


NASA Tech Briefs

National
Aeronautics and
Space
Administration



This fireplace-installed wood-burning heater is one of several commercial products protected by a coating originally developed for spacecraft. By reflecting rather than absorbing radiant energy, the coating keeps surfaces cool — even the metal surfaces exposed to 1,800° F in the wood burner. [See the bottom of page A1.]

About the NASA Technology Utilization Program

The National Aeronautics and Space Act of 1958, which established NASA and the United States civilian space program, requires that "The Administration shall provide for the widest practicable and appropriate dissemination of information concerning its activities and the results thereof."

To help carry out this objective, NASA's Technology Utilization (TU) Program was established in 1962. Now, as an element of NASA's Technology Transfer Division, this program offers a variety of valuable services to help transfer aerospace technology to nonaerospace applications, thus assuring American taxpayers maximum return on their investment in space research; thousands of spinoffs of NASA research have already occurred in virtually every area of our economy.

The TU program has worked for engineers, scientists, technicians, and businessmen; and it can work for you.

NASA Tech Briefs

Tech Briefs is published quarterly and is free to engineers in U.S. industry and to other domestic technology transfer agents. It is both a current-awareness medium and a problem-solving tool. Potential products . . . industrial processes . . . basic and applied research . . . shop and lab techniques . . . computer software . . . new sources of technical data . . . concepts . . . can be found here. The short section on New Product Ideas highlights a few of the potential new products contained in this issue. The remainder of the volume is organized by technical category to help you quickly review new developments in your areas of interest. Finally, a subject index makes each issue a convenient reference file.

Further Information on Innovations

Although some new technology announcements are complete in themselves, most are backed up by Technical Support Packages (TSP's). TSP's are available without charge and may be ordered by simply completing a TSP Request Card found at the back of this volume. Further information on some innovations is available for a nominal fee from other sources, as indicated. In addition, Technology Utilization Officers at NASA Field Centers will often be able to lend necessary guidance and assistance.

Patent Licenses

Patents have been issued to NASA on some of the inventions described, and patent applications have been submitted on others. Each announcement indicates patent status, if applicable.

Other Technology Utilization Services

To assist engineers, industrial researchers, business executives, city officials, and other potential users in applying space technology to their problems, NASA sponsors Industrial Applications Centers. Their services are described on page A7. In addition, an extensive library of computer programs is available through COSMIC, the Technology Utilization Program's outlet for NASA-developed software.

Applications Program

NASA conducts applications engineering projects to help solve public-sector problems in such areas as safety, health, transportation, and environmental protection. Applications teams, staffed by professionals from a variety of disciplines, assist in this effort by working with Federal agencies and health organizations to identify critical problems amenable to solution by the application of existing NASA technology.

Reader Feedback

We hope you find the information in *NASA Tech Briefs* useful. A reader-feedback card has been included because we want your comments and suggestions on how we can further help you apply NASA innovations and technology to your needs. Please use it; or if you need more space, write to the Director, Technology Transfer Division, P. O. Box 8757, Baltimore/Washington International Airport, Maryland 21240.

NASA TU Services

A3 Technology Utilization services that can assist you in learning about and applying NASA technology.



New Product Ideas

A9 A summary of selected innovations of value to manufacturers for the development of new products.



Tech Briefs

409 **Electronic Components and Circuits**



417 **Electronic Systems**



425 **Physical Sciences**



445 **Materials**



455 **Life Sciences**



465 **Mechanics**



483 **Machinery**



493 **Fabrication Technology**



509 **Mathematics and Information Sciences**



Subject Index

515 Items in this issue are indexed by subject; a cumulative index will be published yearly.



COVERS: To find out more about the Reflecting Coating, Circle 79 on the TSP Request Card at the back of this issue of NASA Tech Briefs. Information on the Pipe Flexibility and Analysis Program [MEL-21] may be obtained from COSMIC [see page A8] by Circling R on the COSMIC Request Card.

About This NASA Publication

NASA Tech Briefs, a quarterly publication, is distributed free to qualified U.S. citizens to encourage commercial application of U.S. space technology. For information on publications and services available through the NASA Technology Utilization Program, write to the Director, Technology Transfer Division, P. O. Box 8757, Baltimore/Washington International Airport, Maryland 21240.

"The Administrator of National Aeronautics and Space Administration has determined that the publication of this periodical is necessary in the transaction of the public business required by law of this Agency. Use of funds for printing this periodical has been approved by the Director of the Office of Management and Budget."

Change of Address

If you wish to have NASA Tech Briefs forwarded to your new address, use one of the Subscriptions cards enclosed in the back of this volume of NASA Tech Briefs. Be sure to check the appropriate box indicating change of address.

Communications Concerning Editorial Matter

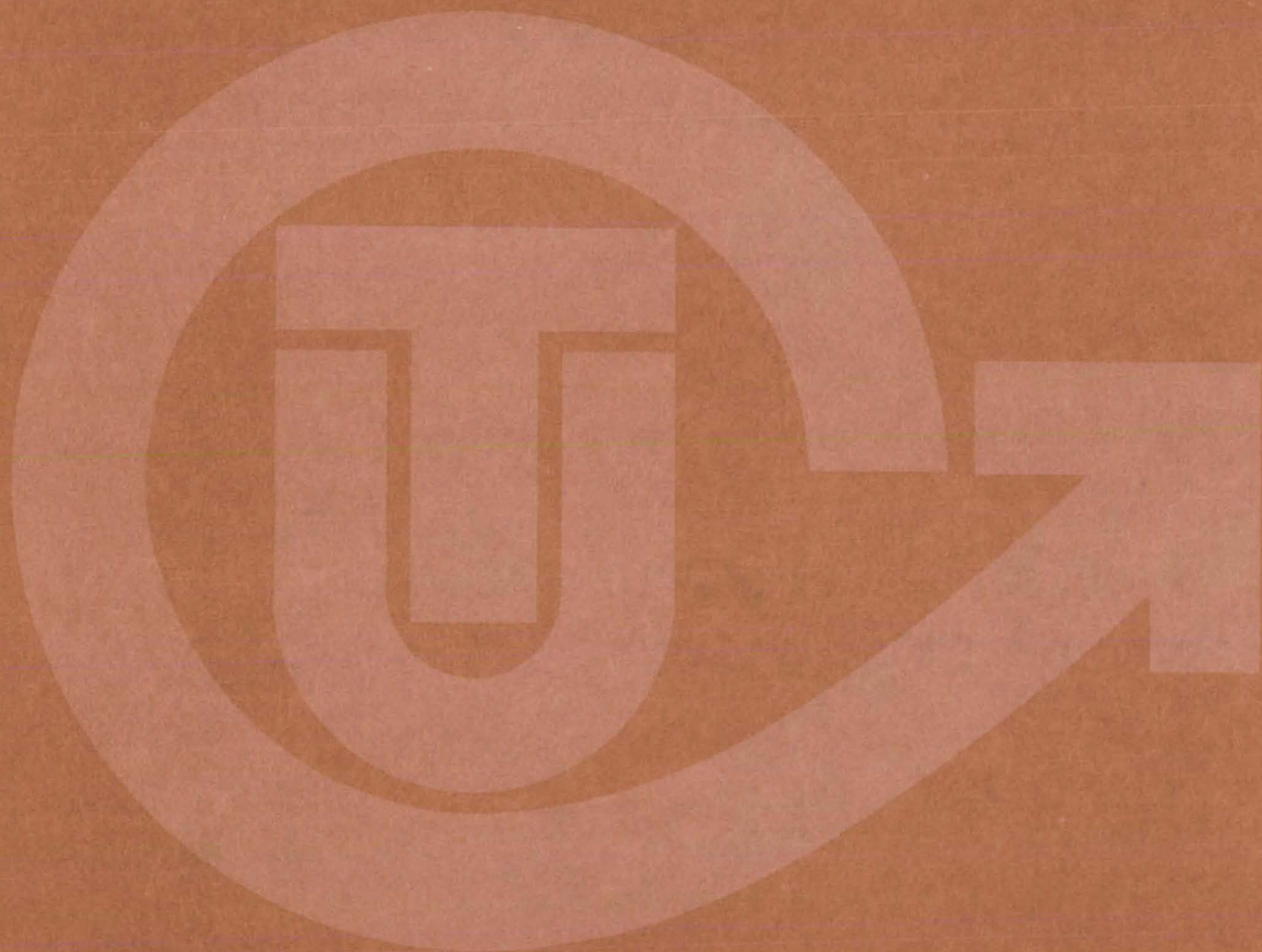
For editorial comments or general communications about NASA Tech Briefs, you may use the Feedback card in the back of NASA Tech Briefs, or write to: The Publications Manager, Technology Transfer Division (ETD-6), NASA Headquarters, Washington, DC 20546. Technical questions concerning specific articles should be directed to the Technology Utilization Officer of the sponsoring NASA Center (addresses listed on page A4).

Acknowledgements

NASA Tech Briefs is published quarterly by the National Aeronautics and Space Administration, Technology Utilization Branch, Washington, DC: Administrator: **Robert A. Frosch**; Director, Technology Transfer Division: **Floyd I. Roberson**; Publications Manager: **D. W. Orrick**. Prepared for the National Aeronautics and Space Administration by **Logical Technical Services Corp.**: Editor-in-Chief: **Jay Kirschenbaum**; Art Director: **Ernest Gillespie**; Senior Editor: **Jerome Rosen**; Chief Copy Editor: **Oden Browne**; Staff Editors: **Donald Blattner**, **Larry Grunberger**, **Ted Selinsky**, **George Watson**; Graphics: **Concetto Auditore**, **Conrad Carlock**, **Luis Martinez**, **Janet McCrie**; Editorial & Production: **Richard Johnson**, **Jeanne Bonner**, **Rose Giglietti**, **Marena Gutman**, **Kathi Norklun**, **Vincent Susinno**, **John Tucker**, **Ernestine Walker**.

This document was prepared under the sponsorship of the National Aeronautics and Space Administration.. Neither the United States Government nor any person acting on behalf of the United States Government assumes any liability resulting from the use of the information contained in this document, or warrants that such use will be free from privately owned rights.

NASA TU SERVICES



NASA TECHNOLOGY UTILIZATION NETWORK

★ TECHNOLOGY UTILIZATION OFFICERS

Ben Padrick
Ames Research Center
Code AU: 240-2
Moffett Field, CA 94035
(415) 965-5151

Gussie Anderson
Hugh L. Dryden Flight Research Center
Code OD/TU Office - Room 2015
Post Office Box 273
Edwards, CA 93523
(805) 258-3311, Ext. 787

Donald S. Friedman
Goddard Space Flight Center
Code 702.1
Greenbelt, MD 20771
(301) 344-6242

John T. Wheeler
Lyndon B. Johnson Space Center
Code AT-3
Houston, TX 77058
(713) 483-3809

U. Reed Barnett
John F. Kennedy Space Center
Code PT-SPD
Kennedy Space Center, FL 32899
(305) 867-2780

John Samos
Langley Research Center
Mail Stop 139A
Hampton, VA 23665
(804) 827-3281

Harrison Allen, Jr.
Lewis Research Center
Mail Code 7-3
21000 Brookpark Road
Cleveland, OH 44135
(216) 433-4000, Ext. 6422

Aubrey D. Smith
George C. Marshall Space Flight Center
Code AT01
Marshall Space Flight Center, AL 35812
(205) 453-2224

D. W. Orrick
NASA Headquarters
Code ETD-6
Washington, DC 20546
(202) 755-2244

John H. Warden
NASA Resident Office-JPL
4800 Oak Grove Drive
Pasadena, CA 91103
(213) 354-6420

Gilmore H. Trafford
Wallops Flight Center
Code OD
Wallops Island, VA 23337
(804) 824-3411, Ext. 201

● INDUSTRIAL APPLICATIONS CENTERS

Aerospace Research Applications Center
1201 East 38th Street
Indianapolis, IN 46205
John M. Ulrich, director
(317) 264-4644

Computer Software Management and Information Center (COSMIC)
Suite 112, Barrow Hall
University of Georgia
Athens, GA 30602
Harold G. Hale, Jr., director
(404) 542-3265

Kerr Industrial Applications Center
Southeastern Oklahoma State University
Durant, OK 74701
Robert Oliver, director
(405) 924-0121, Ext. 413

NASA Industrial Applications Center
701 LIS Building
University of Pittsburgh
Pittsburgh, PA 15260
Paul A. McWilliams, executive director
(412) 624-5211

New England Research Applications Center
Mansfield Professional Park
Storrs, CT 06268
Daniel Wilde, director
(203) 486-4533

North Carolina Science and Technology Research Center
Post Office Box 12235
Research Triangle Park, NC 27709
Peter J. Chenery, director
(919) 549-0671

Technology Applications Center
University of New Mexico
Albuquerque, NM 87131
Stanley Morain, director
(505) 277-3622

NASA Industrial Applications Center
University of Southern California
Denny Research Building
University Park
Los Angeles, CA 90007
Robert Mixer, acting director
(213) 743-6132

■ STATE TECHNOLOGY APPLICATIONS CENTERS

NASA/University of Florida State Technology Applications Center
311 Weil Hall
University of Florida
Gainesville, FL 32611
Ronald J. Thornton, director
Gainesville: (904) 392-6760
Orlando: (305) 275-2706
Tampa: (813) 974-2499

NASA/University of Kentucky State Technology Applications Program
109 Kinkead Hall
University of Kentucky
Lexington, KY 40506
William R. Strong, manager
(606) 258-4632



◆ PATENT COUNSELS

Robert F. Kempf
Asst. Gen. Counsel for patent matters
NASA Headquarters
Code GP-4
400 Maryland Avenue, SW.
Washington, DC 20546
(202) 755-3954

Darrell G. Brekke
Ames Research Center
Mail Code: 200-11A
Moffett Field, CA 94035
(415) 965-5104

Paul F. McCaul
Hugh L. Dryden Flight Research Center
Code OD/TU Office - Room 2015
Post Office Box 273
Edwards, CA 93523
(213) 354-2734

John O. Tresansky
Goddard Space Flight Center
Mail Code: 204
Greenbelt, MD 20771
(301) 344-7351

Marvin F. Matthews
Lyndon B. Johnson Space Center
Mail Code: AM
Houston, TX 77058
(713) 483-4871

James O. Harrell
John F. Kennedy Space Center
Mail Code: SA-PAT
Kennedy Space Center, FL 32899
(305) 867-2544

Howard J. Osborn
Langley Research Center
Mail Code: 279
Hampton, VA 23665
(804) 827-3725

Norman T. Musial
Lewis Research Center
Mail Code: 500-311
21000 Brookpark Road
Cleveland, OH 44135
(216) 433-4000, Ext. 346

Leon D. Wofford, Jr.
George C. Marshall Space Flight Center
Mail Code: CC01
Marshall Space Flight Center, AL 35812
(205) 453-0020

Monte F. Mott
NASA Resident Office-JPL
Mail Code: 180-601
4800 Oak Grove Drive
Pasadena, CA 91103
(213) 354-2700

▲ APPLICATION TEAMS

William N. Fetzner, director
Advisory Center for Medical Technology and Systems
University of Wisconsin
1500 Johnson Drive
Madison, WI 53706
(608) 263-2735

Edmund R. Bangs, director
IIT Research Institute
10 West 35th Street
Chicago, IL 60616
(312) 567-4191

Doris Rouse, director
Research Triangle Institute
Post Office Box 12194
Research Triangle Park, NC 27709
(919) 541-6256

Tom Anyos, director
SRI International
333 Ravenswood Avenue
Menlo Park, CA 94026
(415) 326-6200, Ext. 2864

Eugene Schmidt, program coordinator
Stanford University School of Medicine
Cardiology Division
Biomedical Technology Transfer
703 Welch Road, Suite E-4
Palo Alto, CA 94304
(415) 497-5353

David MacFadyen, project director
Technology + Economics
2225 Massachusetts Avenue
Cambridge, MA 02140
(617) 491-1500

TECHNOLOGY UTILIZATION OFFICERS

Technology transfer experts can help you apply the innovations in NASA Tech Briefs.

The Technology Utilization Officer at each NASA Field Center is an applications engineer who can help you make use of new technology developed at his center. He brings you NASA Tech Briefs and other special publications, sponsors conferences, and arranges for expert assistance in solving technical problems.

Technical assistance,

in the form of further information about NASA innovations and technology, is one of the services available from the TUO. Together with NASA scientists and engineers, he can often help you find and implement NASA technology to meet your specific needs.

Technical Support Packages (TSP's) are prepared by the center TUO's. They provide further technical details for articles in NASA Tech Briefs. This additional material can help you evaluate and use NASA technology. You may receive most TSP's free of charge by using the TSP Request Card found at the back of this issue.

Technical questions about articles in NASA Tech Briefs are answered in the TSP's. When no TSP is available, or you have further questions, contact the Technology Utilization Officer at the center that sponsored the research [see page A4].



NASA INVENTIONS AVAILABLE FOR LICENSING

Over 3,500 NASA inventions are available for licensing in the United States — both exclusive and nonexclusive.

Nonexclusive licenses

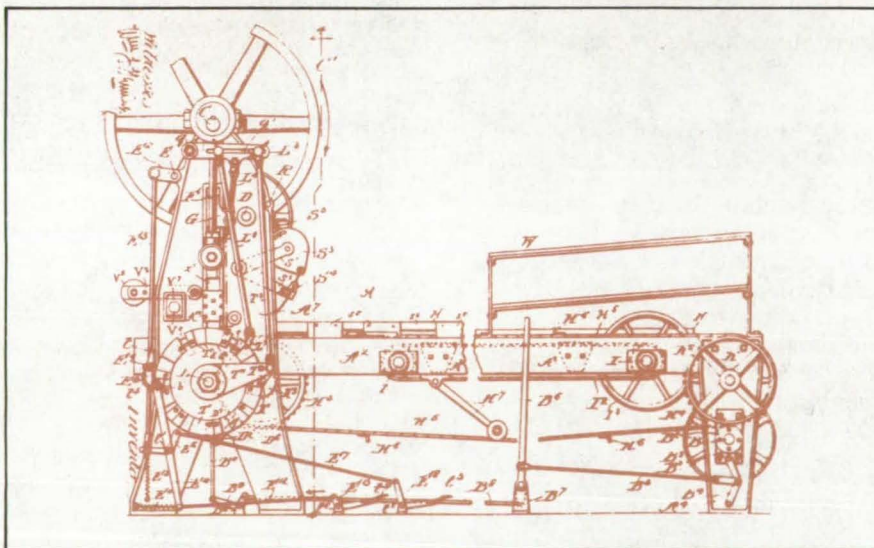
for commercial use of NASA inventions are encouraged to promote competition and to achieve the widest use of inventions. They must be used by a negotiated target date but are usually royalty-free.

Exclusive licenses

may be granted to encourage early commercial development of NASA inventions, especially when considerable private investment is required. These are generally for 5 to 10 years and usually require royalties based on sales or use.

Additional licenses available

include those of NASA-owned foreign patents. In addition to inventions described in NASA Tech Briefs, "NASA Patent Abstract Bibliography" (PAB), containing abstracts of all NASA inventions, can be purchased from National Technical Information Service, Springfield, VA 22161. The PAB is updated semiannually.



Patent licenses for Tech Briefs

are frequently available. Many of the inventions reported in NASA Tech Briefs are patented or are under consideration for a patent at the time they are published. The current patent status is described at the end of the article; otherwise, there is no statement about patents. If you want to know more about the patent program or are interested in licensing a particular invention, contact the Patent Counsel at the NASA Field Center that sponsored the research [see page A5]. Be sure to refer to the NASA reference number at the end of the Tech Brief.

APPLICATION TEAMS

Technology-matching and problem-solving assistance to public-sector organizations

Application engineering projects

are conducted by NASA to help solve public-sector problems in such areas as safety, health, transportation, and environmental protection. Some application teams specialize in biomedical disciplines; others, in engineering and scientific problems. Staffed by professionals from various disciplines, these teams work with other Federal agencies and health organizations to



identify critical problems amenable to solution by the application of existing NASA technology.

Public-sector organization

representatives can learn more about application teams by contacting a nearby NASA Field Center Technology Utilization Office [see page A4].

INDUSTRIAL APPLICATIONS CENTERS

Computerized access to nearly 10 million documents worldwide

Computerized information retrieval

from one of the world's largest banks of technical data is available from NASA's network of Industrial Applications Centers (IAC's). The IAC's give you access to 1,800,000 technical reports in the NASA data base and to more than 10 times that many reports and articles found in 140 other computerized data bases.

The major sources include:

- 750,000 NASA Technical Reports
- Selected Water Resources Abstracts
- NASA Scientific and Technical Aerospace Reports
- Air Pollution Technical Information Center
- NASA International Aerospace Abstracts
- Chem Abstracts Condensates
- Engineering Index
- Energy Research Abstracts
- NASA Tech Briefs
- Government Reports Announcements

and many other specialized files on food technology, textile technology, metallurgy, medicine, business, economics, social sciences, and physical science.

The IAC services

range from tailored literature searches through expert technical assistance:



- **Retrospective Searches:** Published or unpublished literature is screened, and documents are identified according to your interest profile. IAC engineers tailor results to your specific needs and furnish abstracts considered the most pertinent. Complete reports are available upon request.
- **Current-Awareness Searches:** IAC engineers will help design a program to suit your needs. You will receive selected monthly or quarterly abstracts on new developments in your area of interest.

- **Technical Assistance:** IAC engineers will help you evaluate the results of your literature searches. They can help find answers to your technical problems and put you in touch with scientists and engineers at appropriate NASA Field Centers.

Prospective clients

can obtain more information about the services offered by NASA IAC's by contacting the nearest IAC [see page A4] or by checking the IAC box on a TSP Request Card in this issue.

STATE TECHNOLOGY APPLICATIONS CENTERS

Technical information services for industry
and state and local government agencies

Local government and industry

in Florida and Kentucky can utilize the services of NASA's State Technology Applications Centers (STAC's). The STAC's differ from the Industrial Applications Centers described on page A7, primarily in that they are integrated into existing state technical assistance programs and serve only

the host state, whereas the IAC's serve multistate regions.

Many data bases,

including the NASA base and several commercial bases, are available for automatic data retrieval through the STAC's. Other services such as document retrieval and special

searches are also provided. (The STAC's normally charge a fee for their services.)

To obtain information

about the services offered by NASA STAC's, write or call the STAC in your state [see page A4].

COSMIC®

An economical source of computer programs
developed by NASA and other government agencies

A vast software library

is maintained by COSMIC — the Computer Software Management and Information Center. COSMIC gives you access to approximately 1,600 computer programs developed for NASA and the Department of Defense and selected programs for other government agencies. Programs and documentation are available at reasonable cost.

Available programs

range from management (PERT scheduling) to information science (retrieval systems) and computer operations (hardware and software). Hundreds of engineering programs perform such tasks as structural analysis, electronic circuit design, chemical analysis, and the design of fluid systems. Others determine building energy requirements and optimize mineral exploration.

COSMIC services

go beyond the collection and storage of software packages. Programs are checked for completeness; special announcements and an indexed software catalog are prepared; and programs are reproduced for distribution. Customers are helped to

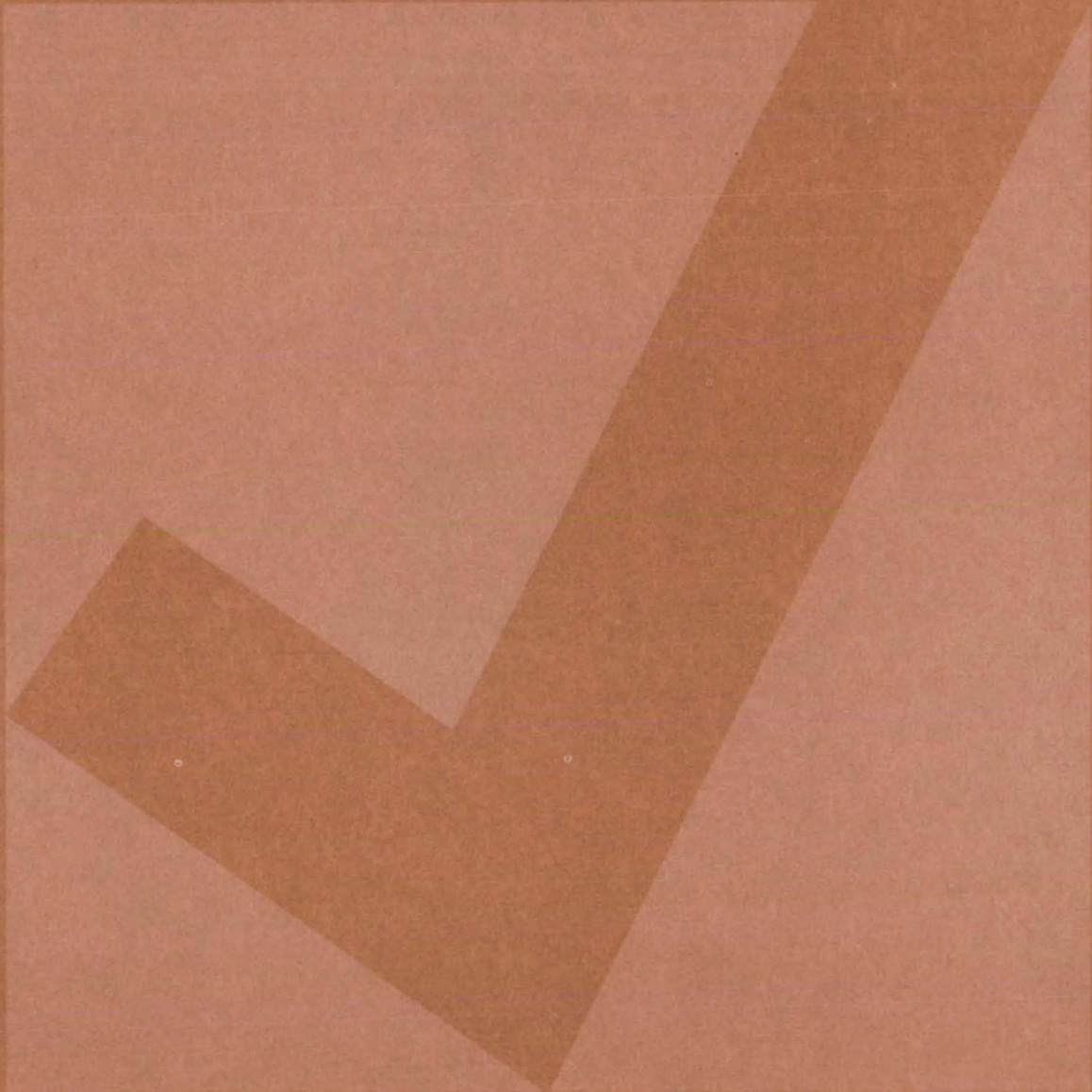
identify their software needs; and COSMIC follows up to determine the successes and problems and to provide updates and error corrections. In some cases, NASA engineers can offer guidance to users in installing or running a program.

Information about programs

described in NASA Tech Briefs articles can be obtained by completing the COSMIC Request Card at the back of this issue. Just circle the letters that correspond to the programs in which you are interested.



NEW PRODUCT IDEAS



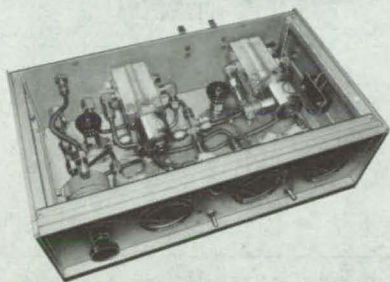
Hardware, Techniques, and Processes

- 411 Improved Battery Charger for Electric Vehicles
- 412 Multijunction High-Voltage Solar Cell
- 413 Solar Cell Is Housed in Light-Bulb Enclosure
- 413 Simple JFET Oscillator
- 414 Speed Control for Synchronous Motors
- 415 Low-Resistance Continuity Tester

of glass-filled material. Successive turns of the strip are spirally wrapped in a groove machined into one of the flange surfaces. Closing the joint compresses the gasket. (See page 502.)

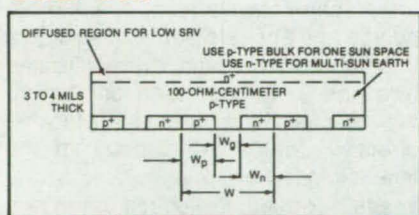
Pneumatic-Power Supply

A new portable compressed-air supply has two or more outputs at pressures that can be adjusted from 20 to 100 psi. It can be used to operate production equipment, to spray paint and lubricants, to pressurize refrigeration systems, and for other applications. The supply filters the air from a standard high-pressure line, reduces it to working pressure,



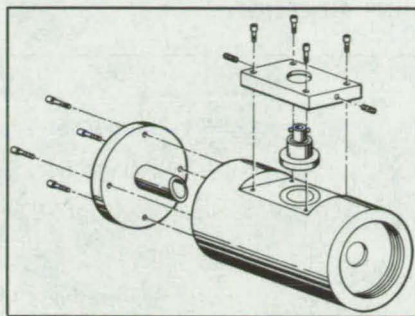
and adds a lubricant if required. An accurate regulator supplies the low-pressure air to the output channels. On the channel lines, vernier-control valves select the output pressures. (See page 486.)

Multijunction High-Voltage Solar Cell



The fabrication of a high-voltage solar cell on a single semiconductor wafer is possible with a new multijunction cell. A photovoltaic energy source using the new cell could be combined on a wafer with the circuit it is to power. For example, a computer module could be built on a silicon wafer with the energy for the internal information processing, and even readouts, derived from an external light source. The new cell consists of many voltage-generating regions that are interconnected internally or externally to give the desired voltage-and-current combination. (See page 412.)

Gas-Laser Power Monitor

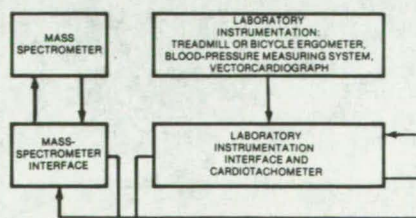


Attached to the front of a laser housing, a gas-laser power monitor reads the power output continuously while the laser is in use. It is calibrated to read either the total power output of the laser or the power generated in a test volume. No modifications to the laser are required — the monitor simply attaches to the laser end cap. It is fabricated from four black-anodized aluminum parts. A piece of crown glass positioned at the Brewster angle reflects a small fraction of the beam into a photodiode, which is calibrated for an electrical output proportional to the laser power. (See page 430.)

New Pressure-Sensitive Silicone Adhesive

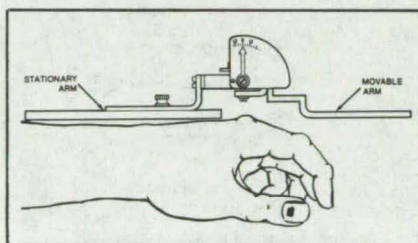
A new pressure-sensitive silicone adhesive for high or low temperatures does not stretch severely under load. The blend of silicone tackifier and cured rubbery silicone is used without solvents. It is produced by combining an intermediate-molecular-weight pressure-sensitive silicone adhesive, which does not cure, with a silicone resin, which generally cures with a catalyst to a rubbery tack-free state. The ratio of silicone tackifier to silicone resin is varied to obtain different degrees of tack, creep resistance, and tensile strength. (See page 452.)

Cardiopulmonary Data-Acquisition System



A computerized cardiopulmonary data-acquisition system controls and monitors bicycle and treadmill cardiovascular stress tests. It acquires and reduces stress data and displays in real time the heart rate, blood pressure, workload, respiratory rate, exhaled-gas composition, and other variables. The data are printed on a hard-copy terminal every 30 seconds so that the operator can quickly respond to the subject throughout the test. The ergometer workload is controlled in real time according to the experimental protocol, and the collected data are stored directly on tape in analog form and on floppy disks in digital form for posttest data processing. (See page 457.)

Gage for Evaluating Rheumatoid Hands

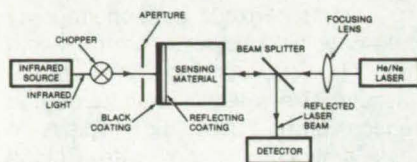


A two-axis goniometer accurately measures the movements of the fingers about the knuckle joints. It can help to diagnose hands that have structurally changed because of rheumatoid arthritis. The new goniometer measures lateral movement which is small in normal knuckle joints but increases in diseased joints. The instrument is basically two connected protractors that simultaneously measure angles in perpendicular planes. Its dials are offset to clear the bony protuberances that result from rheumatoid arthritis. Extension and offset adjustments span any hand size. (See page 461.)

Compact Infrared Detector

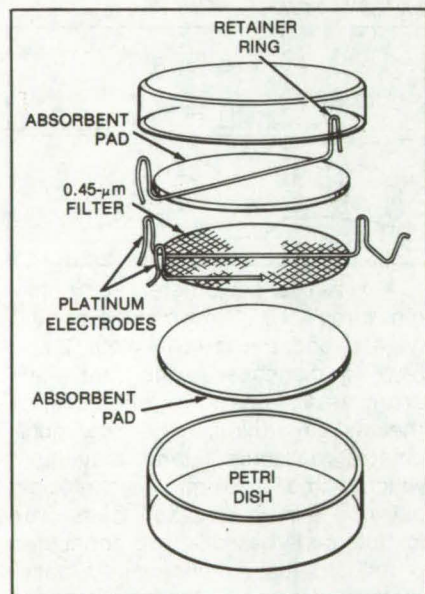
Compactness, high responsivity, and high noise immunity are among the advantages of a new broadband IR detector that could be integrated into a compact package for pollution monitoring and weather prediction. The sensing material is a transparent sheet, metalized with a reflecting coating and then overcoated with a

(continued on next page)



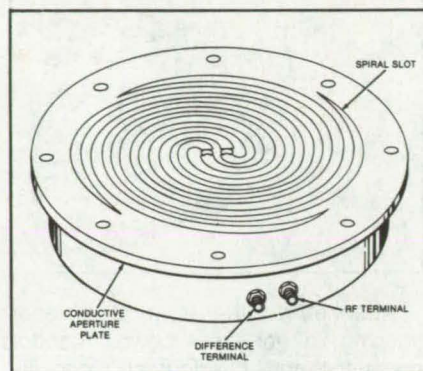
black material on the same side. Each pulse produced by chopping the infrared source beam with a shutter creates a transient "thermal lens" that temporarily defocuses a reflected laser-beam probe. The defocusing increases as the infrared intensity increases. A detector monitors the probe beam, which weakens as the infrared light becomes more intense. (See page 475.)

Improved Microbe Detection in Water Samples



Membrane filtration and electrochemical microbial detection are combined in a new method for detecting micro-organisms in water samples. Combined, the techniques give fast response and better detection of low concentrations. Cells are collected by a membrane filter placed on a moistened absorbent pad; platinum-wire electrodes are positioned on the surface of the filter. Another moistened pad is placed on top of the electrodes and filter. A retainer ring maintains constant pressure and close contact between pads, filter, and electrodes, which are contained in a petri dish to reduce moisture loss. (See page 460.)

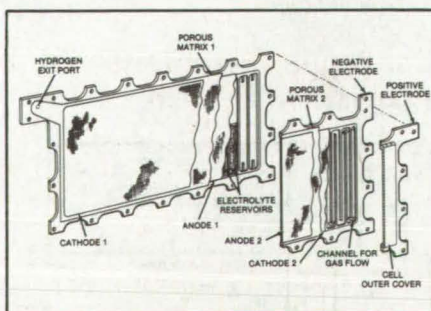
Cavity-Backed Spiral-Slot Antenna



A new flush-mounted antenna can be switched to give either a radiation peak or a null on the axis, with circular polarization in either case. It is compact and can withstand severe mechanical and thermal loads. The radiating elements consist of two pairs of center-fed interleaved spiral slots in a conductive plane. Each slot in each pair lies between the slots of the other pair. At the center feedpoint of each pair of slots, a balanced feed assembly drives the slot from a split-tube coaxial balun. The entire apparatus is reciprocal, so that the circularly polarized patterns represent received signals as well as transmitted signals. (See page 421.)

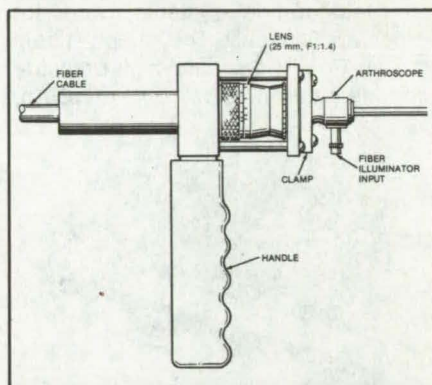
Improved Cell for Water-Vapor Electrolysis

Water vapor in such gases as steam or ordinary room air is decomposed into hydrogen and oxygen by improved continuous-flow electrolytic cells. A new sintered iridium oxide catalytic anode coating yields dissociation rates over a hundredfold greater than those obtained using conventional platinum black. Each cell consists of two mirror-image cells, with a dual cathode sandwiched between two anodes.



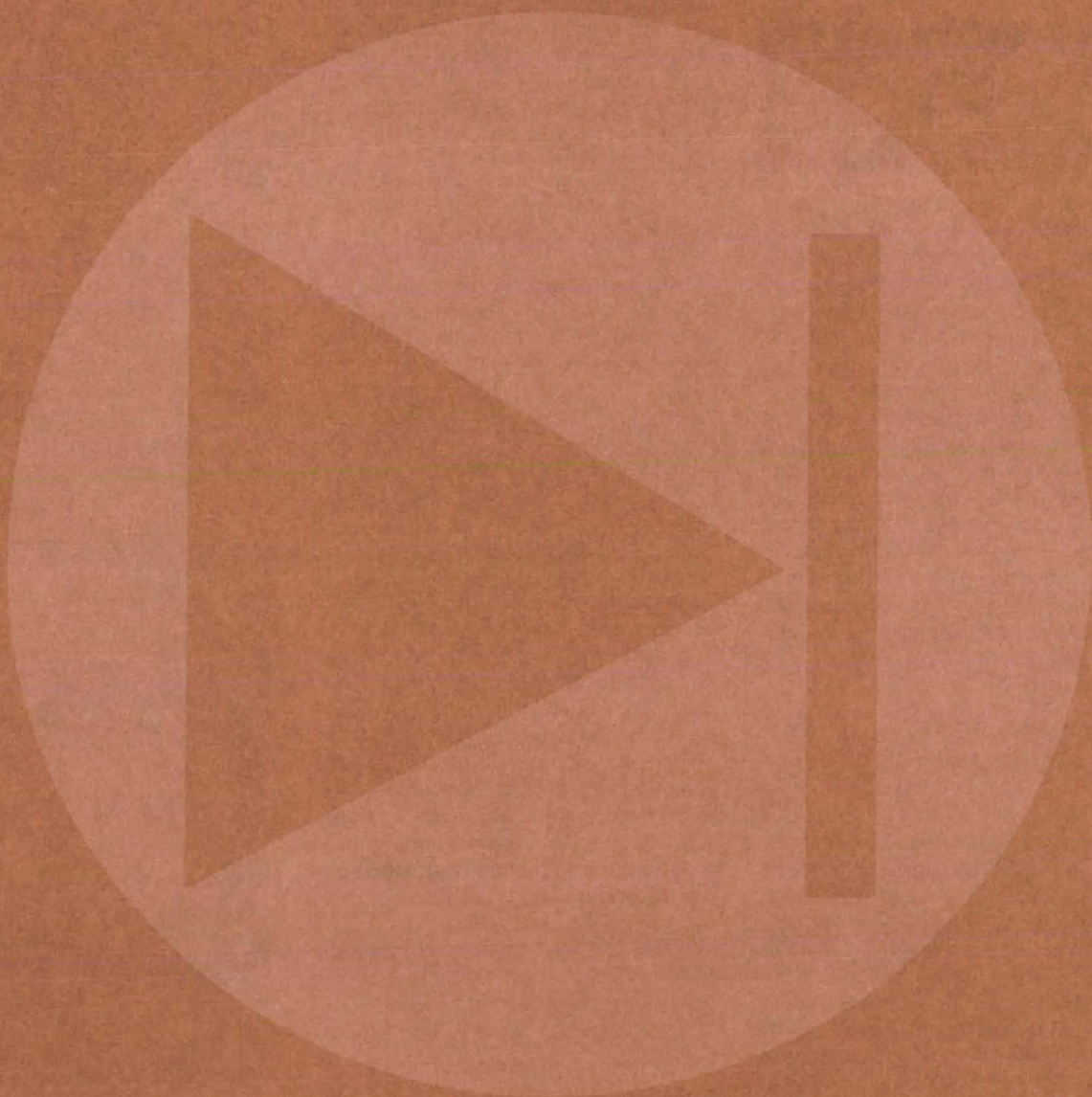
Vapor-laden gas traverses serpentine channels within each cell and is dissociated at the anode into hydrogen ions and free oxygen. The oxygen mingles with the gas stream, while the hydrogen migrates through a porous, electrolyte-saturated matrix and is liberated as hydrogen gas at the cathode. (See page 447.)

Hand-Held Coupler for Arthroscope



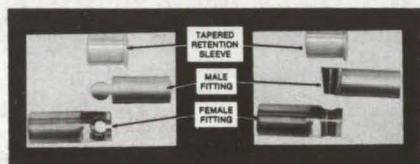
A new, hand-held coupler images the output of an arthroscope onto a coherent fiber bundle. The arthroscope allows surgeons to examine internal structures and organs through a small incision or natural opening in the body. The coupler also can be used for engine inspection, instrument repair, and visual inspection through small openings. The image from the arthroscope travels along the flexible bundle and appears at the other cable end, where the image is recollimated by a lens. The image seen looking into the lens is the same as if looking directly into the arthroscope. If the lens is placed at the eyepiece, a real image is formed. Projection of the real image on a color-TV camera increases the image size and makes it easier to view, enhancing the surgical procedure. The hand-held portion of the coupler permits easy positioning and rotation of the arthroscope. (See page 462.)

Electronic Components and Circuits



NEW PRODUCT IDEAS are just a few of the many innovations described in this issue of NASA Tech Briefs and having promising commercial applications. Each is discussed further on the referenced page in the appropriate section in this issue. If you are interested in developing a product from these or other NASA innovations, you can receive further technical information by requesting the TSP referenced at the end of the full-length article or by writing the Technology Utilization Office of the sponsoring NASA center (see page A4). NASA's patent-licensing program to encourage commercial development is described on page A8.

Interlocking Wedge Joint Is Easily Assembled

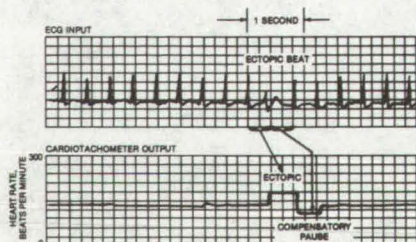


Two structural members in manual-, remote-, or automated-assembly operations are linked by a new interlocking wedge joint. The joint is simple enough to be assembled by undersea divers, workers in nuclear reactors, and others wearing gloves or bulky clothing. An expanding sleeve and male and female endpieces are joined in a single locking stroke. The joint has a high mechanical advantage that overcomes structural misalignments and forces the assembly into the true position as the locking sleeve moves into place. The joint transmits all structural loads, including tension, compression, bending moments, and torsion.

(See page 485.)

Microprocessor-Based Cardi tachometer

A new cardi tachometer operates reliably even with stress-test electrocardiogram (ECG) signals that are subject to noise, baseline wandering, and amplitude change. It records heart rate from a preamplified, single-lead ECG input signal and produces digital and analog heart-rate outputs, which can be fed to other instruments or computers. Analog hardware processes the ECG input signal,

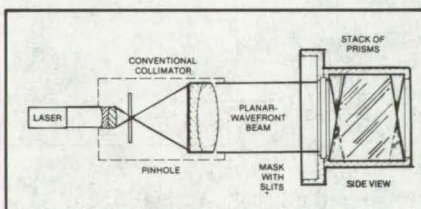


producing a 10-ms pulse for each heartbeat. The resulting pulse train is analyzed by a microprocessor computer program that identifies irregular heartbeats and maintains a stable output during ECG lead switching. Since the analysis logic is part of the computer program, it is easily modified.

(See page 459.)

Multibeam Collimator

Many precisely-divergeant light beams are created by a new optical instrument that can be used to

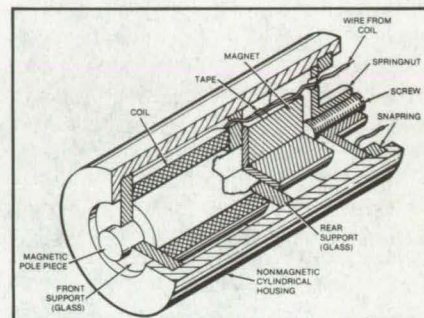


measure angles in surveying land, aligning machine elements, and other applications. The angles and refractive indices of a stack of prisms are selected to divert an incoming laser beam by small increments, different for each prism. Thus, the angles of the emerging beams differ by small, precisely controlled amounts. The instrument is nearly immune to vibration, changes in gravitational force, temperature variations, and mechanical distortion.

(See page 427.)

Vibration Transducer for Extreme Environments

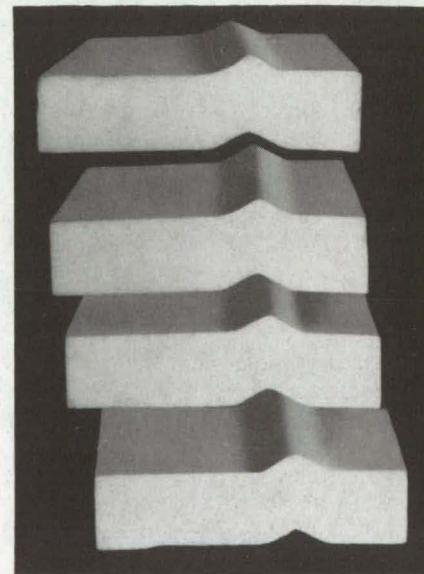
An improved transducer with a temperature limit of 500° C and a pressure limit of up to 10 kilobars responds to mechanical vibrations up to 20 kHz. Constructed of high-temperature-resistant materials, the new vibration pickup should perform well in nuclear reactors, turbines, and other extreme environments. Outgassing and "virtual" leakage, problems experienced at very low pressures with previous transducers potted in



epoxy, are eliminated by using only glass and metal supports. The interior is open to the atmosphere to prevent the buildup of pressure-induced stresses. A spring holds the transducer parts against the housing to reduce distortion due to pressurization and thermal strain.

(See page 471.)

Low-Temperature Seal



A spiral-wound cryogenic gasket is made from just one component, requires no encapsulant, and can be produced with self-locking or other features. Fabricated from a continuous strip, the seal can be "active" (be opened and closed), or it can be permanent. It is made by skiving a strip from the circumference of a disk

Improved Battery Charger for Electric Vehicles

Polyphase chopper circuit would significantly reduce ripple and EMI.

NASA's Jet Propulsion Laboratory, Pasadena, California

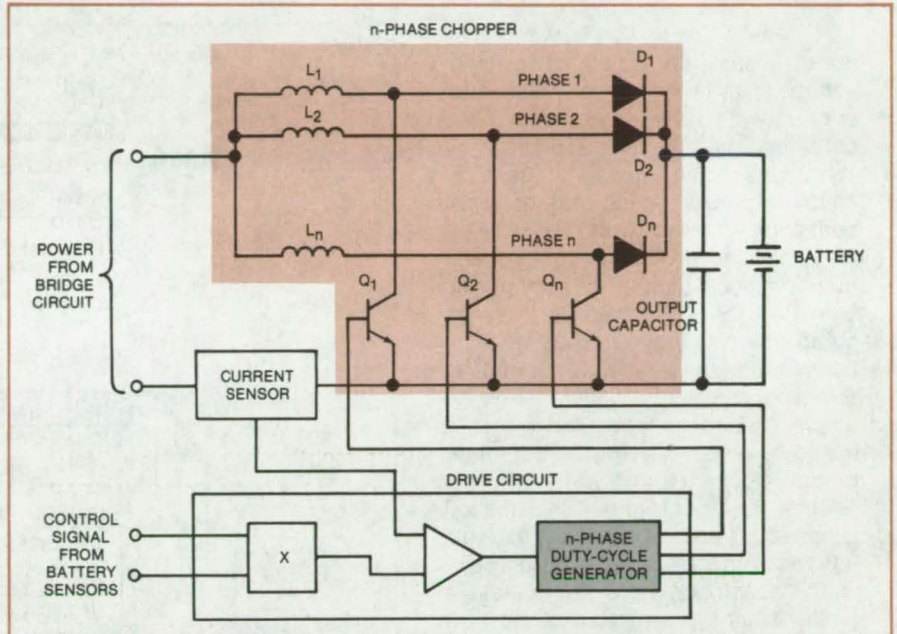
While the single-phase "boost chopper" is already superior to most conventional battery chargers for electric vehicles, a proposed polyphase version is expected to give even better performance. Calculations show that when the number of choppers is increased to two, three, or more, ripple and electromagnetic interference (EMI) are substantially reduced and efficiency is improved. The basic advantages of the boost chopper — compactness, high efficiency, and power factors approaching unity — are retained.

The elementary boost chopper has a bridge-based power circuit and a drive circuit that adjusts the rate of charge in response to changes in key battery parameters. An inductor, a transistor, and a diode in the power circuit make up the chopper, which boosts the bridge output so that current is delivered to the battery. The drive circuit adjusts the chopper duty cycle to give a near-unity power factor.

In the n -phase chopper, diagramed in the figure, each inductor carries $1/n$ of the current handled by the inductor of the analogous single-phase circuit. A modulator controls the duty cycle of the transistors, making the instantaneous current through the inductors proportional to the instantaneous bridge output voltage. With this proportionality, the charger operates at a power factor near unity.

Because the ripple in the different chopper phases tends to cancel, the net ripple is low, as is the EMI produced by the charger. Switching spikes are lowered, because the current steps are reduced below that of the single-phase chopper.

For example, a three-phase chopper reduces ripple to one-ninth its single-phase value. At the same time,



Drive circuit of **n-Phase Boost Chopper** incorporates an n -phase duty-cycle generator. Each chopper is composed of an inductor, a transistor, and a diode.

the ripple frequency is increased three times, and the ripple can therefore be more easily filtered out by small inductors and capacitors. The value of capacitance used to clamp switching spikes and protect the switching transistors is reduced to one-ninth its single-phase value. Thus a smaller and less-expensive capacitor can be used.

In general, an n -phase chopper reduces the ripple magnitude by a factor of n^2 while increasing the ripple fundamental frequency n times. The output capacitance is reduced by at least $1/n$. Although ripple theoretically falls rapidly with increasing phases, it is probably not practical to increase n beyond three or four, because the inductors must be more closely matched as n increases, the transistor

drive signals must be more closely matched, and the polyphase generator becomes more expensive.

The charger can be operated by single-phase or three-phase alternating current, at 115 or 230 volts, for example, or by direct current. With dc, it is possible for one electric vehicle to charge another in a road emergency.

This work was done by Wally E. Rippel of Caltech for NASA's Jet Propulsion Laboratory. For further information, Circle 1 on the TSP Request Card.

Inquiries concerning rights for the commercial use of this invention should be addressed to the Patent Counsel, NASA Resident Office-JPL [see page A5]. Refer to NPO-14964.

Multijunction High-Voltage Solar Cell

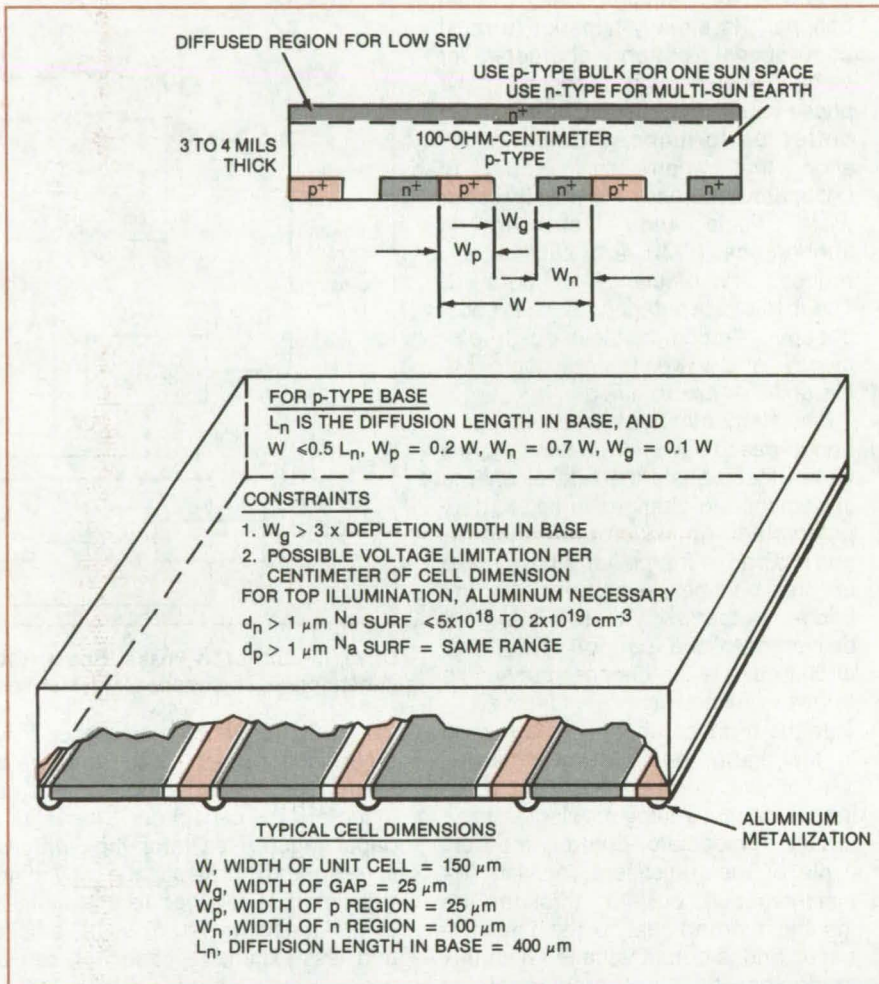
Integrated unit cells could yield 50 volts per linear inch on a single semiconductor wafer.

Lewis Research Center, Cleveland, Ohio

A recent innovation now makes possible the fabrication of a high-voltage solar cell on a single semiconductor wafer. Experimentation has confirmed that a solar cell may be divided into voltage-generating regions, called unit cells, which may be interconnected internally or externally to result in desired voltage and current output combination. The finding also opens up the field of usage in which photovoltaic energy sources may be combined on a wafer with the circuits they are designed to power. For example, it can be speculated that it would be possible to build a computer module upon a silicon wafer with the energy for the internal information processing and even the readouts derived from an external light source.

The accompanying sketch details a typical solar-cell structure of the new planar multijunction (PMJ) high-voltage cell. The starting material for the cited example is high-lifetime, single-crystal, Czochralski-grown silicon. As shown, the device has a thickness of 3 to 4 mils with a textured or planar surface and with an antireflection coating applied to the illuminated surface. In this surface, divided into regions located over the unit voltage-generating unit cells, are implanted or diffused dopants resulting in a front-surface field or a front junction, depending upon the chosen dopant type. When p-type silicon of any resistivity from 1 to 20,000 ohm-cm is used for the base material, a front junction of n^+ dopant such as phosphorus or front surface field of p^+ material such as boron or aluminum may be used. Some benefit is derived from the use of high-resistivity and high-lifetime material for the base.

In any unit voltage-generating unit cell, as shown, a p^+ diffused or implanted region approximately 25 micrometers wide is diffused into a junction depth of 1 micrometer. Next to this narrow band of dopant, an undoped band of the same width is left. Next to the undoped region a wide band of n^+ dopant is inserted to a depth of 1 micrometer. The width of the n^+ region is 100 micrometers, bringing



The Planar Multijunction Solar Cell is shown with doped regions and gaps (not to scale). Unit cells are combined in series, using aluminum metalization bars, to yield the required output voltage and current.

the unit cell width to a total of 150 micrometers. Since the nominal voltage of each such unit cell is one-half volt, it may be possible to produce approximately 50 volts per linear inch of the solar cell while still maintaining optimized size. Smaller or larger unit cells may be used with some penalties, if higher voltages or currents are desired. The overall output voltage of the solar cell is the sum of the unit cell voltages and is collected at the opposite edges of the cell with metal contacting bars as shown on the first p^+ bar and the last n^+ region.

This work was done by John C. Evans, Jr., Chandra Goradia, and An Ti Chai of Lewis Research Center. Further information may be found in NASA TM-81389 [N80-16914/NSP], "Planar Multijunction High Voltage Solar Cells" [\$5]. A copy may be purchased [prepayment required] from the National Technical Information Service, Springfield, Virginia 22161.

Inquiries concerning rights for the commercial use of this invention should be addressed to the Patent Counsel, Lewis Research Center [see page A5]. Refer to LEW-13400.

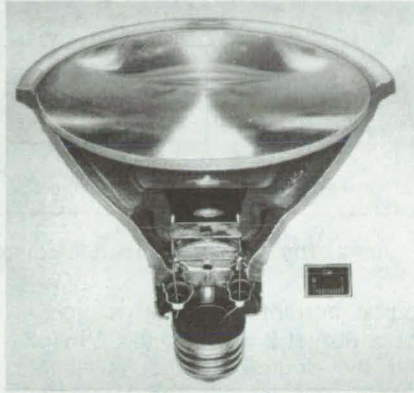
Solar Cell Is Housed in Light-Bulb Enclosure

An inexpensive solar-cell module uses a standard outdoor light-bulb enclosure.

Lewis Research Center, Cleveland, Ohio

With the advent of a recently announced innovation in solar cell fabrication, the planar multijunction (PMJ) high voltage solar cell [see preceding article "Multijunction High Voltage Solar Cell" (LEW-13400)], a number of uses for the new cell have been found. Shown in the accompanying photographs is the first working model of the "light-electric bulb," which uses the focusing principle of the electric lamp in reverse to produce electric power from Sunlight.

Housed in a conventional weather-proof outdoor or yard light enclosure, the new cell, located within the concentrated circle of Sunlight where the lamp filament is conventionally placed, converts radiant energy to electricity. Use of this standard outdoor light enclosure provides a relatively low-cost housing, and one which serves to concentrate Sunlight in the solar cell. A unit as shown is capable of producing approximately 1 watt of electric power.



The **Low-Cost Housing** is seen in the bulb at the left and in the bulb generating 1 watt at about 5 volts on the right.



The new solar cells are made by the same microminiaturization techniques presently employed to make the integrated circuits so familiar in the pocket calculator.

This work was done by John C. Evans, Jr., of Lewis Research Center.

No further documentation is available.

Inquiries concerning rights for the commercial use of this invention should be addressed to the Patent Counsel, Lewis Research Center [see page A5]. Refer to LEW-13418.

Learning High-Quality Soldering

Soldering techniques for high-reliability electronic equipment are taught in a 5-day course. Among the areas covered are: new circuit assembly; reworking printed-wiring boards; parts replacement; and making circuit changes by cutting traces, changing wiring, and adding terminals. (See page 499.)

CADAT Integrated-Circuit Artwork Program

Artwork data are converted into mask patterns by the CADAT integrated-circuit artwork program. The program generates signals for controlling mask-fabricating equipment. An extensive utility package enables the user to create new pattern libraries. (See page 508.)

Trislot-Cavity Microstrip Antenna

A disk radiator sandwiched between conducting planes, so that it is enclosed in a cavity, has greater bandwidths and beamwidths than an unenclosed disk radiator. The cavity antenna, fabricated by conventional microstrip techniques, can be flush mounted on the surface of a moving vehicle. (See page 422.)

Simple JFET Oscillator

Stable high-frequency signal source is compatible with integrated-circuit techniques.

Goddard Space Flight Center, Greenbelt, Maryland

A junction field-effect transistor (JFET) connected in a simple circuit makes a stable sine-wave oscillator for such applications as mixers, modulators, and function generators.

The oscillation frequency can be tuned over a narrow band about the design value. The JFET circuit is convenient for either compact discrete-component assemblies or integrated circuits.

The frequency of this oscillator is in the rolloff portion of the JFET characteristic curve, somewhat above the 3-dB point. As the transconductance
(continued on next page)

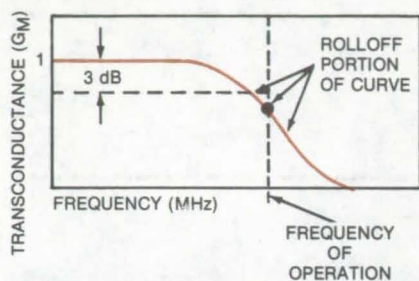


Figure 1. The **Operating Frequency** for the depletion-mode, junction field-effect transistor is in the rolloff portion of its transconductance-vs.-frequency characteristic, around the point where phase shift between source current and gate voltage is 90° .

of the transistor rolls off with increasing frequency (see Figure 1), the phase angle between the source current and the gate voltage increases. The frequency of operation is selected so that the source current is about 90° out of phase with the voltage at the gate and a source capacitor produces an additional 90° of phase shift. Positive feedback then occurs that causes oscillation.

An example of this circuit design is the 2-MHz oscillator shown in Figure 2. The 2N5163 is a depletion-mode JFET that is normally operated at frequencies well below 2 MHz. The drain of the transistor is connected directly to a power supply of +15 volts. The source terminal of the JFET is connected to one end of the parallel combination of resistor R_1 (20 k Ω) and capacitor C_1 (22 pF). The other end of the combination is connected to ground. The phase angle between

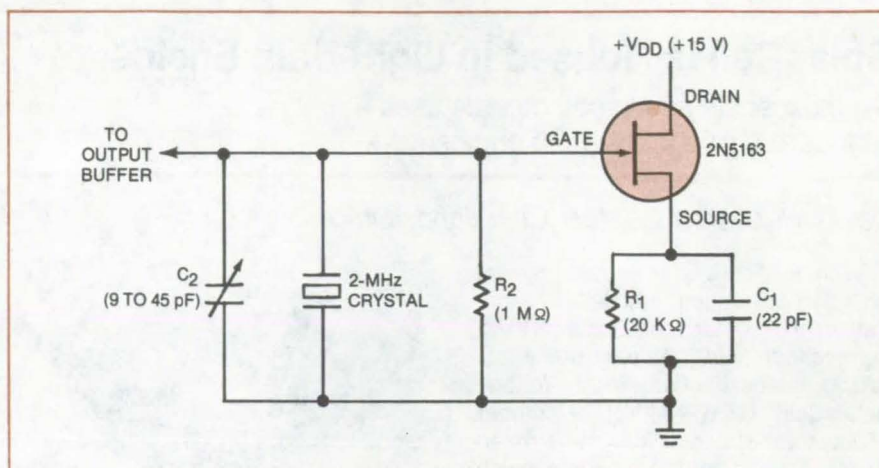


Figure 2. The **Oscillator Circuit** is compact, and has low power consumption.

source current and gate voltage is about 90° at 2 MHz for the 2N5163, and the source voltage is shifted another 90° in C_1 . The total 180° phase shift provides positive feedback that drives a 2-MHz crystal (or a 2-MHz LC tank circuit) at resonance. A variable capacitor, C_2 , connected across the resonator allows fine tuning, and a 1-M Ω resistor supplies a dc return path around the crystal.

The circuit of Figure 2 oscillates at 2.0009255 MHz, without varying more than 0.1 hertz. Its waveform is sinusoidal, with low distortion. The signal is 0.6 volt peak-to-peak at the source and 1.8 volts peak-to-peak at the gate. Outputting from the JFET gate, as shown, is preferred to outputting from the JFET source.

The frequency range, stability, linearity, and low power drain of this

oscillator make it particularly suitable for use in communications receivers and transmitters and in such digital systems as microprocessors, computers, and displays. Its circuit simplicity also allows for ease of monolithic construction. The only components external to the chip would be the crystal or coil and the tuning capacitor.

*This work was done by Leonard L. Kleinberg of **Goddard Space Flight Center**. For further information, Circle 2 on the TSP Request Card.*

This invention is owned by NASA, and a patent application has been filed. Inquiries concerning nonexclusive or exclusive license for its commercial development should be addressed to the Patent Counsel, Goddard Space Flight Center [see page A5]. Refer to GSC-12555.

Speed Control for Synchronous Motors

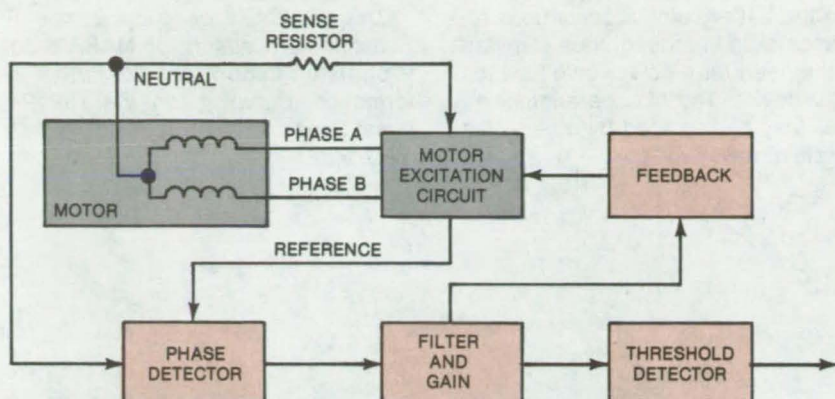
Hunting is either suppressed or enhanced by a phase-sensitive feedback circuit.

Lyndon B. Johnson Space Center, Houston, Texas

A feedback circuit controls fluctuations in the speed of an ac synchronous motor. Small speed variations are detected and either suppressed or enhanced by applying a correction voltage to the motor excitation circuit. Among possible applications of the new speed control is reducing the wow and flutter of audio turntables and tape recorders.

Although an ideal synchronous motor runs at constant speed, small changes in loading, for example, in bearing resistance, cause the speed to "hunt" about the synchronous value at a fairly-constant low frequency. The hunting may be compared to the vibration of a spring, with the motor inertia analogous to the spring mass and the magnetic flux lines equivalent to the elastic spring.

To control hunting in a polyphase motor, the circuit senses the phase difference between the line currents in the motor windings. The phase angle varies in step with the speed variation. A voltage proportional to the angle is developed by a phase detector, rectified, amplified, compared to a threshold, and applied back to the motor excitation circuit. If the correction



Hunting in a Polyphase Synchronous Motor Is Detected by sensing the phase of the current through the neutral line, relative to the phase on one of the motor windings. A similar circuit is used for a split-capacitor synchronous motor.

signal is applied as negative feedback, it suppresses hunting. In some applications, such as gyroscope motors, enhanced hunting may be needed. In those cases, positive feedback is used.

In effect, the feedback alters the motor magnetic field, which is analogous to altering the stiffness of a spring. It is not necessary to apply the feedback to all the windings of a polyphase motor; applying it to just one winding is sufficient. An analogous circuit is used for split-capacitor synchronous motors.

This work was done by Henry Packard and James Schott of Northrop Corp. for **Johnson Space Center**. For further information, Circle 3 on the TSP Request Card.
MSC-18680

Low-Resistance Continuity Tester

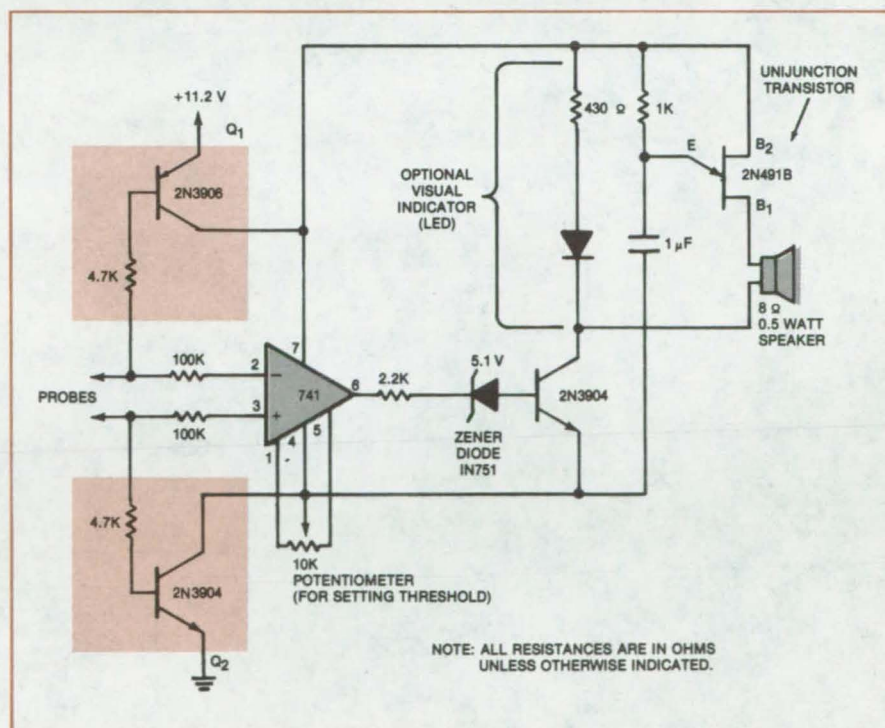
A low-current-drain continuity tester measures resistances as low as 0.1 ohm.

NASA's Jet Propulsion Laboratory, Pasadena, California

Continuity checks of integrated-circuit socket connections with their many parallel paths frequently involve measuring resistances less than 1 ohm. A tester has been devised that measures resistances as low as 0.1 ohm while using little power. The circuit utilizes the inexpensive 741 operational amplifier operating on an 11.2-volt battery.

The operational amplifier controls an audio oscillator that drives a small loudspeaker or an LED visible display for indicating continuity. The probes are applied across the path for which continuity is to be checked. A low resistance across the input probes (see figure) unbalances the operational amplifier to produce a positive output. Threshold response is set by a 10-kilohm potentiometer. When setting the desired threshold resistance by means of the 10-kilohm potentiometer, a 0.5-ohm precision resistor may be used for calibration. A Zener diode in series with the output of the operational amplifier and the base of the bipolar switch transistor prevents the oscillator from operating until the positive output of the operational amplifier has sufficient amplitude, when the probe circuit is closed.

(continued on next page)



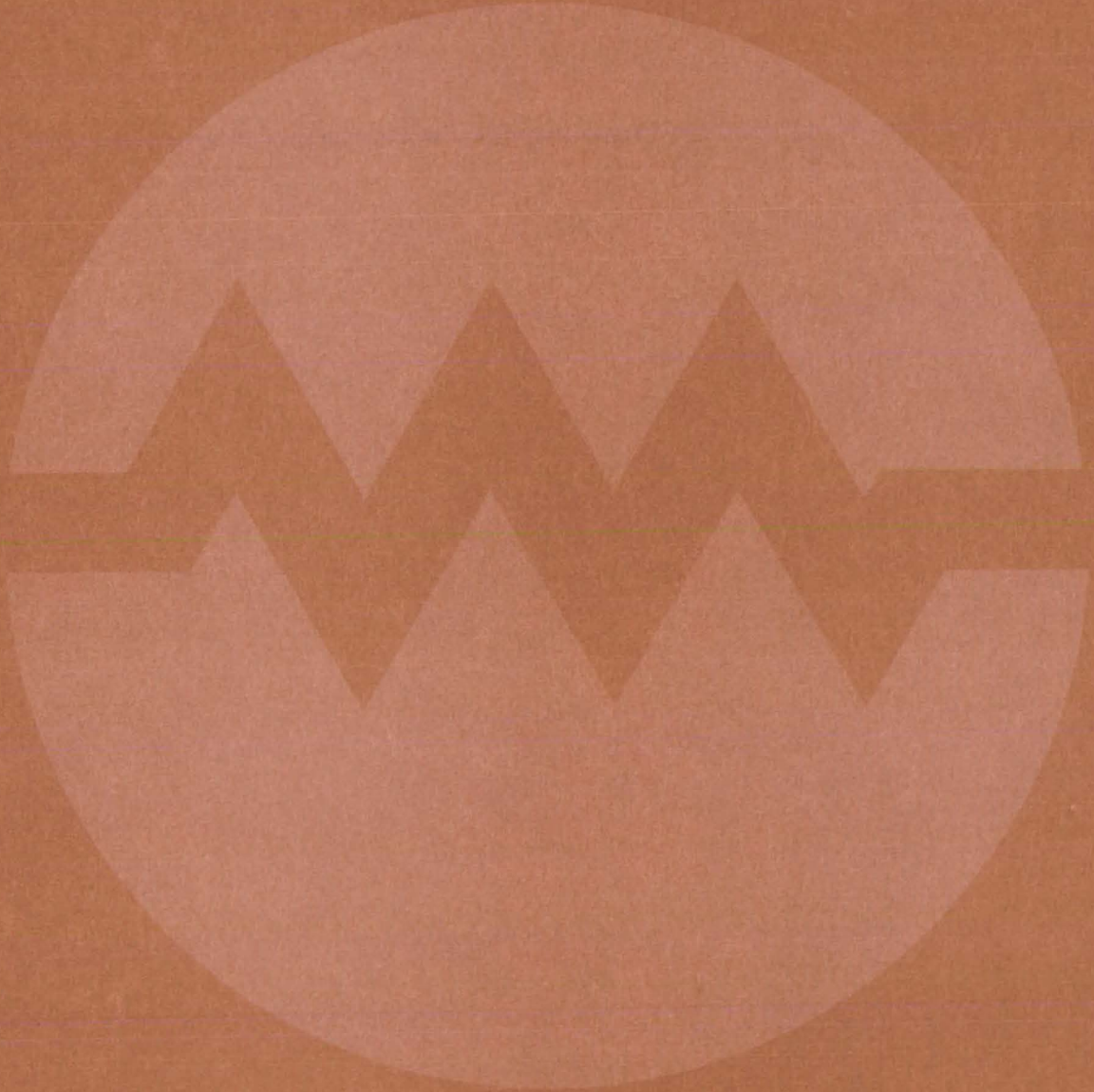
The **Low-Resistance Continuity Tester** can be used to check IC printed-circuit boards. Two 4.7-kilohm resistors and the transistors connected to them prevent current flow through the operational amplifier until the probe circuit is completed. The Zener diode in series with the operational amplifier output prevents audio oscillator operation until the positive output of the operational amplifier has sufficient amplitude.

The oscillator uses a unijunction transistor to generate an audio tone. No current is drawn by the unijunction and switch transistors until the collector of the switch transistor goes low. Transistors Q_1 and Q_2 prevent current flow through the operational amplifier

from the battery until a continuous resistance path is probed, thus eliminating the need for a power on/off switch for the device. The 741 operational amplifier may be replaced by others that operate at lower voltages.

*This work was done by Ronald B. Reasoner of Caltech for **NASA's Jet Propulsion Laboratory**. For further information, Circle 4 on the TSP Request Card.*
NPO-14881

Electronic Systems



Hardware, Techniques, and Processes

- 419 Superconducting Gyrocon Would Be Very Efficient
- 420 High-Power Dual-Directional Coupler
- 421 Cavity-Backed Spiral-Slot Antenna
- 422 Timing Signal Propagates Without Phase Shift
- 422 Trislot-Cavity Microstrip Antenna

Computer Programs

- 423 Developing Experiment Instrument Packages

Superconducting Gyrocon Would Be Very Efficient

Cryogenic operation of a gyrocon can increase gain and efficiency.

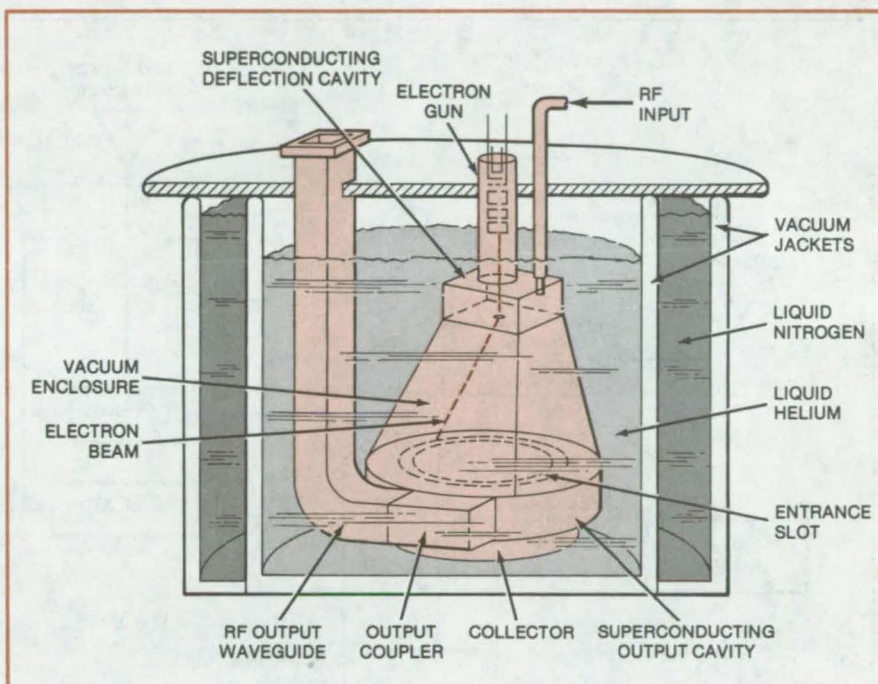
NASA's Jet Propulsion Laboratory, Pasadena, California

A theoretical analysis shows that the gyrocon can be a very efficient microwave amplifier, oscillator, or frequency multiplier when built with superconducting materials and operated at liquid-helium (4.2 K) temperature. Whereas room-temperature operation limits gyrocon gain to less than 15 dB and overall efficiency to about 80 percent despite excellent dc-to-RF conversion efficiency (at least 90 percent), superconductors would up this gain to more than 50 dB and increase the efficiency to more than 90 percent.

As shown in the figure, a gyrocon consists of five parts: the electron gun, the deflection cavity, the output cavity, the collector, and the output coupler. In the superconducting version, the cavities are made of lead or niobium, and are immersed in a cryostat. The electron gun generates a collimated electron beam that acquires very large kinetic energy from the high accelerating voltage between cathode and anode. The beam passes through the deflection cavity, where the field produced by the input RF signal causes the beam to follow an expanding helical path.

The gyrating beam traverses the output cavity through slots in the top and bottom of the cavity waveguide. The phase velocity of the waveguide field and the gyration velocity of the beam can be made to match, so that the beam experiences the same fields each time it sweeps around. The beam energy is thereby converted into waveguide-field RF energy, and the beam slows down almost to a halt. The RF power is taken out through the output coupler, and the electron beam continues on to the collector.

Performance is improved in the superconducting gyrocon because the RF surface resistance for supercon-



The **Superconducting Gyrocon** would have input and output cavities made of superconducting lead or niobium. Operation at frequencies to 50 GHz appear practical.

ducting materials is smaller than that of room-temperature copper by a factor of at least 10^4 to 10^6 , depending on the surface conditions. Thus, for the same field strength, the RF losses in a superconducting cavity are substantially reduced. Calculations using an optimized gyrocon operated at 2.45 GHz with a dc beam power of 1.809 MW show that room-temperature overall efficiency is 0.818 and RF power gain is 13.4 dB; whereas, at superconducting temperature, the overall efficiency is 0.916 and RF power gain is 53.8 dB.

Another advantage of the superconducting gyrocon is that continuous operation becomes practical at very high power levels, and the efficiency

does not suffer when the tube is operated at levels as low as 10 kW. Room-temperature gyrocons are practical only for pulsed operation and have to be operated at beam power levels near 1 MW.

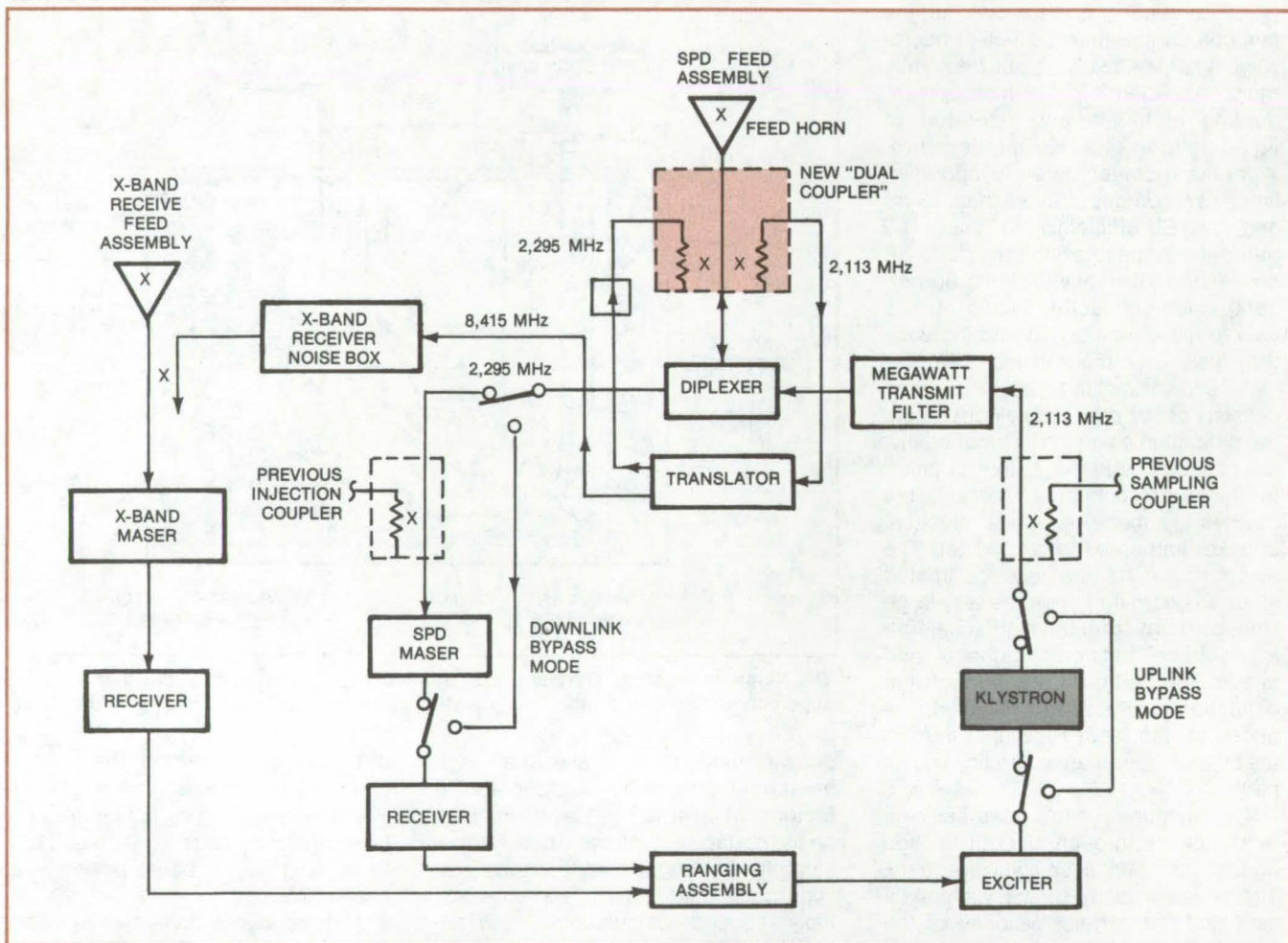
This work was done by Huan-Chun Yen of Caltech for **NASA's Jet Propulsion Laboratory**. For further information, Circle 5 on the TSP Request Card.

This invention is owned by NASA, and a patent application has been filed. Inquiries concerning nonexclusive or exclusive license for its commercial development should be addressed to the Patent Counsel, NASA Resident Office-JPL [see page A5]. Refer to NPO-14975.

High-Power Dual-Directional Coupler

A water-cooled coupler can pass 400 kW of CW microwave energy without arcing.

NASA's Jet Propulsion Laboratory, Pasadena, California



New Dual Coupler Installed in the S-band polarization diversity (SPD) cone is used in calibrating the receiving-station relay. The coupler operates successfully at 400 kW and permits accurate calibration of the entire system below the antenna feed horn.

During the Voyager near-Earth calibration sequence, the power levels received at the traveling-wave maser (TWM) inputs were high enough to saturate the ground station receivers, and the high-power uplink could have saturated the spacecraft receiver. A solution to this problem was to bypass the klystron (see figure); i.e., to use the exciter only and to bypass both the S-band and the X-band TWM's.

To calibrate the station delay for this bypass, as well as for the normal configuration, it was necessary to move the calibration sampling-injection points for the system closer to the S-band feed horn from their positions near the klystron and maser. Installa-

tion of the two existing couplers close to the feed horn was physically unfeasible, and a single compact dual coupler was therefore developed. This compact coupler was fitted with two 54-dB loop coupler modules, each only 5 cm in length, and was water-cooled. Tests showed that the coupler had good directivity, contributed less than 0.01 K to the system noise temperature, and was able to pass 400 kW of CW microwave energy without arcing.

The coupler was installed near the feed horn in the SPD (S-band polarization diversity) cone and has since been used as part of the range-delay calibration system. In the previous

configuration, some of the component delays below the feed horn had to be calculated or precalibrated before installation into the system. In the new configuration, the test translator signal is injected at a point as near the feed horn as possible, allowing a direct range-delay measurement at that point of all parts of the system below the feed horn. As a result, the system is more accurately calibrated.

This work was done by Tommy Y. Otoshi and Kenneth B. Wallace of Caltech for NASA's Jet Propulsion Laboratory. For further information, Circle 6 on the TSP Request Card. NPO-14713

Cavity-Backed Spiral-Slot Antenna

A compact, rugged, flush-mounted antenna operates in sum or difference modes with circular polarization.

Lyndon B. Johnson Space Center, Houston, Texas

A new flush-mounted antenna can be switched to give either a radiation peak or a null on the axis, with circular polarization in either case. The structure is compact and can withstand severe mechanical and thermal loads.

The radiating elements (see Figure 1) consist of two pairs of center-fed interleaved spiral slots in a conductive

plane. Each slot in each pair lies between the slots of the other pair.

The aperture plate is the top of a cavity that is a quarter-wavelength deep. At the center feedpoint of each pair of slots, a balanced feed assembly drives the slot from a split-tube coaxial balun. Both baluns extend down through the bottom of the cavity to a four-port hy-

brid; the input to the hybrid can be switched to feed the pairs of slots either in a sum mode or a difference mode (i.e., in the same phase or 90° out of phase).

The arrayed spiral-slot elements radiate circularly polarized patterns of the general shape shown in Figure 2. The sum (Σ) mode radiation pattern has a null on the axis, and the difference (Δ) mode has a pattern that peaks on the axis. The entire apparatus is reciprocal, so these patterns represent received signals as well as transmitted ones.

The length of the spiral trace of each half of a slot pair is approximately $3\frac{1}{2}$ wavelengths, which yields a relatively large bandwidth. Longer slots would afford still greater bandwidths.

This work was done by Haynes Ellis, Jr., of Rockwell International Corp. for **Johnson Space Center**. For further information, Circle 7 on the TSP Request Card.

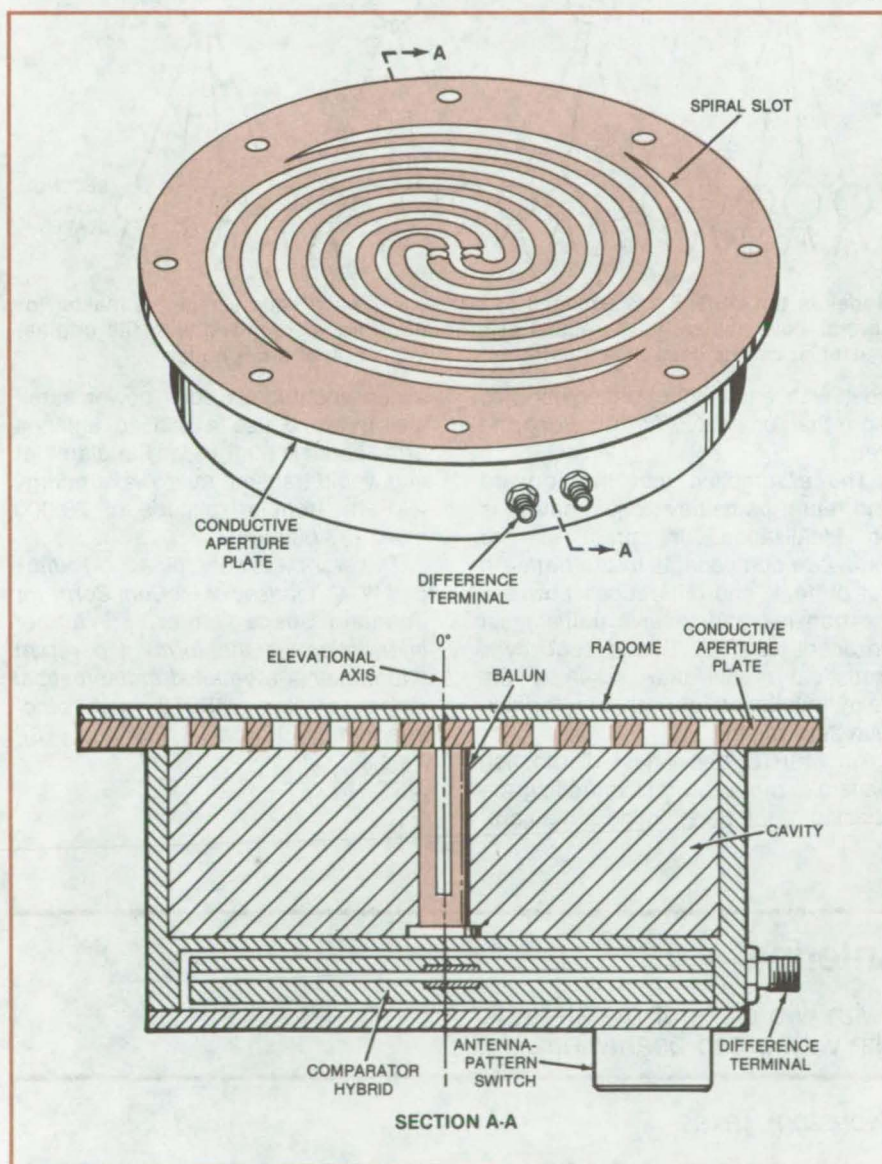


Figure 1. A Spiral-Slot Antenna consists of two pairs of center-fed interleaved spiral slots in a conductive aperture plane. At the center feedpoint of each slot pair is a balanced feed assembly. Each of these center points is fed from a split-tube coaxial balun, which passes through a cavity that is a quarter-wavelength deep. A radome covers the aperture plate.

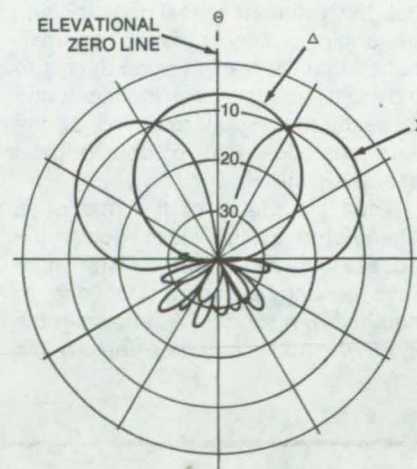


Figure 2. Radiation Patterns differ, depending on whether the antenna is in the sum (Σ) mode or the difference (Δ) mode.

This invention is owned by NASA, and a patent application has been filed. Inquiries concerning nonexclusive or exclusive license for its commercial development should be addressed to the Patent Counsel, Johnson Space Center [see page A5]. Refer to MSC-18532.

Timing Signal Propagates Without Phase Shift

Continuous monitoring of transmission delay corrects for phase shift.

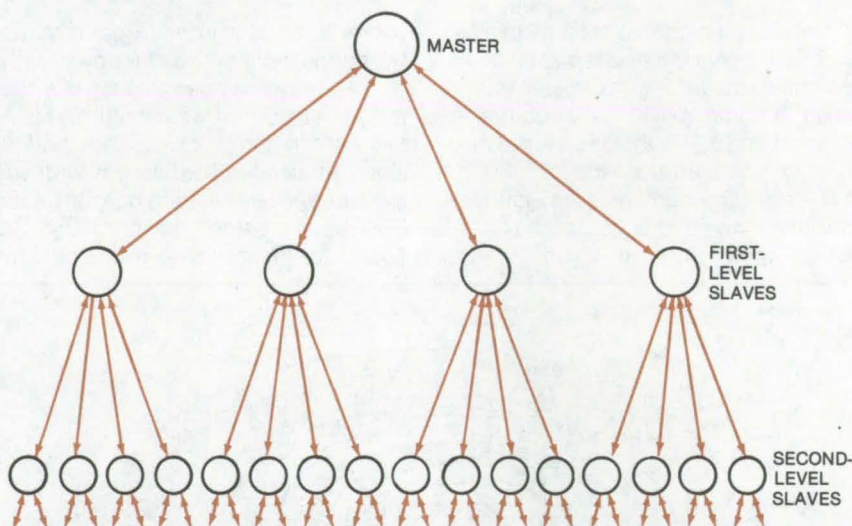
Lyndon B. Johnson Space Center, Houston, Texas

In synchronized electronic systems, such as the phased microwave antenna array a solar-power satellite would use or the accurate clock-distribution systems in avionics and computers, performance depends critically on fixing the phase relationship between system components, or nodes. To maintain synchronization, a master timing signal at a fixed phase and frequency must be available at each node.

Such a timing signal is propagated without phase shift through an array of nodes by the master/slave returnable timing system (MSRTS). The MSRTS actively compensates for phase-shift drift caused by changing transmission delay between nodes.

The basic idea of the MSRTS is to cancel the transmission delay by returning back to the master a sample of the signal received at the slave. The phase transmitted from the master is then advanced until it leads the original phase by the same amount that the returned signal lags behind the original. Then, to the approximation that the transmission delays to and from the slave are identical, the phase of the signal received at the slave matches that of the original master signal.

Since the phase of the master is regenerated at the slave node, the process can be repeated, with each slave serving as master for one or more following nodes. As shown in the figure, the nodes can be arranged in a



Nodes in the MSRTS are arranged as a tree, with each node serving as master for several slave nodes. As the signal at each slave is synchronized with the original master, it can be used as a master to synchronize other slave nodes.

tree, with each node transmitting to more than one slave further along the tree.

The assumption that the forward and return paths have equal delays is an idealization. In practice, the hardware components in the path are not perfect, and differences between the transmit and receive paths must be accounted for. This is done by a statistical model that assumes the delay imbalance is a random variable with zero mean.

An MSRTS tree phase-distribution system is proposed for controlling the phasing of the transmitting antenna of

a geosynchronous solar-power satellite. It would use a phased antenna array about 0.6 mi (1 km) in diameter and would transmit microwave energy to Earth from an altitude of 23,000 miles (37,000 km).

This work was done by A. V. Kantak and W. C. Lindsey of LinCom Corp. for Johnson Space Center. For further information, in the form of a report that presents a detailed mathematical model of the MSRTS and other information, Circle 8 on the TSP Request Card.
MSC-18777

Trislot-Cavity Microstrip Antenna

Flush-mountable assembly, made with two disks of metal-clad dielectric board, has wide bandwidth with broad beamwidth.

Lyndon B. Johnson Space Center, Houston, Texas

A simple disk radiator mounted over a conducting plane can be used as a flush-mounted microwave antenna. However, better antenna characteristics are achieved by placing another

conducting plane above the disk, connecting the top and bottom planes so that the disk is enclosed in a cavity, and cutting a Y-shaped slot in the top plane. The cavity is excited by the microwave

energy from the disk and radiates from the trislot aperture in the top plate.

The figure shows details of the trislot-cavity antenna, including the arrangement for feeding the signal to the disk.

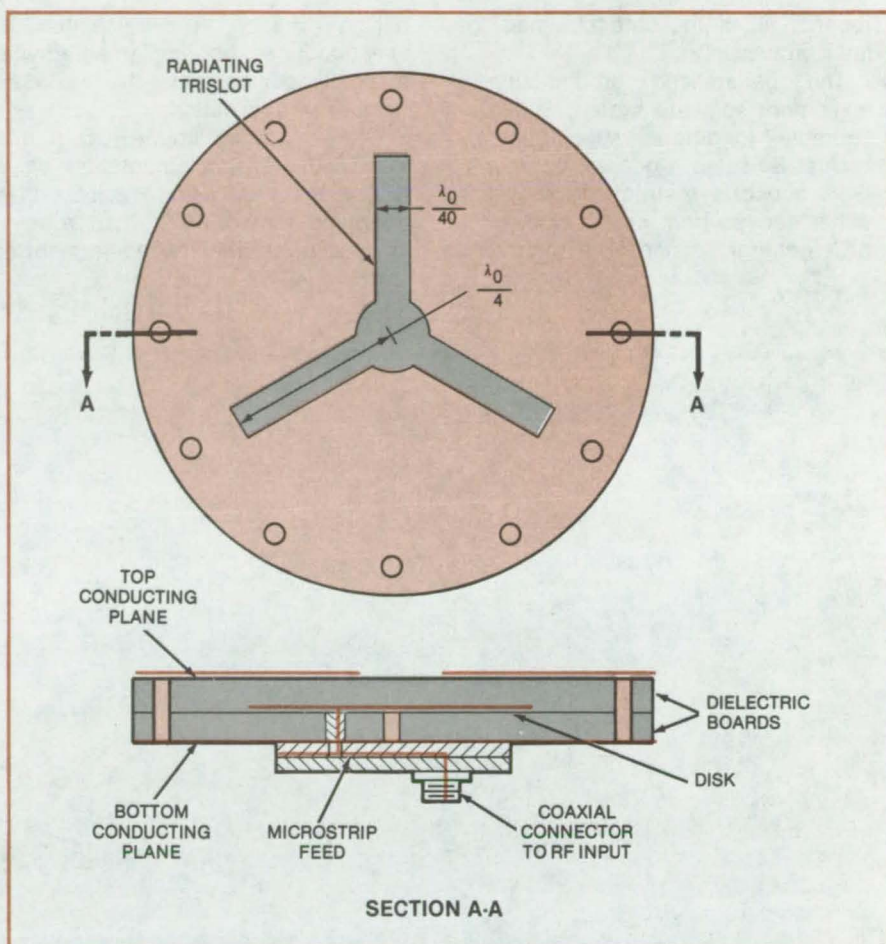
The three slots are 120° apart, are $\lambda_0/4$ long (where λ_0 is the free-space wavelength at the center frequency of the microwave signal), and are $\lambda_0/40$ wide. The conductors that pass through the dielectric boards to connect the top and bottom metal planes are spaced 30° apart, at a radius that is greater than the slot length by the thickness of the antenna.

The excitation disk has a radius of $\lambda_0/4\epsilon$; i.e., less than the slot length by a factor equal to the dielectric constant ϵ of the construction boards. A conducting post connects the center of the disk to the bottom conducting plane. Two feedpoints are located off-center and driven by a quadrature hybrid RF circuit.

The radiation bandwidth (determined by a voltage standing-wave ratio below 1.5:1) is 2 percent for the trislot-cavity arrangement as compared to 0.5 percent for an unenclosed disk. A plot of the radiation patterns for the two configurations shows a 25-percent increase in the 3-dB beamwidth of the trislot over that of the disk antenna.

This work was done by Haynes Ellis, Jr., of Rockwell International Corp. for Johnson Space Center. For further information, Circle 9 on the TSP Request Card.

Inquiries concerning rights for the commercial use of this invention should be addressed to the Patent Counsel, Johnson Space Center [see page A5]. Refer to MSC-18793.



The **Trislot-Cavity Microstrip Antenna** is made from two circular pieces of metal-clad dielectric circuit board. It is applicable to communications systems that use flat-plate antennas and gives greater bandwidths and beamwidths than simple disk antennas.

Computer Programs

These programs may be obtained at very reasonable cost from COSMIC, a facility sponsored by NASA to make new programs available to the public. For information on program price, size, and availability, circle the reference letter on the COSMIC Request Card in this issue.

Developing Experiment Instrument Packages

Software support for development, calibration, and testing of experiment packages

The GSE (ground-support equipment) system supports the development, calibration, and integration of instrument packages for scientific experiments. It can also be used for "quick-look" processing and for data analysis once the experiment is operating. The user of GSE interacts with incoming telemetry data, performs computations, and controls the execution of procedures. The procedures provide for the timely execution of commands and assure the repeatability of system actions.

Facilities to command GSE, to command the scientific instruments, and to configure the system for different operational environments are provided

through the Experiment Command Interactive Language (ECIL). ECIL is a versatile, interactive, procedural control language.

Most instruments, especially spaceborne ones, are vigorously tested to assure that their performances meet specifications. Usually they are precalibrated against known data sources. Once the instrument is calibrated, its electronics package is placed in its final enclosure and is installed at the experiment site. When the instrument is operating, its behavior under severe environmental conditions must often be analyzed quickly. These complex processes are monitored and supported by GSE, which

(continued on next page)

records all of the data obtained for later processing.

The generalized ground-support equipment software system is "configurable" for different specific instruments. By using a general approach, GSE supports instruments that are either derived from or are extensions of a general version. The overriding

design criterion in developing GSE was that it could be implemented with minimal modification for the maximum number of applications.

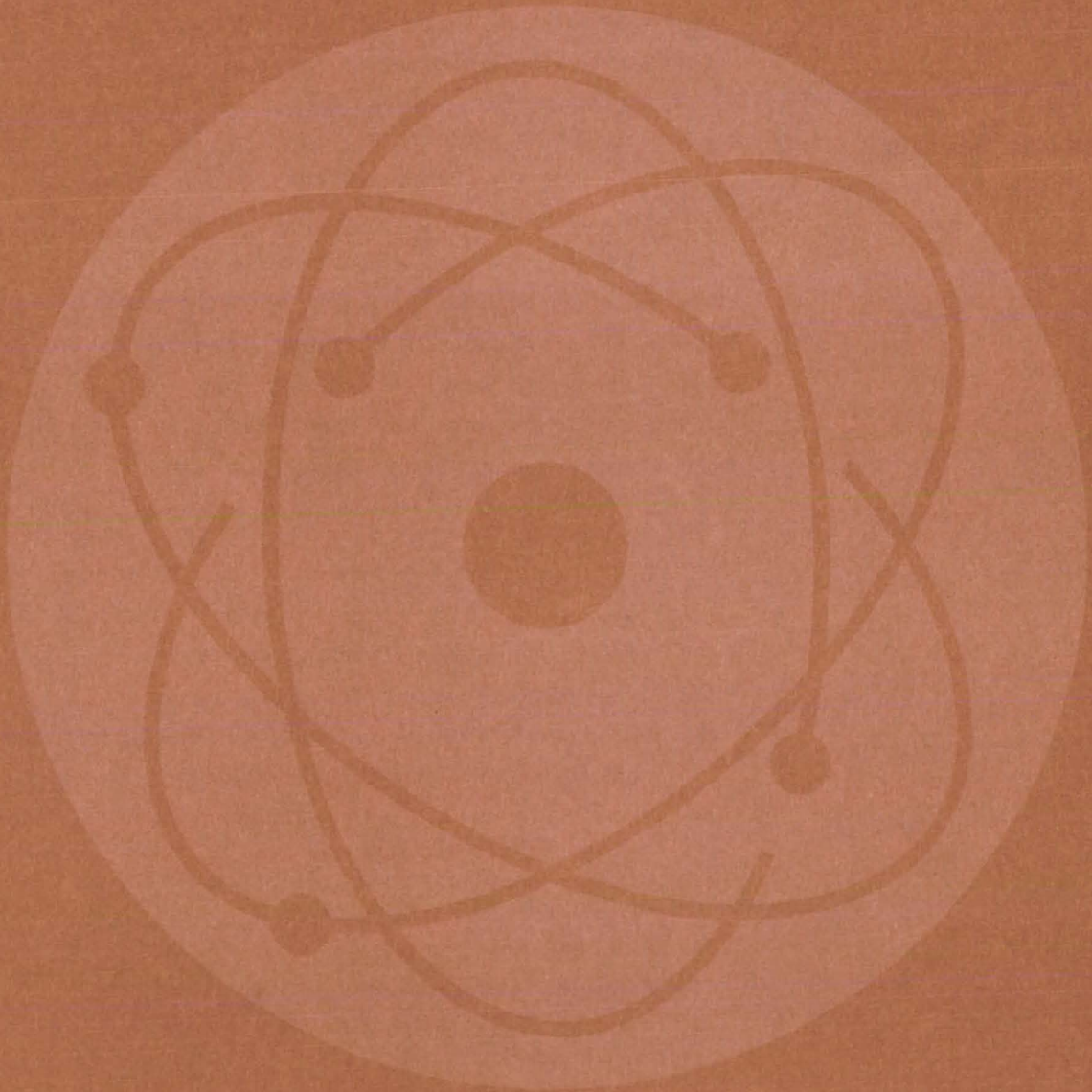
GSE is written in MARCO II and FORTRAN for implementation on a DEC PDP-11/34 using the RSX-11M operating system. GSE has a minimum central memory requirement of

approximately 42K of 16-bit words. It was developed in 1979.

*This program was written by Rodney Herreid of **Goddard Space Flight Center**. For further information, Circle A on the COSMIC Request Card.*

GSC-12536

Physical Sciences



Hardware, Techniques, and Processes

- 427 Multibeam Collimator Uses Prism Stack
- 428 Pulse-Shaping Circuit for Laser Excitation
- 429 Field Limiter for Solar Radiometer
- 430 Gas-Laser Power Monitor
- 430 Fiber Optics Transmit Clock Signal More Reliably
- 431 Reduced Viscosity Interpreted for Fluid/Gas Mixtures
- 432 Tunable Pulsed Carbon Dioxide Laser
- 433 Short-Range Self-Pulsed Optical Radar

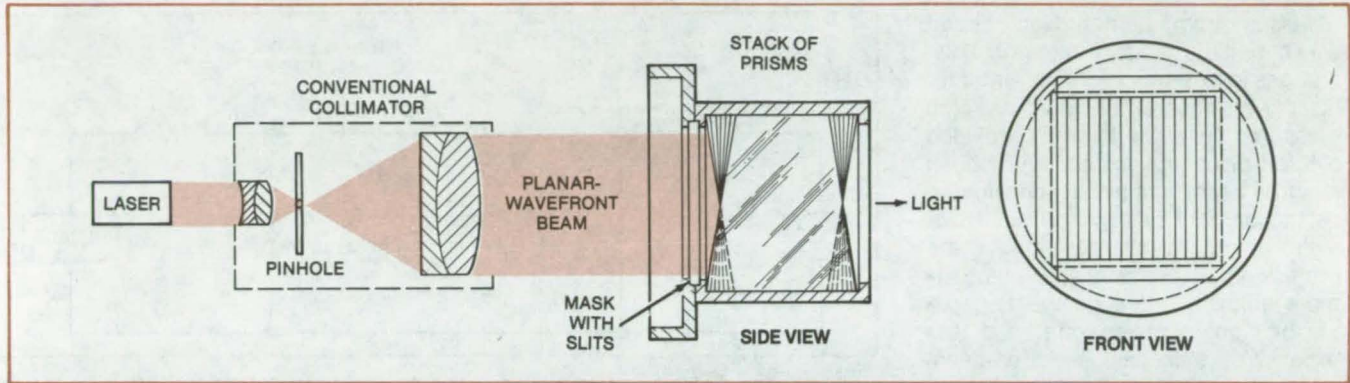
Books and Reports

- 433 Solar-Site Test Module
- 434 Evaluation of an Evacuated-Tube Liquid Solar Collector
- 434 Solar Water Heater Design Package
- 434 Five-City Economics of a Solar Hot-Water System
- 435 Economic Evaluation of a Solar Hot-Water System
- 435 Residential Solar-Heating System Uses Pyramidal Optics
- 436 Solar-Heated Bank — Marks, Mississippi
- 436 Solar Water-Heating Performance Evaluation — San Diego, California
- 436 Solar-Heated and Cooled Savings and Loan Building — Leavenworth, Kansas
- 437 Solar-Energy Landmark Building — Columbia, Missouri
- 437 Solar Heating for an Observatory — Lincoln, Nebraska
- 438 Two-Story Residence With Solar Heating — Newnan, Georgia
- 438 Solar-Energy Heats a Transportation Test Center — Pueblo, Colorado
- 438 Single-Family-Residence Solar Heating — Carlsbad, New Mexico
- 439 Multimode Solar-Heating System — Columbia, South Carolina
- 439 Solar-Heated Swimming School — Wilmington, Delaware
- 439 Winter Performance of a Domestic Solar-Heating System — Duffield, Virginia
- 440 One-Year Assessment of a Solar Space/Water Heater — Clinton, Mississippi
- 440 Fire-Station Solar-Energy System — Kansas City, Missouri
- 440 Solar-Heated Ranger Station — Glendo, Wyoming
- 441 Economic Evaluation of a Solar Hot-Water System — Palm Beach County, Florida
- 441 Residential System — Lansing, Michigan
- 442 Solar Space-Heating System — Yosemite National Park, California
- 442 Motel Solar-Hot-Water System — Dallas, Texas
- 442 Motel Solar-Hot-Water System With Nonpressurized Storage — Jacksonville, Florida
- 443 Closed-Circulation System for Motel Hot Water — Savannah, Georgia
- 443 Solar Heating for a Restaurant — North Little Rock, Arkansas
- 443 Motel Solar Hot-Water Installation — Atlanta, Georgia
- 444 Building With Integral Solar-Heat Storage — Starkville, Mississippi

Multibeam Collimator Uses Prism Stack

A stack of prisms at minimum angular deviation generates divergent light beams for surveying.

Goddard Space Flight Center, Greenbelt, Maryland



A Fanlike Stack of Prisms separates a beam of light into many beams, each having a precise directional relationship to the others. The light source, a helium/neon laser, was selected for its high intensity and the ease with which it can be collimated. A mask with aligned parallel slits is mounted at the entrance to the prism stack.

Many precisely divergent beams are created from a single laser beam by a stack of prisms in a new optical instrument. Each beam points in a slightly different direction with a precise angular relationship to the others. The multiprism collimator can be used to measure angles in surveying land and aligning machine elements.

Unlike many other devices for measuring angles, the multiprism collimator is nearly immune to vibration, changes in gravitational force, temperature variations, and mechanical distortion. It is accurate within 1 microradian in its present form, and it would be even more accurate if it were built in larger sizes.

As shown in the figure, the beam from a helium/neon laser is expanded and collimated by a conventional optical collimator. The beam is then directed onto a stack of prisms, so that each prism intercepts a different portion of the wave front. The angles of the front and rear prism faces and their refractive indices are selected to

divert the beam by a given amount, different for each prism. The angle of the emerging beam thus changes by increments from one end of the prism array to the other. For example, the direction may vary from $+7^\circ$ to -7° from one side of the array to the other, with the prisms providing 1° increments and the deviation of the center wedge being 0° .

The prisms are mounted at their positions of minimum deviation. This means that the angle of incident light is at the minimum of the deviation-vs.-incidence-angle curve. In this region, the directions of the emerging beams are least sensitive to changes in incidence angle. The accuracy of the deviation, therefore, is relatively unaffected by dimensional distortions. Mechanical motion of the collimator causes all the beams to shift in unison but does not change the angular separation between the beams.

The glass used for the prisms is selected for its low-temperature coefficient of refractive index. This property ensures that the instrument

accuracy is hardly affected by temperature changes.

In a collimator that has been built, the prisms are 4.7 mm thick and 82.5 mm wide. A stack of 15 such prisms in the mounting fixture provides a clear aperture 70.7 mm high and slightly more than 70.7 mm wide.

Prism arrays can be designed to produce various increments and ranges of deviation, since the parameters are determined chiefly by the angles of the entrance and exit faces for a given index of refraction. The important constraint is that the deviation of an individual prism should approximate the minimum deviation.

This work was done by Peter O. Minott of Goddard Space Flight Center. For further information, Circle 10 on the TSP Request Card.

This invention is owned by NASA, and a patent application has been filed. Inquiries concerning nonexclusive or exclusive license for its commercial development should be addressed to the Patent Counsel, Goddard Space Flight Center [see page A5]. Refer to GSC-12608.

Pulse-Shaping Circuit for Laser Excitation

Narrower, impedance-matched pulses would initiate stabler electric discharges for gas lasers.

NASA's Jet Propulsion Laboratory, Pasadena, California

Pulses from a proposed circuit would initiate stable electric discharges in rare-gas excitation-transfer lasers. Previously, the relatively high pressures in such lasers precluded electric-discharge excitation, and an electron beam was usually considered as the primary energy source. However, electric-discharge circuits are preferred because they are potentially more efficient, more compact, capable of high repetition rate, and less expensive than an electron-beam apparatus.

Self-sustained discharges in high-pressure rare-gas mixtures are difficult to control because the gas tends to break down and form localized arcs. In addition, high-voltage and high-energy charging circuits usually have large inductances that reduce voltage rise times below that required for optimum gas excitation.

The proposed network compresses the width of high-voltage pulses from a relatively-slow rise-time voltage generator and gradually grades the circuit impedance from the inherent high impedance of the generator to the low impedance of the gas.

As shown in the block diagram (Figure 1), the network consists of two saturable inductor switches, each with a distributed-capacitance energy-storage device at its input. Each inductance switch has a core formed of nonmagnetic material with a laminate wrapped around it. The laminate is formed of a thin layer of high-permeability material ($>2,000\mu_0$) deposited on a flexible backing. Possible energy-storage devices are coaxial cables, multiple coaxial cables, or parallel-plate transmission lines.

The output from the primary voltage source as shown in Figure 2(a) is a

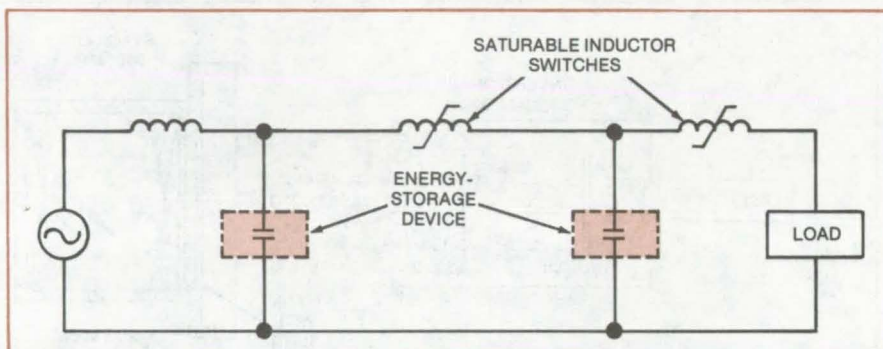


Figure 1. The **Pulse-Forming Network** was developed to deliver excitation pulses to a high-pressure rare-gas laser. The proposed circuit would generate pulses greater than 100 kilovolts, having energies of the order of hundreds of joules. Pulse durations would be less than 100 nanoseconds and rise times on the order of a few nanoseconds. Output impedance would be $1.0\ \Omega$ or less.

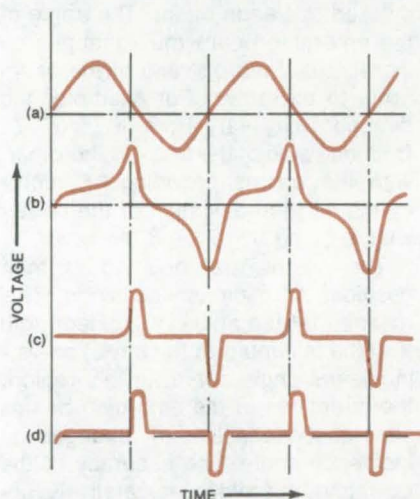


Figure 2. The **Change in the Waveform** as it passes through the circuit of Figure 1 is shown here.

sinusoidal wave that is slightly compressed, as in (b), prior to the time of switch saturation. When the first inductor switch saturates, the energy stored in the first distributed-capacitance storage device is transferred to

the second distributed-capacitance energy-storage device as shown in waveform (c). As this occurs, the second inductor switch saturates, impressing a highly compressed voltage, shown in waveform (d), across the load.

The high-permeability material wound on the saturable inductor switch core has a thickness within an order of magnitude of the skin depth at a frequency corresponding to a desired rise time of the output pulse. For a 10-nanosecond-rise-time pulse-shaping network, the skin depth would be on the order of 1 to 2 microns.

This work was done by James B. Laudenslager and Thomas J. Pacala of Caltech for **NASA's Jet Propulsion Laboratory**. For further information, Circle 11 on the TSP Request Card.

This invention is owned by NASA, and a patent application has been filed. Inquiries concerning nonexclusive or exclusive license for its commercial development should be addressed to the Patent Counsel, NASA Resident Office-JPL [see page A5]. Refer to NPO-14556.

Field Limiter for Solar Radiometer

Lenses project the solar image onto an aperture to exclude circumsolar radiation.

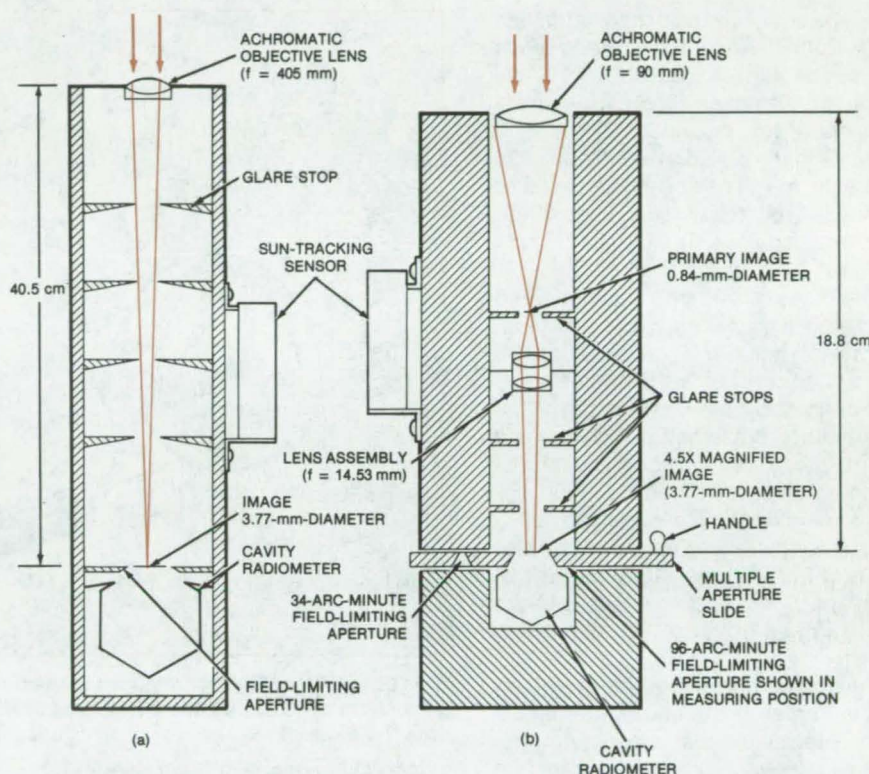
NASA's Jet Propulsion Laboratory, Pasadena, California

Two proposed field limiters for controlling the acceptance angle of a solar radiometer or pyrheliometer are shown in the figure. The units accept radiation strictly from the solar disk, eliminating circumsolar radiation (radiation scattered by dust and the atmosphere). By eliminating the circumsolar inputs, more-precise measurements can be made of energy captured by the receiver apertures of highly-concentrating solar thermal-energy converters.

Version (a) field limiter, 16 in. (41 cm) long, uses an achromatic objective lens (similar to those used in small refractor telescopes) to form an image of the Sun at an aperture just ahead of the radiometer cavity. Version (b) is shorter, 7.4 in. (18.8 cm), and hence more convenient. Its shorter-focal-length achromatic objective forms a smaller image that is magnified by another lens and imaged onto an aperture.

The diameter of the image at the aperture (3.8 mm) is the same in both versions. Aperture diameter determines the instrument acceptance angle; i.e., the aperture is a field stop. An aperture the same diameter as the solar image would prevent circumsolar radiation from entering the radiometer cavity.

Concentrating or focusing solar-energy collectors form an image of the Sun on the collecting element. The Sun subtends an angle of 32 arc minutes. Practical solar collectors accept radiation from a somewhat larger angle to avoid having the intense solar image fall on anything but the collector element. The angle required depends on collector aiming accuracy and image definition.



The **Cavity Radiometer Field Limiters** are designed for use with a standard 5°-field-angle radiometer with a cavity aperture 0.44 inch (1.13 cm) in diameter. The drawings are not to scale. Both radiometers give the same size image and have the same cavity sizes. The lengths, though, are different.

A collector performance evaluation requires accurate radiation measurements with the same acceptance angle as the collector. Measurements of radiation from the solar disk alone are also needed for comparison. Either type of measurement can be made by placing an aperture of the proper diameter in the field limiter.

Either version of the field limiter would require calibration against a

standard radiometer because reflection and absorption losses in the lenses prevent accurate sensitivity calculations from geometry alone. A solar-tracking mount keeps the Sun image centered on the field-limiting aperture.

This work was done by C. Martin Berdahl of Caltech for NASA's Jet Propulsion Laboratory. For further information, Circle 12 on the TSP Request Card.
NPO-14781

Gas-Laser Power Monitor

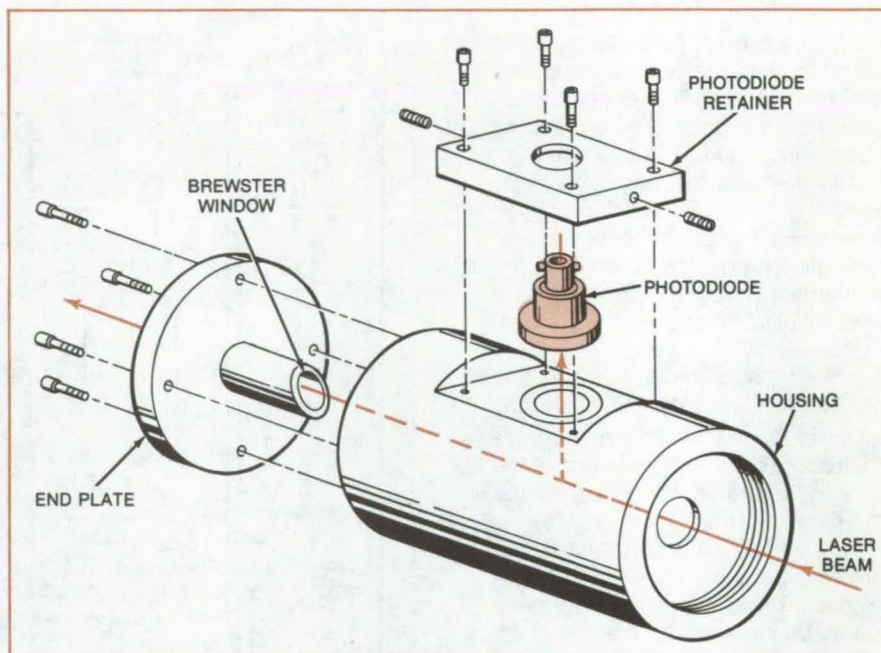
Power output is continuously monitored while the laser is in use.

Langley Research Center, Hampton, Virginia

A gas-laser power monitor attaches to the front of a laser housing and reads the power output continuously while the laser is in use. Although originally developed for one commercial gas laser (Coherent Radiation, Model 53), the basic design can be applied to other lasers as well. No modifications to the laser are required. The monitor simply attaches to the laser end cap.

The new power monitor is fabricated from four black-anodized aluminum parts (see figure). A piece of crown glass positioned at the Brewster angle (determined by the wavelength of the laser) reflects a small fraction of the beam into a photodiode. The photodiode is calibrated for an electrical output proportional to the laser power in watts. Using crown glass at a Brewster angle of $56^{\circ}41'$, calculated for a wavelength of $5,145 \text{ \AA}$, the reflected beam is only 0.33 percent of the total beam power.

Previously, power was measured by a calorimeter at the end of the optical path. However, the calorimeter response time was slow, and the system was susceptible to optical misalignment. The built-in power monitor does not interrupt the laser beam, as did the calorimeter; and the diode has much faster response, allowing instantaneous



This **Laser Power Monitor** attaches to the front end cap of a high-power gas laser. Only a small fraction (0.33 percent) of the total beam power is diverted by the Brewster window into the photodiode.

ous tracking of power fluctuations. The monitor can be calibrated to read either the total power output of the laser or the power generated in a test volume, making it more convenient for data reductions.

This work was done by Courtney E. Russ, Jr., of Langley Research Center. No further documentation is available. LAR-12682

Fiber Optics Transmit Clock Signal More Reliably

Optical automatic gain control smooths maser clock amplitude fluctuations without introducing phase shift.

NASA's Jet Propulsion Laboratory, Pasadena, California

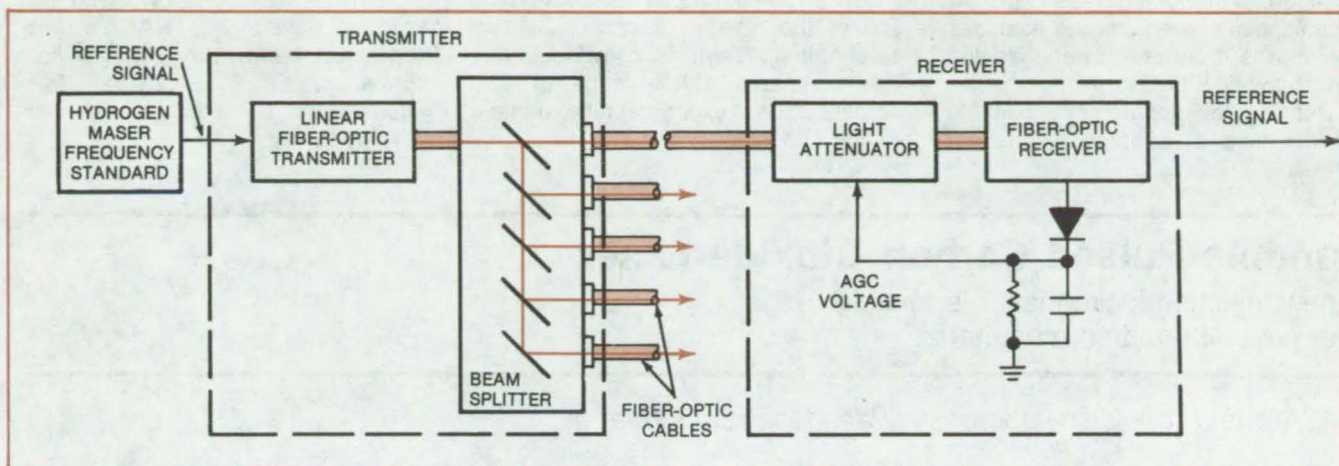
A proposed fiber-optic system would distribute a precise reference signal from a hydrogen maser frequency standard over 1 kilometer. The signal is propagated with near-zero phase shift as a function of automatic gain control (AGC) and with constant amplitude. The optical system, developed for the Deep Space Station complex to deliver reference signals to

receiver and signal-processing equipment, is less complex and more reliable than electrical transmission circuits, which introduce phase shifts as a function of attenuation and require compensating phase-locked loops.

The maser, as shown in the block diagram, feeds the reference signal to a linear fiber-optic analog transmitter

that emits a modulated laser beam, which is directed to an optical beam splitter. The beam splitter consists of dichroic mirrors and associated lenses for distributing the beam to several output ports. Fiber-optic cables attached to each port then guide the signals to the receiving station.

The cables up to 1 km long are terminated in a closed-loop automatic-gain-



The **Fiber-Optic Clock-Signal Distribution System** can use plastic fiber if the transmitter selected emits visible light. Infrared transmitters are also available. The light attenuator in the receiver is controlled by an AGC signal obtained by rectifying the clock-signal output of the fiber-optic receiver.

controlled fiber-optic receiver utilizing a light attenuator, such as a Kerr cell (or a servo with a tapered opacity disk), that varies the transmitted light amplitude in response to a dc variable voltage.

The variable optical output of the attenuator is applied to the receiver. A part of the receiver output is rectified

by an additional diode circuit furnishing dc to the light attenuator for automatic gain control. This AGC maintains the output amplitude at the level required for further processing.

This work was done by George F. Lutes, Jr., of Caltech for **NASA's Jet Propulsion Laboratory**. For further information, Circle 13 on the TSP Request Card.

This invention is owned by NASA, and a patent application has been filed. Inquiries concerning nonexclusive or exclusive license for its commercial development should be addressed to the Patent Counsel, NASA Resident Office/JPL [see page A5]. Refer to NPO-14749.



Reduced Viscosity Interpreted for Fluid/Gas Mixtures

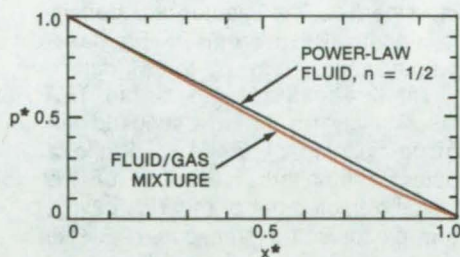
An analysis predicts the decrease in fluid viscosity with gas admixture.

NASA's Jet Propulsion Laboratory, Pasadena, California

A theoretical analysis predicts the observed decrease in viscosity of a non-Newtonian fluid when the fluid is mixed with a gas. The understanding of this effect can assist in the design of flow systems for petroleum, coal, chain, polymers, paints, food products, and other materials.

In the analysis, the fluid is taken to be viscous, non-Newtonian, and incompressible; the gas, to be an ideal gas; and the flow, to be inertia-free, isothermal, and one-dimensional. The gas is assumed to be homogeneously dispersed as bubbles in the fluid as the mixture flows in a tube of constant radius. Surface tension is neglected.

The problem is formulated by introducing the equation of state of the



The Pressure Profile of a Fluid/Gas Mixture is compared with that of a power-law fluid; p^* is the normalized pressure p/p_0 , and x^* is the normalized axial distance x/L , where p_0 is the reservoir pressure and L is the tube length.

gas, equations of conservation of mass and momentum, and a relationship between the wall shear stress and the fluid/gas velocity. Combining these equations yields a differential equation for the pressure. The exponent n in a relationship between the fluid viscosity and the shear rate is taken to be $1/2$, a value typical of polyethylene plastics. When the boundary-value pressures are imposed, discrete solutions are obtained for the axial pressure, velocity, density, volumetric flow rate, and shear-stress profiles.

Values of typical constants for low-density polyethylene are chosen for a representative calculation. The predicted pressure profile is compared in

the figure to that of a gas-free fluid. At the midpoint of the tube, the fluid/gas pressure is 8 percent lower than the power-law fluid pressure.

Defining the apparent viscosity to be the ratio of average wall shear

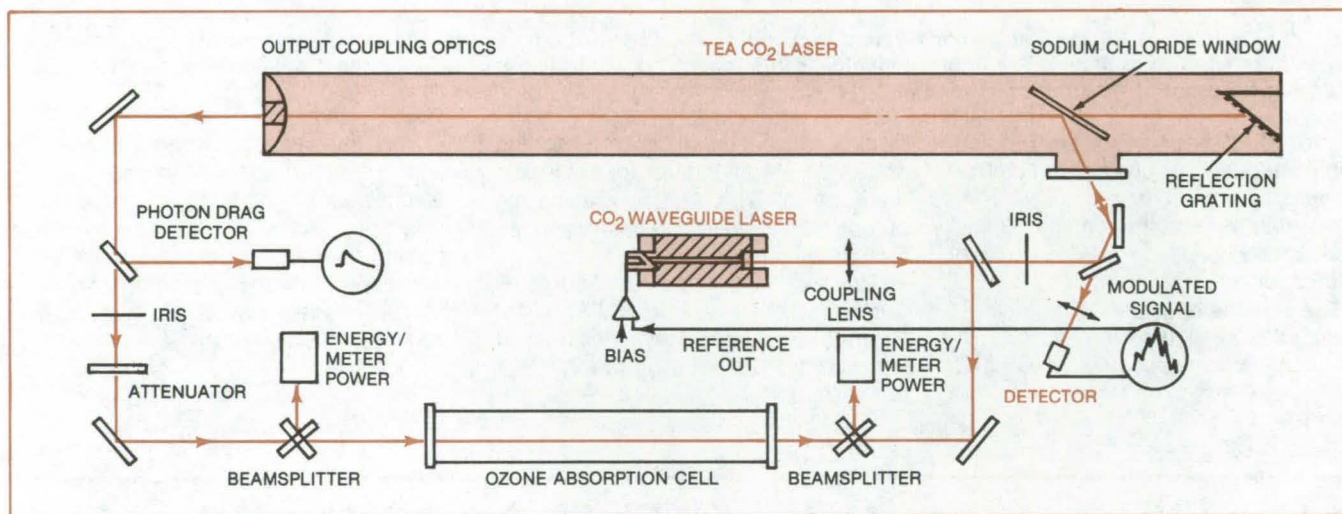
stress to shear rate at the reservoir end of the tube, a decrease of 16 percent in apparent viscosity is found. This compares with a value of 22 percent found experimentally under similar conditions.

This work was done by David H. Lewis of Caltech for **NASA's Jet Propulsion Laboratory**. For further information, Circle 55 on the TSP Request Card.
NPO-14976

Tunable Pulsed Carbon Dioxide Laser

A new injection-locked laser is tunable over several hundred megahertz.

NASA's Jet Propulsion Laboratory, Pasadena, California



A **Tunable Laser** is used to measure an absorption line of ozone. The beam splitters at either end of the absorption cell are in one orientation for the observation of waveguide laser absorption and are in the orthogonal orientation for observation of the pulsed TEA-laser absorption.

A transverse electrically-excited-atmosphere (TEA) laser is continuously tunable over more than 300 MHz about the centers of various spectral lines of CO₂. It is operated in a single longitudinal mode (SLM) by injection of the beam from a continuous-wave, tunable-waveguide CO₂ laser, which serves as a master frequency-control oscillator.

The laser is diagramed in the figure. A diffraction grating in the CO₂ waveguide laser selects the spectral line of interest. A piezoelectric transducer varies the cavity length of the waveguide laser to tune it within its pressure-dependent gain bandwidth. Average continuous-wave output power is typically around 300 mW. The

beam passes through a collimating lens and enters the TEA laser cavity by partial reflection from a sodium chloride flat. The injected flux density is about 60 mW/cm². TEA laser output ranges from 0.2 to 0.6 joule.

The 2.3-meter length of the TEA laser cavity results in a longitudinal-mode spacing of 65 MHz. While a detector monitors a portion of the signal reflected out of the TEA cavity, the piezoelectric transducer in the waveguide-laser cavity is adjusted for maximum detected signal, thus matching the two cavity resonances.

The output of the TEA CO₂ laser can be scanned across absorption features of molecules in the 9- to 12-micron spectral region. For example,

it has been used to record absorption about the 9.488-micron line of ozone. With improvements in frequency control of the TEA cavity and in the waveguide tuning range, the new laser could be used to monitor atmospheric trace species.

This work was done by Gerard J. Megie and Robert T. Menzies of Caltech for **NASA's Jet Propulsion Laboratory**. For further information, Circle 14 on the TSP Request Card.

This invention is owned by NASA, and a patent application has been filed. Inquiries concerning nonexclusive or exclusive license for its commercial development should be addressed to the Patent Counsel, NASA Resident Office-JPL [see page A5]. Refer to NPO-14984.

Short-Range Self-Pulsed Optical Radar

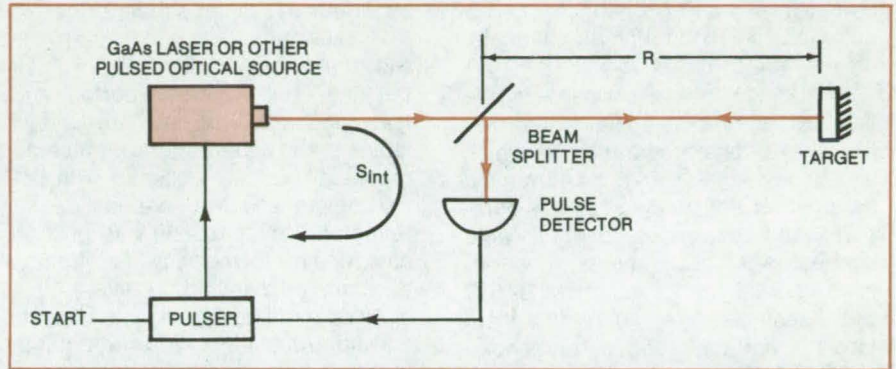
Distances up to 500 m are accurately measured.

NASA's Jet Propulsion Laboratory, Pasadena, California

A short-range optical radar uses a laser pulse that is sent out and reflected back by the target; the reflected pulse triggers the next pulse, which in turn triggers another pulse, and so on. The target range is computed from the number of pulses triggered in a precise period of time, say 1 second.

Typical optical radar for measuring longer distances determines range by measuring the time of flight of a single pulse. The new radar, shown in the figure, would accurately measure distances up to about 500 m. It could be used for measuring the surface shape of reflectors in large, high-gain, highly directional antennas and for other short-range surveying.

For a typical target range, say 150 m, the range-measurement accuracy of the new optical radar can be estimated as follows: Knowing the speed of light, (3×10^8 m/s), the range R of 150 m (pulse round-trip distance 300 m) would produce a pulse frequency $f = c/2R = 10^6$ Hz. If the frequency is measured by counting pulses for 1 second and the count is accurate to 1 pulse, the frequency — and hence the range — will be known to an accuracy of 1 part in 10^6 . For a range of 150 m, the range error would be 0.15 mm. The accuracy of the frequency-measuring equipment sets



The **Laser for an Optical Radar** is retrIGGERED when the previous laser pulse is reflected back from the target. The target range R is computed from the number of pulses triggered in a time interval.

an ultimate limit on how well the range is measured.

The distance determined from the frequency measurement includes not only the external distance $2R$ covered by the pulse but an effective internal distance S_{int} due to pulse travel and propagation delay inside the radar. The true range R is therefore

$$R = \frac{c}{2f} - S_{int}$$

The internal range S_{int} can be determined by rotating the beam splitter through 90° so that it reflects the laser pulse directly to the detector. In effect, this sets R to zero. The value of S_{int} can be determined from the

resulting pulse frequency f_{int} ; i.e., $S_{int} = c/2f_{int}$.

This setup may overtax the laser or may produce a frequency that is inconvenient to measure. This can be dealt with by introducing a known delay into the system and modifying the range relation accordingly. Otherwise, S_{int} could be determined by measuring the frequency for an accurately known range and solving the range relation for S_{int} .

This work was done by C. Martin Berdahl of Caltech for NASA's Jet Propulsion Laboratory. For further information, Circle 15 on the TSP Request Card. NPO-14901

Books and Reports

These reports, studies, and handbooks are available from NASA as Technical Support Packages (TSP's) when a Request Card number is cited; otherwise they are available from the National Technical Information Service.

Solar-Site Test Module

Small test set interrogates solar-energy data-acquisition systems.

A 32-page report describes a portable test module used for onsite checkout of DOE/NASA solar-energy demonstration installations. Although the report and the module are specific to the DOE/NASA application, the report nonetheless contains some general information and ideas that may assist engineers and others designing similar units.

A commercial portable microcomputer is the basic hardware of the test module. It is custom programmed to monitor the status of an operating solar-energy installation. The site is

fully instrumented with temperature sensors, flow-rate monitors, and other transducers; and data are collected and stored by an instrument called the SDAS (site data acquisition system). The portable unit interfaces with the SDAS.

The test unit consists of a microcomputer with keyboard, alphanumeric display, and printer; a cassette recorder/player for storing programs and data; and a cable for connecting to the SDAS. It weighs only about 10 lb (4.5 kg), including integral power supply and carrying case.

(continued on next page)

The unit is operated by a taped program written in BASIC (for ease of communication with the trouble shooter) and Assembly language (for speed of communication with the SDAS). The program gives the troubleshooter the option of (1) manually monitoring any sensor channel; (2) periodically and automatically monitoring from 1 to 10 channels; or (3) automatically monitoring all channels, either once or repeatedly.

In addition to a description of the test unit, the report contains information on site-data preparation (in which sensor channels and performance parameters are defined for the computer) and appendixes covering cable connector-pin assignments, descriptions and listings for both the BASIC and Assembler programs, data-input formats, and operating instructions.

This work was done by Ralph R. Kissel and Donald R. Scott of Marshall Space Flight Center. Further information may be found in DOE/NASA TM-78291 [N80-30899/NSP], "Solar Site Test Module" [\$6]. A paper copy may be purchased [prepayment required] from the National Technical Information Service, Springfield, Virginia 22161. The report is also available on microfiche at no charge. To obtain a microfiche copy, Circle 16 on the TSP Request Card.

MFS-25543

Evaluation of an Evacuated-Tube Liquid Solar Collector

Indoor and outdoor thermal performances are compared.

The thermal performance of an evacuated-tube solar collector described in several previous NASA Tech Brief articles [see for example "Indoor Tests of the Concentric-Tube Solar Collector" (MFS-25390) on page 39 of Vol. 5, No. 1] is documented in a 42-page report. Tests were conducted outdoors and indoors, on an indoor solar simulator, and data were obtained for diffuse and specular reflectors.

The evacuated-tube collector uses water or water/glycol as the working fluid. Liquid flows in series through the 24 evacuated tubes (concentric glass tubes with an evacuated space

between the cylinders) and the collector manifold. The external dimensions of the collector are 4 by 8 ft (1.2 by 2.4 m). The tubes are 44 in. (112 cm) in length and 2 in. (5 cm) in diameter. When filled with approximately 9 gallons (34 liters) of water, the unit weighs 185 lb (84 hg).

Excellent correlation was found between the solar-simulator-derived test results and the outdoor test results with the collector mounted on a Sun-tracking table. Thermal performance test conditions and data are listed in tables in the report and are presented graphically for the collector with both the diffuse and the shaped specular reflectors. Comparisons with previous data for a prototype show the effects of an improved manifold.

All-day efficiency of the collector and time constants were determined. Incident-angle-modifier tests were made for angles of 0°, 10°, 20°, 30°, 40°, 50°, and 60° from normal to the collector surface. All-day efficiency with a diffuse reflector was comparable to the performance with the standard shaped specular reflector.

This work was done by the Solar Energy Systems Division of Wyle Laboratories for Marshall Space Flight Center. Further information may be found in DOE/NASA CR-161421 [N80-24745/NSP], "Comparison of Indoor-Outdoor Thermal Performance for the Sunpak Evacuated Tube Liquid Collector" [\$6]. A paper copy may be purchased [prepayment required] from the National Technical Information Service, Springfield, Virginia 22161. The report is also available on microfiche at no charge. To obtain a microfiche copy, Circle 17 on the TSP Request Card.

MFS-25450

Solar Water Heater Design Package

Documentation for preliminary design review

A 112-page design package contains documents pertaining to the preliminary design of a commercial domestic-hot-water heater. The system has roof- or rack-mounted solar collectors. It is adaptable to specific needs and may be installed in a new dwelling or fitted to an existing gas or

electric hot-water system. Two systems are currently being installed: one in Tempe, Arizona, and the other in San Diego, California.

Each collector (a system may have more than one) weighs 100 lb (45.5 kg) when filled with water. System elements include a storage tank of 50 to 120 gallons (190 to 450 liters), an automatic control system, a pump, cascade (two-position diverter) valves, and associated plumbing. Automatic circulation of stored hot water and an automatic "dump" insure protection against freezing.

The design package includes:

- A list of drawings of system configurations, elements, parts, and installation methods;
- A description of the automatic control logic;
- Definitions of measurements that will be used to evaluate system performance;
- A description of proposed changes in the initial design;
- A list of materials in contact with potable water;
- A list of special tools for handling, installation, and maintenance;
- A manual for installation, operation, and maintenance; and
- An analysis of hazards from pressure, electricity, toxicity, flammability, gas, and hot water or steam.

This work was done by Elcam, Inc., for Marshall Space Flight Center. Further information may be found in DOE/NASA CR-150605 [N80-27518/NSP], "Preliminary Design Package for Sunspot Domestic Hot Water Heating System" [\$9]. A paper copy may be purchased [prepayment required] from the National Technical Information Service, Springfield, Virginia 22161. The report is also available on microfiche at no charge. To obtain a microfiche copy, Circle 18 on the TSP Request Card.

MFS-25521

Five-City Economics of a Solar Hot-Water System

Energy savings and system costs are projected for five sites.

An analysis based on technical and economic models for a solar-energy, domestic hot-water (DHW) system for

single-family residences at five sites provides such data as estimated year of payback and cumulative savings for replacing a conventional hot-water system with the solar-energy system. The system was actually installed at a site in Togus, Maine. Alternative parameters were evaluated for Albuquerque, Fort Worth, Madison (Wisconsin), and Washington, D.C. System design variables were derived from operation of the system at Togus.

Water is heated by circulating a silicone fluid through a flat-plate solar-collector array. The fluid then circulates through a double-walled heat exchanger, which transfers solar energy to water from a 120-gallon (454-liter) preheat tank. This tank services a standard electric DHW heater. One operating mode is used: The system turns on when the collector outlet temperature climbs 25° F (14° C) above the temperature of the water in the bottom of the preheat tank; it turns off when this difference falls below 8° F (4° C).

The solar-heating system can supply approximately 75 percent of the domestic hot water needed for a single-family residence in Togus, Maine. The economic payback period for the system at this site is estimated at 19 years.

Economic benefits from this solar-energy system depend primarily on two factors: the maintenance or decrease of the initial investment required and the continuing increase in the cost of conventional energy. The report includes an economic uncertainty analysis that weighs, for all 5 sites, the effect of uncertainty on the 15 variables used to evaluate profitability in the use of the solar-energy system.

This work was done by the Federal Systems Division of IBM Corp. for Marshall Space Flight Center. Further information may be found in DOE/NASA CR-161510 [N80-29854/NSP], "Solar Energy System Economic Evaluation — Final Report for IBM System 2, Togus, Maine" [\$8]. A paper copy may be purchased [prepayment required] from the National Technical Information Service, Springfield, Virginia 22161. The report is also available on microfiche at no charge. To obtain a microfiche copy, Circle 19 on the TSP Request Card.

MFS-25532

Economic Evaluation of a Solar Hot-Water System

An analysis shows economic benefits at six representative sites.

A 103-page report presents the economic analysis of a solar-energy, domestic-hot-water system for six sites that are representative of a wide range of environmental and economic conditions in the continental United States. The two-tank cascade system with a flat-plate collector array, was installed at locations in Tempe, Arizona, and San Diego, California. Projected performances based on available environmental and economic data are forecast for Albuquerque, New Mexico, Fort Worth, Texas, Madison, Wisconsin, and Washington, D.C.

The report can be used to estimate the economic performance of the system for other parts of the country. For example, if it is noted that the environmental parameters of a locale are similar to those of Fort Worth, but that the conventional-energy cost is different, the savings can be scaled accordingly.

The four-mode solar-energy system that heats water for a single-family residence. Water is pumped directly from either the domestic-hot-water tank or the storage tank, through the collectors, and back into the same tank. Also included are freeze protection and auxiliary electrical heating.

Life-cycle costs, including hardware, installation, maintenance, and operating costs, are compared to net energy savings. The model for each site includes variables for long-term average environmental conditions, loads, fuel costs, and other economic factors. Federal tax credits for solar-energy systems and an economic uncertainty analysis are included. The year in which the installation begins to yield positive yearly savings and the year when cumulative savings will have paid back the original investment in the solar system are calculated.

This work was done by the Federal Systems Division of IBM Corp. for Marshall Space Flight Center. Further information may be found in DOE/NASA CR-161492 [N80-31872/NSP], "Solar Energy System Economic Evaluation —

Final Report for Elcam-Tempe, Tempe, Arizona, and Elcam-San Diego, San Diego, California" [\$9]. A paper copy may be purchased [prepayment required] from the National Technical Information Service, Springfield, Virginia 22161. The report is also available on microfiche at no charge. To obtain a microfiche copy, Circle 20 on the TSP Request Card.

MFS-25529

Residential Solar-Heating System Uses Pyramidal Optics

Reflective panels optimize solar-energy collection throughout the year.

A new report describes the operation, installation, and maintenance of a residential solar space-heating and domestic-hot-water system that features pyramidal optics for solar-energy collection. Subsystems include collection, storage, distribution, and control. Required construction and the proper sequence of installation are detailed in the report.

The solar-energy-collecting subsystem uses a partially variable reflector to optimize energy collection annually as the solar altitude changes. Weekly adjustments are made by motor in a moving reflector that concentrates light on a glazed absorber panel; heat is transferred to liquid flowing through the panel. The combination of fixed reflectors and the moving reflector varies the net optical gain, from 3.0 in the winter down to 1.0 in the summer. The entire collector subsystem is fitted into an attic.

Solar-heated fluid flows from the collector panel through a water tank where energy is transferred to storage. Heat exchangers for hot-water preheating and space heating are located in the storage tank. A temperature-differential controller selects among four modes of operation: direct solar heat, solar heat augmented by a heat pump, outside air heated by the same heat pump, and electrical-resistance heat. The pyramidal-optics solar-energy system can heat single-family and multifamily dwellings.



This work was done by Wormser Scientific Corp. for **Marshall Space Flight Center**. Further information may be found in DOE/NASA CR-161203 [N80-33864/NSP], "Installation, Operation, and Maintenance for the Pyramidal Optics Solar System Installed at Yacht Cove, Columbia, South Carolina" [\$9]. A paper copy may be purchased [prepayment required] from the National Technical Information Service, Springfield, Virginia 22161. The report is also available on microfiche at no charge. To obtain a microfiche copy, Circle 21 on the TSP Request Card. MFS-25567

Solar-Heated Bank — Marks, Mississippi

Air solar-energy collectors supply 60 percent of the space-heating load.

A 119-page report describes a solar-heating system installed in a full-service bank. The new building is a contemporary structure with a roof supporting 468 square feet (43.5 square meters) of flat-plate air solar-energy collectors. As the first solar-energy system in the geographical area, the installation has promoted much interest and features onsite temperature- and power-measurement readouts.

Problems of maintenance, system deterioration, freezeup, and control failure are minimized by using air rather than liquid solar collectors. The design also eliminates the need for a heat exchanger for space-heating.

A rock bin stores thermal solar energy. Temperature stratification is maintained by rock storage; thus, the highest available temperature, at the top of the storage bed, is used for space heating. Return air to the collectors is from the bottom of storage at a reduced temperature.

Solar-heated air is distributed to the space-heating load or to storage by an air-handling unit with both motorized and gravity-operated dampers. The solar-heating system is integrated to function with a backup heat pump and electric-resistance heating. A thermostatically-controlled exhaust fan vents the attic in hot weather.

This work was done by the First National Bank of Clarksdale for **Marshall Space Flight Center**. Further information may be found in DOE/NASA CR-161549 [N80-33858/NSP], "Solar Heating System at Quitman County Bank, Marks, Mississippi — Final Report" [\$9]. A paper copy may be purchased [prepayment required] from the National Technical Information Service, Springfield, Virginia 22161. The report is also available on microfiche at no charge. To obtain a microfiche copy, Circle 22 on the TSP Request Card. MFS-25558

Solar Water-Heating Performance Evaluation — San Diego, California

Energy is saved by replacing a domestic, conventional natural-gas heater with a solar-energy system.

A recently released report describes the 6-month performance of a solar-energy system that heats domestic hot water for a single-family residence in Encinitas, California, near San Diego. Energy savings for the test period averaged 1.089 million Btu (1.149 billion joules) per month. After the operating energy required for energy collection and storage is deducted, an average net monthly savings of 1.026 million Btu (1.083 billion joules) or 301 kWh is obtained.

A light load on the system prevented energy savings from reaching their potential during the test season; on the average as much as twice the hot water could have been used. Collector efficiency was 40 percent.

Solar energy from the 65-square-foot (6-square-meter) collector array is supplied to either a 66-gallon (250-liter) preheat tank (solar storage) or a 40-gallon (151-liter) domestic-hot-water tank. The temperatures of the water in the collectors, the preheat tank, and the domestic-hot-water tank are measured, and a programable controller pumps water from one of the tanks through the collectors and back to the same tank. At preset tank temperatures or at preset temperature differences between the tank and

collector water, the controller switches the cascade valve to divert the flow to the proper tank.

The collector cover is 1/8-inch (3-millimeter) tempered glass. Freeze protection is provided by circulating hot water from the domestic-hot-water tank through the collectors when necessary. Auxiliary energy is supplied by natural gas.

This work was done by the Federal Systems Division of IBM Corp. for **Marshall Space Flight Center**. Further information may be found in DOE/NASA CR-161481 [N80-27806/NSP], "Solar Energy System Performance Evaluation — Seasonal Report for Elcam San Diego, San Diego, California" [\$7]. A paper copy may be purchased [prepayment required] from the National Technical Information Service, Springfield, Virginia 22161. The report is also available on microfiche at no charge. To obtain a microfiche copy, Circle 23 on the TSP Request Card. MFS-25502

Solar-Heated and Cooled Savings and Loan Building — Leavenworth, Kansas

A heating and cooling system for a two story building

A 310-page report describes a solar-heating and cooling system installed in the Citizens Mutual Savings and Loan Association, Leavenworth, Kansas. The system is expected to furnish 90 percent of the annual heating load, 70 percent of the cooling load, and all of the domestic hot-water load of the two-story structure. The building has two floors with 9,000 square feet (836 square meters) of conditioned space.

Flat-plate solar-energy collectors are roof-mounted and oriented to face south with a slope 40° to the horizontal. Nine computer-run comparisons were made to determine the optimum collector type and area. The building contains fully-automated temperature controls and is divided into five separate temperature-load zones, each with an independent heat pump.

Three different rates of flow are possible through the collector panels.

The lowest rate produces hot water for the absorption chillers, and the other two collect energy for heating. Two storage tanks are provided: one tank for summer use and both tanks for winter use when maximum storage is needed.

The control system is pneumatic and includes step controllers for sequential control of the five absorption-chilling units. A fan system cools from outdoor air until outside temperatures become too high. Also, the high vaulted ceiling of the main banking area results in temperature stratification, permitting the installation of dual return-air dampers. One near the roof peak recovers hot air for winter recycling, and the other near the floor recovers cooler air for summer.

This work was done by the Citizens Mutual Savings & Loan Association of Leavenworth, Kansas, for Marshall Space Flight Center. Further information may be found in DOE/NASA CR-161484 [N80-29848/NSP], "Solar Heating and Cooling System Installed at Leavenworth, Kansas — Final Report" [\$17]. A paper copy may be purchased [prepayment required] from the National Technical Information Service, Springfield, Virginia 22161. The report is also available on microfiche at no charge. To obtain a microfiche copy, Circle 24 on the TSP Request Card.
MFS-25520

Solar-Energy Landmark Building — Columbia, Missouri

An attractive installation supplies space heating for a four-story, campus Visitors Center.

The 299-page final report on a solar-energy system at the Visitors Center on the Stephens College campus in Columbia, Missouri, includes design, cost, installation, maintenance, and performance details of the project. The four-story center will house the Admissions Office, the Faculty Lounge, a two-story art gallery, and nine rooms for guests of the college. The building is situated adjacent to a well-traveled intersection and is a highly visible landmark.

The solar-energy system, designed to meet 71 percent of the heating load for the building, includes 176 hydronic flat-plate collectors and a water-to-water heat exchanger. Solar-heated water is stored in a 5,000-gallon (18,900-liter) water-storage tank located in the basement equipment room. A natural-gas-fired boiler supplies hot water to the heating system when the solar-heat supply fails to meet the demand.

The collector array is mounted several inches (centimeters) off the roof on brackets that reduce the number of roof penetrations required, thereby minimizing the chance of roof leaks. The roof slopes 50° from the horizontal and faces south.

Building construction started in November 1977 and was completed in January 1979. The solar-energy-system installation and acceptance test were completed in May 1979. With the exception of some problems in the control system, performance has been exceptional. Although the site is not fully instrumented, an operating panel with various readouts, including an integration (British thermal unit) meter, gives interested visitors a quick summary of the system operation.

This work was done by the Building and Grounds Department of Stephens College for Marshall Space Flight Center. Further information may be found in DOE/NASA CR-161485 [N80-29849/NSP], "Solar Space Heating For the Visitors Center, Stephens College, Columbia, Missouri — Final Report" [\$17]. A paper copy may be purchased [prepayment required] from the National Technical Information Service, Springfield, Virginia 22161. The report is also available on microfiche at no charge. To obtain a microfiche copy, Circle 25 on the TSP Request Card.
MFS-25524

Solar Heating for an Observatory — Lincoln, Nebraska

Most of the space heating for a 50-seat observatory is supplied by solar energy.

A new report describes a solar-energy system that provides 60 percent of the space heating for the 50-seat Hyde

Memorial Observatory in Lincoln, Nebraska. The system includes nine flat-plate collectors, a rock-storage bin, blowers, controls, and ducting. A natural-gas furnace supplies additional energy when Sunlight cannot meet the space-heating demand.

The system has five modes of operation: supplying heat directly from the collectors, supplying heat from storage, storing solar energy, auxiliary heating, and summer venting to protect against high temperatures that are damaging to the collectors.

A total of 224.74 million Btu (237.11 billion joules) was measured in the plane of the collector array during the reporting period. The system collected 35.8 million Btu (37.8 billion joules) of the available energy, for a collector-array efficiency of 16 percent. During periods when the collector array was active, a total of 103.92 million Btu (109.64 billion joules) was measured in the plane of the collector array. Therefore, the operational collector efficiency was 35 percent.

Definitions of performance factors, solar-energy-system performance equations, and long-term average weather conditions are collected in appendixes to the report. Although the insolation was below the long-term average for the Lincoln, Nebraska, site, the net fossil-energy savings for the 12-month report period were measured at 11.31 million Btu (11.93 billion joules) or the equivalent of 1.9 barrels (300 liters) of oil. Unquantified system losses into the heated space from the storage bin and ductwork increase the actual savings beyond this figure.

This work was done by the Federal Systems Division of IBM Corp. for Marshall Space Flight Center. Further information may be found in DOE/NASA CR-161495 [N80-29851/NSP], "Solar Energy System Performance Evaluation — Seasonal Report for SEECO Lincoln, Lincoln, Nebraska" [\$7]. A paper copy may be purchased [prepayment required] from the National Technical Information Service, Springfield, Virginia 22161. The report is also available on microfiche at no charge. To obtain a microfiche copy, Circle 26 on the TSP Request Card.
MFS-25525



Two-Story Residence With Solar Heating — Newnan, Georgia

A warm-air-collector system delivers heat to a two-story building.

A solar-energy system installed in a two-story dwelling about 40 miles (65 kilometers) southwest of Atlanta in Newnan, Georgia, was evaluated over the period from June 1979 through April 1980. The system consists of 14 warm-air collectors with a total area of 392 square feet (36.4 square meters), a rock-thermal-storage bin, an air handler, heat exchangers, a domestic-hot-water (DHW) preheat tank, and associated controls, plumbing, and air ducting. A report featuring an overall performance assessment as well as details on operation and maintenance is now available.

Air-handler blowers deliver hot air either directly from the solar collectors or from the rock-bin storage. Summer venting and DHW preheating is also included; a 40-gallon (151-liter) electric hot-water tank is supplied water from the 80-gallon (303-liter) preheat tank. When outdoor temperatures drop below 15° F (–9° C), auxiliary heating is available from electric resistance heaters and an electric heat pump.

An average building temperature of 72° F (22° C) was maintained during the 11-month reporting period. The measured space-heating load was 23.06 million Btu (24.33 billion joules), with the solar fraction totaling 47 percent. When accounted for, unmeasured losses from the solar-heating system into the heated space approximately doubled the measured net electrical savings for the test period, which were the equivalent of 0.9 barrel (140 liters) of oil.

This work was done by The Federal Systems Division of IBM Corp. for Marshall Space Flight Center. Further information may be found in DOE/NASA CR-161494 [N80-29853/NSP], "Solar Energy System Performance Evaluation — Seasonal Report for Contemporary Newnan, Newnan, Georgia" [\$8]. A paper copy may be purchased [prepayment required] from the National Technical Information

Service, Springfield, Virginia 22161. The report is also available on microfiche copy, Circle 27 on the TSP Request Card. MFS-25526

Solar-Energy Heats a Transportation Test Center—Pueblo, Colorado

Warehouses and similar buildings could be heated by this flat-plate-collector system.

A petroleum-base, thermal-energy transport fluid circulating through 583 square feet (54 square meters) of flat-plate solar collectors accumulates much of the energy needed for space heating and domestic hot water at the U.S. Department of Transportation Test Center in Pueblo, Colorado. A report that is now available describes the operation, maintenance, and performance for this system, possibly suitable for warehouses and similar buildings, along with the energy savings for the test period from February 1979 to January 1980.

The measured daily average incident insolation in the plane of the collector array for the test period was about 10 percent below the long-term daily average for the area. The measured average outdoor ambient temperature for the period when solar heating was necessary was 51° F (11° C). For the report period, the solar-heating fraction was 31 percent, and the hot-water solar fraction was 79 percent. Since losses from transport piping that actually went toward heating the building were not measured and since much stored energy was lost because of the low hot-water consumption, the actual performance of the system can be above these figures.

This work was done by the Federal Systems Division of IBM Corp. for Marshall Space Flight Center. Further information may be found in DOE/NASA CR-161493 [N-80-29850/NSP], "Solar Energy System Performance Evaluation — Seasonal Report for Colt Pueblo, Pueblo, Colorado" [\$8]. A paper copy may be purchased [prepayment required] from the National Technical Information Service,

Springfield, Virginia 22161. The report is also available on microfiche at no charge. To obtain a microfiche copy, Circle 28 on the TSP Request Card. MFS-25527

Single-Family-Residence Solar Heating — Carlsbad, New Mexico

About half of the space-heating and hot-water energy requirement is supplied by the Sun.

A solar-energy system described in a recent report is located in a single-family residence at Carlsbad Caverns National Park, New Mexico. This hot-air, solar-heating and hot-water system includes 408 square feet (38 square meters) of flat-plate air collectors, a rock-storage bin, an energy-transport system, an air-to-water heat exchanger, controls, and a hot-water preheat tank that supplies preheated water to an electric hot-water tank. An oil, hot-air furnace supplies auxiliary space heating. Electricity powers the air-handler blower and hot-water preheat pump.

Measured average daily insolation at the test site for the 12 months of the reporting period was 9 percent below the long-term average for the area, indicating a few more cloudy days than normal. However, space-heating and hot-water loads were near expected values based on results derived from a modified f-chart analysis, which uses measured weather and subsystem loads as inputs. Solar energy provided 43 percent of the space-heating and 53 percent of the hot-water energy. The total net energy savings during the reporting period amounted to 23.072 million Btu (24.34 billion joules or 6,761 kWh).

This work was done by the Federal Systems Division of IBM Corp. for Marshall Space Flight Center. Further information may be found in DOE/NASA CR-161508 [N80-29856/NSP], "Solar Energy System Performance Evaluation — Seasonal Report for IBM System 1B, Carlsbad, New Mexico" [\$7]. A paper copy may be purchased [prepayment required]

from the National Technical Information Service, Springfield, Virginia 22161. The report is also available on microfiche at no charge. To obtain a microfiche copy, Circle 29 on the TSP Request Card.
MFS-25528

Multimode Solar-Heating System — Columbia, South Carolina

Operating-energy needs and control problems reduced winter energy savings.

A six-mode pyramidal-optics solar-energy system in a four-unit townhouse in Columbia, South Carolina, netted unexpectedly-low winter energy savings. Its performance over a 12-month period (from June 1979 through May 1980) is described in a report that is now available.

Control failures, occurring most severely in February, caused electrical strip heaters to turn on unnecessarily while solar heat was available. Consequently, almost 5 million Btu (5 billion joules) were wasted in 1 month.

Even if the controls had operated correctly, fossil-fuel savings would not have been impressive; much of the energy accumulated by the solar collectors was dissipated in losses through heat exchangers and ductwork, while operating-energy requirements for the many motors and lengths of tubing were high.

For this site and solar-energy application, more net energy could have been realized with a system utilizing only a direct space-heating mode or a hot-water-preheating mode. The most inefficient mode of the tested system was the one in which heat pumps mingled alternatively storage or collector energy with electric-heat-strip energy to satisfy the space-heating demand. The direct-solar-heating mode of the same system performed very well in comparison.

This work was done by The Federal Systems Division of IBM Corp. for Marshall Space Flight Center. Further information may be found in DOE/NASA CR-161546 [N80-31880/NSP], "Solar Energy System Performance Evaluation — Seasonal Report

*for Wormser, Columbia, South Carolina" [\$9]. A paper copy may be purchased [prepayment required] from the National Technical Information Service, Springfield, Virginia 22161. The report is also available on microfiche at no charge. To obtain a microfiche copy, Circle 30 on the TSP Request Card.
MFS-25552*

Solar-Heated Swimming School — Wilmington, Delaware

An energy alternative to natural gas pool heating.

During the winter of 1977, with the low availability of natural gas, the Wilmington Swim School in Wilmington, Delaware, was judged to be a nonessential user and as such faced possible cutbacks or the elimination of its gas allocation. Solar energy now supplies much of the total annual building energy load at this school, thus alleviating the dependence on natural gas. A new report describes the operation, installation, and performance of the solar-energy system.

The active solar-energy system is composed of 2,500 square feet (230 square meters) of liquid flat-plate collectors connected to a 3,600-gallon (13,600-liter), concrete storage tank located belowground near the building. An extension of the building completed in 1979 incorporates a vertical-wall, passive collection system that provides about 25 percent of the heated-fresh-air for the office area. The active collector area is the maximum that could fit on the building roofs.

A microcomputer-based control system selects the optimal application of stored energy among the space-heating, domestic-hot water, and pool-heating alternatives. Selection is based on seasonal energy availability and the specific thermal requirements of each load. For example, if winter space heating requires water in excess of 120° F (49° C), stored water below this temperature will be used for pool heating, which only requires temperatures in excess of 85° F (29° C); any heat stored below this temperature may be used for domestic water preheating.

*This work was done by Cooperson Brack Associates for Marshall Space Flight Center. Further information may be found in DOE/NASA CR-161538 [N80-31878/NSP], "Solar Energy System Demonstration Project at Wilmington Swim School, New Castle, Delaware — Final Report" [\$8]. A paper copy may be purchased [prepayment required] from the National Technical Information Service, Springfield, Virginia 22161. This report is also available on microfiche at no charge. To obtain a microfiche copy, Circle 31 on the TSP Request Card.
MFS-25548*

Winter Performance of a Domestic Solar-Heating System — Duffield, Virginia

Sunlight supplies 39 percent of the heat load, saving 9 barrels of fuel oil in one heating season.

The wintertime performance of a solar-energy system in a Virginia home is described in a report that covers the period from October 1979 through March 1980. The house is a two-story, single-family residence with a floor area of approximately 1,940 square feet (180 m²). Solar energy is collected with roof-mounted air flat-plate collectors. It is stored in a rock bin on the lower level of the house and is transferred to a water-preheat tank whenever the system is storing energy. The water is heated to its final temperature by electrical heaters in another tank. A heat pump supplies heat to the house when necessary.

Although the system was designed to furnish 24 percent of the space heating and heat for domestic hot water, it furnished 39 percent, even though the average daily insolation was 34 percent below normal and the average outdoor temperature was 5° F (2.8° C) below normal. The net energy saved by the use of solar energy instead of electricity was the equivalent of approximately 9 barrels (1,400 liters) of oil.

The solar-energy system was designed with the aid of system-solar-fraction charts (f-charts). The discrepancy between the measured system

(continued on next page)



solar fraction of 39 percent and the expected value of 24 percent possibly show that the f-chart simulation is not valid for the Duffield installation. Reasons for the discrepancy are under investigation.

This work was done by the Federal Systems Division of IBM Corp. for Marshall Space Flight Center. Further information may be found in DOE/NASA CR-161507 [N80-30892/NSP], "Solar Energy System Performance Evaluation — Seasonal Report for Solaron-Duffield, Duffield, Virginia" [\$8]. A paper copy may be purchased [prepayment required] from the National Technical Information Service, Springfield, Virginia 22161. The report is also available on microfiche at no charge. To obtain a microfiche copy, Circle 32 on the TSP Request Card.

MFS-25540

One-Year Assessment of a Solar Space/Water Heater — Clinton, Mississippi

Unit is integrated into the space-heating and hot-water systems of a dormitory building.

System 4, a solar-energy system for space heating and domestic-hot-water preheating, was evaluated during 1 year of operation at a training-center dormitory in Mississippi. As stated in a new report, the system satisfied 32 percent of the building heating load.

The system is designed to supply 48 percent of heating needs. The relatively low contribution of solar energy in the installed system is explained by a combination of correctable and uncontrollable factors: The solar array, which is close to a dirt road, became coated with dust during dry spells and did not receive full insolation. Air leakage into the collector array and an open bypass valve also reduced efficiency. In addition, the winter was somewhat cooler than usual.

System 4 is a prepackaged unit. Solar energy is absorbed in flat-plate collectors with air as the heat-transfer medium. The collector area for

the unit evaluated in the report is 259 ft² (24 m²). A blower circulates air from the collector array to a rock storage bed. Another blower circulates air to the building from either the collector array or the rock storage bed. A heat exchanger at the bed absorbs heat for domestic hot-water use. Auxiliary heat is furnished by a 4-kW electric heater in each of two hot-water tanks and a 20-kW strip heater in an air duct.

The report describes the performance of the system and each of its subsystems (collector array, storage, hot water, and space heating). It presents operating energy requirements (the energy needed to transport solar energy to the point of use) and energy savings. Appendixes contain definitions of performance factors and solar terms, a listing of equations used in performance assessment, and a tabulation of long-term average weather conditions.

This work was done by the Federal Systems Division of IBM Corp. for Marshall Space Flight Center. Further information may be found in DOE/NASA CR-161509 [N80-30893/NSP], "Solar Energy System Performance Evaluation — Seasonal Report for IBM System 4 at Clinton, Mississippi" [\$8]. A paper copy may be purchased [prepayment required] from the National Technical Information Service, Springfield, Virginia 22161. The report is also available on microfiche at no charge. To obtain a microfiche copy, Circle 33 on the TSP Request Card.

MFS-25539

Fire-Station Solar-Energy System — Kansas City, Missouri

Screen-walled solar collectors are part of an award-winning architectural design.

About half of the space heating and 75 percent of the heat for domestic hot water at a Kansas City fire station are provided by a solar-energy system, described in a 157-page report. A historical narrative of the project is included, along with detailed drawings, charts, and product literature.

The fire station has two areas: an operations area occupied by the firemen and the apparatus bay occupied by the fire equipment. The operations area covers 2,800 square feet (260 square meters) and has a winter design temperature of 70° F (21° C); the apparatus bay covers 6,000 square feet (560 square meters) with a winter design temperature of 50° F (10° C). The solar collectors, are an integral part of the apparatus bay. Two arrays of flat-plate, air solar collectors are mounted on the roof, and one large array extends from the roof to the ground, forming the south wall. Ninety-six collectors are integrated into the wall.

East and west screen walls create an attractive profile for the fire station without significantly affecting collector performance. A regional association awarded a certificate of design excellence to the architect for the conception of these screens. A concrete-box storage subsystem, a domestic-hot-water preheat tank, blowers, pumps, heat exchangers, air ducting, controls, and plumbing complete the solar-energy system.

This work was done by the city of Kansas City, Missouri, for Marshall Space Flight Center. Further information may be found in DOE/NASA CR-161513 [N80-30895/NSP], "Solar Heating and Domestic Hot Water System Installed at Kansas City Fire Station, Kansas City, Missouri — Final Report" [\$11]. A paper copy may be purchased [prepayment required] from the National Technical Information Service, Springfield, Virginia 22161. The report is also available on microfiche at no charge. To obtain a microfiche copy, Circle 34 on the TSP Request Card.

MFS-25538

Solar-Heated Ranger Station — Glendo, Wyoming

Solar energy heats a Wyoming residential ranger station.

The Glendo Reservoir Ranger Station in Wyoming, occupying 1,078 square feet (100 square meters), is the residence of a State park ranger. A solar-energy system to provide 46

percent of the space-heating and 80 percent of the building domestic-hot-water energy requirements was installed in the existing building, and system performance was monitored from January through December 1979. A report that is now available describes the system and each of its subsystems: collector-array, storage, hot-water, and space-heating. Long-term average and actual weather conditions are included in the report for the test site, as well as system performance values and energy savings.

Water is the only heat-transfer medium used at the installation. A 1,000-gallon (3,785-liter) hot-water-storage tank is supplied with energy from 294 square feet (27.3 square meters) of flat-plate collectors. A domestic-hot-water tank, pumps, heat exchangers, and a controller complete the five-mode solar-energy system. A gas furnace supplies auxiliary space heating, and electrical-resistance elements supplement the hot-water supply.

An abnormally high number of cloudy days reduced the measured average daily insolation for the test year. The solar-energy system was able to supply 22 percent of the space-heating and 58 percent of the hot-water energy demand. Net energy savings for the year were about 30 million Btu (32 billion joules).

This work was done by The Federal Systems Division of IBM Corp. for Marshall Space Flight Center. Further information may be found in DOE/ NASA CR-161520 [N80-30896/ NSP] "Solar Energy System Performance Evaluation — Seasonal Report for IBM System 3, Glendo, Wyoming" [\$8]. A paper copy may be purchased [prepayment required] from the National Technical Information Service, Springfield, Virginia 22161. The report is also available on microfiche at no charge. To obtain a microfiche copy, Circle 35 on the TSP Request Card.

MFS-25537

Economic Evaluation of a Solar Hot-Water System — Palm Beach County, Florida

Solar-energy costs and savings for a residential hot-water system are projected over a 20-year life cycle.

A solar-energy system designed to supply 90 percent of the domestic-hot-water energy requirements for the home of the refuge manager of the Loxahatchee National Wildlife Refuge in Palm Beach County, Florida, is the subject of a recent report. An economic evaluation of the system at this site uses technical and economic models with inputs based on the actual working characteristics of the installed system and on local conditions. The analysis relates system cost to anticipated savings over a 20-year period. Based on the analysis of the Loxahatchee site, economic viability is calculated for four other sites in the continental United States.

Tables of variables enable the prediction of the economic performance of the solar hot-water system at various locations, with different values for insolation and fossil-fuel cost. For example, at an Albuquerque, New Mexico, site, the total initial cost of the system in 1980 dollars, before adjustment for Federal tax credit, is \$2,604. The 1980 value of fuel costs and other costs anticipated over a 20-year period without solar energy is \$6,282; with solar energy, it is \$2,364. The figures indicate positive savings with the solar installation in 1 year and total payback of investment costs after 10 years of operation.

This work was done by the Federal Systems Division of IBM Corp. for Marshall Space Flight Center. Further information may be found in DOE/ NASA CR-161512 [N80-30894/ NSP], "Solar Energy System Economic Evaluation — Final Report for Semco-Loxahatchee, Loxahatchee National Wildlife Refuge, Palm Beach County, Florida" [\$8]. A paper copy may be purchased [prepayment required] from the National Technical Information Service, Springfield, Virginia 22161. The report is also available on microfiche at no charge. To obtain a microfiche copy, Circle 36 on the TSP Request Card.

MFS-25536

Residential System — Lansing, Michigan

Air collectors are combined with water storage.

A performance evaluation of a solar-energy system supplying space heating and hot water to a 1,300-square foot (121-square-meter) residence in Lansing, Michigan, is featured in an 87-page report, along with a discussion of typical system operation, operating energy, energy savings, and maintenance. During the reporting period from April 1979 to March 1980, the measured average outdoor ambient temperature was 48° F (9° C). Solar energy supplied 15 percent of the measured load for hot water and space heating.

The Lansing installation uses 278 square feet (25.8 square meters) of hot-air flat-plate collectors, three 120-gallon (454-liter) meter storage tanks, a liquid/air heat exchanger, an energy transport module, pumps, controls, and transfer lines. The unusual combination of water storage with an air collecting medium stores heat in about one-third the space of a rock-bin system, but with consequent loss of heat-exchanging efficiency.

Unusual operating conditions during the report period made it difficult to assess performance. A large amount of hot-water was consumed in the final 7 months — generally over 225 gallons (852 liters) per day, and as a result almost all the solar energy collected during this period was used in support of the hot-water subsystem. Solar-energy support was greatly reduced for the space-heating subsystem, contrary to design expectations. Nonetheless, net savings were approximately 21 million Btu (22 billion joules).

This work was done by the Federal Systems Division of IBM Corp. for Marshall Space Flight Center. Further information may be found in DOE/ NASA CR-161491 [N80-29855/ NSP], "Solar Energy System Performance Evaluation — Seasonal Report for Fern Lansing, Lansing, Michigan" [\$8]. A paper copy may be purchased [prepayment required] from the National Technical Information Service, Springfield, Virginia 22161. The report is also available on microfiche at no charge. To obtain a microfiche copy, Circle 37 on the TSP Request Card.

MFS-25530



Solar Space-Heating System — Yosemite National Park, California

Performance over 12 months suffered from low insolation and equipment breakdown.

A report on a solar-heating system in the Visitors Center at Yosemite National Park, California, assesses system performance from May 1979 through April 1980. The installation has 980 square feet (91 square meters) of liquid flat-plate solar collectors, water energy storage, heat exchangers, pumps, controls, and plumbing.

Design expectations that over half the annual heating demand would be supplied by solar energy were not met due to large building-heat loss, below-average insolation, and maintenance downtime during the test period. Several large pine trees that add to the attractiveness of the Visitors Center also shade the building and cause significant performance penalties. Nonetheless, fossil-energy savings amounted to 109 million Btu (116 billion joules); the potential savings with fewer equipment failures is higher.

The system has four modes of operation:

- Collector to storage via a heat exchanger, when the temperature difference between the two is sufficient;
- Storage to space heating via a second heat exchanger upon demand, when storage temperature exceeds 105° F (58° C);
- Mixed solar and conventional heating, at storage temperatures down to 90° F (32° C); and
- Conventional heating, using an oil-fired boiler to deliver hot water for building space heating to a third heat exchanger.

This work was done by the Federal Systems Division of IBM Corp. for Marshall Space Flight Center. Further information may be found in DOE/NASA CR-161539 [N80-31883/NSP], "Solar Energy System Performance Evaluation — Seasonal Report for Colt Yosemite, Yosemite National Park, California" [8]. A paper copy may be purchased [prepayment required] from the National Technical

Information Service, Springfield, Virginia 22161. The report is also available on microfiche at no charge. To obtain a microfiche copy, Circle 38 on the TSP Request Card. MFS-25553

Motel Solar-Hot-Water System — Dallas, Texas

Solar energy meets most of the hot-water requirements of a large motel.

A report describes a solar-energy system designed to satisfy up to 64 percent of the hot-water demands of a 120-room motel. Key system components include a 1,000-square-foot (93-square-meter) roof-mounted collector array, a 1,000-gallon (3,800-liter) storage tank, a tube-in-shell heat exchanger, and three domestic hot-water tanks.

The collector array comprises 30 water-filled units in a series/parallel arrangement. A pump circulates water from the bottom of the storage tank, through the collectors, and back into the storage tank. A second pump circulates water from the storage tank, through the shell side of the heat exchanger, and back into the storage tank. A third pump circulates water between the domestic hot-water tanks and the tube side of the heat exchanger.

The pumps and valves are automatically controlled at preset temperature differences between the collectors and storage tank and between the storage tank and one of the domestic hot-water tanks. Pressure gages are installed for performance monitoring and manual valves are included for maintenance.

The report contains calibration instructions for the differential-temperature controllers, emergency-shutdown instructions, maintenance procedures, and a suggested form for operating records and performance analysis. Manufacturers' data sheets on system components are also included.

This work was done by Day's Inn of America, Inc., for Marshall Space Flight Center. Further information may be found in DOE/NASA CR-161570 [N81-10521/NSP], "Solar

Hot Water System Installed at Day's Inn Motel, Dallas, Texas [Valley View]" [6]. A paper copy may be purchased [prepayment required] from the National Technical Information Service, Springfield, Virginia 22161. The report is also available on microfiche at no charge. To obtain a microfiche copy, Circle 39 on the TSP Request Card. MFS-25575

Motel Solar-Hot-Water System With Nonpressurized Storage — Jacksonville, Florida

Energy is transferred to pressurized domestic-hot-water tanks.

A solar-energy system providing 65 percent of the domestic-hot-water (DHW) demand at a Jacksonville, Florida, motel uses a 1,000-gallon (3,780-liter) nonpressurized storage tank to supply solar energy to existing motel hot-water lines, which are pressurized. Heat is transferred to each of three domestic-hot-water tanks by circulating water from these tanks through the tube side and water from the storage tank through the shell side of a tube-and-shell heat exchanger. The parts and operation of this system are described, along with maintenance, performance, and warranty information, in a report that is available upon request.

The modular roof-mounted solar-energy collectors have copper absorber plates. They are painted flat black, glazed, and insulated on the back. The collector array and piping are graded to drain into the storage tank whenever the collector circulating pump is not operating. The storage tank is vented to the atmosphere, and two vacuum breakers for the collectors admit air during draindown to speed drainage and prevent vapor problems.

When the absorber plate of one collector becomes 12° F (7° C) warmer than the bottom of the storage tank, the collector circulating pump turns on to fill all the collectors and begin their operation. When the temperature difference drops to a predetermined level, the pump turns off and the collectors drain back into storage.

If the temperature at the top of the storage tank is 30° F (17° C) greater than the temperature at the bottom of any of the three DHW tanks, water from the cold tanks is circulated through the heat exchanger, along with hot water from the storage tank. This heat-exchanger system, operating independently of the solar-collector system, shuts off again when the temperature differences decrease to 15° F (8° C).

This work was done by Day's Inn of America, Inc., for Marshall Space Flight Center. Further information may be found in DOE/NASA CR-161560 [N81-10523/NSP], "Solar Hot Water System Installed at Day's Inn Motel, Jacksonville, Florida" [\$6.50]. A paper copy may be purchased [prepayment required] from the National Technical Information Service, Springfield, Virginia 22161. The report is also available on microfiche at no charge. To obtain a microfiche copy, Circle 40 on the TSP Request Card. MFS-25569

Closed-Circulation System for Motel Hot Water — Savannah, Georgia

Solar-energy collectors are supported by guy wires.

A solar-energy hot-water-supply system installed in a Savannah, Georgia, motel has roof-mounted solar collectors supported by guy wires. The collectors circulate a 50-percent ethylene glycol solution rather than relying on a drain system for freeze protection. A heat exchanger transfers energy to the domestic hot water. A recent report describes the equipment and its operation and maintenance. The system is well tested, and at the Savannah installation no major problems were encountered with its operation.

The 1,000-gallon (3,780-liter) fiberglass storage tank contains two heat exchangers: One heats water in the storage tank with fluid from the solar collectors; and the other preheats the cold-water supply as it passes through to the domestic hot-water heaters, which have electrical elements for supplementing energy from the Sun.

Temperature sensors are located in the collector plates and in the storage tank, and controller pumps are turned on or off according to the measured temperature differential.

Costly structural-steel mounting for the solar collectors was bypassed by using guy wires to secure the collector array to the roof. Although no roof penetrations were required over the occupied space, the mounting system is rated to withstand 120-mile-per-hour (193-kilometer-per-hour) winds. The solar-energy system provides an average of 2,440 gallons (9,240 liters) of 140° F (60° C) water at the installation.

This work was done by Day's Inn of America, Inc., for Marshall Space Flight Center. Further information may be found in DOE/NASA CR-161561 [N81-10522/NSP], "Solar Hot Water System Installed at Day's Inn Motel, Savannah, Georgia" [\$6.50]. A paper copy may be purchased [prepayment required] from the National Technical Information Service, Springfield, Virginia 22161. The report is also available on microfiche at no charge. To obtain a microfiche copy, Circle 41 on the TSP Request Card. MFS-25572

Solar Heating for a Restaurant — North Little Rock, Arkansas

Large building hot-water consumption affects solar-energy-system design.

A solar-heating system designed to supply a major portion of the space heat and water heat for a restaurant in North Little Rock, Arkansas, was installed in December 1979. The system uses flat-plate liquid collectors circulating an antifreeze solution. Equipment specifications and modifications to existing building heating and hot-water systems are described along with other information in a report that is now available.

Four rows of roof-mounted solar collectors at the North Little Rock site are surrounded by an architectural screen for an attractive building profile. Solar-collector area was determined by optimizing building load,

collector output, and cost. Architectural considerations led to two of the collectors being tilted at an angle of only 25°, although the optimum is greater; the performance penalty for this modification is slight.

Because of the continual demand for domestic hot water at the restaurant, storage is less important than at other sites; storage capacity is equal to the estimated daily hot-water requirement. Two heat exchangers between the collector fluid and the potable hot-water supply prevent water contamination from the antifreeze solution flowing through the collectors. Water is pumped directly from storage through a coil for space heating. A purge coil in the collector loop protects against failure when more heat is collected than can be used or stored.

This work was done by Shoney's South, Inc., for Marshall Space Flight Center. Further information may be found in DOE/NASA CR-161557 [N81-10520/NSP], "Solar Heating and Hot Water System Installed at Shoney's Restaurant, North Little Rock, Arkansas — Final Report" [\$11]. A paper copy may be purchased [prepayment required] from the National Technical Information Service, Springfield, Virginia 22161. The report is also available on microfiche at no charge. To obtain a microfiche copy, Circle 42 on the TSP Request Card. MFS-25568

Motel Solar Hot-Water Installation — Atlanta, Georgia

An analysis of motel hot-water requirements insures compatibility with solar-energy system design.

Such considerations as the hardness of local water, average insolation for the site, and daily hot-water requirements are studied in a report describing two new solar-energy hot-water units at a motel in Atlanta, Georgia. The two units are designed to supply 81 percent of the total motel hot-water demand annually. Demand is based on an anticipated 85 percent

(continued on next page)



occupancy in the two buildings, each of which is served by a separate solar-energy system.

The report includes drawings, operating and maintenance instructions, and test results for 1 day of system operation.

Both buildings use 16 liquid flat-plate solar-energy collectors; the systems differ only in having slightly different controllers. Each includes a cement-lined steel tank for hot-water storage. As domestic hot water is consumed, water flows into them from the storage tanks.

Electric resistance units in the hot-water tanks heat the solar-heated water, if necessary, to reach the thermostat setting. When collector temperatures approach freezing or when there is an interruption in electrical power, the collectors drain to prevent failure. When working conditions are reinstated, the collectors are automatically refilled.

*This work was done by Day's Inn of America, Inc., for **Marshall Space Flight Center**. Further information may be found in DOE/NASA CR-161559 [N81-10519/NSP], "Solar Hot Water System Installed at Day's Lodge, Atlanta, Georgia" [\$5]. A paper copy may be purchased [prepayment required] from the National Technical Information Service, Springfield, Virginia 22161. The report*

is also available on microfiche at no charge. To obtain a microfiche copy, Circle 43 on the TSP Request Card. MFS-25564

Building With Integral Solar-Heat Storage — Starkville, Mississippi

The roof-supporting column houses a rock-storage bin.

A solar space-heating system in a Starkville, Mississippi, bank has a rock thermal-storage bin that is an integral part of the building design. The bin is a steel container, with the exterior insulated and plastered, that runs from floor to ceiling in the bank lobby. Roof-supporting trusses are cantilevered from the steel column. A description of the system, including technical installation and operation data, is included in a report that is now available.

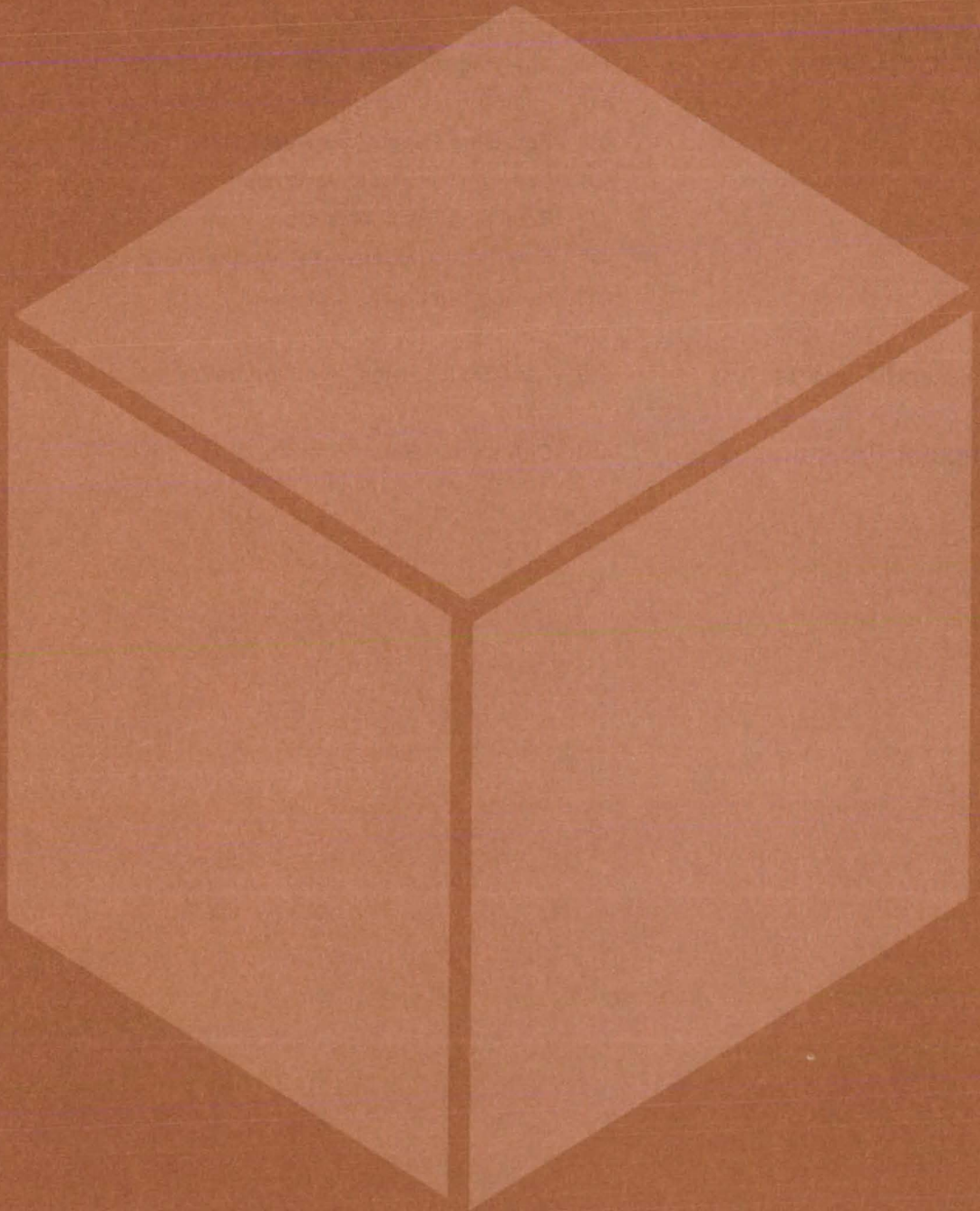
The solar-energy system supplies more than half the building space-heating load. Since very little hot water is used, hot water is supplied by conventional heaters. A special air-handling unit, with low-leakage dampers and a motor with high-temperature insulation, moves air over the solar

collectors and into storage and connects to the conventional building cooling and air-duct distribution system. A two-stage electric-resistance heater in the ductwork makes up any additional building heat required.

The rock-storage bin in the lobby column is deeper and narrower than is normally recommended, due to its unusual location. To keep the airflow resistance at a minimum, individual pebble size was increased from the standard 3/4 to 1-1/2 in. (2 to 4 cm) to 2 in. (5 cm). A building thermostat integrates the following modes of operation: heating from collectors, heating from storage, storing heat, conventional backup heat, and conventional cooling.

*This work was done by Security State Bank, Starkville, Mississippi, for **Marshall Space Flight Center**. Further information may be found in DOE/NASA CR-161550 [N81-10518/NSP], "Solar Heating System at Security State Bank, Starkville, Mississippi — Final Report" [\$9.50]. A paper copy may be purchased [prepayment required] from the National Technical Information Service, Springfield, Virginia 22161. The report is also available on microfiche at no charge. To obtain a microfiche copy, Circle 44 on the TSP Request Card. MFS-25559*

Materials



Hardware, Techniques, and Processes

- 447 Improved Cell for Water-Vapor Electrolysis
- 448 Applying the Helium Ionization Detector in Chromatography
- 449 Photoproduction of Halogens Using Platinized TiO₂
- 450 Recycling Paper-Pulp Waste Liquors
- 451 User Chooses Coating Properties
- 452 Removing Freon Gas From Hydraulic Fluid
- 452 New Pressure-Sensitive Silicone Adhesive
- 453 Driving Bubbles Out of Glass

Books and Reports

- 453 Less-Toxic Corrosion Inhibitors

Computer Programs

- 454 Diffusion in Single-Phase Binary Alloys

Improved Cell for Water-Vapor Electrolysis

A sintered iridium oxide anode coating sharply increases the rate of dissociation of water vapor.

Lyndon B. Johnson Space Center, Houston, Texas

Water vapor in such gases as steam or ordinary room air is decomposed into hydrogen and oxygen by improved continuous-flow electrolytic cells akin to fuel cells. A new iridium oxide catalytic anode coating, demonstrated in over 1,000 hours of testing, yields dissociation rates over a hundredfold greater than those obtained using conventional platinum black (see Figure 1). Conversely, at equal current density, the iridium cell operates at approximately 0.45 volt lower potential, allowing practical dissociation rates at voltages below the threshold (2.1 volts) for significant ozone production. Power consumption is correspondingly reduced.

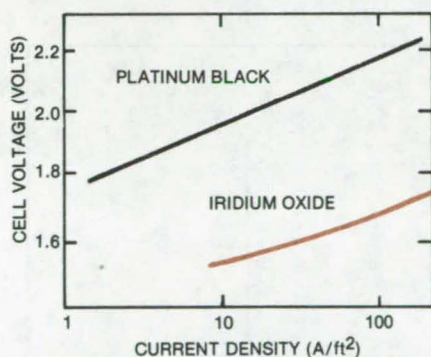


Figure 1. **Comparative Performance** of iridium oxide catalyst and conventional platinum black is shown in these I/V curves. The difference is a factor of over 100 in current density at fixed voltage, or about 0.45 volt at fixed current density.

A typical cell, originally developed for continuous oxygen enrichment of the atmosphere in manned space vehicles, is shown in Figure 2. Each unit actually consists of two mirror-image cells, with a dual cathode sandwiched between two anodes. Any number of dual cells can be stacked in parallel to handle the volume of water vapor at the input.

Vapor-laden gas traverses the serpentine channels within each cell and is dissociated at the anode into hydrogen ions and free oxygen. The oxygen mingles with the gas stream, while the

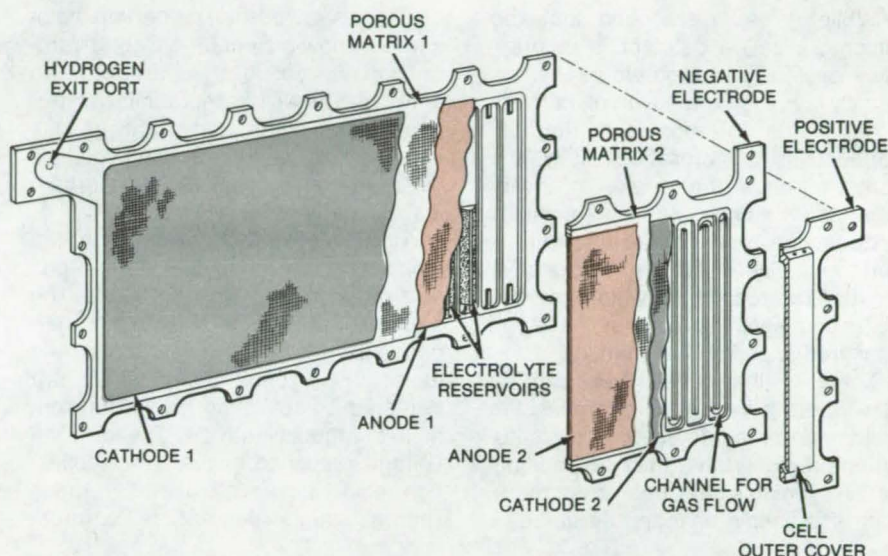


Figure 2. A **Dual-Cell Element** such as this would be part of a multicell stack, with blower, power supply, and control instrumentation.

hydrogen migrates through a porous, electrolyte-saturated matrix and is liberated as hydrogen gas at the cathode, exiting by a separate port.

Porous-metal electrolyte reservoirs lie against the anode. With variations in the humidity of the gaseous stream, electrolyte passes back and forth through the anode to the matrix to maintain the proper electrolyte level.

The anode substrate is a foraminous metal screen or expanded mesh, containing from 500 to over 1,500 pores/in.² (80 to over 230 pores/cm²). It may be titanium, gold, or tantalum (the latter is best, as it is inexpensive, inert, and resistant to hydrogen embrittlement). The matrix is made from a compounded asbestos such as blue asbestos, which will not decompose in the electrolyte — a mixture of sulfuric and phosphoric acid — yet will be adequately wetted.

The catalytic anode coating consists of 70 to 85 percent iridium oxide; the remainder is a high-temperature binder such as polytetrafluoroethylene resin. A soluble iridium compound, such as chloroiridic acid or iridium chloride, is dissolved in water and applied to sodium nitrate; after drying, the mixture is oxidized at 400° C. The fused

cake is leached with water, and iridium oxide is filtered out and mixed in water with polytetrafluoroethylene. After another filtration, the mesh is pressed into the mixture to receive a coating of about 20 mg/cm². It is then sintered at 310° C for 5 minutes, producing a highly adherent coating on one side and in the pores of the mesh.

In a prototype cell, efficiencies greater than 99 percent are obtained at ambient temperatures, using atmospheric air and a current density of about 60 A/ft² (650 A/m²). The cell may be operated at superatmospheric pressures and elevated temperatures, such as with steam.

This work was done by John R. Aylward of United Technologies Corp. for **Johnson Space Center**. For further information, Circle 45 on the TSP Request Card.

This invention is owned by NASA, and a patent application has been filed. Inquiries concerning nonexclusive or exclusive license for its commercial development should be addressed to the Patent Counsel, Johnson Space Center [see page A5]. Refer to MSC-16394.

Applying the Helium Ionization Detector in Chromatography

When modified to operate in its saturation region, the helium ionization detector can be ideal for gas chromatography.

Lyndon B. Johnson Space Center, Houston, Texas

While it can be argued that the helium ionization detector is theoretically ideal for gas chromatography, it is usually bypassed in favor of conventional flame-ionization and thermal-conductivity detectors. Ironically, the same features that make it advantageous — namely, its high sensitivity and responsiveness to nearly all atoms and molecules — are also responsible for its shortcomings, which include high noise levels and oversensitivity to background and contamination.

Many of the deficiencies can be eliminated, however, by operating the helium ionization detector in its "saturation" region, rather than its "multiplication" region as has been customary. With this simple change, the detector

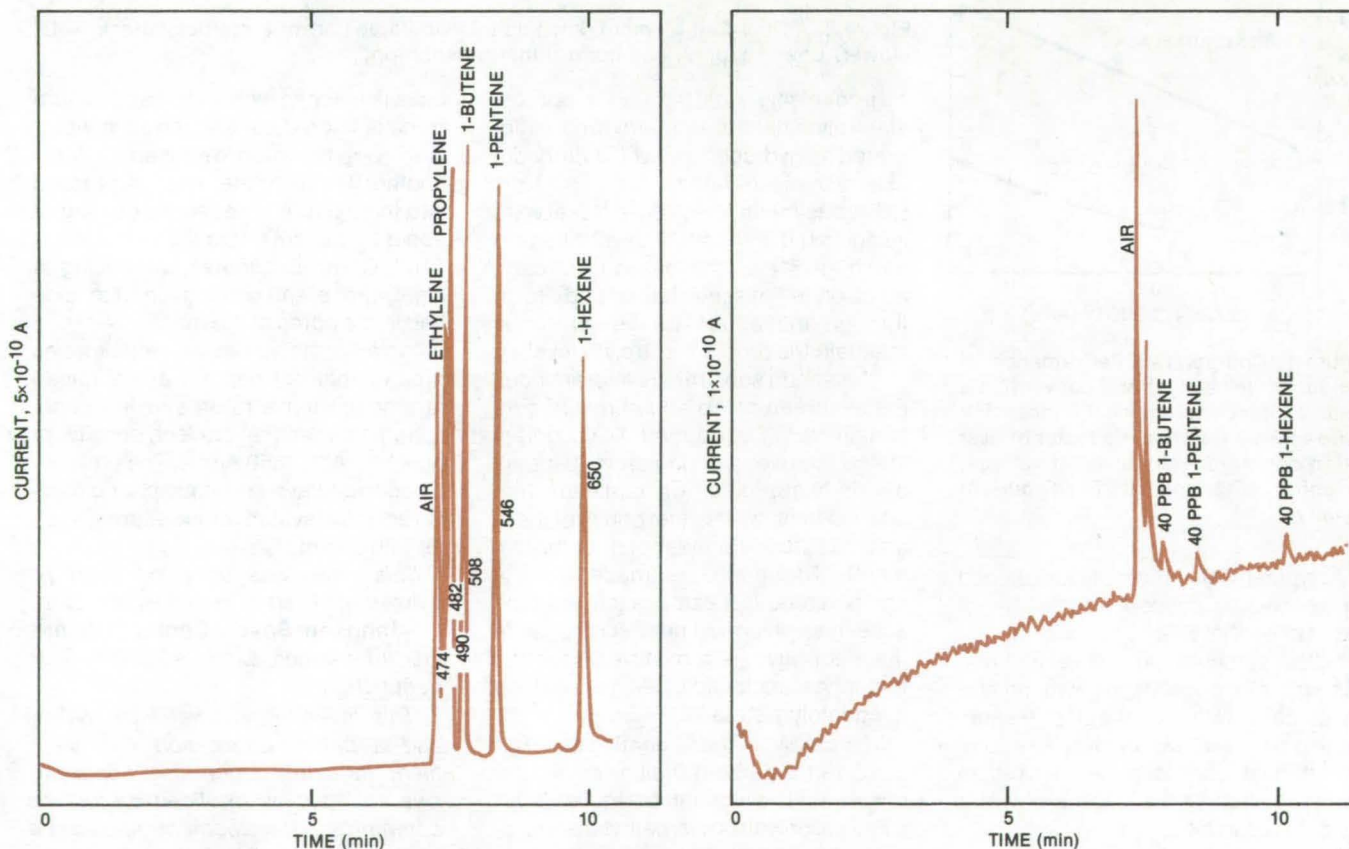
can be used to analyze certain halo-carbons, low-molecular-weight hydrocarbons, hydrogen cyanide, and ammonia, as well as inorganics (water, phosphorus, sulfur, and nitrous gases). It is also suitable for detecting volatiles released from pyrolyzed metals, organics, and geological samples.

A radioactive beta emitter in the ionization detector excites helium gas to a metastable state at 19.8 eV. The metastable helium is sufficiently energetic to ionize nearby atoms and molecules (except neon), which are detected by collecting the ion current at a charged electrode. The current/voltage response has a linear collection region at low voltage, a saturation region where current is voltage-

independent, and an exponential multiplication region at high voltage, resulting from the participation of secondary electrons.

Conventionally, the detector is operated in the multiplication region, where response is high; but so too are background current and noise. To minimize background current induced by atmospheric diffusion, some experimenters have even gone so far as to operate the entire chromatograph in a helium atmosphere.

In contrast, when the detector is operated in its saturation region — where its current output is independent of applied voltage, the result is low background current, low noise, high stability, and high sensitivity. To



The **Detector Response**, when operating in its saturation region, to 17 parts per million of ethylene, propylene, 1-butene, 1-pentene, and 1-hexene is shown in the curve at the left. The curve on the right shows the response to 40 parts per billion. Chromatograph column temperature is 60° C; detector temperature is 175° C; and sample size is 100 microliters.

achieve these conditions, the bucking circuit of a commercial detector is modified for operation in the 20- to 200-volt saturation range and is calibrated to allow absolute measurement of the detector output current. The modified detector has a detection limit in the picogram range for organic compounds (see figure), and its response is linear over more than six orders of magnitude of concentration.

While a conventional detector is operated at a flow rate exceeding 45 cm³/min to suppress the background

and increase stability, the modified detector is stable at flow rates below 20 cm³/min. Moreover, the system does not require expensive research-grade (99.9995-percent-purity) helium; standard high-purity-grade (99.995-percent-purity) helium, most often used in chromatography, gives excellent results while eliminating problems of signal-polarity reversal experienced with certain gases.

Many organic compounds are liquids at room temperature and must be directly injected with a syringe. This

requires a simple modification to a standard commercial injection port to avoid introducing air that could overload the detector and obscure parts of the chromatogram.

This work was done by Everett K. Gibson of Johnson Space Center, Fikry F. Andrawes of Lockheed Engineering and Management Services Co., Inc., and Roswitha S. Brazell of the University of Houston. For further information, Circle 46 on the TSP Request Card.
MSC-18835

Photoproduction of Halogens Using Platinized TiO₂

A powdered photocatalyst dramatically increases the rate of production of I₂, Br₂, and Cl₂.

Langley Research Center, Hampton, Virginia

The halogen molecules, I₂, Br₂, and Cl₂, are produced efficiently by the ultraviolet irradiation of electrolyte solutions containing halide anions (I⁻, Br⁻, Cl⁻) and a suspension of platinized titanium dioxide powder. The new technique requires no external power other than a source of ultraviolet radiation, in contrast to the currently most popular technique for generating these halogens — electrolysis of the salt solutions containing the halide ions, which uses electricity directly to drive the electrolysis reaction.

In electrolysis cells containing n-type semiconductors, light having energy greater than the band-gap energy initiates oxidation processes at the semiconductor/electrolyte interface at smaller (more-negative) potentials than at metal electrodes. This

allows the oxidation/reduction reactions, which normally occur at very low rates or which may be thermodynamically unfavorable, to occur at higher rates in the presence of semiconductors and light. Platinized, powdered TiO₂ can photocatalyze some reactions that otherwise proceed slowly. Such powders are analogous to a system of many short-circuited photoelectrolysis cells; but the powder is less expensive than commercial electrodes, and it has a much higher surface-area-to-weight ratio — an important criterion for a good catalyst.

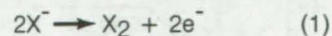
The Pt/TiO₂ powder is prepared by illuminating with ultraviolet radiation a solution of 15 ml platonic acid (H₂PtCl₆), 15 ml glacial acetic acid, and 2 grams of TiO₂ powder. The powder is of the anatase phase and can be doped or undoped. In a typical preparation, the resulting catalytic powder is 1:10 by weight of doped Pt:TiO₂.

Typically, 100 to 200 mg of this catalyst are suspended in a solution containing 35 ml of I⁻, Br⁻, or Cl⁻ salts (about 2M concentration) and irradiated with ultraviolet light from a 1,000-watt high-pressure mercury lamp. After several hours of irradiation, the color typical of the halogen molecule of interest appears in the solution: brown for I₂; yellow-brown for Br₂; yellow-green for Cl₂.

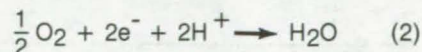
The amount of halogen produced is determined by two methods. In the first method, a known amount of As (III) is introduced into the halide solution. After irradiation, the solution is titrated with iodine in the presence of starch. The difference in the amount of As (III) before and after irradiation indicates the amount of halogen produced. In the second method, the solution is first saturated with O₂, and the reaction cell is closed. After irradiation, the amount of halogen produced is determined by titration in the presence of starch. (In the cases of Br₂ and Cl₂, KI is added before titration.)

The rate of production of halogen is summarized in the table. For comparison, the rate of production of halogen is also given in the presence of unplatized TiO₂ powders.

The reduction of O₂ molecules occurs simultaneously with the halide oxidation. While the halide oxidation occurs on the illuminated side of the particle according to



(where X is the halide ion) oxygen is being reduced on the "dark" side of the particle according to

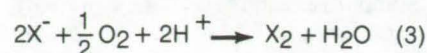


(continued on next page)

Halogen	Micromoles of Halogen Produced After 1 Hour of Illumination	Suspension
I ₂	120	Pt/TiO ₂
I ₂	1	TiO ₂ (anatase)
Br ₂	80	Pt/TiO ₂
Br ₂	0	TiO ₂
Cl ₂	56	Pt/TiO ₂
Cl ₂	0	TiO ₂

Halogen Photoproduction is compared for platinized and unplatized TiO₂ powder. The technique, using platinized TiO₂, produces halogen molecules easily and inexpensively, without using electricity directly.

The overall reaction, therefore, is



The half reaction in equation (2) determines the overall rate of the reaction in equation (3). The Pt on the powders affects the overall rate by decreasing the overvoltage for oxygen reduction.

Other useful reactions could possibly be photocatalyzed or photosynthesized effectively by the plantinized semiconductor powders. The technique can use light, such as solar radiation, and a brine solution containing a suspension of platinized semiconductor powder to produce halogen molecules; or it can be used to oxidize hazardous materials such as CN^- in wastewater or to convert carbon monoxide to CO_2 .

This work was done by Benjamin Reichman of Christopher Newport College and Charles E. Byvik of Langley Research Center. For further information, Circle 47 on the TSP Request Card.

Inquiries concerning rights for the commercial use of this invention should be addressed to the Patent Counsel, Langley Research Center [see page A5]. Refer to LAR-12713.

Recycling Paper-Pulp Waste Liquors

Lignosulfonates are converted to an ion-exchange resin and sugars are recovered.

NASA's Jet Propulsion Laboratory, Pasadena, California

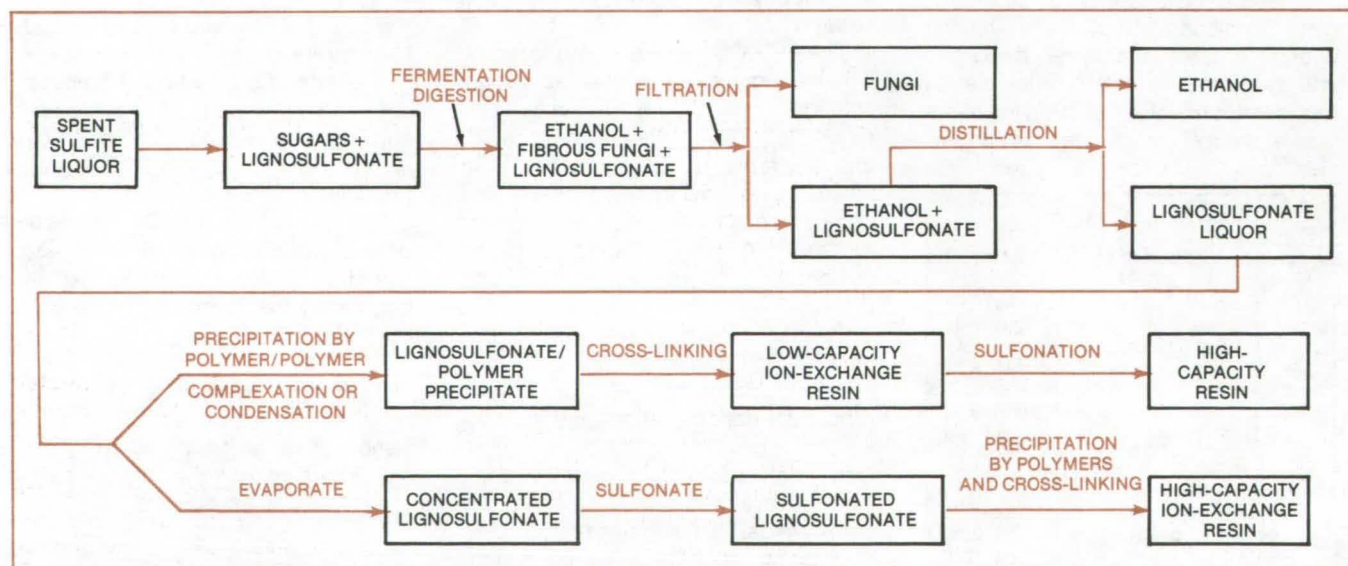
Papermills in the United States annually produce about 3 million tons (1978 figure) of sulfite waste-liquor solids. Although about 10 percent of the solids can be used, disposal of the remainder poses a serious environmental problem for the woodpulp industry. The sulfite waste liquor contains 10 to 15 percent solids, of which approximately 25 percent are monomeric sugars and the balance are lignosulfonates.

Sugars are recovered, and the lignosulfonates are converted to a useful ion-exchange resin in a new pulp-waste-liquor treatment now

under development. In the new process, the sugars are converted to ethanol/single-cell protein and removed by distillation; a gelatin or a polymer similar to polyethyleneimine precipitates the lignosulfonates, which are then cross-linked to form the ion-exchange resin (see figure). Because of its high cost and potential environmental hazard, polyethyleneimine is being considered only as a model for identifying other, more practical, candidates for the process.

In laboratory tests, a 50-percent aqueous solution of sulfite waste liquor containing 13 percent sodium ligno-

sulfonate was mixed with a 10-percent aqueous solution of gelatin. The precipitate, which was highly swollen and rubbery, was separated by centrifugation and vacuum-dried to obtain a 40-percent yield of lignosulfonate/gelatin resin (based on the weight of gelatin added). The swelling and rubberiness of the precipitate are attributed to only the high-molecular-weight lignosulfonates forming a complex with the gelatin. The precipitate was then cross-linked by heating with 37 percent formaldehyde at the boiling point of the aqueous solution for 5 minutes to form a lignosulfonate/



The **Recovery of Lignosulfonates** from sulfite waste liquor involves cross-linking the lignosulfonates to form a solid ion-exchange resin. Contamination of the sugars in the waste liquor is avoided by first converting them to ethanol and removing the ethanol by distillation.

gelatin/formaldehyde ion-exchange resin. The resin formed this way has a relatively-low exchange capacity of 1.3 milliequivalents per gram (dry).

Still better results were obtained when the procedure was repeated using a polyethyleneimine in place of the gelatin. All the lignosulfonates separated, and the supernatant was colorless. The complex that formed

was stable and had an exchange capacity of 1.6 to 1.9 milliequivalents per gram (meg) (compared to about 4.5 meg for commercial resins). The precipitate weight increased as the molecular weight of polyethyleneimine increased. The exchange capacity of the resin was doubled by further sulfonation by a simple heat treatment in 98 percent sulfuric acid (or 30

percent oleum) in the presence of about 20 percent alumina at 250° to 270° C.

This work was done by Mohammad N. Sarbolouki of Caltech for NASA's Jet Propulsion Laboratory. For further information, Circle 48 on the TSP Request Card. NPO-14797

User Chooses Coating Properties

Anodizing technique allows the independent selection of coating thermal emittance and solar absorption.

Langley Research Center, Hampton, Virginia

A versatile thermal-control coating is prepared by modified chromic acid anodizing of aluminum. The coating, with ranges of 0.10 to 0.72 for thermal emittance (ϵ_T) and 0.2 to 0.4 for solar absorptance (α_S), allows the selection of any value of ϵ_T or α_S in the specified range to within an accuracy of ± 0.02 .

Other thermal-control coatings include conversion coating (Alodine), other anodic coatings, and dielectric films and paints. These, however, have limited ranges of ϵ_T and α_S and do not allow the independent selection of these properties.

The variable anodic thermal-control coating process has three phases: initial material processing, anodizing, and material postprocessing. The initial processing prepares the material for anodizing and establishes the initial values of ϵ_T and α_S . The aluminum is immersed in a metal-cleaning bath, rinsed, immersed in a deoxidizer solution, and rinsed by physical agitation to remove all particulates from the aluminum surface.

The aluminum is anodized by immersing it in a chromic acid solution containing 3 to 10 percent CrO_3 (by weight) balanced with water. The voltage is applied between the aluminum and the chromic acid solution at a predetermined rate up to a selected voltage and is maintained for a selected period of time. The rate, voltage, and time, along with the initial values of ϵ_T and α_S , temperature of the chromic acid solution, acid concentration, and material to be anodized, determine the final values of ϵ_T and α_S . Material postprocessing involves rinsing with

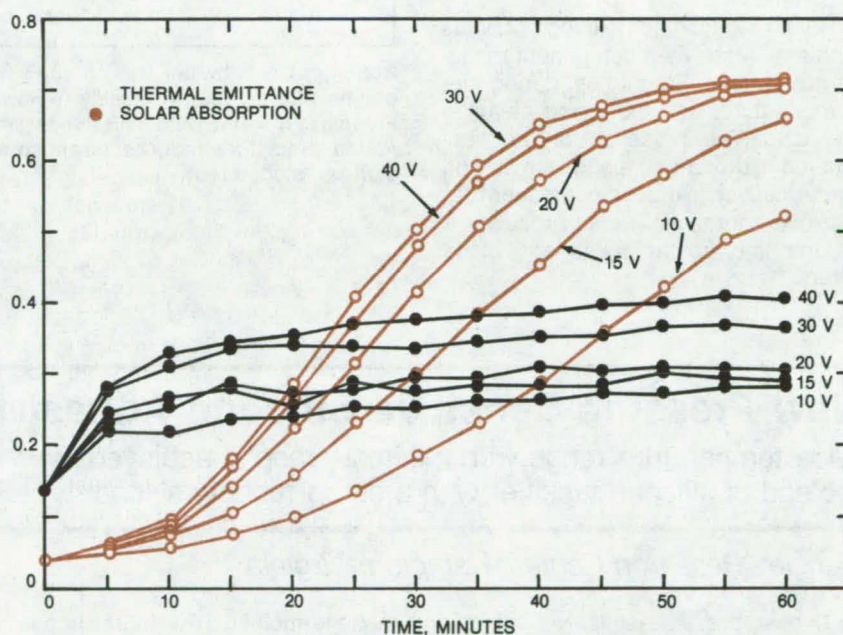
water, placing in a sealing bath of clear water at 180° F (82° C), and drying with filtered forced air.

Typical results are shown in the figure, where ϵ_T and α_S are plotted for various anodizing voltages and times. The anodic process has been applied on 6061, 1145, and 2024 aluminum with thicknesses as low as 0.001 inch (0.003 cm). Preliminary stability tests in vacuum have shown less than 15 percent degradation over a 2,000-hour solar exposure. The technique is sensitive to voltage, the rate of voltage application, time, temperature, acid concen-

tration, material pretreatment, and sealing. However, consistent results are obtained if the processing parameters remain constant.

This work was done by Charles S. Gilliland and Roy J. Duckett of Langley Research Center. For further information, Circle 49 on the TSP Request Card.

Inquiries concerning rights for the commercial use of this invention should be addressed to the Patent Counsel, Langley Research Center [see page A5]. Refer to LAR-12719.



Thermal Emittance and Solar Absorption of the anodic thermal-control coating are shown for various anodizing times and voltages. The cell voltage is increased to the operating voltage in 30 seconds in these examples. Solution temperature is 95° F (35° C), and the pH is 0.5.

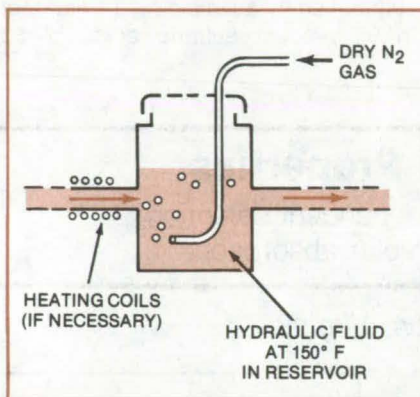
Removing Freon Gas From Hydraulic Fluid

Sparging the heated fluid with dry nitrogen speeds removal and lowers the final level of contamination.

Lyndon B. Johnson Space Center, Houston, Texas

Dissolved Freon gas can be removed from hydraulic fluid by raising the temperature to 150° F (66° C) and bubbling dry-nitrogen gas through the fluid reservoir (see figure). The procedure can be carried out while the fluid is circulating through the hydraulic system. Agitating a liquid with piped-in gas is called sparging; the dry-nitrogen sparging of the hydraulic fluid not only removes gas faster than simple heating does but also results in a lower final level of contamination.

Hydraulic fluid sometimes becomes contaminated when component manufacturers use Freon gas during the manufacture, assembly, and cleaning of parts. The presence of the fluorinated hydrocarbon along with air and water causes hydraulic components to corrode; moreover, it also produces a sludge that contaminates and clogs filters.



Bubbling Dry-Nitrogen Gas through hydraulic fluid at 150° F quickly removes Freon gas from the fluid. This decontamination procedure reduces parts corrosion and sludge formation.

Specifications for Space Shuttle ground-support equipment limit the content of fluorinated hydrocarbon in hydraulic fluid to less than 100 parts per million. In the past, high temperatures were used to reduce the contamination to this level, but other design constraints now limit the fluid temperature to 165° F (74° C) at the most.

An application of the procedure successfully prevented corrosion and sludge resulting from dissolved Freon. The sparging was accomplished simply by immersing a tube in the hydraulic fluid after removal of the reservoir cover.

This work was done by Billy B. Williams, Shirley M. Mitchell, and Theodore S. State of Rockwell International Corp. for Johnson Space Center. No further documentation is available. MSC-18740

New Pressure-Sensitive Silicone Adhesive

Wide temperature range with minimal creep is achieved by a blend of silicone tackifier with a cured rubbery silicone.

Langley Research Center, Hampton, Virginia

A new pressure-sensitive silicone adhesive can be used at high or low temperatures with minimal creep. A blending of silicone tackifier and cured rubbery silicone, the new adhesive can be used without solvents.

Pressure-sensitive adhesives are typically made from a polymer above its glassy transition temperature. The polymers usually have intermediate molecular weight (if they were of lower molecular weight, they would be liquid; and if of higher molecular weight, they would be solid with no tack). The adhesives are prepared from the tacky resins alone or from a blend with other polymers and/or fillers. For silicone systems, the only available pressure-sensitive adhesives are those for which the tacky inter-

mediate-molecular-weight silicone is used alone or in conjunction with mineral fillers. Polymer binders other than silicones have also been used.

Conventional pressure-sensitive silicone adhesives have a tendency to creep or stretch severely when they are placed under a stress or load. Other polymeric binders can alleviate this problem in some instances; however, no other polymer systems have the unique properties of the silicones when temperature extremes (between -115° and 250° C) are experienced.

The new adhesive system is produced by blending an intermediate-molecular-weight pressure-sensitive silicone adhesive, which does not cure, with a silicone resin, which

generally cures with a catalyst to a rubbery tack-free state. The result is a pressure-sensitive silicone adhesive that can be used for structural or load-bearing applications without creeping. The ratio of silicone tackifier to silicone resin can be varied to obtain different degrees of tack, creep resistance, and tensile strength. Various formulations were tested:

- 50/50 (tackifier/cured resin) — tack remains for up to 48 hours, low creepage under load;
- 75/25 (tackifier/cured resin) — tack remains over 3 months, low creepage under load; and
- 80/20 (tackifier/cured resin) — tack remains for over 3 months, creeps under load.

Flatwise tensile strengths of various formulations range from 10 to 19 psi (69×10^3 to 131×10^3 N/m²) at room temperature.

The pressure-sensitive silicone adhesive has been successfully tested at temperatures from -45° to 232° C with

minimal creep under structural loading. It can also be used without solvents in both atmospheric and vacuum environments.

This work was done by James L. Leiffer, William E. Stoops, Jr., Terry L. St. Clair, Vernon E. Watkins, Jr.,

and Thomas P. Kelly of Langley Research Center. No further documentation is available.

Inquiries concerning rights for the commercial use of this invention should be addressed to the Patent Counsel, Langley Research Center [see page A5]. Refer to LAR-12737.

Driving Bubbles Out of Glass

A surface-tension gradient forces gas bubbles to the surface.

Marshall Space Flight Center, Alabama

Gas bubbles have been eliminated from molten glasses by a surface-tension gradient in the melt. The bubbles move to a region of lower surface tension. Since surface tension decreases with increasing temperature in most molten glasses, bubbles rise to the surface if the temperature of the melt increases from bottom to top. Although developed by NASA for possible materials processing in space, the same technique should work for glasses and other liquids in normal gravity.

Traditionally, bubbles have been removed by buoyant "fining," in which the denser glass sinks, forcing the bubbles to move to the surface and burst. In chemical fining, also used to remove bubbles, chemicals are added to the melt to dissolve the gas contained in the bubbles so that they shrink and disappear.

Buoyant fining can be exceedingly slow in viscous glasses. (It does not occur at all in the absence of gravity.) Chemical fining is even slower, espe-

cially for large bubbles, since a sizable volume of gas must be absorbed.

In experiments to test the surface-tension-gradient method on simple borax glasses, 250- μ m bubbles have been moved at rates as high as 30 μ m/s. A few glasses have greater surface tension at higher temperatures, in which case the bubbles migrate to a cooler region. A few other glasses show hardly any variation in surface tension with temperature, and a temperature gradient would be expected to have no effect.

Although the requisite heat for the high-temperature part of the melt can be furnished by stationary electrical or natural-gas heaters, it may also be possible to use induction heating to create a moving hot zone that sweeps through the glass, driving bubbles before it, much as in zone refining of semiconductors. Laser heating is also a possibility, perhaps aiming the beam directly at a bubble to move it along.

The new method could remove the gases that are inevitably generated in

glass processing and which reduce strength and transparency. It may therefore be useful in making glass-to-metal and glass-to-ceramic seals in such devices as high-pressure lamps and cathode-ray tubes; in "gassivating" integrated circuits — that is, coating them with a protective layer of glass; and in applying porcelain enamels to metals. The method may have even broader applications. For example, it may be adapted to removing unwanted bubbles in processes that involve conversions between liquid and solid phases or for controlling bubble formation in flowing fluids to prevent turbulence.

This work was done by D. M. Mattox of Westinghouse Electric Corp. for Marshall Space Flight Center. No further documentation is available.

Inquiries concerning rights for the commercial use of this invention should be addressed to the Patent Counsel, Marshall Space Flight Center [see page A5]. Refer to MFS-25414.

Books and Reports

These reports, studies, and handbooks are available from NASA as Technical Support Packages (TSP's) when a Request Card number is cited; otherwise they are available from the National Technical Information Service.

Less-Toxic Corrosion Inhibitors

Combinations of low-toxicity inhibitors effectively protect aluminum from corrosion in water.

Various combinations of borates, nitrates, nitrites, phosphates, silicates, and sodium mercaptobenzo-

thiazole (NaMBT) were tested for their effectiveness in preventing or reducing the corrosion of aluminum parts immersed in corrosive freshwater. The inhibitors are intended to replace chromates and other water additives that are effective against corrosion but are subject to governmental restrictions.

The inhibitors were tested in combination because when used individually, they are only partly effective.

(continued on next page)

The chemicals were added to a corrosive test solution of distilled water containing 138 parts per million (ppm) sodium bicarbonate, 148 ppm sodium sulfate, and 165 ppm sodium chloride. Also present in some of the tests were 0.2 ppm copper sulfate. Test specimens of 2219-T87 aluminum were cut into small sheets, immersed in 300 ml (10 oz) of solution, and stored at room temperature. Exposure times varied from 1 to 14 months, depending upon the amount of corrosion observed and upon the nature of the solution.

Of 50 inhibitor combinations tested, 8 are effective and compare favorably with sodium chromate. While highly

alkaline solutions are normally corrosive to aluminum, it was nevertheless observed that the most effective inhibitor combinations contained trisodium phosphate and were alkaline.

One disadvantage of the successful inhibitor combinations is that each must be formulated with the prescribed amounts of four to six of the chemicals mentioned above, with a total concentration of 500 to 1,000 ppm, whereas only 100 to 200 ppm of sodium chromate are required for effective inhibition. Under extended service (longer than 6 months) or the nonmonitoring of concentrations, the inhibitor dosage should be increased to allow for depletion. From an

economic point of view, inhibitors that are effective at low concentration are preferred.

This work was done by T. S. Humphries of Marshall Space Flight Center. Further information may be found in NASA TP-1279 [N78-28226/NSP], "Low Toxic Corrosion Inhibitors for Aluminum in Fresh Water" [\$5]. A paper copy may be purchased [prepayment required] from the National Technical Information Service, Springfield, Virginia 22161. The report is also available on microfiche at no charge. To obtain a microfiche copy, Circle 50 on the TSP Request Card. MFS-25496

Computer Programs

These programs may be obtained at very reasonable cost from COSMIC, a facility sponsored by NASA to make new programs available to the public. For information on program price, size, and availability, circle the reference letter on the COSMIC Request Card in this issue.

Diffusion in Single-Phase Binary Alloys

Exact solutions for systems with planar, cylindrical, or spherical interfaces

The DBAS 1 computer program provides the analyst with a set of simple algorithms for exact solutions of diffusion in single-phase binary/alloy systems with planar, cylindrical, or spherical interfaces. This exact approach typically takes much less time than finite-difference calculations.

The analysis of diffusion-controlled processes requires the prediction of the interaction between different components for a given set of exposure equations. Exact solutions are available in the literature for diffusion in single-phase binary-alloy systems with constant diffusion coefficient and zero-flux boundary conditions. These solutions, however, have not been widely utilized because of their complexity and convergence problems.

Two algorithms are provided for each of the three interface geometries. One algorithm converges rapidly for short diffusion times; the other algorithm converges rapidly for long diffusion times. The algorithms in the DBAS 1 program, along with an established methodology for selecting the appropriate algorithm for a given situation, can rapidly solve diffusion problems.

For planar geometry, the long-time algorithm is a trigonometric solution. The short-time algorithm is the classical double-error-function solution

generalized to account for multiple reflections.

For cylindrical geometry, the long-time algorithm is based on Bessel functions and the roots of a Bessel equation. The short-time algorithm involves integration, using a Gauss-Legendre quadrature formula, over a modified Bessel function.

For spherical geometry, the long-time algorithm is based on roots of a trigonometric equation. The short-time algorithm involves error functions.

DBAS 1 is written in FORTRAN IV for batch execution and has been implemented on a CDC 6600 computer with a central memory requirement of approximately 33K (octal) of 60-bit words. The program was developed in 1979.

This program was written by Darrel R. Tenney of Langley Research Center and Jalaiah Unnam of VPI and State University. For further information, Circle B on the COSMIC Request Card. LAR-12665

Life Sciences



**Hardware,
Techniques, and
Processes**

- 457 Cardiopulmonary Data-Acquisition System
- 458 Microprocessor-Controlled Ultrasonic Plethysmograph
- 459 Microprocessor-Based Cardiotachometer
- 460 Improved Microbe Detection in Water Samples
- 461 Gage for Evaluating Rheumatoid Hands
- 462 Fiber-Optics Couple Arthroscope to TV
- 463 Beef Grading by Ultrasound

Cardiopulmonary Data-Acquisition System

A computerized system controls stress tests and displays real-time physiological data.

Lyndon B. Johnson Space Center, Houston, Texas

A computerized cardiopulmonary data-acquisition system controls and monitors bicycle and treadmill cardiovascular stress tests. It acquires and reduces stress data and displays in real time the heart rate, blood pressure, workload, minute volume, respiratory rate, exhaled-gas composition, and other variables.

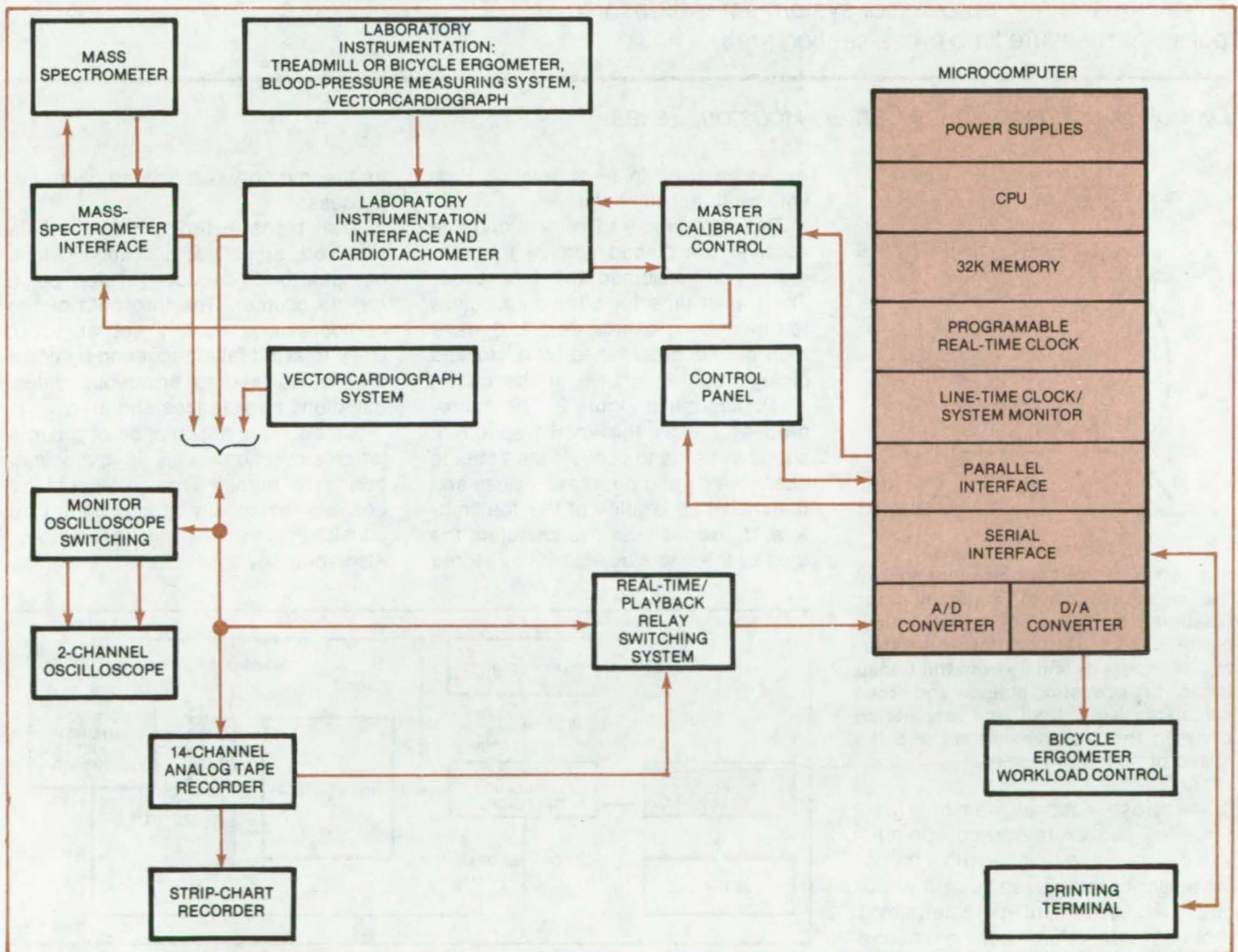
A block diagram of the microcomputer-based system is shown in the figure. The data are printed on a hard-copy ter-

minal every 30 seconds so that the operator can quickly respond to the subject throughout the test. The ergometer workload is controlled in real time according to the experimental protocol, and the collected data are stored directly on tape in analog form and on floppy disks in digital form for posttest data processing.

One of the main advantages of the system is its simplicity. Many conventional near-real-time data-collection

systems are more difficult to use or lack automatic calibration and accurate exhaled-gas analysis. Others have no real-time data display or are not as easily adapted to changing test requirements.

Major system components include a microcomputer operating with assembly-language and higher-level-language programs, a custom analog signal interface and control unit, a
(continued on next page)



The **Block Diagram of the Cardiopulmonary Data-Acquisition System** shows the flow of data and control signals. A self-calibrating function compensates for drift or small changes in gain. The most critical calibrations (mass-spectrometer calibrations for the three respiratory gases) are checked through the entire system before each test and during the automatic calibration sequence.

beat-by-beat (nonaveraging) cardiometer [also see "Microprocessor-Based Cardiometer" (MSC-18775) on page 459 of this issue], and a mass-spectrometer interface/control. Many of the components are commercially available.

The system includes a multipole latching relay panel for switching to backup operating modes. All automatic functions can be overridden at the flip of a switch, and testing can continue even if major components fail, including the microcomputer.

A computer control panel with seven labeled pushbutton switches is used for executing a stress test. Once the stress program is started, only those switches that are illuminated under program control can be used. (Unilluminated buttons are deactivated). The only electrical connections to the test subject are those of the ECG machine.

This work was done by William G. Crosier and Roy A. Reed of Technology Inc. for Johnson Space Center. Further information may be found in:

NASA CR-160608 [N80-33083/NSP], "Final Report on the Cardiopulmonary Data Acquisition System, Version 2.0, Volume 1, User's Guide" [\$7]; and NASA CR-160609 [N80-33084/NSP], "Final Report on the Cardiopulmonary Data Acquisition System, Version 2.0, Volume 2, Detailed Software/Hardware Documentation" [\$12].

Copies of these reports may be purchased [prepayment required] from the National Technical Information Service, Springfield, Virginia 22161.
MSC-18783

Microprocessor-Controlled Ultrasonic Plethysmograph

A noninvasive microprocessor system times ultrasonic pulses to measure limb cross-section area.

Lyndon B. Johnson Space Center, Houston, Texas

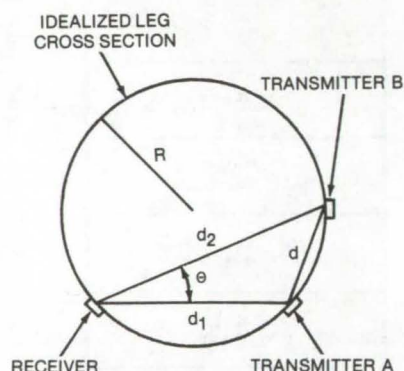


Figure 1. For the **Area Measurement** of the cross section of a person's leg (assumed to be round), a microprocessor-based plethysmograph determines chords d_1 and d_2 from the transit times of acoustic pulses and then calculates area from the separation between the two transmitters and the speed of sound in tissue.

The cross-sectional area of a person's leg can be measured noninvasively, safely, and reliably with a microprocessor-based ultrasonic plethysmograph (an instrument for determining changes in the volume of an organ or a limb). The automated instrument is easy to operate and requires no calibration. Since the new plethysmograph does not confine leg movement,

it can be used in tests relating limb volume to activity level.

Two ultrasonic transmitters and one receiver are placed against the subject's calf, assumed to be circular. The transit time for ultrasonic pulses to travel along chords d_1 and d_2 (see Figure 1) is determined by a clocked binary counter, shown in the circuit block diagram in Figure 2. The microprocessor uses the known speed of sound in tissue to convert the times to distances d_1 and d_2 ; these values and the known separation of the transmitters, d , are then used to calculate the area of the circle by algorithms stored

in the memory associated with the processor.

The transmitted ultrasound is received, amplified, and applied to a comparator to produce a stop pulse for the counter. The threshold of the comparator is usually set at about 0.2 V to avoid false triggering by noise that would lead to erroneous determinations of distances and area.

Although the assumption of a circular cross section is only an approximation to a human limb, it should be possible to modify the program to consider more realistic geometries. Also, for many applications the change

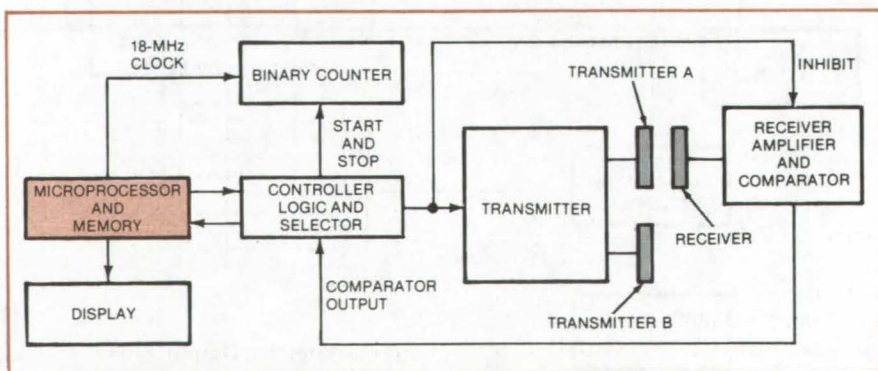


Figure 2. The **Two-Transmitter Ultrasonic Plethysmograph** is designed around an 8080 microprocessor. The controller logic and selector control the flow of information through the system, select a transmitter for a chord length measurement, and provide a count proportional to the measured transit time for display. The transmitted ultrasound is received and used by the comparator to stop the binary counter.

in area rather than the absolute area is of interest, and in these cases the error introduced by assuming a circular cross section is not very large.

Analysis of other factors affecting the system accuracy shows that errors due to body-temperature changes and timing roundoff are insignificant. Also,

the uncertainty in chord length caused by variations of the comparator threshold affects the area precision by less than 1 percent.

This work was done by P. K. Bhagat and V. C. Wu of the University of Kentucky for **Johnson Space Center**. For further information, including cir-

cuit diagrams and equations for calculating limb area, Circle 51 on the TSP Request Card.

Inquiries concerning rights for the commercial use of this invention should be addressed to the Patent Counsel, Johnson Space Center [see page A5]. Refer to MSC-18759.

Microprocessor-Based Cardi tachometer

Heart rate is measured with better than 1 percent accuracy in rest or exercise stress testing.

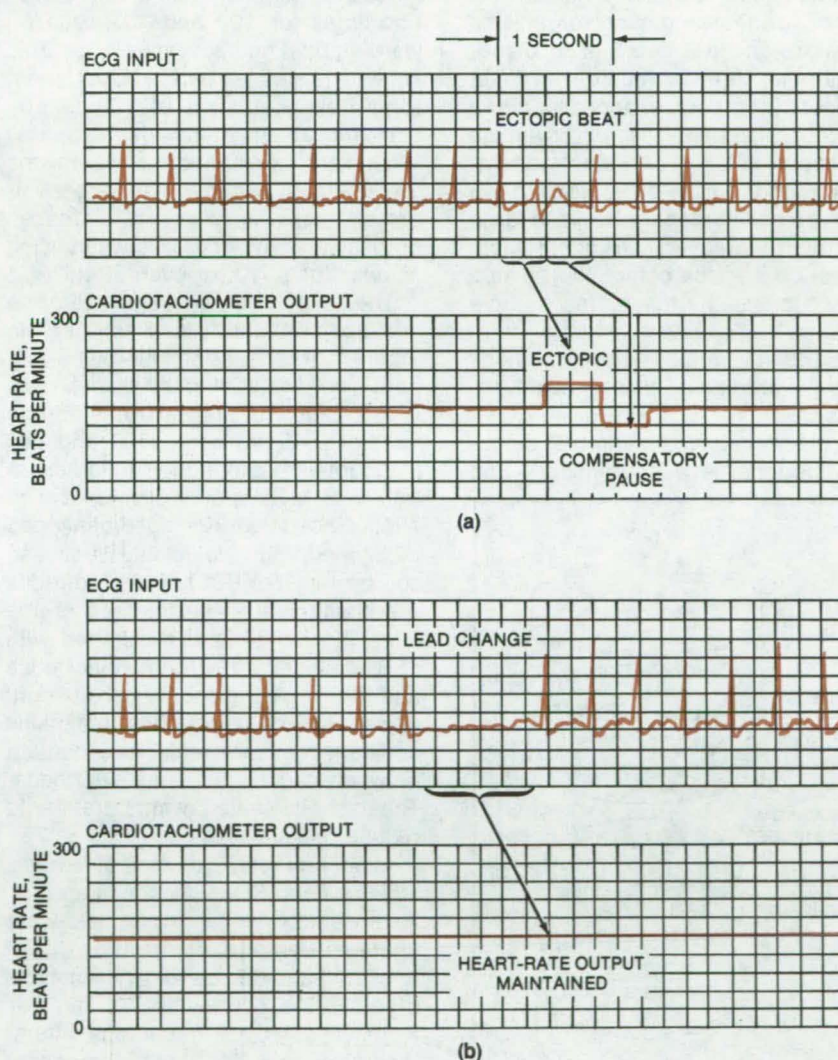
Lyndon B. Johnson Space Center, Houston, Texas

A new cardi tachometer operates reliably even with stress-test electrocardiogram (ECG) signals that are subject to noise, baseline wandering, and amplitude change. The unit, successfully used in a stress-test facility for over a year, records heart rate via a preamplified, single-lead ECG input signal and produces both digital and analog heart-rate outputs, which can be fed to other instruments or computers. [Also see "Cardiopulmonary Data-Acquisition System" (MSC-18783) on page 457 of this issue.] The accuracy of the unit is better than 2 percent over the full range, 30 to 300 beats per minute, and is typically better than 1 percent up to 230 beats per minute.

Analog hardware, including a filter for ECG noise rejection and an improved R-wave detector, processes the ECG input signal, producing a 10-ms pulse for each heartbeat. The resulting pulse train is analyzed by a microprocessor computer program stored in a 2-kilobyte erasable programed read-only memory (EPROM).

As the recordings in the figure show, the program, written in Assembly language, can identify ectopic (irregular) heartbeats and maintain a stable output during signal interruptions that occur during ECG lead switching.

Since the analysis logic is part of the computer program, it can be easily modified. For example, the present program produces a heart-rate output computed from the period of time between the two most recent beats. The program can be revised for additional or different features, such as a continuously-updated averaged heart-rate output or digital filtering.



Cardi tachometer Output Signal recording (a) shows heart-rate changes with an ectopic beat, but recording (b) does not show any heart-rate change during a longer interruption caused by ECG lead switching. The microprocessor program contains the decisionmaking logic for interpreting such ECG signal artifacts. The time intervals interpreted as indicating various artifacts depend on the current heart rate, on when an early ectopic beat has occurred, and the like. The program updates these reference values with each heartbeat.

The unit also includes internal heart-rate calibration signals of 60 and 180 beats per minute. These are derived from the crystal-controlled clock controlling the microprocessor.

This work was done by William G. Crosier and John A. Donaldson of Technology Inc. for Johnson Space Center. Further information may be found in NASA CR-160607 [N80-33082/NSP], "Final Report — A Mi-

croprocessor-Based Cardiometer" [8]. A copy may be purchased [prepayment required] from the National Technical Information Service, Springfield, Virginia 22161. MSC-18775

Improved Microbe Detection in Water Samples

Combined membrane filtration and electrochemical detection give fast response and better detection of low concentrations.

Langley Research Center, Hampton, Virginia

Two techniques, membrane filtration and electrochemical microbial detection, are combined in a new method for detecting micro-organisms in water samples. When used alone, membrane filtration requires at least 24 hours for growth to appear, and an operator must be available to examine and count colonies. The electrochemical method, on the other hand, often misses small numbers of cells in large volumes. Moreover, an appreciable lag period elapses before the buildup of enough cells for a measurable response. The new technique combines the advantages of both methods while overcoming these disadvantages.

In electrochemical microbial detection, the time between challenge and

the initial increase in voltage is a function of the number of cells in the inoculum. For *Escherichia coli*, detection times for 10^5 and 10^1 cells/ml were 4 and 8 hours, respectively. This lag time is dictated by the requirement for a cell population of 10^6 to 10^7 cells/ml at the time of response. When very low numbers of organisms are present, especially in large volumes, there is also an increased probability of missing cells when using samples of 1, 10, or even 50 ml.

The experimental setup for the combined method is illustrated in Figure 1. It consists of a 60- by 15-mm petri dish, two absorbent pads 47 mm in diameter, a standard membrane filter of 0.45- μ m pore size, and two platinum-wire electrodes in a length ratio of 2:1. Cells are collected by the filter placed on an absorbent pad moistened with 2.0 ml of Trypticase soy broth (TSB,BBL); the electrodes are positioned on the surface of the filter. The other pad, moistened with TSB, is placed on top of the electrodes and filter. A retainer ring at right angles to the electrodes maintains constant pressure and close contact between pads, filter, and electrodes. The dish is sealed with parafilm to reduce moisture loss.

In dose-response studies of *Escherichia coli* and *Staphylococcus aureus*, volumes from a tenfold series were filtered. Bacteria from 100 ml of undiluted and 10^{-1} and 10^{-2} dilutions of estuarine or freshwater samples were collected on membrane filters. Viable counts for both the dose-response studies and the water samples were made by spreading appropriate dilutions from a tenfold series on Trypticase soy agar (BBL) and counting colonies after 24 hours incubation at 35° C.

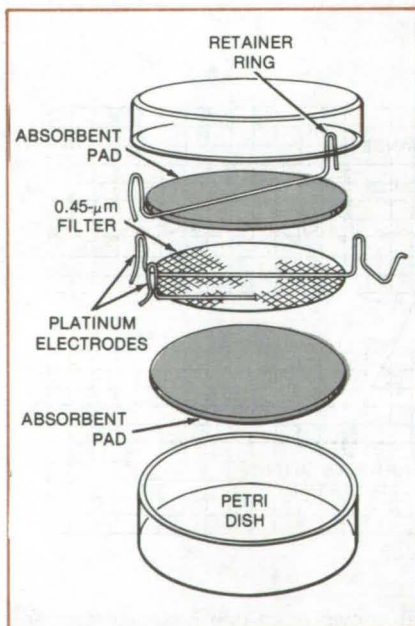


Figure 1. The experimental Apparatus for the Combined Technique requires only standard, commercially-available laboratory items.

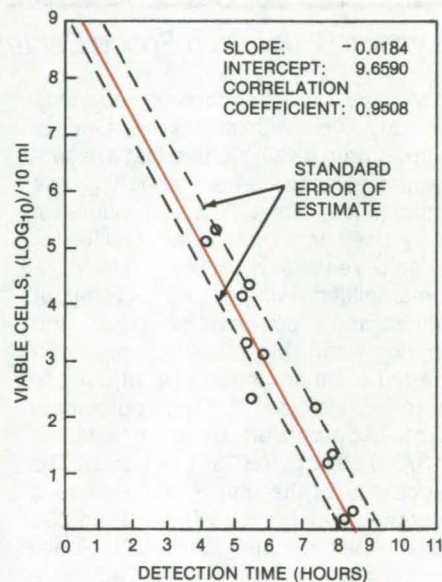


Figure 2. The relationship between the Number of "*Escherichia coli*" Cells retained on membrane filters and detection times obtained with the platinum electrode electrochemical method is shown here.

Prior to connecting the electrodes to the strip-chart recorder, each channel was set at a zero reference point. The 25-mm and 50-mm electrodes were connected to the positive and negative terminals, respectively, of the recorder. The electrodes were allowed to equilibrate for 60 to 80 minutes before establishing a baseline that was generally offset slightly from the recorder zero reference point in the positive direction. Responses upward from the baseline were considered positive and downward as negative. Detection time endpoints (lag time) were recorded as the time between challenge and the initial increase in voltage.

The dose-response curve for *Escherichia coli* is illustrated in Figure 2, and the linear regression parameters are shown. These results compare favorably with previously published data in which platinum electrodes were tested in a broth/test-tube experiment. Favorable results were also achieved with 50 estuarine and 46

freshwater samples tested with the combined technique. Results with *Staphylococcus aureus*, however, were erratic and not reproducible. The overall results indicate that the combined technique can be an effective and rapid method for estimating the microbial loading of water samples.

This work was done by Judd R. Wilkins and David C. Grana of

Langley Research Center and Susan C. Fox of The Bionetics Corp. For further information, Circle 52 on the TSP Request Card.

Inquiries concerning rights for the commercial use of this invention should be addressed to the Patent Counsel, Langley Research Center [see page A5]. Refer to LAR-12709.

Gage for Evaluating Rheumatoid Hands

Lateral mobility of knuckle joints is measured simply and reliably.

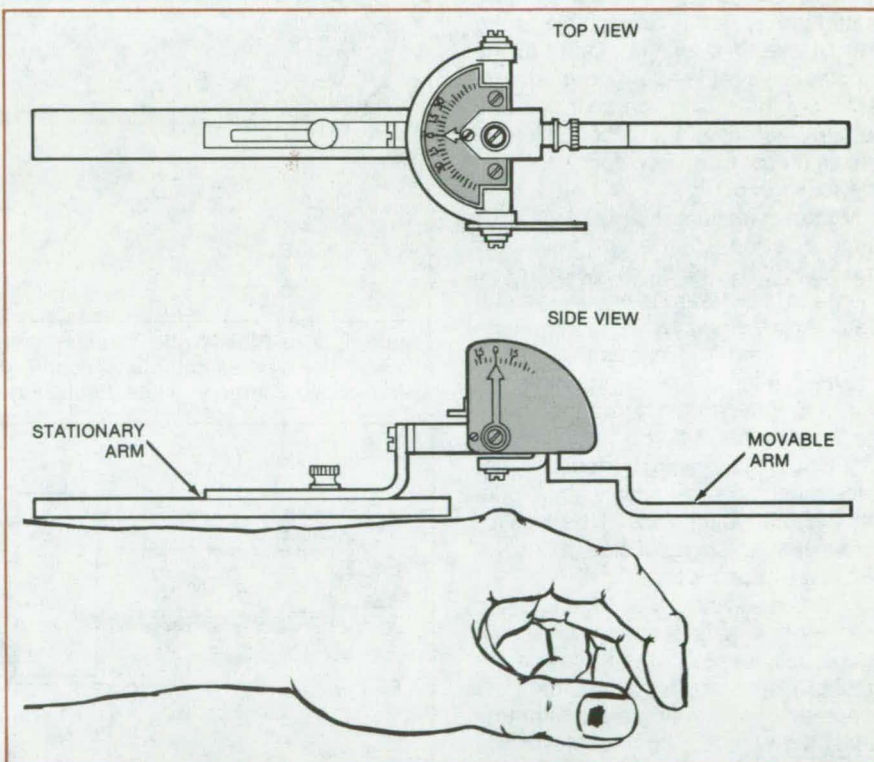
Goddard Space Flight Center, Greenbelt, Maryland

A two-axis goniometer accurately measures the movements of the fingers about the metacarpophalangeal (knuckle) joints. It can be used to help diagnose hands that have structurally changed because of rheumatoid arthritis. The new goniometer measures lateral movement of a knuckle joint when it is flexed 70° to 90°. This lateral movement is small in normal joints but increases in diseased joints.

The new diagnostic instrument, constructed of stainless steel and brass, basically consists of two connected protractors that simultaneously measure angles in perpendicular planes. The goniometer dials are offset to clear the bony protuberances that result from rheumatoid arthritis. Extension and offset adjustments span any size hand. The pivots are friction damped, so that readings are retained even if the goniometer is accidentally jostled. The unit weighs about 4.5 ounces (128 grams).

The movable arm of the goniometer operates in two mutually perpendicular planes (see figure), a plane perpendicular to the back of the hand (dorsal-volar plane) and a plane through the bones of the forearm (radio-ulnar plane). The measurement procedure begins by drawing a line on the middle of the back surface of each finger, along its axis. The stationary platform arm of the goniometer rests on the back of the hand in alignment with the bones between the knuckle and wrist of the fingers being measured. It is held in position by the measurer.

The knuckle joint is flexed 70° to 90° with the movable goniometer arm aligned with the line drawn on the finger.



The **Two-Axis Goniometer** measures flexion in the radio-ulnar plane (top view) and in the dorsal-volar plane (side view). The dial offset shown in the side view accommodates protuberances at the joint.

With the joint flexed the finger and goniometer are passively moved in the radio-ulnar plane, and the total range of motion is recorded.

The two-axis goniometer and measurement procedure can be used with a minimum of training. Reliability studies show very good agreement of measurements by the same and by different measurers. The accuracy and reliability of measurement are important in as-

essment and treatment planning, in the documentation of joint changes over time, and for gathering research data.

This work was done by James C. Houge and Kenneth A. Plautz of the University of Wisconsin for **Goddard Space Flight Center**. For further information, Circle 53 on the TSP Request Card.

GSC-12610

Fiber-Optics Couple Arthroscope to TV

A hand-held flexible coupler links the arthroscope to a color-TV camera.

Langley Research Center, Hampton, Virginia

A new, hand-held coupler images the output of an arthroscope onto a coherent fiber bundle. The image travels along the flexible bundle and appears at the other cable end, where the image is recollimated by a lens. The image seen looking into this lens is the same as if looking directly into the arthroscope.

The arthroscope allows surgeons to examine internal structures and organs through a small incision or natural opening in the body. Its output is a collimated image that is acceptable to the normal eye. If a lens is placed at the eyepiece, a real image is formed. Projection of the real image on a color-TV camera increases the image size and makes it easier to view, enhancing the surgical procedure.

Methods for directly coupling a TV camera to the arthroscope have several problems. First, the camera is bulky and is awkward to handle in a surgical environment. Second, the time taken to wrap the camera in sterile drapings often exceeds the time required to perform the operation. Third, the 6- to 10-pound (3- to 5-kg) camera is difficult to hold for long periods. Finally, since the image size is only about one-fifth the major dimension of the monitor screen, the actual resolution of the system is less than optimal.

In the new system (see Figure 1), the image intensity is reduced somewhat by the bulk losses in the fiber and the Fresnel losses at the fiber ends. (The oriented 10-micron fibers are 3 meters in length.) With moderate quality fibers and short cable lengths, however, the losses are not significant. The collimated output is directed into the lens of the TV camera. The camera-lens focal length is chosen so that the image will fill the monitor screen.

The hand-held portion of the coupler is shown in Figure 2. The handle permits easy positioning and rotation of the

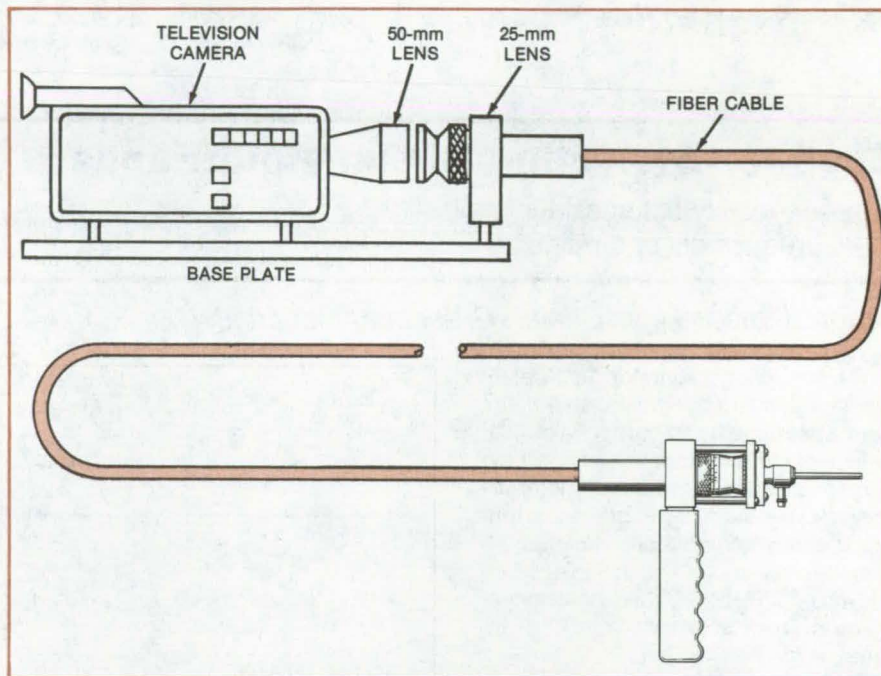


Figure 1. The **Fiber-Optic Coupler** links an arthroscope with a color-television camera. The flexible cable and hand-held coupler make it easy to manipulate the arthroscope in surgery, while displaying the arthroscope image on the TV monitor.

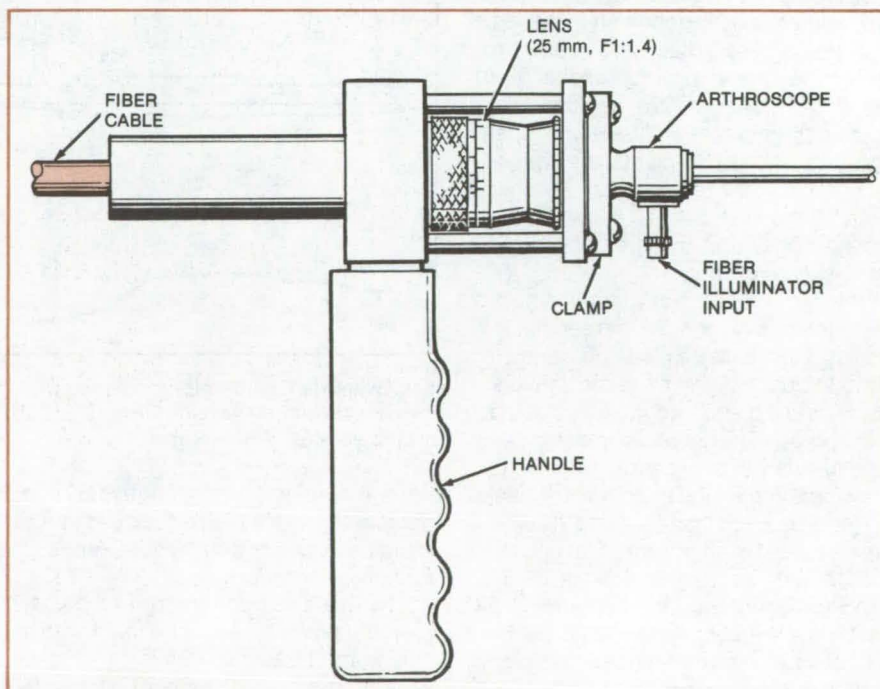


Figure 2. The **Hand-Held Portion** of the coupler has a pistol grip and a lens for imaging the arthroscope output on the fiber bundle.

arthroscope. The ultimate resolution of the system is limited by the resolution of the arthroscope and TV monitor (routine resolution is better than 100 mi-

crons). In addition to its medical applications, the coupler can be used for engine inspection, instrument repair, and visual inspection through small openings.

This work was done by John M. Franke and David B. Rhodes of **Langley Research Center**. No further documentation is available.
LAR-12718

Beef Grading by Ultrasound

The richness of reflections in ultrasonic A-scan signatures indicates the USDA grade of beef.

NASA's Jet Propulsion Laboratory, Pasadena, California

A proposed method for grading beef quality uses ultrasonic inspection. In the method, the grade of beef carcasses is determined by analysis of the ultrasonic A-scan signatures from the marbling within the muscle. Since the reflections from within the muscle are determined primarily by the fat/muscle interface, the richness of such reflections is a direct indication of the degree of marbling and quality. The method is intended to replace the present subjective method of sight and feel of individual USDA graders and ultimately to yield both the grade and yield of live cattle.

Though no work has been done on live animals, tests on butchered-beef specimens indicate a definite trend between ultrasonic signatures and grade. A typical scan of each grade is shown in Figure 1. The reflection content is seen to be greater for the better grades; i.e., prime is richer in reflections than the other grades, and the reflection content of standard is poorer than the other grades.

The area studied was about 1 inch (2.54 cm) below the surface of the steak. The external fat was trimmed off and the transducer aimed in the direction shown in Figure 2. The

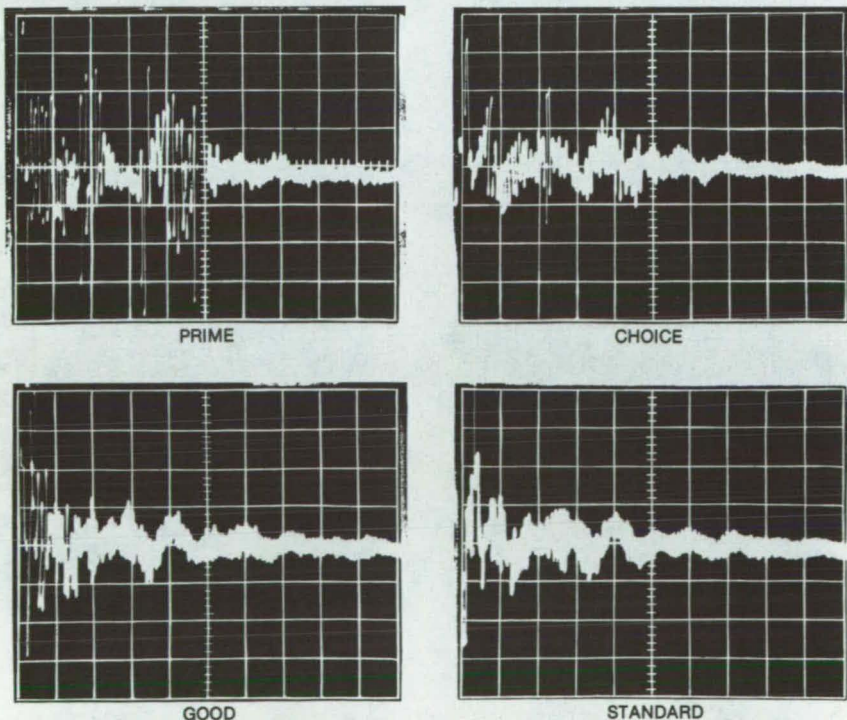


Figure 1. Typical Ultrasound Patterns for four USDA grades show the decrease in richness of reflections from best quality (prime) to lesser quality (standard) beef.

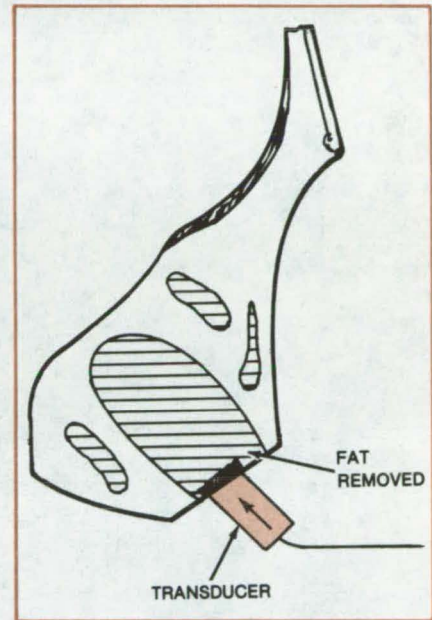


Figure 2. The Ultrasonic Transducer is positioned and oriented on the meat to measure the marbling and quality. The fat has been removed so that the signal attenuation is reduced.

electronics were gated so that the picture displayed covers the range of 20 to 70 mm from the transducer, each graticule division being 5 mm. The reflection content or the density of moderate-amplitude (about 1-graticule-high) reflections is an indication of the fine structure of a specimen.

As the sound wave propagates through fluid and soft tissues of the body, about 0.01 to 1 percent of the energy is reflected back toward the transducer at each interface. If the interface is approximately perpendicular to the transducer, a strong specular reflection is received, and the distance of the interface from the transducer can be measured with an
(continued on next page)

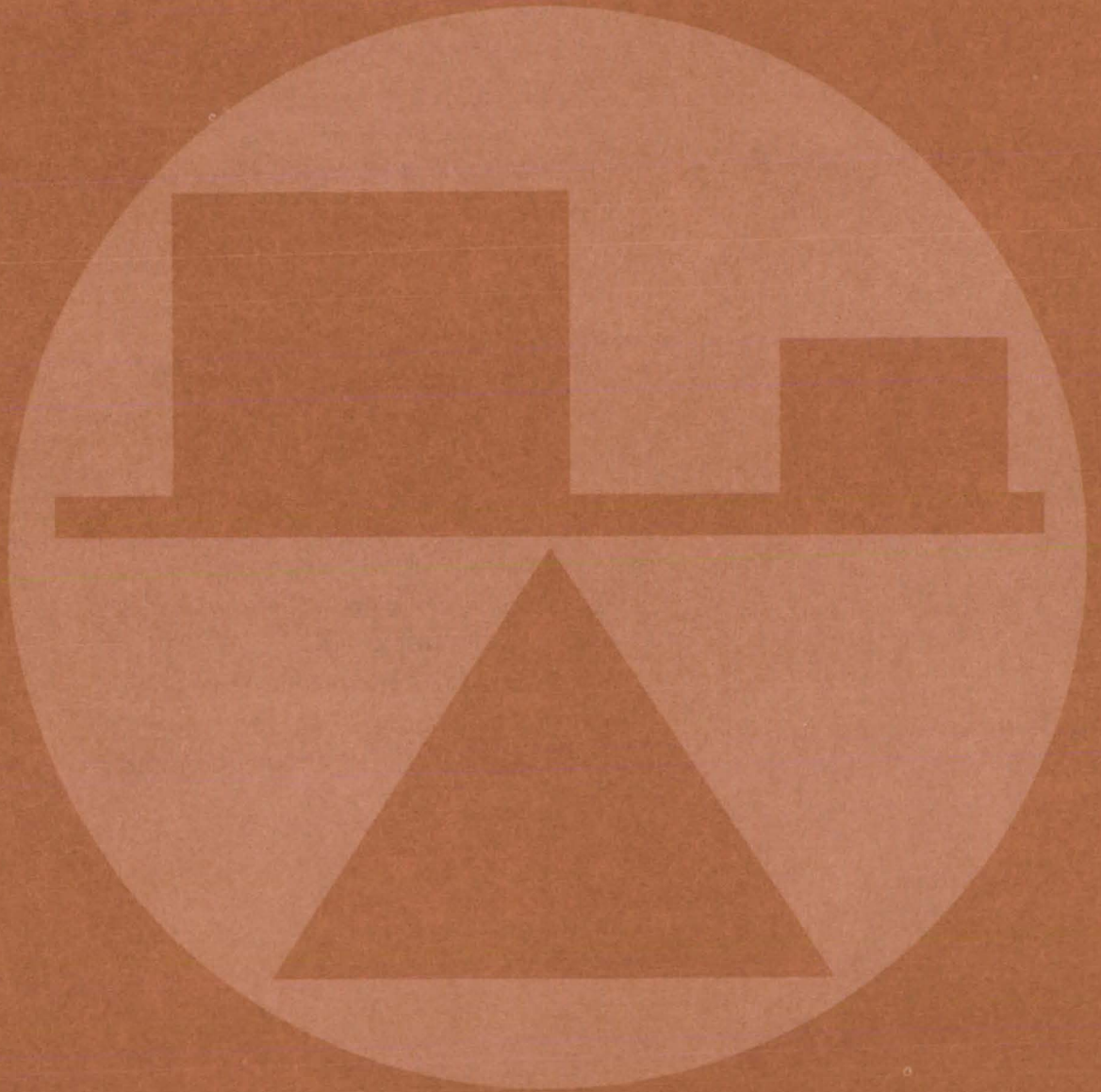
A-scan instrument.

In the feasibility experiments performed, a 2.25-MHz unfocused ultrasonic transducer of 0.5 in. (1.27 cm) diameter and moderate damping was used to transmit and receive direct and specular reflections from different

tissue areas of marbled beef. The 2.25-MHz ultrasonic bursts were 20 milliwatts in power and lasted about 1 microsecond. A wideband receiver without a rectifying detector was used in order not to reduce the information content of the signal.

*This work was done by Paul M. Gammell of Caltech for **NASA's Jet Propulsion Laboratory**. For further information, Circle 54 on the TSP Request Card.*
NPO-14812

Mechanics



Hardware, Techniques, and Processes

- 467 An Oven for Many Thermocouple Reference Junctions
- 468 Isolation and Measurement of Rotor Vibration Forces
- 469 Improved LEEM Ranges Over Four Decades
- 470 Imager Displays Free Fall in Stop Action
- 471 Transducer for Extreme Temperatures and Pressures
- 471 Bulk Lifetime Indicates Surface Contamination
- 472 Biaxial Method for In-Plane Shear Testing
- 474 Gas Absorption/Desorption Temperature-Differential Engine
- 474 Instrument Measures Cloud Cover
- 475 Compact Infrared Detector
- 476 Fast Calibration of Gas Flowmeters
- 477 Wind-Simulation Tester for Solar Modules
- 478 Heat Pipes Cool Probe and Sandwich Panel

Computer Programs

- 479 Thermodynamic and Transport Properties of Air/Water Mixtures
- 479 Calculating Linear A,B,C, and D Matrices From a Nonlinear Dynamic Engine Simulation
- 480 Structural Design With Stress and Displacement Constraints
- 481 An All-FORTRAN Version of NASTRAN for the VAX
- 481 Potential Flow in Two-Dimensional Deflected Nozzles
- 481 The Design and Analysis of Low-Speed Airfoils
- 482 Transonic Flow Over Wing/Fuselage Configurations

An Oven for Many Thermocouple Reference Junctions

A compact oven holds many junctions at a stable temperature.

Dryden Flight Research Center, Edwards, California

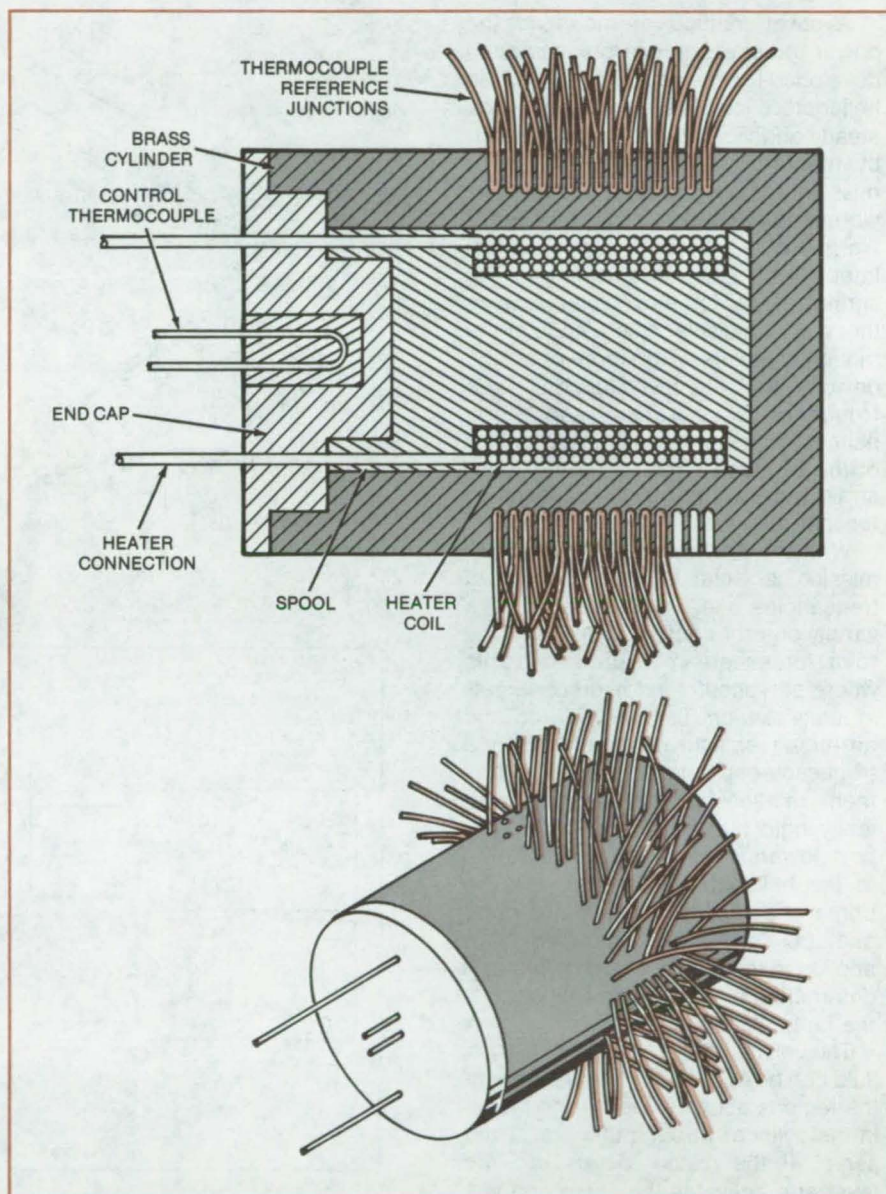
Thermocouples are widely used for temperature measurement because they are inexpensive and reliable. They are accurate if their reference junctions are held at a constant known temperature. When many reference junctions are mounted in an oven for stable temperature control, temperature gradients in the oven or among the junctions may require special heating arrangements or special calibration measures.

To prevent nonuniformity in junction temperature, a compact, lightweight, multijunction oven has been designed with a symmetry of geometry, heating, and thermocouple-junction location (see figure). The oven has a cylindrical wall made of a material that is a good thermal conductor, such as brass. Inside the cylinder is a cylindrical heating coil, wound on a spool that is also made of brass. The end cap that closes the cylinder extends into the spool, with a temperature-sensing element (shown here as a control thermocouple). The sensor controls the power supplied to the heating coils so as to maintain the cylinder wall at a constant temperature.

Numerous holes are bored radially into the cylinder wall, and the thermocouple junctions are inserted in these holes. Because of their common distance from a common heating coil in a good conductor, the junctions are held at a common temperature.

This oven was originally developed for an airborne data-acquisition system used in flight tests. Its light weight, compactness, and low-power requirements, compared to other ovens for the same purpose, allowed the use of more thermocouples than would have been possible otherwise.

This work was done by Louis P. LeBlanc of Dryden Flight Research Center. For further information, Circle 56 on the TSP Request Card.



All of the **Thermocouple Reference Junctions** mounted in this cylindrically symmetrical oven are held at the same stable temperature.

This invention is owned by NASA, and a patent application has been filed. Inquiries concerning nonexclusive or exclusive license for its

commercial development should be addressed to the Patent Counsel, Dryden Flight Research Center [see page A5]. Refer to FRC-10112.

Isolation and Measurement of Rotor Vibration Forces

Active vibration isolators couple transmission gearbox to helicopter frame and provide load measurement.

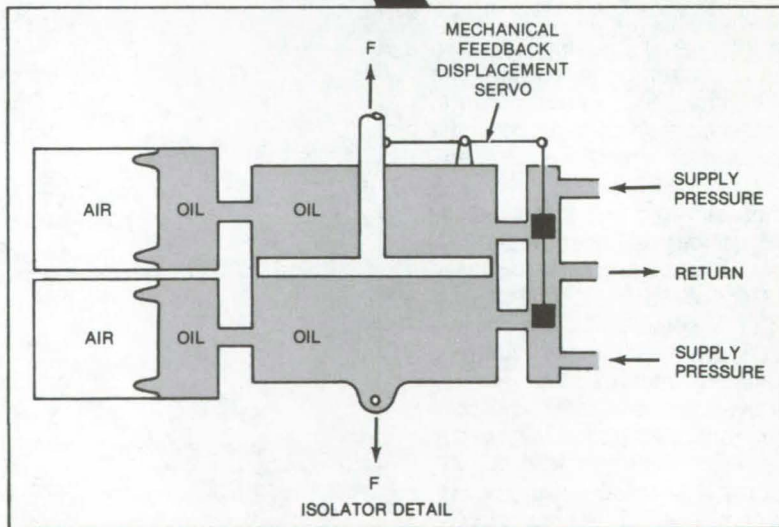
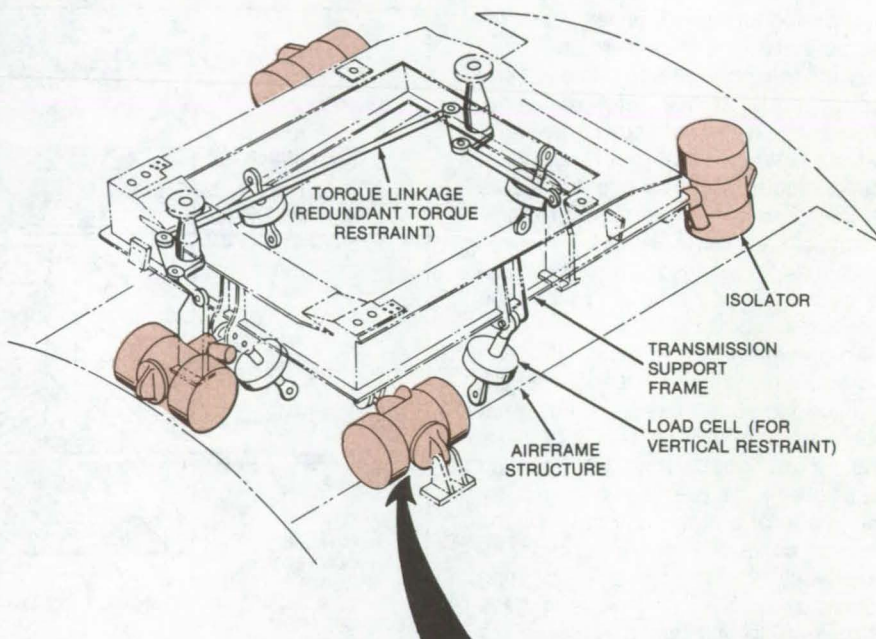
Langley Research Center, Hampton, Virginia

A novel method of mounting the power transmission gearbox has been developed for use on a NASA research helicopter. This system measures the steady and vibratory forces generated by the rotor and isolates the transmission from the airframe so that rotor vibrations are substantially reduced.

Previously the transmission was isolated from the airframe either by springs or by force-opposing devices that create a displacement node at the mounting points. The force-opposing devices are effective for only one frequency of vibration; and since neither method includes measurement of the vibration forces from the rotor, strain gages would have to be installed for that purpose.

With the new mounting, the transmission is isolated over a range of frequencies allowing the testing of a variety of rotor configurations, and the rotor forces are measured at points where servocontrolled hydropneumatic units attach the gearbox to the airframe (see figure). The units have a frequency-dependent load/displacement relationship that gives a statically rigid but dynamically soft support, lowering the vibration transferred to the helicopter. The units are the primary load path between the rotor and the airframe; thus the loads applied to the airframe by the rotor are determined by measuring the loads in the units.

The unit is "active" in that hydraulic fluid can be supplied under pressure to the regions above or below the piston in the cylinder through the use of the servo. If the piston moves up, the lever arm activates the servo and lets oil into the top region and lets oil out of the lower region. High-pressure fluid is pumped into the top of the cylinder until the piston is recentered — hence the static rigidity of the mounting. At frequencies above about 2 Hz, however, too little fluid can be pumped in to change loads, so the air in the air reservoirs acts as a simple pneumatic spring — hence the dynamic softness. Load is measured simply by meas-



Four Vibration Isolators restrain the transmission support frame against in-plane motion. For the current configuration, standard load cells are used for vertical restraint; however, they could be replaced by vibration isolators.

uring the differential pressure across the piston.

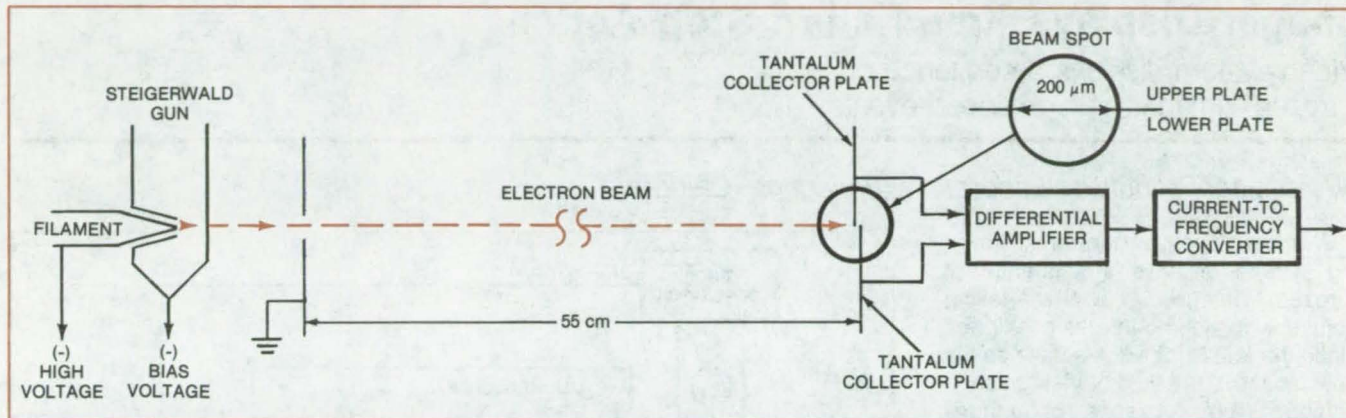
This work was done by Irwin Kenigsberg and John F. Madden of United Technologies Corp. for **Langley Research Center**. Further information may be found in "The RSRA

Active Isolation/Rotor Balance System." A copy may be purchased [\$7, paper copy; \$3, microfiche] from the Technical Information Service, American Institute of Aeronautics and Astronautics, Inc., 555 West 57th Street, New York, New York 10017. [Request document A79-18654.] LAR-12476

Improved LEEM Ranges Over Four Decades

A low-energy electron magnetometer would be suitable for terrestrial and aerial magnetic-field measurements.

Langley Research Center, Hampton, Virginia



A Beam of Low-Energy Electrons strikes two tantalum collector plates, and the differential current is amplified and converted to frequency. The current difference increases as the beam deflection increases, providing a measure of the local magnetic field. The drawing is not to scale.

A proposed new low-energy-electron magnetometer (LEEM) would measure magnetic fields as low as 10^{-3} nanotesla. Its anticipated performance in selected applications compares favorably with that of more-complex high-resolution magnetometers.

Other magnetometers currently available include pivoted needle instruments, compensation-type variometers, fluxgate instruments, proton precession magnetometers, optically pumped magnetometers, and the highly-sensitive superconducting quantum interference device (SQUID) magnetometer. A SQUID magnetometer is essentially a superconducting flux transformer tightly coupled to a SQUID.

The SQUID and the optically pumped magnetometers can meet the 0.01-nT sensitivity requirement of many geomagnetic and interplanetary field measurements. However, the SQUID requires liquid helium for its operation and thus seems more appropriate for laboratory measurements. The sensitivity of the LEEM compares favorably with that of optical absorption magnetometers. Using modern solid-state technology, LEEM response time can be reduced to the microsecond range for analyzing fast magnetic transients and for magnetic-signature analysis in large engineering systems.

Fraction of Instrument Range	Ratio of Actual to Measured Magnetic Field	Actual Field, nT
0.001	1.0000	0.059
0.01	1.0000	0.59
0.05	0.9996	2.95
0.10	0.9983	5.90
0.20	0.9933	11.80
0.30	0.9848	17.70
0.40	0.9727	23.60
0.50	0.9566	29.50
0.60	0.9363	35.40
0.70	0.9109	41.30
0.80	0.8796	47.20
0.90	0.8400	53.00
1.00	0.7854	59.00

Predicted LEEM Response to fields over a range of four decades is shown in this table.

The improved LEEM is diagramed in the figure. The low-energy monoenergetic electron beam would be produced by high Rydberg atoms, by photoionization, or by a hot-filament source. Calculations show that if the current from each collector plate is fed to a current-to-frequency converter with a conversion factor of $1 \text{ Hz}/10^{-14} \text{ A}$, the system sensitivity would be about $4.31 \times 10^4 \text{ Hz/nT}$. Thus, a measurement of magnetic fields as low as 0.01 nT could be made with high accuracy in a 1-second counting time. A measurement of 0.1 nT could be made with moderate accuracy in a counting time of 10 milliseconds.

The response of the new LEEM to magnetic fields from 0.059 nT to 59.00 nT is shown in the table. As seen, the LEEM is linear to ± 1 percent over three decades, from under 10^{-2} nT to over 10^1 nT. Since the nonlinearity of the instrument is known, it is easily corrected for, extending the useful range to four decades, from 5.9×10^{-3} nT to 5.9×10^1 nT.

This work was done by Jag J. Singh and George M. Wood, Jr., of Langley Research Center, Grayson H. Rayborn of the University of Southern Mississippi, and Frederick A. White of Rensselaer Polytechnic Institute. Further information may be found in (continued on next page)

NASA TM-80172 [N80-13429/NSP], "A Low Energy Electron Magnetometer" [\$4], a copy of which may be purchased [prepayment required] from the National Technical Informa-

tion Service, Springfield, Virginia 22161.

This invention is owned by NASA, and a patent application has been filed. Inquiries concerning nonexclu-

sive or exclusive license for its commercial development should be addressed to the Patent Counsel, Langley Research Center [see page A5]. Refer to LAR-12706.

Imager Displays Free Fall in Stop Action

Video system displays a sequence of "frozen" images of high-speed events.

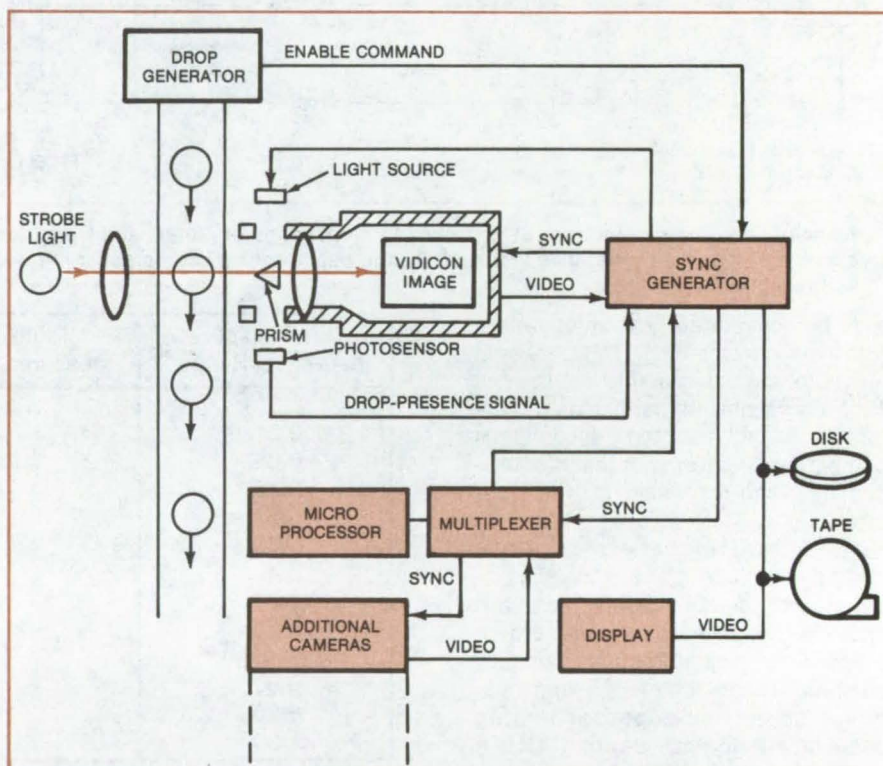
NASA's Jet Propulsion Laboratory, Pasadena, California

A microprocessor-controlled imaging system displays a sequence of "frozen" images of a free-falling object using video cameras positioned along the fall. Strobe lights flash as the object passes the field of view of each camera. The sequence of images stored on video disk and displayed on a television monitor is a stop-action record of the dynamics of the falling object. With appropriate modifications, the system can monitor other high-speed phenomena using one or several cameras.

The basic configuration, developed to observe the dynamics of hollow liquid glass pellets formed by a drop generator, is shown in the diagram. As the generator releases a molten bubble, it generates an enable pulse that initiates the camera sequence.

As the object enters the field of view of each camera, photosensors detect light reflected from its surface and fire the strobe light. The photosensor signals also activate the video multiplexer and establish the connection to the first track on the video disk. At the beginning of the next available television frame, determined by the sync generator, a scan of the camera commences, and the video information is written on the disk. The arrival of the object in the field of view of the next camera initiates an analogous sequence, resulting in a series of single-frame exposures recorded on disk and displayed on the TV screen.

The enable pulse creates an erase scan in the camera to clear the system and establishes the black level. The beam or scan drive can be returned to x and $y = 0$ to wait the next command. This prevents loss of the image by leakage if the object arrives midframe.



In the **High-Speed Imager** the drop generator outputs an enable command that initiates the sequence for visualizing the moving bubble. Each strobe light is controlled to flash during the camera retrace period. The system utilizes the intrinsic capability of the vidicon or CCD camera to store the image until it is scanned.

A microprocessor accepts the enable command from the drop generator and controls the cameras. It also supervises the writing of the image pixels on the video disk. The strobe light is triggered by sync pulses from the microprocessor. Similarly, the multiplexer function of the microprocessor enables the cameras in sequence and synchronizes the video format. The microprocessor can also be programmed to image a single object in a train of objects by rejecting objects that arrive at the cameras at

the wrong time.

The system can be modified to use a charge-coupled-device (CCD) camera and a strobed circular LED array arranged around the camera lens instead of the strobe light. In addition the image can be digitized by the microprocessor.

This work was done by Robert E. Frazer of Caltech for NASA's Jet Propulsion Laboratory. For further information, Circle 58 on the TSP Request Card.
NPO-14779

Transducer for Extreme Temperatures and Pressures

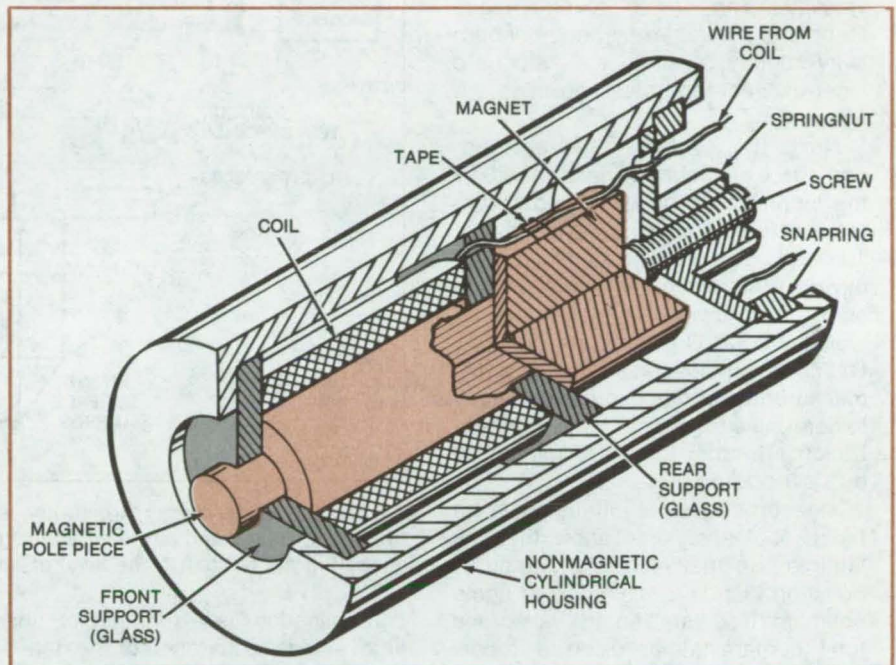
Transducer functions under high pressure and in vacuum.

Lyndon B. Johnson Space Center, Houston, Texas

An improved transducer with a temperature limit of 500° C and a pressure limit of up to 10 kilobars responds to mechanical vibrations up to 20 kHz. Constructed of high-temperature-resistant materials, the new vibration pickup should perform well in nuclear reactors, turbines, and other extreme environments. Outgassing and "virtual" leakage, problems experienced at very low pressures with previous transducers potted in epoxy, are eliminated by using only glass and metal supports. The interior is open to the atmosphere to prevent the buildup of pressure-induced stresses.

As with other transducers of this type, the new pickup senses the motion of a magnetic material attached to the test object. The motion changes the flux in a magnetic pole piece within a pickup coil, which generates an emf and current in the external circuit. A magnet attached to the pole piece biases the transducer at its operating point.

The transducer parts (see figure) are supported and positioned in a nonmagnetic housing. Glass supports orient the magnetic pole piece centrally and axially. Since the supports are open to the external atmosphere, there is no differential pressure on them. The magnet, which is Alnico 8 or similar material, clamps to the pole piece magnetically. All of the parts are held firmly against the housing shoulder by a snap-



The **Pole Piece** of the transducer is attached to the test object and measures its mechanical vibration. By holding the parts against the housing with a spring, distortion due to pressurization and thermal strain is eliminated.

ring, a springnut (a flanged nut that can apply a bending load to a mating shoulder), and a screw. The coil, which is held in place by the glass spacers, is made of ceramic-insulated copper wire, or similar material.

To relieve strain on the electrical connection, insulated copper leads are welded to the coil terminations, taped

to the magnet, and exit through the springnut. Holding the parts against the housing with a spring also reduces distortion due to pressurization and thermal strain.

This work was done by Harry Nadler of Rockwell International Corp. for Johnson Space Center. No further documentation is available.
MSC-18778

Bulk Lifetime Indicates Surface Contamination

An indirect measurement of wafer surface impurities has a sensitivity of 300 monolayers.

NASA's Jet Propulsion Laboratory, Pasadena, California

A new method of determining the level of surface contamination on semiconductor wafers has a sensitivity of approximately 10^{10} impurities per cm^2 . Surface contamination of this magnitude results, on heat treatment, in a bulk impurity concentration of

10^{12} cm^{-3} (for a sample 0.02 cm in thickness), which is sufficient to degrade the minority-carrier recombination lifetime.

In the new technique, a sample is annealed at high temperature to redistribute the surface impurities

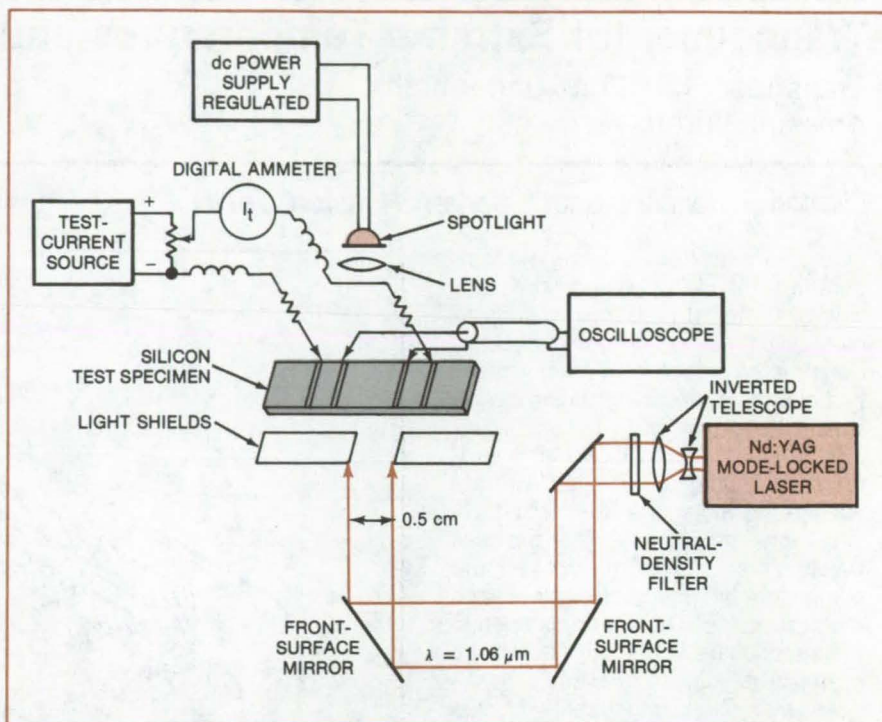
uniformly throughout the bulk. The bulk impurity concentration is determined before and after annealing by measuring the recombination lifetime. The method can be used to evaluate wafer-cleaning techniques, to qualify
(continued on next page)

the purity of chemicals and deionized water used in these techniques, or to monitor a production process.

In tests to evaluate cleaning procedures, specimens are cut from high-resistivity silicon. Contacts are applied, and the surface is etched to control the surface recombination velocity. The initial recombination lifetime is measured by photoconductivity decay, using the standard laser-excited apparatus shown in the figure.

Next, the contacts are removed, and the wafer surface is cleaned by the technique to be evaluated. High-temperature annealing, typically at 1,000° C in a mixture of 95 percent oxygen and 5 percent hydrochloric acid, is followed by slow cooling, typically at 1° C per minute, to 200° C. The recombination lifetime is again measured by photoconductivity decay to determine the bulk impurity concentration. Thermal traps are minimized by slow cooling.

Measurements of lifetime as a function of rinse time show that the lifetime is a maximum (i.e., impurity concentration is a minimum) at some optimum rinse time. An analysis of the total contamination, using a model that postulates that the cleaning solution leaves a residue of salts, yields an expression for the net



Photoconductivity-Decay Apparatus is used to determine the bulk recombination lifetime in semiconductor materials. Impurity levels in the bulk before and after annealing are related to the level of surface contamination.

contamination as a function of rinse time. A least-squares fit of the data to this expression determines the optimum rinse time.

This work was done by Phillip D.

Blais of Westinghouse Electric Corp. for NASA's Jet Propulsion Laboratory. For further information, Circle 59 on the TSP Request Card. NPO-14966

Biaxial Method for In-Plane Shear Testing

A method for obtaining uniform shear deformation yields more accurate values for material mechanical properties.

Langley Research Center, Hampton, Virginia

A biaxial method for measuring in-plane shear properties applies a more-uniform shearing deformation to orthotropic and isotropic materials than uniaxial picture-frame techniques. The forces applied by the biaxial method are one-half the magnitude required by the uniaxial method, reducing the transmitted force and consequently reducing pin deformations.

In the biaxial method, shown in Figure 1, a square sandwich specimen is installed in a very stiff fixture with pinned corners. Equal tensile and compressive forces are applied along the frame diagonals through the corner pins. The frame deformation, depicted

in Figure 2b, creates a parallelogram with sides that are straight and unchanged in length. With the conventional, uniaxial method of loading, the sides are extended and bent, as shown in Figure 2a.

The deformation caused by the biaxial method is that required to subject the test specimen to a uniform shear strain. For orthotropic or isotropic materials, this is equivalent to subjecting the material to a uniform shear stress.

The tensile load is applied vertically by a standard tensile-test machine, and the compressive load is applied horizontally by a hydraulic cylinder, load cell, and tension bar. The compressive

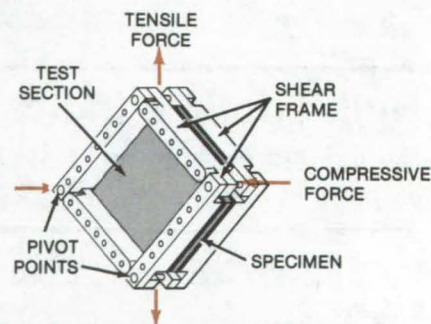


Figure 1. In the Biaxial Method, the square sandwich specimen is installed in a very stiff frame with pinned corners. Applied loads are one-half those required in the uniaxial method.

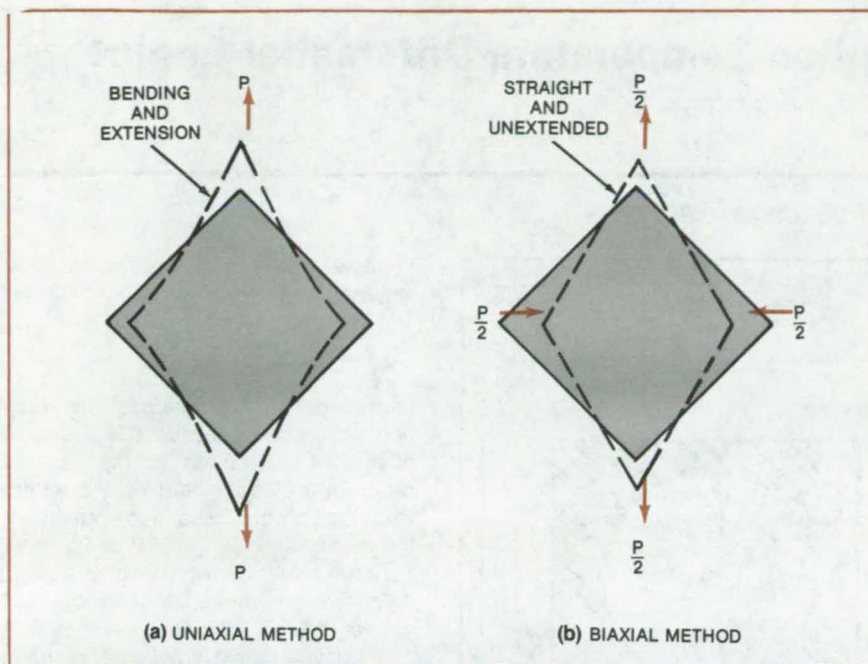


Figure 2. The Uniaxial and Biaxial Deformations are compared. The uniaxial method (a) causes the edges to undergo both extension and bending; the biaxial method (b) deforms the frame into a parallelogram with sides that are straight and unchanged in length.

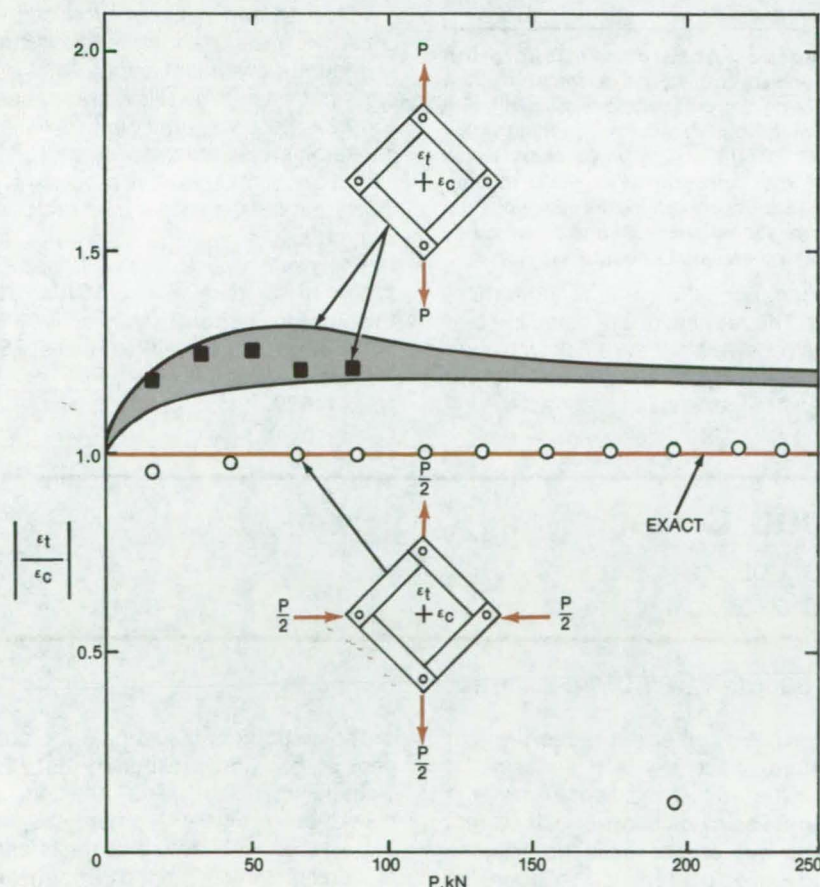


Figure 3. Strain Ratio Data are shown in the shaded area for the uniaxial method; biaxial data falls along the straight line $|\epsilon_t/\epsilon_c| = 1$, indicating a uniform shearing deformation.

load is measured by the load cell, while the tensile load is measured by a similar transducer built into the tensile-test machine. Output from both load cells is recorded electronically. A test machine with biaxial load capability (tension and compression) could also be used.

To quantify the difference between uniaxial and biaxial loading, four identical aluminum-faced sandwich specimens with aluminum honeycomb core were fabricated and instrumented with strain gages. Three of the specimens were tested uniaxially to failure. The fourth was initially tested uniaxially in the elastic range and then tested biaxially to failure. Results of these tests are shown in Figure 3, where the average value of the principal tensile-to-compressive strain ratio $|\epsilon_t/\epsilon_c|$ over the specimen face is plotted as a function of total applied load.

A specimen subjected to a uniform shearing deformation will exhibit equal principal tensile and compressive strains, yielding a strain ratio of 1. The three uniaxially tested specimens (data in shaded area) did not exhibit a uniform shear deformation, either in the elastic or inelastic range. The fourth specimen (data denoted by squares) showed similar behavior when tested uniaxially in the elastic range. However, when tested biaxially to failure, a uniform shearing deformation was achieved in both the elastic and inelastic regions (circles along $|\epsilon_t/\epsilon_c| = 1$).

In addition, tests showed that frictional effects in the shear frame and loading apparatus had a negligible effect on the experimental results. Also, the stiffening effect of honeycomb core on the in-plane shear response of a sandwich panel was identified, and a method was found for considering this effect.

This work was done by Harold G. Bush of Langley Research Center and Tanchum Weller of the National Academy of Sciences. Further information may be found in NASA TM-74070 [N78-21489/NSP], "A Biaxial Method for Inplane Shear Testing" [5]. A copy may be purchased [prepayment required] from the National Technical Information Service, Springfield, Virginia 22161. LAR-12680

Gas Absorption/Desorption Temperature-Differential Engine

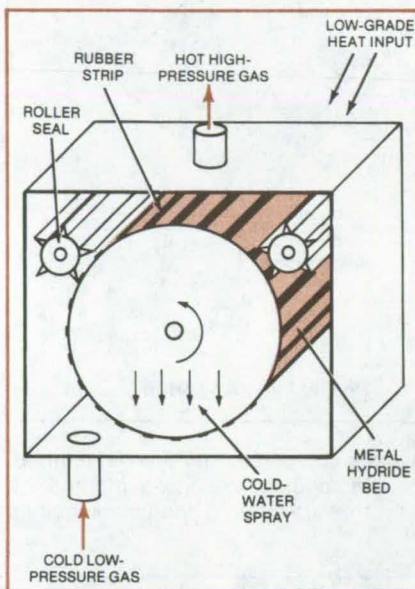
Almost 90 percent of gas-turbine-plant energy can conceivably be converted to electricity.

NASA's Jet Propulsion Laboratory, Pasadena, California

A compressor concept is proposed that would be well suited to work in conjunction with a continuous Brayton-cycle gas-turbine plant for converting high-temperature energy to electricity. The compressor operating in a continuous mode would assist the plant in converting almost 90 percent of heat to electricity. Conventional turbine plants work in a batch mode and operate at 40 percent efficiency.

The compressor would utilize a reversible metal hydride reaction to supply hydrogen that would serve as the working fluid. The hydrogen gas would be compressed by cyclic absorption/desorption in a metal hydride matrix embedded on a rotating drum (see figure). The absorption process would release heat, and the desorption process would absorb low-grade heat.

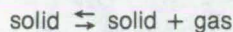
Two thermal inputs could be used to operate the hydride compressor: a low-temperature input ($T \approx 100^\circ \text{C}$), supplied by low-grade solar, geothermal, or waste heat; and a cold low-pressure gas input. For a continuous-acting heat pump that would replace a batch process, fixed locations for the heat would be maintained, and the absorbent material would be moved on a drum from one temperature region to the other and back. The compressed hot gas from the continuous-acting temperature-differential absorption/desorption



Proposed Absorption/Desorption Compressor would use a metal hydride matrix on the outer surface of a rotating drum to generate the working gas, hydrogen. The rolling valve seals would allow the compressor to work continuously. During operation, the gas would be absorbed to release heat and desorbed by absorbing low-grade heat.

gas pump could then go to the turbine plant. The rotating drum, being in compression, need not be thick and thus would allow good heat exchange between its inner and outer surfaces.

Metal hydrides are not the only substances that can be used on the rotating drum. Any reactant of the form:



can be used. The choice of the reaction would be based on the speed of absorption/desorption in the desired temperature range and on the effectiveness of the roll seal used outside of the drum.

Some materials would not seal well. A gas leak would be tolerable but would reduce efficiency. A possible sealing alternative would be to have the roller in the form of a toothed star, as shown, that meshes with rubber seal strips on the drum. The active material on the drum would then be between the rubber strips.

The proposed concept promises to conserve nuclear and fossil fuels and to reduce powerplant capital and operating costs. When low-grade heat sources become abundant, existing gas-turbine powerplants can be modified to accommodate this process and thus increase the output by a factor of 2 or more.

This work was done by Charles G. Miller of Caltech for NASA's Jet Propulsion Laboratory. For further information, Circle 60 on the TSP Request Card.
NPO-14528

Instrument Measures Cloud Cover

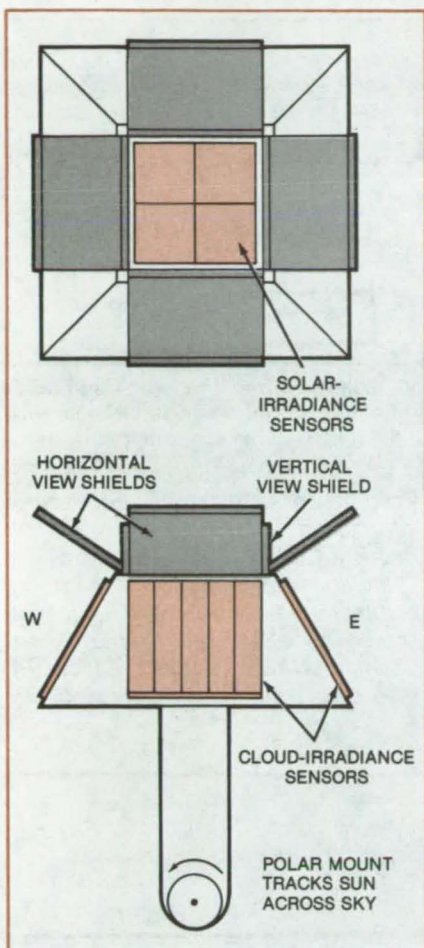
The voltage ratio derived from two sets of solar cells equals the fractional cloud cover.

NASA's Jet Propulsion Laboratory, Pasadena, California

The outputs of eight solar cells are utilized in an instrument that makes an instantaneous measurement of cloud cover—a factor that is of interest to meteorologists as an aid in weather forecasting. The instrument includes a tracking mechanism so that one of the set of four solar cells always faces the

Sun, while another set faces the four quarters of the sky. On an overcast day, the cloud-irradiance sensors generate as much short-circuit current as the sun-sensor cells do. As the cloud cover decreases, so does the output of the cloud sensors.

The instrument is just past the concept stage, with preliminary data indicating that the basic principle is sound; however, development still has to be done. Such factors as the effects of cloud reflection into the Sun sensors and erroneous readings caused by



small clouds blocking the Sun remain to be evaluated. Nonetheless, the sensor shows promise as a simple, inexpensive monitor of cloud cover.

The cloud-cover monitor is shown in the figure. Its base is a truncated four-sided pyramid, with a polar mount that rotates at 15° per hour to track the Sun across the sky. Thus the Sun-sensing solar cells on top of the truncated pyramid always face directly toward the Sun.

The four sides of the pyramid are at an angle of approximately 60° to the central axis of the pyramid. Each side supports one square silicon photovoltaic cell, with the electrical output of each cell connected in series. These cloud-irradiance sensors are loaded so that 100 mW/cm^2 (normal incidence) produce an output of 25 mV on each cell. The solar-irradiance sensor, on top of the truncated pyramid, consists of four smaller, square solar cells, also connected in series and also loaded so that 100 mW/cm^2 produce an output of 25 mV on each cell. Cloud cover is obtained by dividing the total

series voltage obtained from the cloud-irradiance cells by the total series voltage obtained from the solar-irradiance cells.

View-limiting shields separate the fields of view of the two sets of solar cells. The nearly vertical limiters shield the solar-irradiance sensors from infrared radiation reflected by the clouds, while the horizontal limiters shield the cloud-irradiance sensors from direct or reflected solar irradiance. Horizontal limiters may also be needed near the bottom edges of the cloud-irradiance sensors to shield them from energy reflected from the ground.

This work was done by Eric G. Laue of Caltech for **NASA's Jet Propulsion Laboratory**. For further information, Circle 61 on the TSP Request Card.

This invention is owned by NASA, and a patent application has been filed. Inquiries concerning nonexclusive or exclusive license for its commercial development should be addressed to the Patent Counsel, NASA Resident Office-JPL [see page 5]. Refer to NPO-14936.

The **Solar Cells** (in color) sense radiation from the Sun and from the rest of the sky. The ratio of cloud-sensor voltage to Sun-sensor voltage is the numerical measure of the cloud cover.

Compact Infrared Detector

A new photothermal detector has a sensing area only 0.1 mm on a side.

NASA's Jet Propulsion Laboratory, Pasadena, California

Compactness, high responsivity, and high noise immunity are among the advantages of a new detector that uses the "transient thermal lens" effect to measure infrared radiation. Tested successfully with a sensing area only 0.1 mm on a side, the broadband IR detector could be integrated into a compact package for pollution monitoring, weather prediction, and other applications.

The sensing material is a transparent sheet (plastic, for example), metalized with a reflecting coating and then overcoated with a black material on the

same side. The reflecting coating can be either silver or aluminum, and the black coating can be either gold black or platinum black. The spectral range of the radiation detected depends only on the absorptivity of the black coating.

The infrared light passes through a shutter, which chops the light into pulses. The light strikes the black coating on the plastic sheet, where it is absorbed and transmitted to the plastic (see figure). Each pulse thus creates a transient region of hot material with an altered index of refraction in the plastic microvolume.

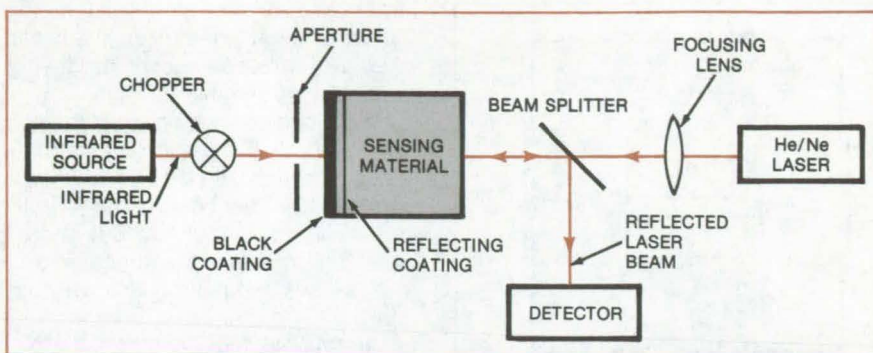
A beam of laser light is directed into the sensing material from a direction opposite to that of the infrared light. The laser beam is reflected by the metal coating under the black infrared-absorptive coating and is directed by a beam splitter into a detector.

The hot transient region generated by an infrared pulse acts as a lens that defocuses the laser beam. The defocusing increases as the infrared intensity increases. Thus the detector monitors a probe beam that weakens as the infrared light becomes more
(continued on next page)

intense. The detector could be a point detector such as a photomultiplier or an area detector such as a vidicon or a charge-coupled device. For the area detector, a two-dimensional profile of the IR beam is imaged. It is possible to pack a 20by20 matrix within a 1-cm² area detector.

Because the black absorbent layer on the sensing material absorbs equally well over a wide range of wavelengths, the infrared meter is sensitive over a broad band. Electrical noise is virtually eliminated because the sensor is non-electronic, except for the last stage. Noise is also reduced because the infrared light is chopped and its transient rather than steady-state effects are measured.

The responsivity of the tested detector — the volts produced per unit flux — is 2×10^9 V/W/cm² for a detector 0.1 mm on a side. Responsivity potentially can be further improved by substituting a transparent, highly



The **Sensing Material**, only 0.1 mm on an edge, receives infrared radiation that defocuses the laser beam. Each pulse produced by chopping the infrared source beam with a shutter creates a transient "thermal lens" in the microvolume and temporarily defocuses the reflected laser beam.

polarizable material for the plastic sensing material. Such polarizable materials experience a higher change in index of refraction for a given change in temperature.

This work was done by Amitava Gupta, Su-Don Hong, and Jovan Moacanin of Caltech for **NASA's Jet**

Propulsion Laboratory. For further information, Circle 62 on the TSP Request Card.

Inquiries concerning rights for the commercial use of this invention should be addressed to the Patent Counsel, NASA Resident Office-JPL [see page A5]. Refer to NPO-14864.

Fast Calibration of Gas Flowmeters

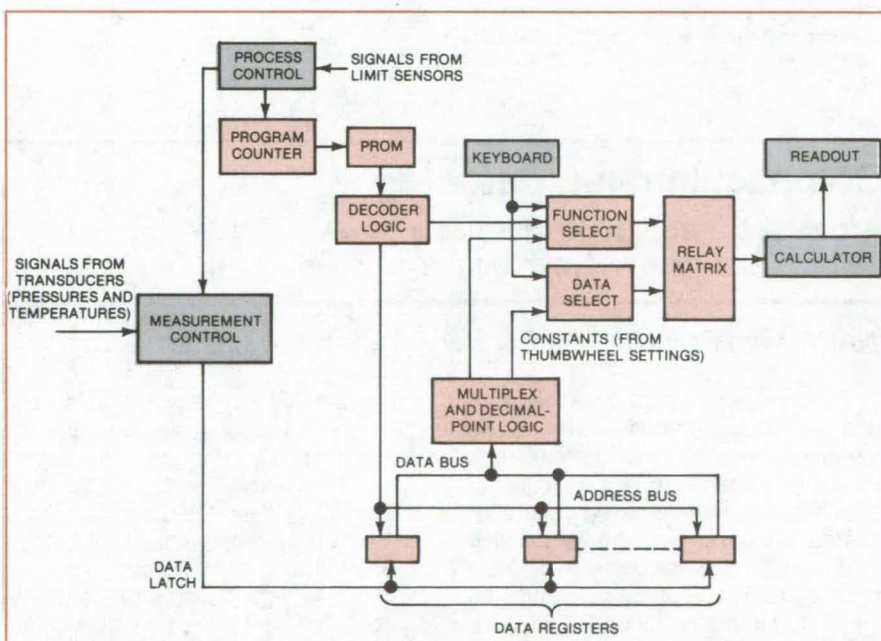
Digital unit automates the calibration sequence.

John F. Kennedy Space Center, Florida

Digital logic and memory (see figure) are the key elements of an instrument that calibrates gas flowmeters quickly and accurately. The new instrument uses a calculator IC and a programable read-only memory (PROM) to solve the calibration equations. Infrared sensors start and stop the calibration sequence.

The instrument collects a known volume of gas, which displaces a piston, while simultaneously measuring the elapsed time. It calculates the meter flow rate from the volume, the time, and preset constants. Measured values of temperature and pressure in the instrument and in the flowmeter are entered in the calculations to adjust the calibration for differences in these variables at the two locations. The instrument calibrates either mass flowmeters or rotameters, in which flow measurement is based on mass or volume, respectively.

To calibrate, the operator connects a flowmeter to one of three cylinders and adjusts the piston upper-limit sensor for



Flowmeter Calibration Instrument Circuitry consists of hard-wired transistor/transistor logic (TTL) IC's, except for the calculator set, which are of metal-oxide-semiconductor (MOS) devices. The calibration program is stored in a programable read-only memory (PROM). Data are fed to the calculator serially from the data registers.

the volume to be collected. Six constants for the flow-rate equation are dialed on thumbwheel switches. The operator then turns on the gas to the flowmeter and presses a start button. From that point, the calibration proceeds automatically.

As gas flows through the meter, it drives the piston upward. When the piston passes the lower-limit sensor, the instrument starts timing the run. The timing stops as the piston reaches the upper-limit sensor. Four measurements — the pressure and temperature in the meter and in the prover — are made within 15 seconds and transmitted to the calculator. These data, along with the elapsed-time and

volume measurements, are used to compute the flow rate in the flowmeter.

Each piston limit sensor is an infrared light-emitting-diode source and a phototransistor detector. The infrared energy from the source is reflected into the detector by the mercury seal on the moving piston. The pressure transducers are solid-state devices. Their outputs are digitized before they are processed by the calculator. The temperatures are measured by a multichannel digital thermometer. Pressures, temperatures, and the calculated flow rate are displayed on the instrument panels.

By controlling the procedure and performing the calculations automati-

cally, the instrument has reduced operator time by 80 percent. It is more reliable than previous instruments using magnetic-pickup sensors because its components are solid-state devices. Also, because the instrument is digital, its accuracy is determined primarily by the accuracy of the transducers.

This work was done by R. V. Lisle and T. L. Wilson of Kennedy Space Center. For further information, Circle 63 on the TSP Request Card.

Inquiries concerning rights for the commercial use of this invention should be addressed to the Patent Counsel, Kennedy Space Center [see page A5]. Refer to KSC-11076.

Wind-Simulation Tester for Solar Modules

Tester induces cyclic pressure loads across the surface of the module.

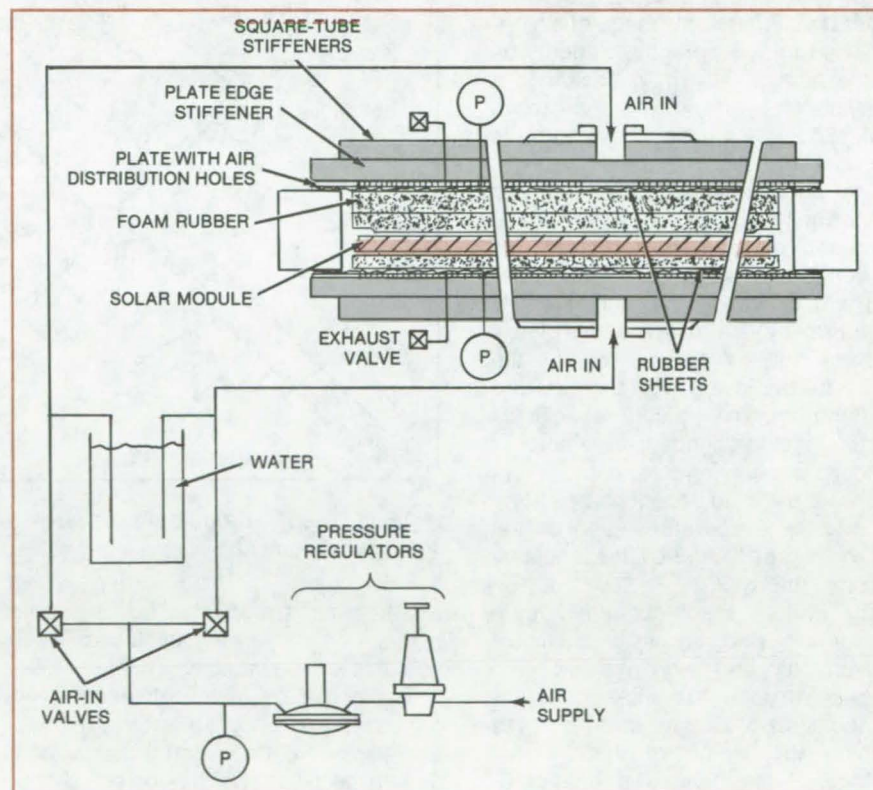
NASA's Jet Propulsion Laboratory, Pasadena, California

By applying pressure cyclically to solar-cell modules, a test fixture simulates wind pressure loads. The fixture was developed to induce peak pressure loads across the surface of the modules at a predetermined pressure, typically 2,400 pascals (0.35 psi). Through gentle test pressure loads upon the solar module, the fixture guarantees the mechanical integrity of the module. The fixture operates at relatively high speed, completing a cycle in 5 seconds.

The module is sandwiched between two stiffened aluminum plates covered with 1/64-in. (0.4-mm) rubber sheets (see figure). To insure that the air pressure is transmitted uniformly to the module, the rubber sheets are slack. All the spaces and nonuniformities between the module and the sheets are filled with foam rubber until the foam is flush to within 5 mm of the module frame.

Automatic front-side and back-side pressure loading is cycled by a pneumatic system on a separate stand. Two loading valves and two exhaust valves alternately pressurize each side of the fixture. The controller for the valves is motor-driven. The applied load is uniform to within 10 percent, as measured by indicators mounted on a bar across the test

(continued on next page)



The **Solar-Cell Module**, to be tested, is sandwiched between two stiffened aluminum sheets that are covered with rubber sheets. Automatic front- and back-side pressure loading is cycled by a pneumatic system on a separate stand. Relief valves prevent overpressurizing.

frame that sense module frame deflections.

To reduce the air pressure from the line level to the desired pressure load, two regulators are used. Relief valves prevent overpressurizing. As an extra

precaution, the air supply lines to the fixture have vents in them that are immersed in a can of water. The water in the can is only slightly deeper than the desired pressure, expressed in inches of water.

This work was done by John S. Griffith of Caltech for NASA's Jet Propulsion Laboratory. For further information, Circle 64 on the TSP Request Card.
NPO-14837

Heat Pipes Cool Probe and Sandwich Panel

Two new concepts integrate heat-pipe technology.

Langley Research Center, Hampton, Virginia

Heat pipes are incorporated in two new design concepts at Langley Research Center: a heat-pipe-cooled jacket for a probe used in hostile high-temperature environments, such as those encountered in the measurement of combustion-gas parameters, and a heat-pipe sandwich panel that combines the structural efficiency of sandwich construction with the thermal efficiency of the heat pipe.

The cylindrical probe-jacket container (see Figure 1) is made of a high-temperature superalloy, such as Hastelloy X or Ti-Ni/Cr. Inside is a stainless-steel arterial or spiral-groove wick. Sodium or other liquid metal is the working fluid.

The cooling jacket transfers heat isothermally to an area of lower temperature where it is rejected by conventional methods, such as radiation and/or free convection. Heat is absorbed by the evaporation of the working fluid in the portion of the probe that is in the high-temperature environment. The heated vapor flows to the finned condenser where it condenses and rejects heat. From there, the liquid condensate flows back to the evaporator region by the action of gravity and by the capillary action of the wick.

The system is self-contained, passive, and has no moving parts, unlike conventional air- and water-cooled probes. An alternate wick configuration consists of narrow spiral grooves running the length of the internal surface of the pipe. The heat-pipe-cooled jacket can be used to cool probes for measuring temperatures or pressures in high-heating environments, such as wind tunnels and

powerplants. It can also be used on high-speed research vehicles or hypersonic cruise vehicles.

The heat-pipe sandwich panel reduces thermal gradients, hence stresses, in a honeycomb sandwich panel that is heated or cooled along one face. Conventional honeycomb structures have a very low transverse thermal conductivity and consequently are often used as insulation. The heat-

pipe sandwich panel concept retains this feature, yet it can also operate as a thermal diode. The sandwich is an insulating barrier when the heat pipes are not operating, and it is a thermally conducting panel that transfers heat efficiently from one face to the other when the heat pipes are operating.

The panel consists of a metallic honeycomb core, two facesheets, and a working fluid. Heat is transferred

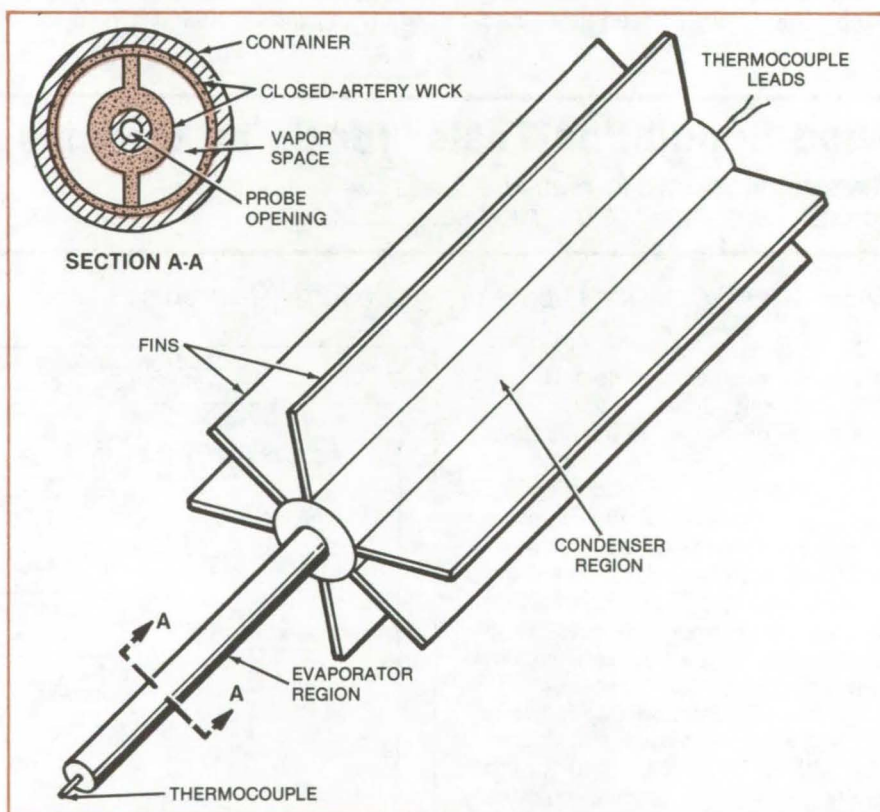


Figure 1. The **Heat-Pipe-Cooled Probe** could be used to measure temperature in a hostile environment.

from the heated face to the cooler face by the evaporation and condensation of the working fluid. The fluid evaporates at the heated face and condenses at the cooler face, and the condensate returns to the evaporator region by the capillary action of the wick. In this application, the wick is the honeycomb and inner surfaces of the facings, which are either scored, etched, or grooved (see Figure 2).

An alternate concept uses a sintered-metal foil-gage screen formed to the honeycomb shape and spot-welded to the facings; or, arbitrary cells can be used as wicking columns. The faces are etched for capillary flow, and the honeycomb cells are notched at both ends to allow flow to cells not in direct contact with the wicking columns.

The heat-pipe sandwich panel can be applied in any situation where it is necessary to transfer heat from one face of the panel to the other, to eliminate thermal gradients and stresses, and/or to minimize thermal distortions. Possible applications in-

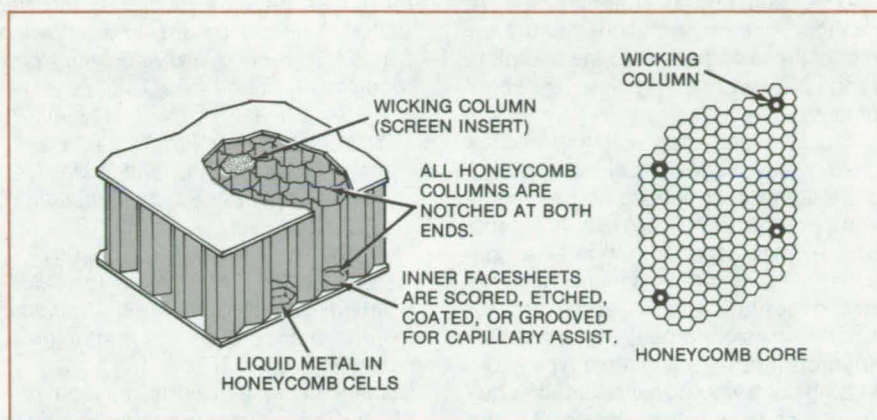


Figure 2. **Heat-Pipe Sandwich Panel** combines sandwich strength with heat-pipe thermal efficiency. Either the honeycomb walls are used as the wicking medium; or, as shown, selected honeycomb cells can contain the wick material.

clude reducing thermal stresses in the walls of jet engines, cooling electronic components, limiting thermal distortions in large structures, and operating as a thermal diode for cryogenic storage vessels.

This work was done by Charles J. Camarda, Lana M. Couch, and H. Neale Kelly of Langley Research

Center. No further documentation is available.

Inquiries concerning rights for the commercial use of this invention should be addressed to the Patent Counsel, Langley Research Center [see page A5]. Refer to LAR-12588 and LAR-12637.

Computer Programs

These programs may be obtained at very reasonable cost from COSMIC, a facility sponsored by NASA to make new programs available to the public. For information on program price, size, and availability, circle the reference letter on the COSMIC Request Card in this issue.

Thermodynamic and Transport Properties of Air/Water Mixtures

Properties of mixtures are calculated up to nearly 1,500 K and 4,500 atmospheres.

The thermodynamic and transport properties of air/water mixtures are calculated by the subroutine WETAIR. Inputs required are the assigned values of either temperature and density, pressure and density, temperature and pressure, pressure and entropy, or pressure and enthalpy. Outputs are the

properties of dry air, water (steam), and the air/water mixtures. Interpolation of property tables is used to obtain the dry-air and water properties, and simple mixing laws are then used to calculate the properties of the air/water mixtures.

Properties of mixtures with water content below 40 percent (by mass) can be calculated at temperatures from 273.2 to 1,497 K and at pressures to 450 MN/m² (4,500 atmospheres). Dry-air properties can be calculated at temperatures as low as 150 K. Water properties can be calculated at temperatures to 1,747 K and at pressures to 100 MN/m². The precision of the air properties is approximately 0.01 percent, and that of the water properties is approximately 0.05 percent, although both show maximums of up to 1 percent for extreme conditions.

Experimental data on air/water-mixture properties are generally lacking in the literature, with the exception of viscosity measurements. Until such data become available, WETAIR represents the state-of-the-art in the calculation of thermodynamic and transport properties of air/water mixtures.

WETAIR has been used in testing gas-turbine engines and components operating in relatively humid air at pressures to 40 atmospheres (40×10^5 N/m²). The program is available in SFTRAN and FORTRAN.

This program was written by Theodore E. Fessler of Lewis Research Center. For further information, Circle C on the COSMIC Request Card. LEW-13432

Calculating Linear A, B, C, and D Matrices From a Nonlinear Dynamic Engine Simulation

Program generates linear state-space models for simulating turbofan and turbojet engines.

Digital computers can accurately simulate the steady-state and transient performance of turbojet and turbofan engines. When nonlinear steady-state

(continued on next page)

and transient physical relationships are included, the computations accurately model these engines over the complete range of power settings and flight conditions.

Most of the analytical approaches used by control designers, however, require linear descriptions of the steady-state and transient engine characteristics. A linear approximation to a nonlinear system can be obtained at a selected operating point and used for small excursions about that point. For an aircraft turbine engine, a typical operating point would be a particular equilibrium condition of power setting and flight condition.

For a system as complex as an aircraft engine, the linear description usually consists of a number of coupled linear algebraic and differential equations. These equations can be written in the so-called "state-space" form, using vector-matrix notation. At an operating point, the linear model is fully described by the set of matrices, commonly designated as: a system matrix A, a control matrix B, an output matrix C, and a feed-forward matrix D. To describe an engine over its complete operating envelope, a number of operating points are defined, and a set of matrices is obtained for each point.

A digital computer program DYGABCD generates linear state-space models of simulated turbofan and turbojet engines. DYGABCD also contains DYNGEN, a program that simulates nonlinear steady-state and transient cases for one-spool and two-spool turbojet engines or two-spool and three-spool turbofan engines. Consequently, DYGABCD can be used exactly as DYNGEN to simulate nonlinear engine steady-state and transient performance. In addition, DYGABCD calculates the state-space matrices A, B, C, and D for any turbine engine that can be simulated with DYNGEN. The method used in DYGABCD to generate A, B, C, and D could also be used in any other transient simulation that uses a backward difference integration technique.

DYGABCD is written in FORTRAN IV for batch execution and has been implemented on an IBM 360-series computer with a central memory requirement of approximately 314K of 8-bit bytes. DYGABCD was completed in 1977.

This work was done by Lucille C. Geyser of Lewis Research Center. For

further information, Circle D on the COSMIC Request Card. The following two NASA reports are necessary prerequisites for use of DYGABCD:

NASA TP-1295 [N78-33110/NSP], "DYGABCD — A Program for Calculating Linear A, B, C, and D Matrices from a Nonlinear Engine Simulation" [\$13]; and NASA TN D-7901 [N75-25620/NSP], "DYNGEN — A Program for Calculating Steady-State and Transient Performance of Turbojet and Turbofan Engines" [\$13].

Copies of these reports may be purchased [prepayment required] from the National Technical Information Service, Springfield, Virginia 22161. LEW-13250

Structural Design With Stress and Displacement Constraints

A program for synthesizing minimum-weight linear elastic structures with upper limits on stresses and displacements

Every structural design task is either directly or indirectly governed by certain optimality criteria. The designer is seldom required to create a structure that will only serve its primary function. Instead, the design is usually expected to meet such objectives as minimum weight and cost.

The DESAP1 program synthesizes linear elastic structures under static loads. Its design objective is to find the element sizes that minimize the total weight without changing the layout of the structure. The primary constraints in the synthesis algorithm are upper limits on stresses and displacements. These stress limits are prescribed as yield criteria and local instability criteria. DESAP1 also allows secondary constraints consisting of minimum allowable element sizes and size-proportion constraints.

An iterative process is used in the synthesis, with each iterative step consisting of three parts: First, the current structure is analyzed. Next, the results of that analysis are evaluated in terms of structure optimization. Finally, the

results of the evaluation are used to redesign the structure.

The classical stress-ratio method is employed in the redesign with respect to stress constraints. This procedure drives the final design to the fully stressed design, which may not coincide with the design having minimum weight. For the displacement constraints, the redesign formula is obtained from the minimum-weight criterion with element sizes being driven toward a design having optimal weight. In the presence of both stress and displacement constraints, each iterative redesign operation first determines the element sizes from the stress-ratio method. These results are then used as minimum-size constraints during the application of the displacement-constrained redesign formulas. The result of the synthesis is a minimum-weight structure adhering to the prescribed constraints.

Inputs to DESAP1 consist of an initial finite-element model of the structure and a set of constraints. Basic structural elements available in DESAP1 include three-dimensional bars, three-dimensional beams, quadrilateral shear panels, anisotropic plane-stress quadrilaterals and triangles, and anisotropic quadrilateral and triangular plates.

A set of boundary elements is included to represent elastic supports and to apply constraints. The design procedure assumes that the loading is independent of element sizes. Allowances have been made for such size-dependent loads as thermal stresses and gravity loading. Outputs from DESAP1 consist of a redesign history, the final structural weight, and the redesigned element sizes.

The DESAP1 program is written in FORTRAN IV for batch execution and has been implemented on an IBM 360 computer with a central memory requirement of approximately 300K of 8-bit bytes. The DESAP1 program was developed in 1977.

This program was written by J. Kiusalaas and G. B. Reddy of Pennsylvania State University for Marshall Space Flight Center. For further information, Circle E on the COSMIC Request Card. MFS-25235

An All-FORTRAN Version of NASTRAN® for the VAX

A general-purpose finite-element program for structural analysis

An all-FORTRAN version of the level 17.6 NASA structural analysis program NASTRAN® was developed for implementation on the DEC VAX-series computer under the VAX/VMS operating system. The minimum configuration includes half a megabyte of central memory and 50 megabytes of disk space. A recommended configuration includes 4 megabytes of central memory, two 256-megabyte disk drives, two 1,600-bpi tape drives, and the optional floating-point accelerator.

Developed in the mid-1960's, NASTRAN is a general-purpose finite-element computer program for structural analysis. Besides being efficient, versatile, and convenient to use, NASTRAN can be modified easily and expanded to accommodate new problems and new computer configurations without major redevelopment.

Applications of NASTRAN extend to almost every type of linear structure and construction. Structural elements provide for the specific representation of the more-common types of construction, including rods, beams, shear panels, plates, and shells of revolution. More general structures are analyzed by using combinations of these elements and by the use of "general" elements. Control systems, aerodynamic transfer functions, and other nonstructural features can be incorporated by the engineer into the structural analysis problem. A complex structure can be represented as a set of substructures to decrease processing time. NASTRAN includes plotting interfaces that permit the display of structure and substructures with or without deformations.

The range of analysis that can be performed using NASTRAN includes: static response to concentrated or distributed loads, thermal expansion, and enforced deformation; dynamic response to transient loads, steady-state sinusoidal loads, and random excitation; the determination of real and complex eigenvalues for use in vibration analysis; dynamic stability analysis; and elastic stability analysis.

The program also includes a limited capability for the solution of nonlinear problems, including piecewise linear analysis of nonlinear static response and transient analysis of nonlinear dynamic response.

NASTRAN has been specifically designed to treat and solve efficiently large problems with many degrees of freedom. The only limitations on problem size are those imposed by the practical considerations of computer run time and by the ultimate capacity of auxiliary storage devices. To reduce the central memory requirements on the VAX computer, NASTRAN is organized into 16 sections called links. One of these links is a control program that pulls the other links into core only as they are needed. This structure allows NASTRAN to offer the user a large selection of capabilities while requiring only a moderate amount of core resources.

Two new NASTRAN features are available in the VAX version. The program can be executed from a terminal in a manner that permits use of the VAX interactive debugger, and any link can be interactively restarted as often as desired by making a copy of all NASTRAN work files before executing that link for the first time.

This program was written by Lloyd Purves of Goddard Space Flight Center. For further information, Circle F on the COSMIC Request Card. GSC-12600

Potential Flow in Two-Dimensional Deflected Nozzles

An informative approximation to three-dimensional nozzle flow.

Potential flow in two-dimensional deflected-flow nozzles is calculated by three programs: SCIRCL, a geometry definition program; 24Y, an incompressible two-dimensional potential-flow program; and NOZZLEC, a program that combines incompressible potential-flow solutions into solutions of interest and applies a compressibility correction.

SCIRCL uses nozzle geometry segments as input, with each segment

introduced as an analytic curve. The printed output, containing the coordinates, slopes, curvatures, and other features of the entire nozzle surface, is placed in a disk file. An initial screening of candidate nozzles can be made from the printout from this stage of the computation.

Using the results of SCIRCL as input, plus desired points of output, 24Y generates simple two-dimensional basic potential-flow solutions for both on-body and off-body points. The velocity fields are placed on disk files for use as input to NOZZLEC. Since a full three-dimensional nozzle analysis does not now exist, the simpler but more approximate methods of 24Y were developed to analyze real nozzles. Even though actual nozzles are three-dimensional, there are sections of the nozzles for which a two-dimensional analysis is an informative approximation.

The final routine, NOZZLEC, combines the basic solutions from 24Y into solutions of interest having specified values of nozzle mass flow and, if desired, free-stream velocity and angle of attack. NOZZLEC output includes velocities, pressures, flow angles, and mach numbers. If desired, compressibility corrections are also applied.

The program group is written in FORTRAN V and has been implemented on a UNIVAC 1100/42. It requires a memory having approximately 52K of 36-bit bytes. The program was completed in 1979.

This program was written by J. Dennis Hawk and Norbert O. Stockman of Lewis Research Center. For further information, Circle G on the COSMIC Request Card. LEW-13461

The Design and Analysis of Low-Speed Airfoils

Direct and inverse airfoil-flow problems are solved by the program PROFILE.

The flow about an airfoil in free air can be described approximately by a boundary-layer flow near the surface of the airfoil and by a potential flow everywhere else. Boundary-layer theory can be applied to the flow about an airfoil in two ways. First, the



boundary-layer development can be determined for a given potential-flow velocity distribution. This is the direct, or analysis, problem. Second, the potential-flow field, or at least some of its properties, can be determined for a given boundary-layer development. This is the inverse, or design, problem. Both the direct and inverse problems are solved by the program PROFILE.

A conformal-mapping method for the design of airfoils with prescribed velocity-distribution characteristics, a panel method for the analysis of the potential flow about given airfoils, and a boundary-layer method are combined in the PROFILE program. The conformal-mapping method, similar to that of Lighthill, solves most multipoint design problems very simply. The potential-flow analysis method is required for comparison with wind-tunnel tests of given airfoils and for analyses of airfoils generated by the design method and then modified by a flap deflection. This analysis method employs a distributed surface-singularity technique. The boundary-layer method uses integral momentum and energy equations but does not contain a boundary-layer displacement iteration.

PROFILE is written in FORTRAN IV and has been implemented on a CDC 6000-series computer with a central memory requirement of approximately 110K (octal) 60-bit words. The program was developed in 1980.

This program was written by Richard Eppler of the University of Stuttgart and Dan M. Somers of Langley Research Center. For further information, Circle H on the COSMIC Request Card.
LAR-12727

Transonic Flow Over Wing/Fuselage Configurations

Flow-field analysis in the transonic region

The Wing Body Code (WIBCO) simulates the aerodynamics of wing/fuselage configurations at transonic speeds. It can reduce the design cost and improve the performance of high-speed aircraft.

The transonic flow field is characterized by mixed subsonic and supersonic regions, shock waves, and complicated viscous effects. The complexity of such flow often makes a purely experimental approach impractical for solving aircraft design problems in this regime. WIBCO obtains a numerical finite-difference solution of a modified (extended) small-disturbance flow equation on a multiple embedded mesh system. This approach gives high computational resolution and coordinate-system flexibility for treating complex realistic aircraft shapes.

The WIBCO flow equation is a modified extension of the classical transonic small-disturbance equation. This modification includes crossflow terms for resolving shock waves with large sweep angles. The computational space used in solving the flow equation is divided into a global crude grid and embedded fine grids about the wing and body where the gradients are large and the details are important.

The simplicity of the approximate flow equation and planar boundary conditions permit the use of Cartesian coordinates for all grids. The resulting

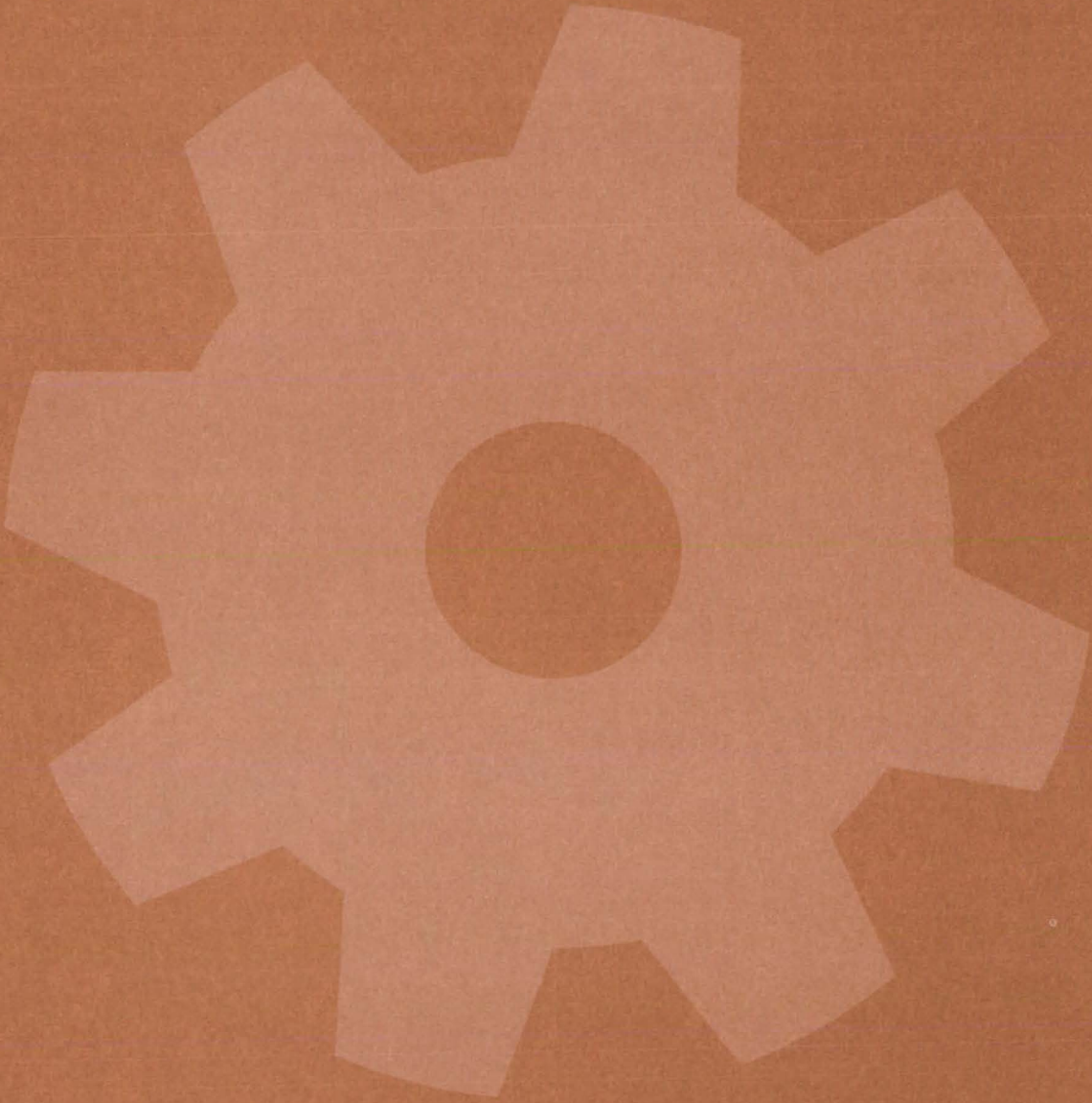
numerical efficiency permits a very dense computational mesh, a benefit in both the resolution of shock waves and the calculation of configuration forces and moments. The embedded meshes are independent and optimized for a particular geometric component, facilitating applications to complex configurations. The flow-field equation is of mixed type for supercritical flow and is solved using a type-dependent finite-difference approximation with planar boundary conditions. A successive-line over-relaxation method is used where vertical columns of mesh points are relaxed starting at the first line (plane) upstream and ending at the last line (plane) downstream in each grid system.

Inputs to WIBCO consist of ambient flow conditions and geometric configuration data, the grid control and relaxation parameters are internally set. Outputs include input data echo; grid system verification; relaxation-solution convergence history; and computed velocities, pressures, forces, moments, reference lengths, and areas. Plotted output for geometry verification is also available. Plotted output can be generated for any offline X/Y plotter.

WIBCO is written in FORTRAN IV for batch execution and has been implemented on a CDC CYBER 175 with a central memory requirement of approximately 226K (octal) of 60-bit words. WIBCO was developed during 1977 to 1979.

This program was written by Charles W. Boppe of Grumman Aerospace Corp. for Langley Research Center. For further information, Circle J on the COSMIC Request Card.
LAR-12702

Machinery



Hardware, Techniques, and Processes

- 485 Interlocking Wedge Joint Is Easily Assembled
- 486 Pneumatic-Power Supply
- 487 Sidewall Penetrator for Oil Wells
- 488 Four-Wheel Dual Braking for Automobiles
- 489 Lock for Hydraulic Actuators
- 490 Gentle Arrestor for Moving Bodies
- 491 Soft Container for Explosive Nuts

Computer Programs

- 491 Cylindrical Bearing Analysis

Interlocking Wedge Joint Is Easily Assembled

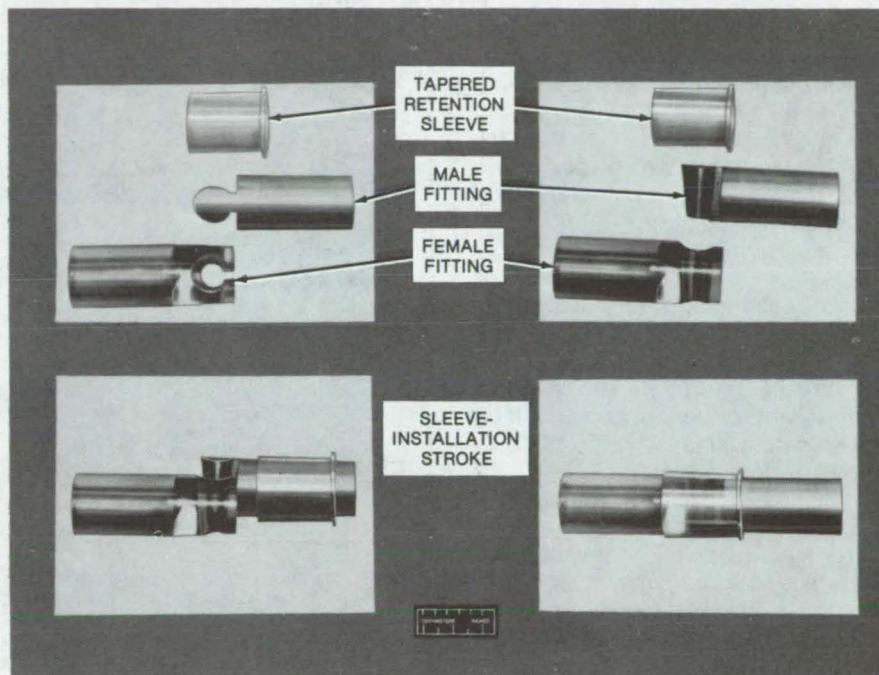
Structural joint is simple enough to be used by workers wearing gloves or bulky clothing.

Langley Research Center, Hampton, Virginia

A new interlocking wedge joint links two structural members in manual-, remote-, or automated-assembly operations. It transmits all structural loads, including tension, compression, bending moments, and torsion. If necessary, electrical powerlines and data-transmission lines can be incorporated within the joint. Originally developed for use by astronauts, the joint is simple enough to be assembled by undersea divers, workers in nuclear reactors, and others wearing gloves or bulky clothing.

The joint consists of a male endpiece, a female endpiece, and a sleeve (see figure). The small end of the male taper is inserted into the large end of the female tapered hole and pressed in until the sleeve slides over the two pieces; then the sleeve is forced up the conical surface to lock the joint. In moving up the conical surface, the sleeve expands to near its yield point or beyond, resulting in a clamping action that holds it in place. The necessary force is furnished by the operator with a special tool or by special mechanisms built into a manipulator or other automated equipment. For release, the assembly steps are reversed.

In large structures, one of the endpieces could be attached to (or an integral part of) a column or strut, and the other endpiece could be an integral part of a cluster with connections for several such members. If electrically nonconductive materials are used for the endpieces, metal inserts cast or molded in place may be used to conduct electrical power or data signals across the joint. Multiple electrical paths are feasible without a separate connector.



In the **New Wedge Joint**, an expanding sleeve and male and female endpieces (top) are joined in a single locking stroke (bottom).

Comparable joints are usually expensive machined mechanisms requiring extremely close tolerances. Few carry bending or torsional loads. The components of the new joint may be formed by machining, casting, or molding. If many are required, casting or molding should reduce costs substantially. The overall size, wedge angle, and conical taper may be varied to handle unusual loads or special assembly problems.

The joint is inherently insensitive to thermal excursions, vibration, and the buildup of machining tolerances. Joints assembled from injection-molded composites, using qualified

materials, should withstand severe environments. The combination of wedging angles on the male/female parts and the sleeve create high mechanical advantages that overcome structural misalignments and force the assembly into the true position as the locking sleeve moves into place.

*This work was done by Moses J. Long of **Langley Research Center**. No further documentation is available.*

Inquiries concerning rights for the commercial use of this invention should be addressed to the Patent Counsel, Langley Research Center [see page A5]. Refer to LAR-12729.



Pneumatic-Power Supply

A pneumatic analog of the portable electric-power supply has adjustable pressure outputs.

Lyndon B. Johnson Space Center, Houston, Texas

Compressed air is used in industrial plants, shops, and laboratories for operating production equipment, spraying paint and lubricants, cleaning, drying, and moving liquids. It is also used for activating valves in high-pressure systems and for pressurizing refrigeration systems.

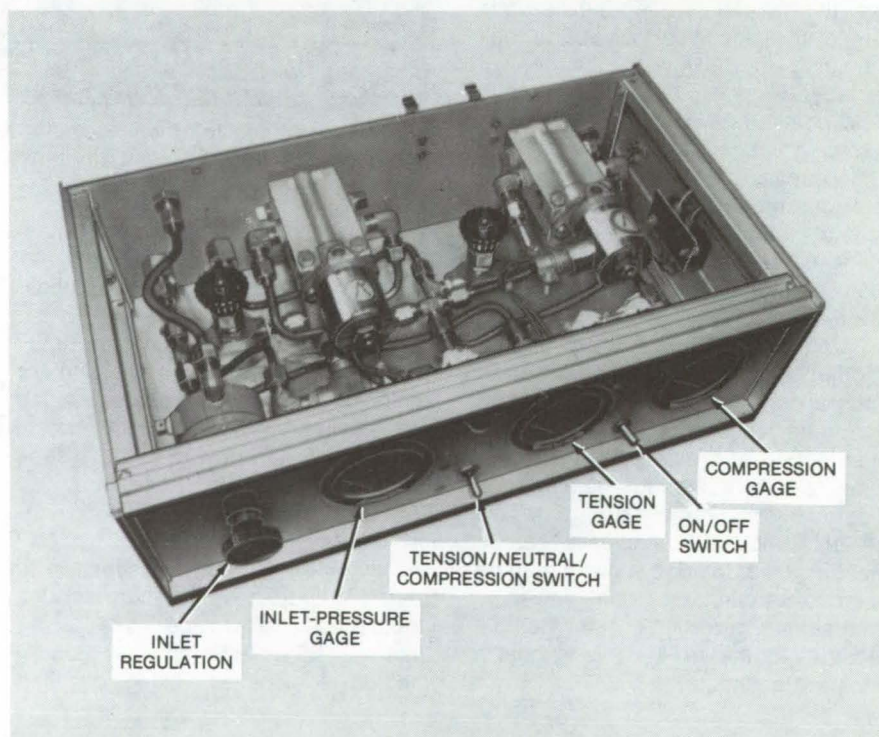
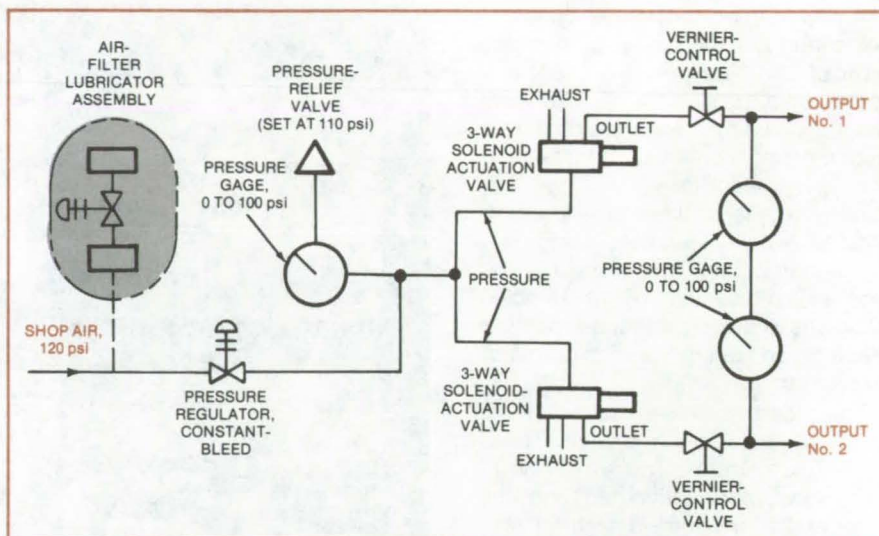
A new portable pneumatic supply that is analogous to the electric-power supplies used throughout industry simplifies these operations. It connects to a standard high-pressure air line (120 psi, or $8.3 \times 10^5 \text{ N/m}^2$) and has two or more outputs at pressures that can be adjusted from 20 to 100 psi (1.4×10^5 to $6.9 \times 10^5 \text{ N/m}^2$).

A portable pneumatic supply with two adjustable outputs is shown in the figure. It accepts plant compressed air, filters out particles larger than 10 microns in diameter, reduces the air to working pressure, and adds a lubricant if required.

An accurate constant-bleed regulator supplies the reduced-pressure air to both output channels. On the channel lines, vernier-control valves select the output pressures. Gages show inlet and channel pressures.

A "momentary-on" toggle switch controls channel selection through two solenoid-operated four-way valves (converted to three-way operation). Safety and convenience features are included, such as a pressure-relief valve, a stand, a carrying handle, and mode-of-operation indicator lights.

This work was done by Ralph C. Kramer of Rockwell International Corp. for **Johnson Space Center**. No further documentation is available.
MSC-18855



Two Adjustable-Pressure Outputs of filtered compressed air are available from the compact portable pneumatic supply shown here in a schematic diagram (top) and a photograph (bottom). The primary source is high-pressure air from a main air line. The actuator valves and indicator lights require standard 120-volt ac electricity.

Sidewall Penetrator for Oil Wells

New penetrator bores horizontal holes in the well casing to increase oil drainage.

NASA's Jet Propulsion Laboratory, Pasadena, California

A sidewall penetrator (see figure) bores horizontal holes 6 in. (15 cm) in diameter, 15 in. (37.5 cm) deep, to extract oil trapped in the adjacent strata. A common drive mechanism turns several penetrators at once to cut multiple holes simultaneously. The penetrators are more efficient than the more-commonly-used armor-piercing bullets and shaped explosive charges, none of which pierces the sidewalls as deeply.

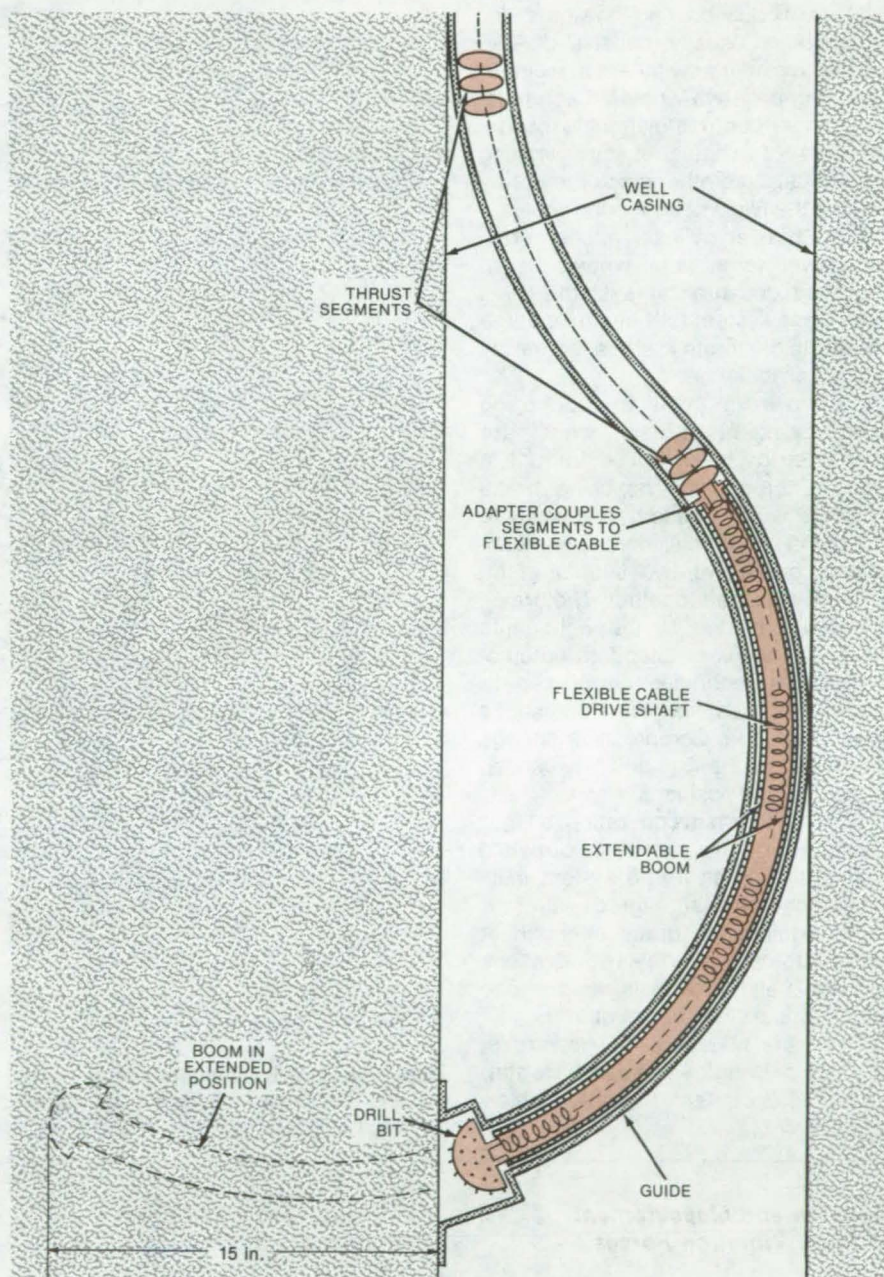
Each penetrator drill bit is turned by a flexible shaft. The shaft, made from a spiraling cable, rotates and thrusts simultaneously through a rigid curvilinear guide tube forcing the bit through the well casing and into the strata.

The shaft is driven by a series of interlocking thrust segments confined in the tube and connected to a drive motor at the mouth of the well. Each segment contains a rotatable hollow sleeve that interlocks with the next one. Drilling fluid feeding through these sleeves flows through ports in the drill bit to cool and lubricate the cutting teeth and to flush chips and debris from the drilled hole. When the drill is retracted, the sleeves disconnect.

Power is applied to the thrust segments via a feeding mechanism coupled to the drive motor. The motor drives several of these feeding mechanism at once. Each feeding mechanism operates in the manner of a lead screw/nut arrangement. A threaded rod, analogous to a lead screw, is thrust forward by a rotating nut driven by a gear reduction mechanism. Simultaneously a rotary drive gear turns the thrust segments.

The rotating segments surge forward, interlock, and apply power to the shaft. The feeding-mechanism gears advance the drill bit slowly in relation to its high rotary speed.

This work was done by Earl R. Collins of Caltech for **NASA's Jet Propulsion Laboratory**. For further information, Circle 67 on the TSP Request Card.



Sidewall Penetrator cuts horizontal holes in oil wells to release oil trapped in the adjacent strata. A number of these penetrators operated by a common drive is inserted into the well at once. The drill bits advance simultaneously in several directions, releasing trapped oil into the well.

Title to this invention has been waived under the provisions of the National Aeronautics and Space Act

[42 U.S.C. 2457(f)], to the California Institute of Technology/Jet Propulsion Laboratory, Pasadena, CA 91103. NPO-14306

Four-Wheel Dual Braking for Automobiles

All four wheels are braked by either of two master cylinders.

Langley Research Center, Hampton, Virginia

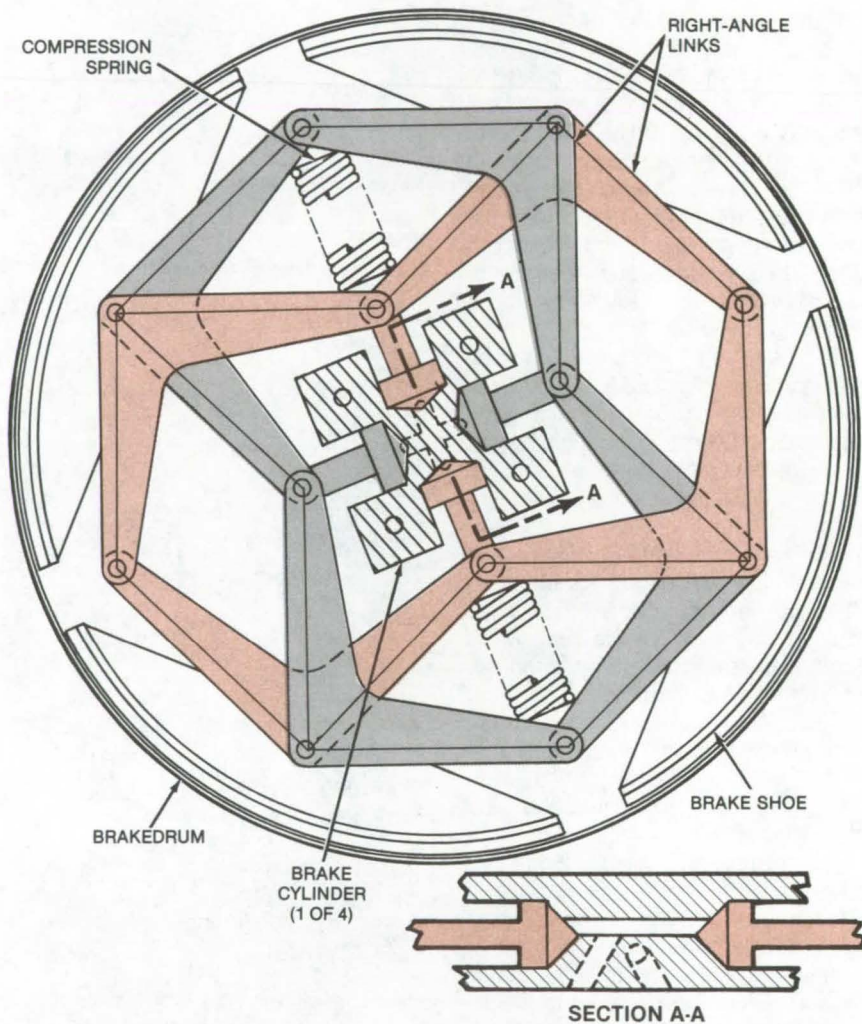
Modern dual-braking systems for automobiles usually consist of two master cylinders, with each cylinder operating only two wheels. Each master cylinder controls diagonally opposing sets of wheels. If one braking system fails, the other stops the car by braking the two wheels it controls.

Each master cylinder applies braking power to all four wheels in an improved dual-braking system. Thus, even if one system fails because of the loss of fluid, the other stops the car by braking all four wheels.

As shown in the figure, opposing brake cylinders at each wheel are connected by holes drilled through a block. Each pair of opposing brake cylinders is connected hydraulically to one of the master cylinders. The mechanism consists of two sets of right-angle links pinned together. The brake-shoes are pinned to the right-angle corners of the links. Standard automotive design techniques are used to place the studs that lock the shoes against rotation. Compression springs return the mechanism and brakeshoes to their neutral positions.

With both systems operating, all four brakeshoes are forced outward against the drum. If one system fails, the mechanism still forces all four shoes against the drum, although at half the force. Nevertheless, all shoes operate in all four wheels whether one or both brake systems are operational.

This work was done by Howard B. Edwards of Langley Research Center. No further documentation is available. LAR-12687



Opposing Brake Cylinders are connected to each other by a hole drilled through the block. Each pair of cylinders, connected hydraulically to one of the master cylinders, operates independently. A model of the linkage has been built.

Isolation and Measurement of Rotor Vibration Forces

A mounting for a helicopter gearbox measures forces generated by the rotor and isolates the transmission from the airframe. The mountings have a frequency-dependent load/displacement relationship that gives a statically rigid but dynamically soft support, which lowers vibratory transfer.

(See page 468.)

Removing Freon Gas From Hydraulic Fluid

Dissolved Freon gas can be removed from hydraulic fluid by raising the temperature to 150° F and bubbling dry-nitrogen gas through it, even while the fluid is circulating through the hydraulic system. This decontamination procedure reduces parts corrosion and sludge formation.

(See page 452.)

Speed Control for Synchronous Motors

A feedback circuit controls fluctuations in the speed of synchronous motor. A voltage proportional to the phase angle is developed by a phase detector, rectified, amplified, compared to a threshold, and applied back to the motor excitation circuit.

(See page 414.)

Lock for Hydraulic Actuators

Two clamps prevent rod travel in deenergized actuators.

Lyndon B. Johnson Space Center, Houston, Texas

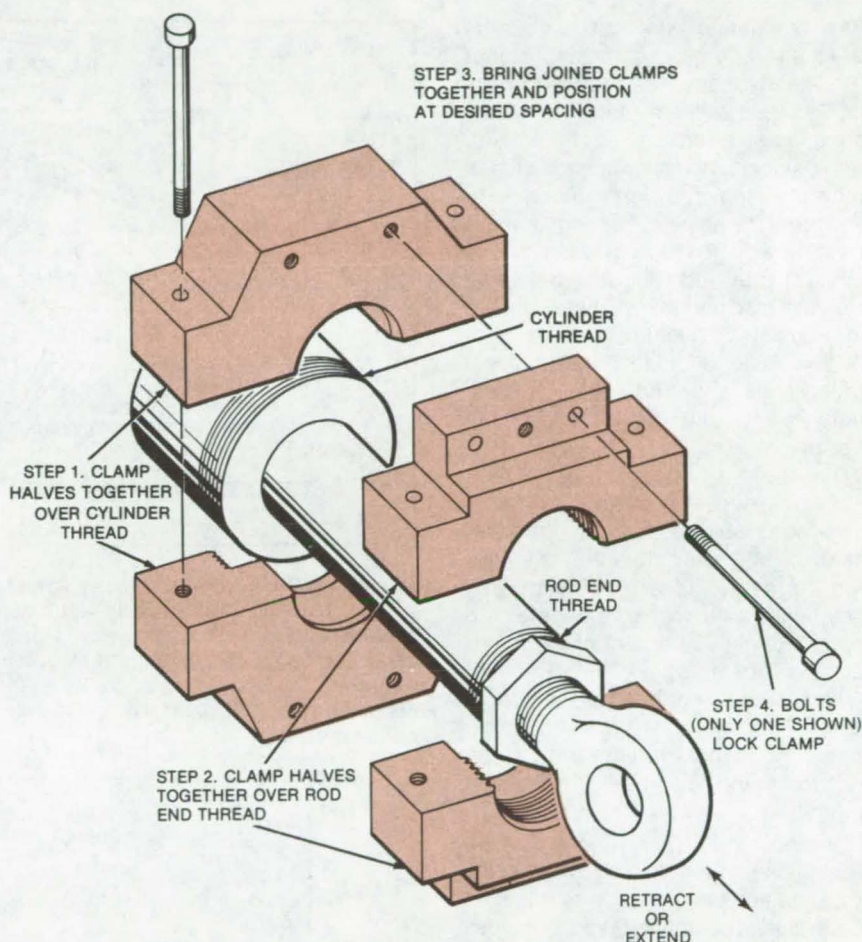
In a hydraulic actuator, a rod is thrust out from a cylinder or is retracted into the cylinder. As long as hydraulic pressure is maintained, the actuator holds the rod at the desired extension. When power is removed, however, the rod can move under the load.

A pair of clamps developed for hydraulic actuators on the Space Shuttle engines prevents the unwanted movement. The clamps are fastened to the rod and cylinder and are then locked together with bolts. Besides preventing the travel of deenergized actuators, the clamps might also serve as a temporary rigid link in a hydraulic system under repair.

A prototype of the locking device is shown in the figure. Both the rod and cylinder are threaded. Each clamp consists of two threaded halves that are assembled around the rod and cylinder threads. The two clamps are then fastened together by bolts that prevent both retraction and extension of the rod. An important feature of the mechanism is that the spacing between the clamps is adjustable through use of the bolts. Thus the actuator can be locked at any rod extension.

The clamps can lock an actuator to be used as a mechanical support or linkage — for example, to support a platform. The mechanism may also be useful as a fail-safe device in case of loss of hydraulic pressure. Potential applications include manufacturing processes and specialized handling and holding devices.

This work was done by Robert H. Wood of Rockwell International Corp. for Johnson Space Center. No further documentation is available.
MSC-18853



This **Adjustable Lock** for a hydraulic actuator can hold the rod in a fixed extension from the cylinder even when power is off, thus converting the actuator into a stiff structural member.



Gentle Arrester for Moving Bodies

A wire cable absorbs energy with reduced shock and rebounding.

Langley Research Center, Hampton, Virginia

An elongating wire cable absorbs the kinetic energy of a moving object more gently than does a conventional elastic-arrest system, such as a coil spring, a net, or an aircraft shock cord. Such devices impart large shock loads to the moving body and cause it to rebound. The new arresting line, in contrast, absorbs energy at a nearly constant rate, reducing the maximum arresting load and minimizing rebounding. Possible applications of the wire-cable arrester include passenger restraint in air and land vehicles, parachute risers, and ground snatch by aircraft.

The new energy arrester (see Figure 1) consists of a wire cable surrounded by a tubular braided sheath of polyester cloth that is longer than the cable. To arrest the moving body, the wire cable elongates to approximately 90 percent of its potential while absorbing all the energy of motion. To be efficient, the cable elongates to near its breaking point. Should it break prematurely, the braided sheath absorbs the remaining energy.

One possible cable material is type 302 stainless steel, which when properly annealed elongates by as much as 40 percent with only a 50-percent loss in strength. The wire cable is routed through the longer tubular suspension line to prevent chafing against adjacent structures during elongation and to prevent a catastrophic failure should the wire cable break. Figure 2 compares the maximum shock loads imparted to the arrested body by the elongating cable and by typical elastic arresters, for equivalent energy absorption.

This work was done by Reid A. Hull of Langley Research Center. No further documentation is available.

This invention is owned by NASA, and a patent application has been filed. Inquiries concerning nonexclusive or exclusive license for its commercial development should be addressed to the Patent Counsel, Langley Research Center [see page A5]. Refer to LAR-12372.

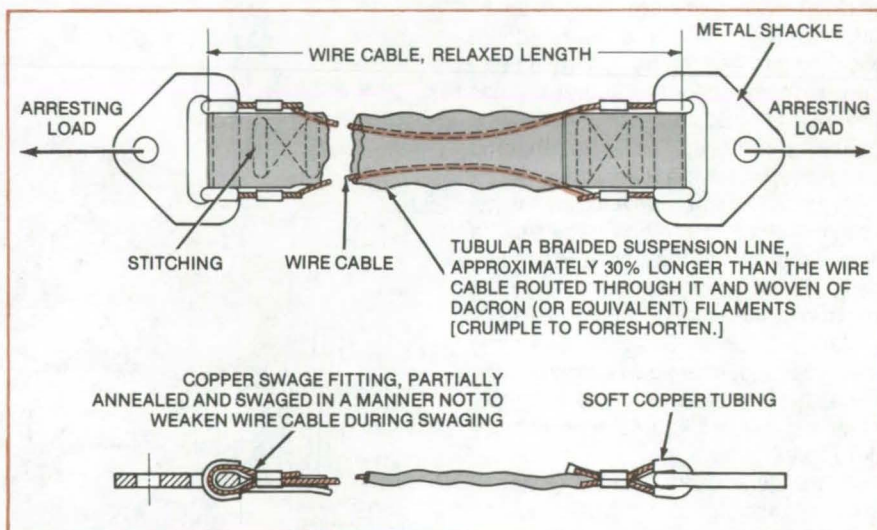


Figure 1. **Moving-Body Velocity Arrester** consists of wire cable surrounded by a braided sheath. The stitching reinforces the assembly. The wire cable is partially annealed so as to have increased elongation potential. [Type 302 stainless-steel cable can be made to elongate as much as 40 percent if cleaned and annealed in a vacuum furnace and that with only a 50-percent loss in strength; subjecting the wire cable to 1,650° F (900° C) for 15 minutes is required to achieve these physical characteristics.]

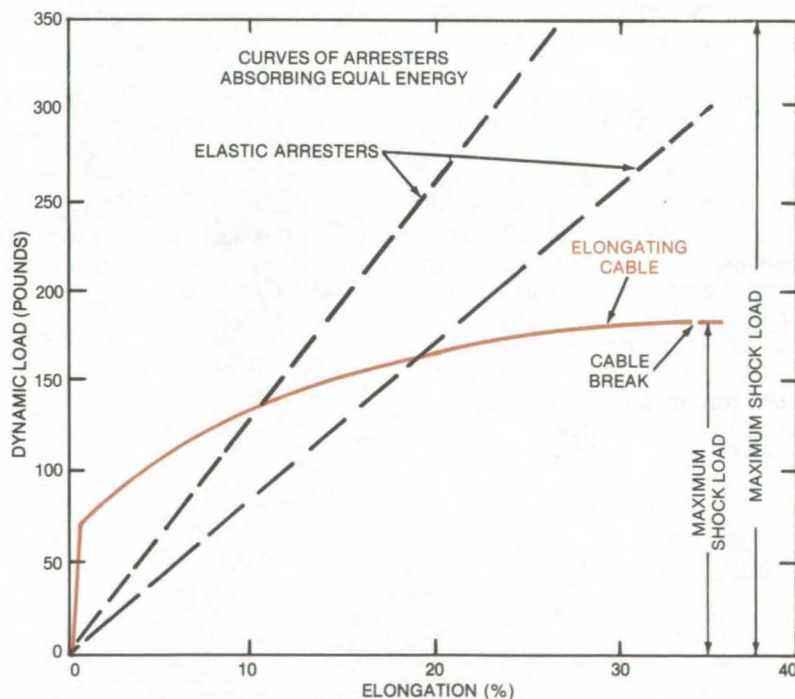


Figure 2. **Dynamic Load Is Compared** for an elongating cable, 1/16 in. (0.16 cm) in diameter, and typical elastic-arrest systems. The cable data were obtained experimentally.

Soft Container for Explosive Nuts

Flexible fabric bag fits over a variety of assembly shapes.

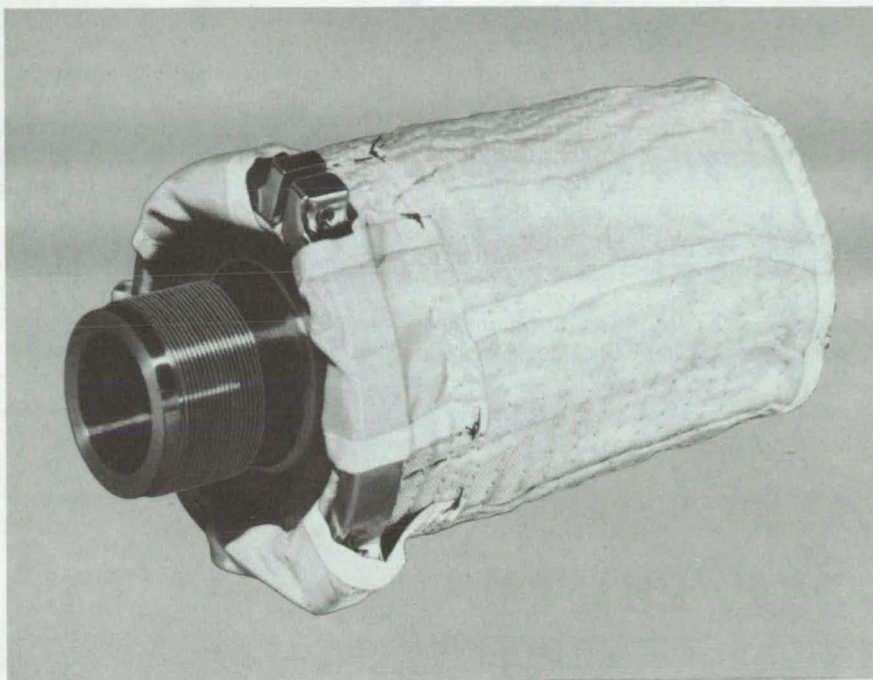
Lyndon B. Johnson Space Center, Houston, Texas

Blasts from explosive nuts and other pyrotechnic devices are contained by a bag sewn from fabric. Unlike conventional metal vessels for blast containment, the bag is light and flexible and readily fits around odd shapes. It could be used to contain not only the debris produced by explosive-nut detonations but also that from safety tests.

The material for the bag is woven aramid (a multifilament polyamide) fabric. Belt loops of the same fabric attach the bag to a three-piece clamp, which retains the bag on a rigid ring. The ring supports the structure for the explosive nut inside the bag. The clamp makes a sewn-on top unnecessary, and the bag can therefore easily be placed over the nut structure and removed after the nut has been detonated.

Thread is stitched around the bag in parallel rings (see figure). The stitches help to absorb energy as the threads break from the shock of the explosion.

This work was done by Dean C. Glenn, William E. Drummond, and Gordon Miller of Johnson Space Center. For further information, Circle 68 on the TSP Request Card.
MSC-18871



Belt Loops Hold the Blast-Container Bag to a clamp. A threaded-neck ring supports the explosive-nut structure and detonator wires. After the nut has been mounted in the ring, the bag and clamp are slipped over it and fastened to it.

Computer Programs

These programs may be obtained at very reasonable cost from COSMIC, a facility sponsored by NASA to make new programs available to the public. For information on program price, size, and availability, circle the reference letter on the COSMIC Request Card in this issue.

Cylindrical Bearing Analysis

Including the effects of bearing geometry, shaft misalignment, and temperature

CYBEAN computes the behavior of cylindrical rolling-element bearings

under conditions that may include high speed and misaligned shafts. Accurate assessment of geometry-induced roller preload is possible for various outer-ring and housing configurations. The analysis considers a flexible outer ring and housing and treats cases where the outer-ring outer surface is not in contact with the housing around its entire perimeter. This would be the case when a two- or three-point out-of-round ring is pressed into a circular mounting hole in the housing.

CYBEAN is structured for the coordinated execution of modules that perform specific analytic tasks. It initiates a computation with geometry, lubricant, and material definitions. To economize on computation, constants are evalu-

ated in structure locations external to iterative calculations.

A repetitive loop is used that addresses the computation of geometry fits. Arbitrary housing and outer-ring profile interactions are considered. Rolling-element load distribution is obtained for the mode of bearing preload defined by the user. Interference-fit effects, including rotation, temperature, and roller-load-induced ring displacements, are evaluated and used to compute the operating diametral clearance. The field-equation set is evaluated for the bearing, which can contain up to 50 rollers. The set of values for the independent variables that satisfies all

(continued on next page)



the equations of equilibrium simultaneously is considered to be a solution.

An accurate initial guess of the variable values can save considerable execution time. However, the nonlinear coupling of the large set of unknowns within a typical physical system makes it difficult to guess accurately. This problem is overcome by first solving the simpler elastic case. The set of variables that satisfy the equilibrium of elastic forces is then used as an initial guess for the more complicated solution, which includes friction. This initial elastic solution is also used to determine the equilibrium load distribution that defines housing-fit pressures.

The general field-equation set is partitioned before it is solved. Independent variables describing the inner-ring position and roller radial position are

addressed in conjunction with field equations governing ring and roller radial equilibrium. Equation cross coupling is established through the roller radial position. This subset is brought to equilibrium by Newton-Raphson iteration.

Once inner-ring equilibrium is satisfied, the field-equation set is again partitioned to include roller axial, radial, skew, and tilt moment equations of equilibrium. Coupling is maintained through the associated displacement variables. At this portion of the analysis, roller end-flange contact forces are equilibrated with raceway-induced loading.

A final partition is made such that the field equations defining force equilibrium in the direction tangent to the pitch circle, moments about the roller

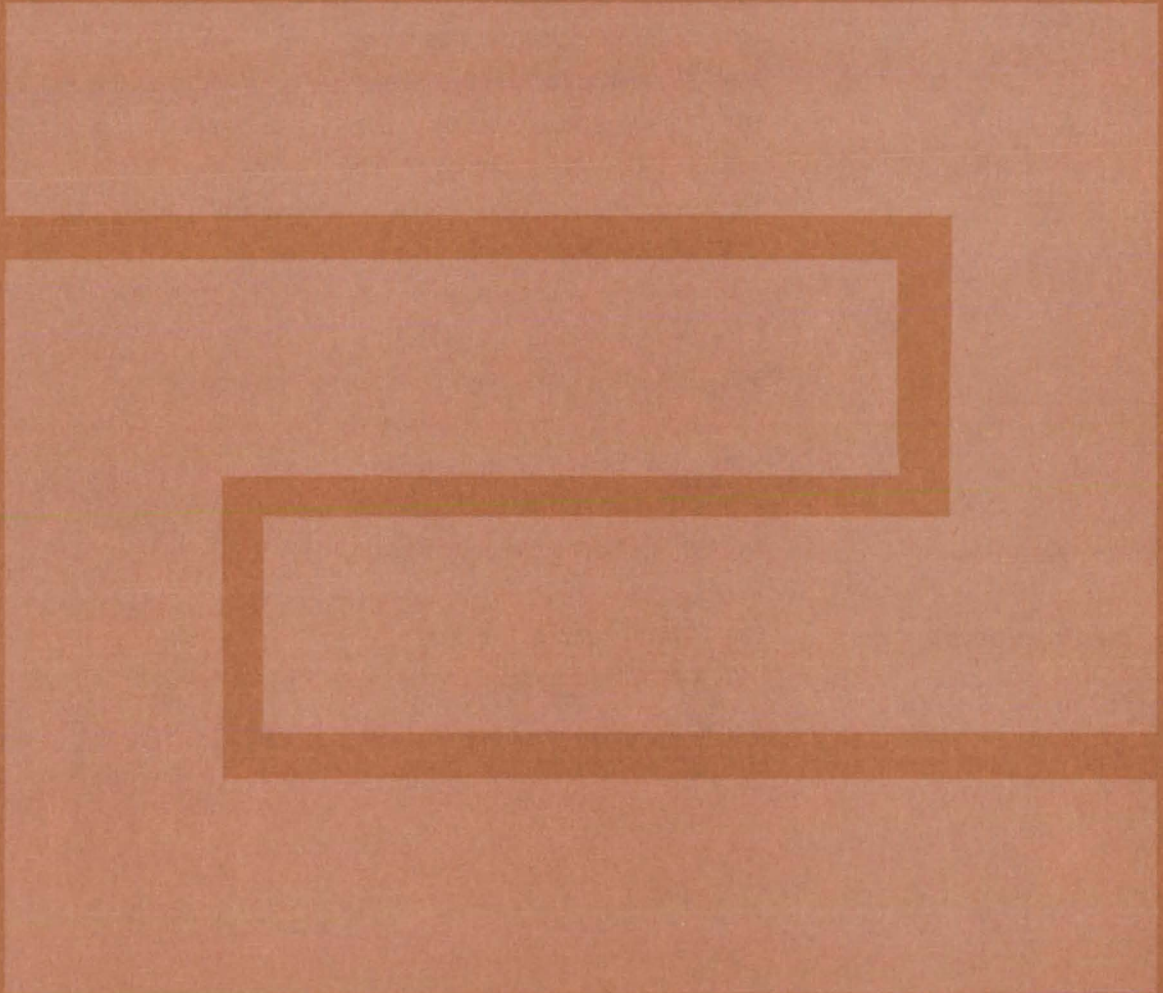
axis, and radial cage equilibrium are considered. Associated variables are: radial position, rotational and orbital speeds, and cage displacements. The set of values of independent variables that simultaneously satisfy these equations is considered a solution.

Satisfactory convergence of the iterative procedure allows the definition of results of a specific temperature. The remaining program structure addresses the computation of steady state and the time-transient system thermal performance.

This program is written in FORTRAN V for use on the UNIVAC 1100/40 computer.

*This program was written by R. J. Kleckner and J. Pirvics of SKF Industries for **Lewis Research Center**. For further information, Circle K on the COSMIC Request Card.*
LEW-13393

Fabrication Technology



Hardware, Techniques, and Processes

- 495 "Densified" Tiles Form Stronger Bonds
- 495 Tile Densification With TEOS
- 496 Repairing High-Temperature Glazed Tiles
- 497 Producing Silicon Continuously
- 498 Mobile Glazing Unit
- 499 Learning High-Quality Soldering
- 500 Eliminating Gaps in Split Rings
- 501 Passivation Layer for Steel Substrate of Solar Cell
- 502 Low-Cost Concentrating Mirrors
- 502 Spiral-Wound Gasket Forms Low-Temperature Seal
- 503 Arc Spraying Solderable Tabs to Glass
- 504 Back Contacts for Silicon-on-Ceramic Solar Cells
- 504 Self-Lubricating Gearset
- 505 Reflecting Layers Reduce Weight of Insulation
- 505 Lightweight Cryogenic Vessel
- 506 Drop Tower With No Aerodynamic Drag

Books and Reports

- 507 Nickel-Doped Silicon for Solar Cells

Computer Programs

- 507 CADAT Network Translator
- 508 CADAT Integrated-Circuit Artwork Program

"Densified" Tiles Form Stronger Bonds

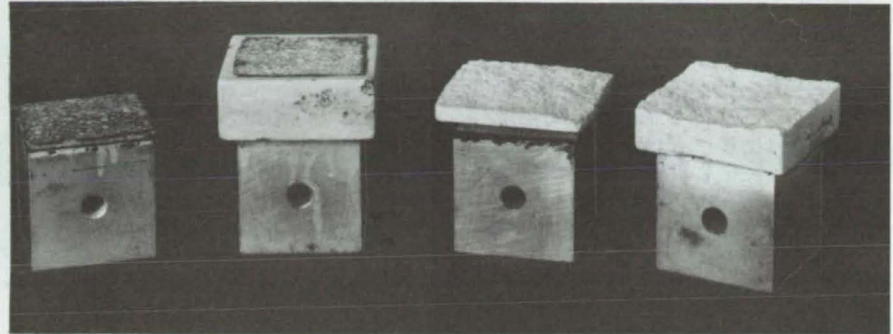
A one-step application of colloidal silica more than doubles the bond strength.

Lyndon B. Johnson Space Center, Houston, Texas

The technique selected for strengthening the Space Shuttle surface-tile/substrate bond could be applied to similar ceramic-tile-attachment problems in other applications. The "densification" process strengthens the surface where the tile attaches to a felt strain-isolator pad, redistributing stresses and preventing failures at that point. Those interested in the technology of bonding delicate ceramics to non-rigid materials should also consider the Shuttle backup tile-strengthening technique, described in the following article, "Tile Densification With TEOS" (MSC-18737).

The reusable surface-insulation tiles that protect the orbiter from repeated high-temperature plunges through the atmosphere are susceptible to failure where they are bonded to felt pads that separate them from the Shuttle frame. In densification, a binder mixture impregnates the bottom of the fibrous ceramic tiles to form a high-strength skin. The platelike layer more than doubles the strength of the tile-to-felt-pad bond. In tests, tiles that were densified did not fracture until they were stressed to the limit of the bulk material (see figure). Undensified tiles, in comparison, fractured at the bond interface and at much lower stresses.

The process uses an aqueous mixture of colloidal silica as a cement and ball-milled silica particles, which — like sand in concrete — act as a reinforcement. Brushing forces the mixture into the interstices of the tile. The depth of



Densified and Undensified Tiles fail at different locations and at different stresses. The undensified specimen (left) failed at about 11 psi (7.5×10^4 N/m²) at its interface with the stress-isolation pad. The densified tile (right) failed at a much higher stress, 23 psi (1.6×10^5 N/m²), and the break occurred in the bulk material.

densification is 0.06 to 0.11 inch (1.5 to 2.8 mm), depending on the original tile density. The outer 0.035 inch (0.9 mm) of densified tile are three to six times as strong as the bulk material. The densified layer is still porous and allows volatile materials to escape as the Shuttle heats up in the atmosphere.

The first step in densification is an application of isopropyl alcohol to the bottom (unglazed) surface of the tile. The alcohol allows the densifying agents to wet and penetrate the water-repellent treatment on the tile. The slurry of colloidal silica and silica powder, with a small amount of pigment added, is painted on the tile. The pigment, an inert ceramic (tetra-boron silicide), makes the slurry easier to see and aids in an even application.

After air-drying for 24 hours and oven-drying at 150° F (66° C) for 2 hours, the tile is weighed to determine the amount of material that has been added. Usually the amount is about 0.5 g/in.² (0.078 g/cm²) of surface area. Finally, the tile is rewater-proofed by exposure to vapors or methyltrimethoxysilane and acetic acid (a catalyst) at 350° F (1.77° C). The tile is then ready for installation.

This work was done by Robert L. Dotts of Johnson Space Center and Jack W. Holt of Rockwell International Corp. For further information, Circle 69 on the TSP Request Card.

Inquiries concerning rights for the commercial use of this invention should be addressed to the Patent Counsel, Johnson Space Center [see page A5]. Refer to MSC-18741.

Tile Densification With TEOS

Tetraethyl orthosilicate is another effective tile densifier.

Lyndon B. Johnson Space Center, Houston, Texas

The alternate densification process for Space Shuttle surface-insulation tiles (see preceding article) uses a brushed or sprayed coating of tetraethyl orthosilicate (TEOS), a commer-

cial bonding agent for refractory brick and constituent of high temperature paint. When applied to the tile surface, TEOS is absorbed and deposits a relatively pure form of silica within the

tile. The thermal expansion of the deposit matches that of the tile closely; and the surface tension of TEOS liquid is low enough that it

(continued on next page)

readily penetrates into the tile, even if the tile has been waterproofed. A TEOS-densified layer in the tile, about 0.2 inch (0.5 cm) deep with a minimum density of 2.5 g/in.³ (0.15 g/cm³), strengthens the tile/pad combination to a level consistent with the full strength of the tile alone.

The liquid is generally applied and cured in three steps, after which the tile is allowed to cool and is weighed. The weight increase will usually average 0.15 g per square centimeter.

The TEOS liquid is prepared by mixing TEOS with 0.05N hydrochloric acid in the correct volume ratio. A dye added to the mixture helps to determine when the constituents are fully

mixed; it also makes the TEOS easier to see when it is applied to the tile. The liquid should be used within 48 hours after preparation.

The TEOS liquid can be applied by brush, spray, or any other means that will ensure an even coating. If the area to be densified is less than the total area of the tile base, the boundary may be marked by a soft pencil (for brush application) or masked (for spraying).

The versatility of TEOS gives it a wide range of applications. Selected areas of tile can be densified to provide stiffer and stronger tile properties; also, a more durable surface is provided for additional coatings. The

penetration of TEOS into a tile can be adjusted from full penetration (saturation) to a controlled localized densification. There is no surface buildup from the use of TEOS; thus, there are no dimensional changes when densifying.

This work was done by Glenn M. Ecord and Calvin Schomburg of Johnson Space Center. For further information, Circle 70 on the TSP Request Card.

Inquiries concerning rights for the commercial use of this invention should be addressed to the Patent Counsel, Johnson Space Center [see page A5]. Refer to MSC-18737.

Repairing High-Temperature Glazed Tiles

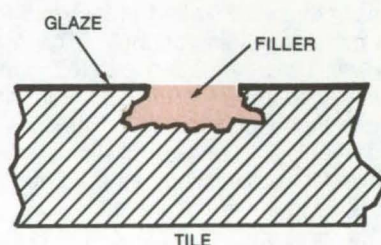
Chips and cracks in glaze are fixed quickly and dependably with a mixture containing tetraethyl orthosilicate.

Lyndon B. Johnson Space Center, Houston, Texas

Surface-damaged insulation tiles (see preceding articles) survive exposure to hostile sonic and temperature environments when they are repaired according to a new procedure. The new method consists of filling damaged areas on the glazed surface of the tile after proper preparation. The primary ingredient in the filler material is tetraethyl orthosilicate (TEOS).

The filler is prepared by mixing hydrolyzed TEOS, silicon tetraboride powder, and pulverized tile material. The silicon tetraboride gives the filler a black color; for white tiles it can be omitted.

To repair a tile, the damaged area is first cleaned. With the aid of dental tools, the edges of the damaged area are undercut (see figure), and any residue is removed. The area is coated with liquid TEOS and dried with heat lamps or a heat gun. After another coat of liquid TEOS is applied to the damaged area, the filler paste is applied to



Undercutting the Edge of a Surface Crack, as shown in this cross section, helps to anchor filler material securely. The filler is carefully built up to the level of the tile glaze. The procedure can be performed in less than 1-1/2 hours.

the crack with a spatula. The paste is carefully worked into the damaged area, including the undercut edges. Packed gently but firmly so as not to crack the surrounding coating, the paste is built up to the surface of the tile. The surface then is heated to dry and cure the filler. Finally, excess

filler is sanded off the tile surface, and a final coat of liquid TEOS is brushed on.

Tiles repaired in this manner survived tests in which they were subjected to intense acoustic emissions, arc jets, and intense heat radiation. The new method is not only more reliable but also is less time-consuming than previously used methods. It can be performed in less than 1-1/2 hours with the tile in any orientation — even facing downward; the tile does not have to be removed for repair.

This work was done by Glenn M. Ecord and Calvin Schomburg of Johnson Space Center. For further information, Circle 71 on the TSP Request Card.

Inquiries concerning rights for the commercial use of this invention should be addressed to the Patent Counsel, Johnson Space Center [see page A5]. Refer to MSC-18736.

Producing Silicon Continuously

Fluid-bed vaporization followed by chemical vapor deposition generates large, semiconductor-grade silicon particles.

NASA's Jet Propulsion Laboratory, Pasadena, California

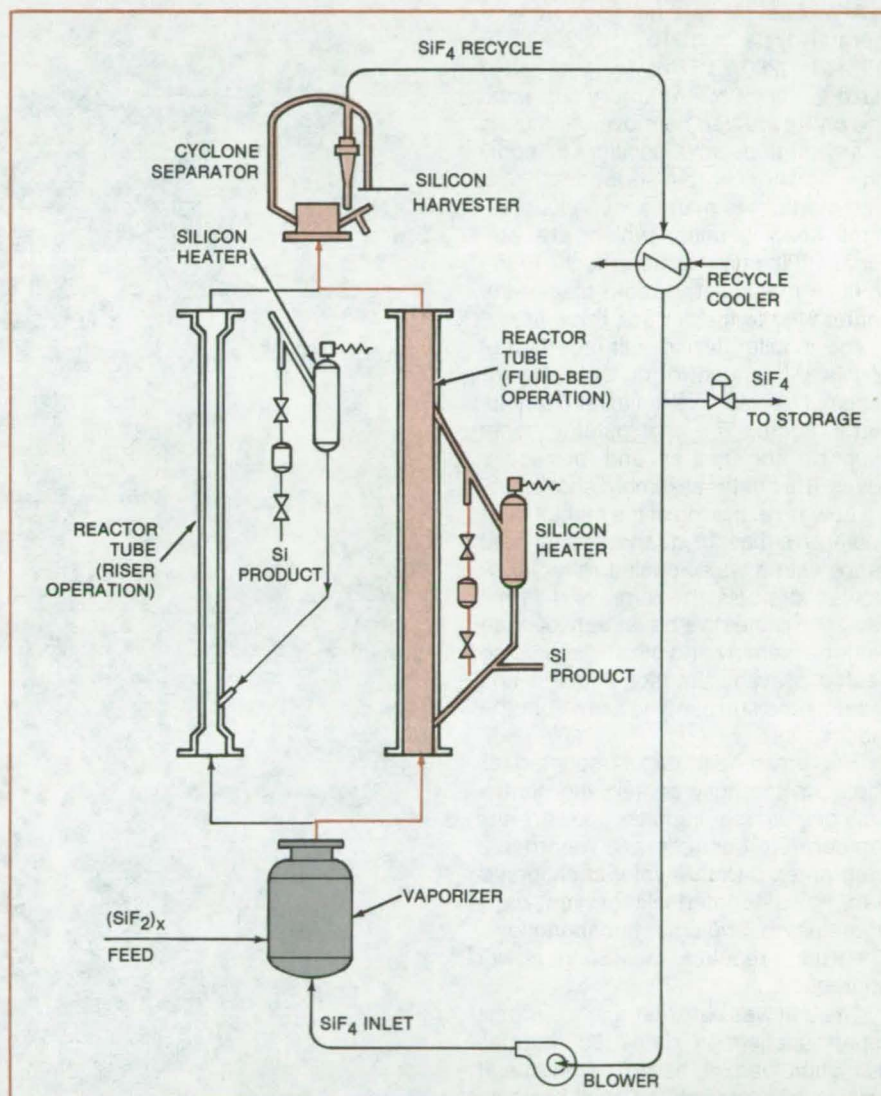
Chunks of semiconductor-grade silicon suitable as "seeds" for single-crystal growth and other applications is harvested continuously from an apparatus that combines a vaporizer with a fluidized bed or riser bed. Now undergoing laboratory development, the apparatus generates only dense silicon particles (no powder) from $(\text{SiF}_2)_x$ polymer feedstock. It shows promise as a more economical, higher volume alternative to previous batch-processing methods.

The apparatus, as shown in the figure, includes a fluid-bed vaporizer, consisting of silicon particles ranging from 1/2-in. (13-mm) to 5-mesh, with a $(\text{SiF}_2)_x$ polymer feed, and a SiF_4 inlet. The temperature of the vaporizer is maintained between 200° and 400° C by controlling the temperature of the inlet SiF_4 . At these temperatures the $(\text{SiF}_2)_x$ is in equilibrium with Si_xF_y homologs that distill out of the vaporizer. Si_xF_y exits the vaporizer and contacts 5-to-80-mesh silicon in heaters at 500° to 1,000° C in the fluidized bed or riser bed. The flow rate and diameter of the reactor tube determine the mode of operation (fluidized or riser). On contacting the hot silicon, the Si_xF_y homologs disproportionate into silicon (which deposits on the hot silicon) and SiF_4 .

The pure silicon is separated from the Si_xF_y in a cyclone separator, and the SiF_4 is recycled after cooling to 250° C. Part of the SiF_4 is stored, and the balance is recycled.

The addition of SiF_4 is regulated in the vaporizer to ensure that the partial pressure of Si_xF_y in the fluidized bed is less than 7 torr. At this low pressure, no silicon powder forms.

The $(\text{SiF}_2)_x$ polymer can be introduced into the duplex vaporizer/harvester by several methods. It could be formed in a heat exchanger/condenser and scraped into a displacement pump, which would force-feed the $(\text{SiF}_2)_x$ polymer into the vaporizer. Alternatively, the polymer could be scraped into a storage hopper and then added to the vaporizer.



Semiconductor-Grade Silicon Chunks, roughly 1 cm in diameter, are produced continuously in a process based on the vaporization of feedstock, chemical vapor deposition in a fluidized bed, the extraction of silicon chunks, and the recycling of SiF_4 .

The product fluidized-bed particles are approximately 0.03 to 0.5 cm in diameter; and the harvested chunks, extracted in a cyclone separator, are about 0.5 to 1.3 cm in diameter. The process is not limited to $(\text{SiF}_2)_x$ polymer feedstock; it can utilize virtually any halosilane intermediate

used in silicon production.

This work was done by William M. Ingle, Richard S. Rosler, and Stephen Thompson of Motorola, Inc., for NASA's Jet Propulsion Laboratory. For further information, Circle 72 on the TSP Request Card. NPO-14796

Mobile Glazing Unit

The unit provides a programmed thermal cycle for in situ repair of ceramic coatings.

John F. Kennedy Space Center, Florida

A mobile glazing unit programs a thermal cycle from 100° to 2,300° F (40° to 1,260° C) for firing ceramic glaze coatings on refractory surfaces. The prototype can be moved and used in any attitude and position to apply high radiant heat to a surface.

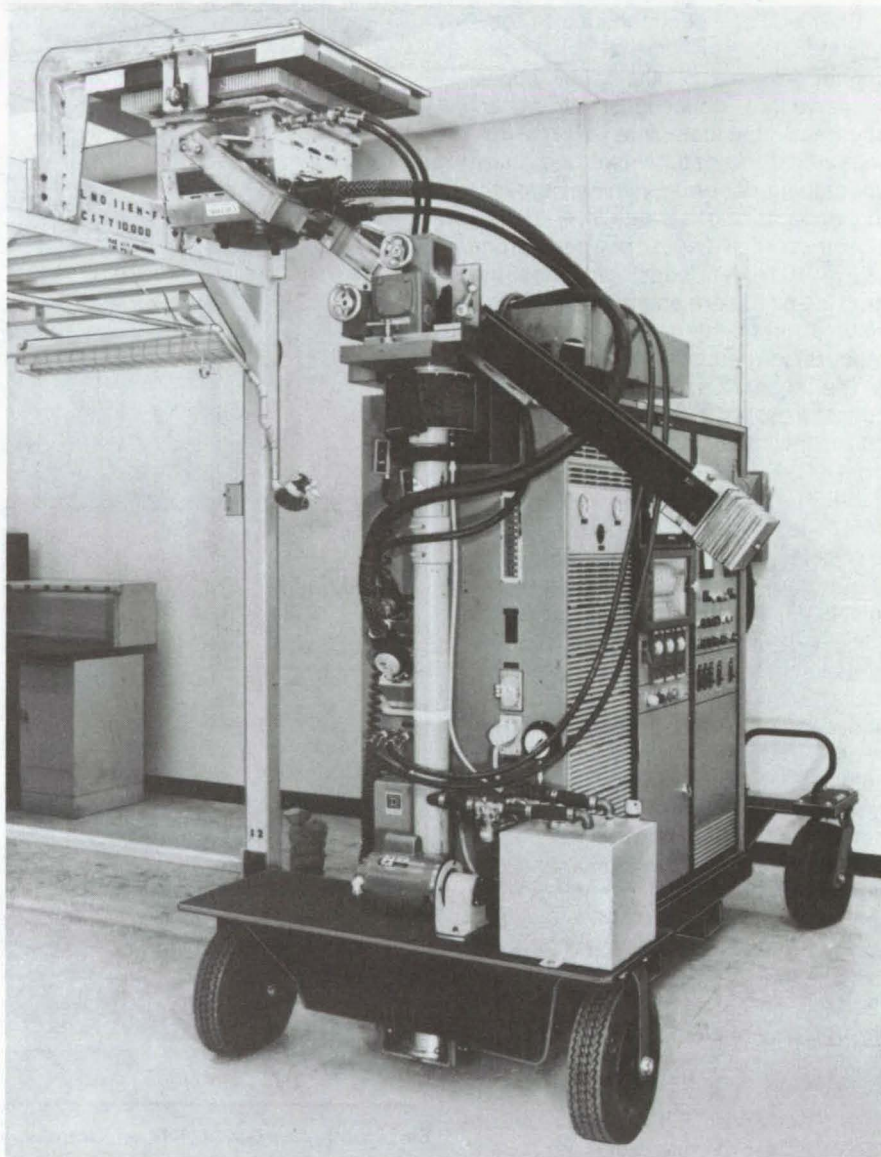
In contrast to many conventional radiant heating units, which are stationary, this unit can be brought to the work. A manipulator boom places the heater next to the surface to be fired.

The mobile glazing unit (see figure) consists of a control console, heater assembly, protective cover, and manipulator boom. The manipulator boom supports the heater and protective cover. The heater assembly, shown facing upward at the top of the manipulator boom arm, has 18 quartz radiant-heat lamps with a water-cooled reflector. A blower air-cools the lamp end terminals. The protective cover between the heater assembly and the surface being heated prevents impact damage and protects the surrounding area from the radiant heat.

The equipment racks mounted directly on the dolly contain the control console, which includes power and temperature controllers, a recorder, a programmer, and the water-cooling system. Fail-safe interlocks prevent damage due to equipment malfunctions. The unit requires a 480-V power source.

The unit was built for firing a ceramic repair coating on damaged thermal-insulation tiles on the Space Shuttle. It was built from off-the-shelf components. The unit should be useful industrially for in situ repair applications of glazing on ceramics or for curing individual refractory blocks during the maintenance of furnaces.

This work was done by Jack W. Holt of Rockwell International Corp. for Kennedy Space Center. Further information may be found in NASA N81-70850/NSP, "Model 1023/8. Mobile Tile Glazing High Density Radiant Heating System—Preliminary Man-



The **Mobile Glazing Unit** consists of a control console, heater assembly, protective cover, and manipulator boom. The heater assembly has 18 quartz radiant-heat lamps and a water-cooled reflector that provide thermal cycling in the temperature range of 100° to 2,300° F.

ual" and "Instruction Manual" [\$20]. A copy may be purchased [prepayment required] from the National Technical Information Service, Springfield, Virginia 22161.

Inquiries concerning rights for the commercial use of this invention should be addressed to the Patent Counsel, Kennedy Space Center [see page A5]. Refer to KSC-11171.

Learning High-Quality Soldering

A 5-day course teaches ultra-high-reliability electronic assembly.

NASA's Jet Propulsion Laboratory, Pasadena, California

	<p>EXERCISE NO: 1</p> <p>EQUIPMENT</p> <p>Special Work Station</p> <p>See L1200 Information Sheet</p> <p>CAUTION: Rework of static sensitive parts require same Special Work Station as for installation of sensitive components.</p>		<p>EXERCISE NO: 5</p> <p>REMOVE IC</p> <p>Repeat step 3 and 4 until all leads are detached, lift IC from board with approved tweezers.</p>
	<p>EXERCISE NO: 2</p> <p>PREPARE WICKING BRAID</p> <p>Select a wicking braid of appropriate size.</p> <p>Flux braid.</p>		<p>EXERCISE NO: 6</p> <p>RESTORE PAD</p> <p>Restore tinned pads to original tinned condition by wicking off excess solder.</p>
	<p>EXERCISE NO: 3</p> <p>REMOVE SOLDER</p> <p>Place fluxed braid over IC lead to be unsoldered and apply soldering iron tip over braid. Limit time of tip on braid to 4 seconds. Remove iron. Trim braid with solder to expose new section and repeat until excess solder of joint is removed. No more than 3 leads can be wicked without re-preparing the soldering iron.</p>		<p>EXERCISE NO: 7</p> <p>CLEAN AND INSPECT</p> <p>Clean PWB Pad area with stiff brush and approved solvent.</p> <p>Inspect pad area to verify original requirements for PWB and tinned pads.</p>
	<p>EXERCISE NO: 4</p> <p>SEPARATE LEAD FROM TRACE</p> <p>After wicking the solder from flat pack joint, place a lead lifting tool under the lead near the juncture of the lead and PWB trace. Heat the lead with a soldering iron and gently press the tool on the joint and slide the tool between the lead and the trace to separate the two.</p>		<p>EXERCISE NO: 8</p> <p>Replace flat pack with new part using original installation criteria per Lesson Plan FS 12.</p>

Exercises in a Lesson Plan show in detail the approved steps for assembly or disassembly operations for electronic circuits — in this case, the removal of an integrated-circuit flat pack. Each step is presented in a simple and straightforward fashion in a training booklet and a video-tape demonstration.

A training course teaches soldering techniques to technicians who work on high-reliability electronic equipment. The course develops student awareness of soldering practices that assure long, failure-free equipment life.

At NASA's Jet Propulsion Laboratory, students attend the course for 5 days, from 8:15 in the morning to 4:15 in the afternoon. Part of their time is spent listening to lectures and watching video-tape demonstrations, but most of their time is devoted to performing step-by-step procedures under the guidance of an instructor.

Topics covered include:

- Hand Soldering;
- Wire and Component-Lead Preparation;
- Eyelet, Hook, Bifurcated, and Turret Terminal Soldering;
- Soldering of Flat and Round Conductors;
- Wire Routing; and
- Component Installation.

In addition to learning how to assemble new circuits, the students learn how to rework printed-wiring boards, to replace parts, and to make circuit changes by cutting traces, changing wiring, and adding terminals. The students are taught the benefits of using approved and calibrated instruments and tools and of performing the operations at properly-equipped and grounded work stations, particularly for complementary metal-oxide-semiconductor (CMOS) integrated circuits.

The instructor demonstrates — and the students practice — the use of flux; cleaning before and after soldering; joint inspection; soldering-iron care, maintenance, and calibration; and wire stripping and forming. The procedures and practices are organized as lesson plans, each plan consisting of step-by-step instructions for a complete assembly or disassembly operation.

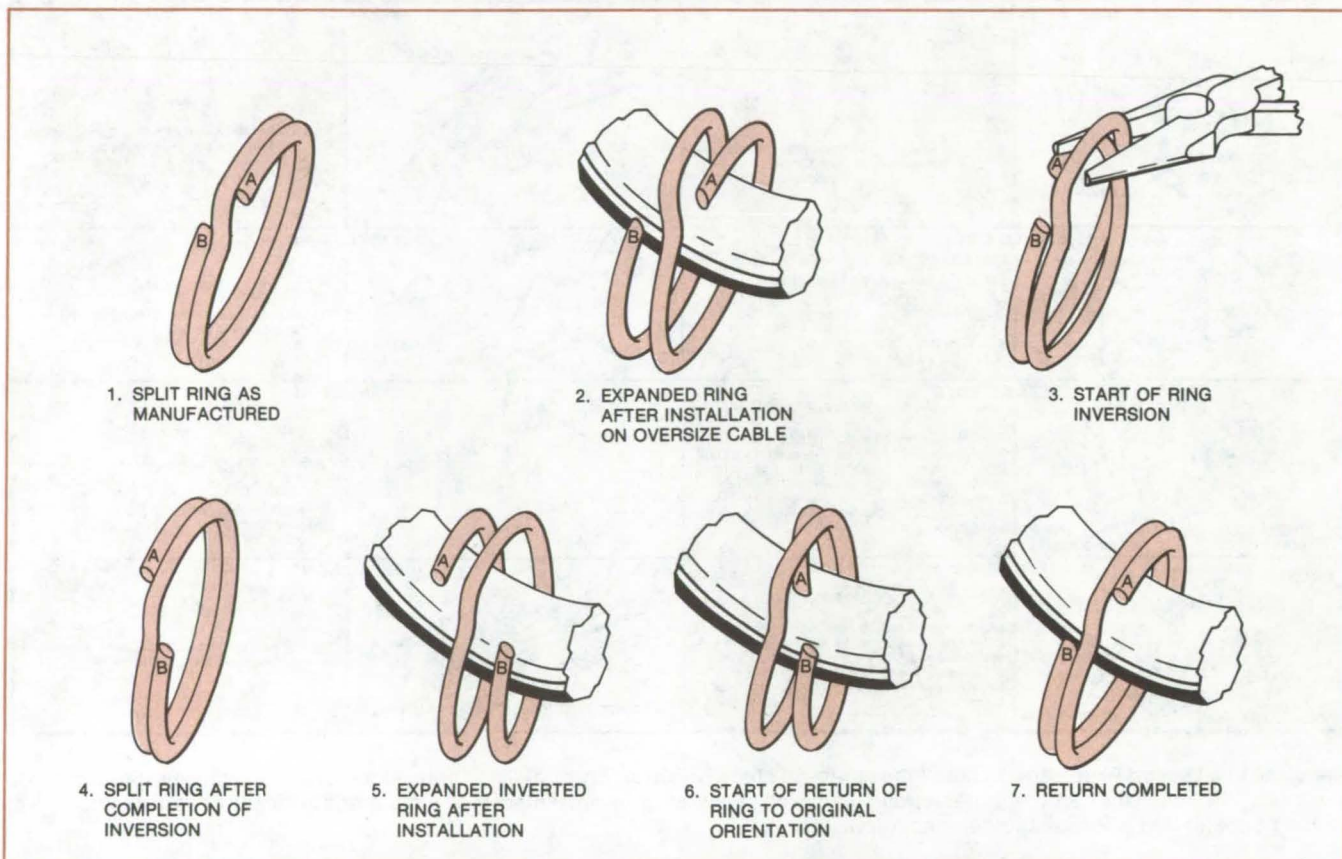
For example, one lesson plan covers the removal of an integrated-circuit flat pack. The student is instructed (through video-tape demonstration and illustrated booklet — see figure) to select a soldering-iron tip and a wicking braid and to apply the iron and braid to each of the flat-pack leads in turn, removing the solder from each. Then the student is told to select a soldering-iron tip of the proper size and shape for the leads, to select a lead-lifting tool as well, and to use these tools to detach each lead in turn from the circuit board. Throughout, the student is shown methods that will prevent damage to the parts and ensure cleanliness.

This work was done by William S. Read of Caltech for **NASA's Jet Propulsion Laboratory**. For further information, Circle 73 on the TSP Request Card.
NPO-14869

Eliminating Gaps in Split Rings

A simple installation method allows smaller, lighter tether rings for cables.

Lyndon B. Johnson Space Center, Houston, Texas



A **Split Ring is Expanded** (views 1 and 2) if it is installed on too large a cable. However, the procedure shown in views 3 through 7 inverts the coils and then returns them to their original position so that the coil gap disappears.

Ordinarily, the split-ring wire coils used to tether objects to a cable or rope have a wire diameter greater than some minimum determined by the cable diameter. Below this thickness, the elastic limit of the wire will be exceeded when its coils are opened wide enough to pass over the cable. The coils then will not snap together after they have passed over the cable, but will remain expanded, with a gap between adjacent coils. In this condition, the ring is not a reliable fastener.

A simple method of attaching split-ring coils to cables prevents such gaps from forming. The method makes it possible to use thinner coils without gaps forming and thus saves cost and weight. In the method, a ring is inverted before it is installed and returned to its original position after it is installed.

The coil installation is shown in the figure. The installer inverts the ends of the ring with a small pair of pliers, pulling one end through the ring and

allowing the coils to follow. The coils are spread, and the ring slides over the cable. This procedure expands the inverted ring, leaving gaps between the coils. Finally, the installer reverses the inversion, pulling one end through the ring so that the coils follow it. The ring is then in its original orientation, and the coils are tightly compressed.

This work was done by Richard W. Gould of Rockwell International Corp. for **Johnson Space Center**. No further documentation is available.
MSC-18854

Passivation Layer for Steel Substrate of Solar Cell

Thin-film solar cell can be fabricated on commercial sheet-steel substrate passivated with tungsten layer.

NASA's Jet Propulsion Laboratory, Pasadena, California

A coating of fine-grain tungsten can passivate steel; i.e., prevent any of the constituents of the steel from interacting with material on the other side of the tungsten. This passivation layer of tungsten allows the use of steel as an inexpensive conducting substrate for thin-film solar cells; the tungsten is deposited on top of the steel, and then the solar cell is fabricated on top of the tungsten passivation layer (see figure).

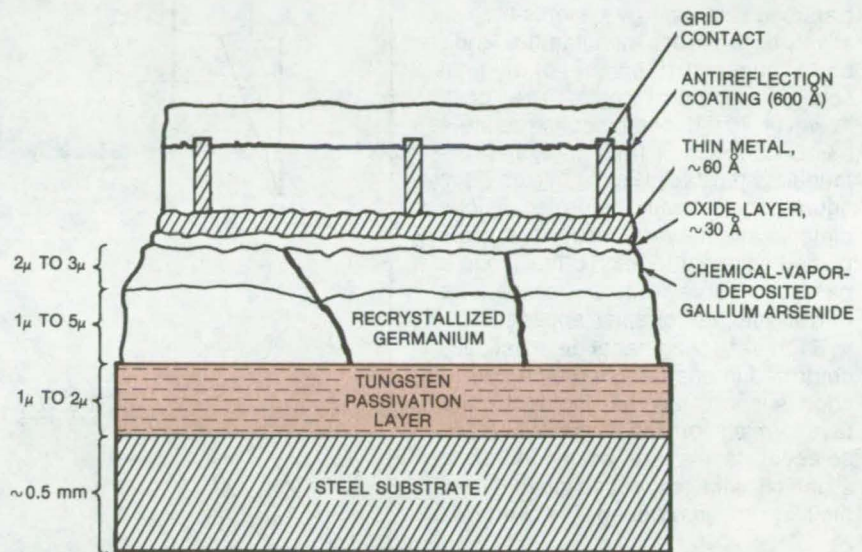
In the thin-film solar cell, germanium (Ge) is deposited and recrystallized on the substrate. Gallium arsenide (GaAs) is then formed by chemical vapor deposition over the germanium. Subsequently, a thin oxide and thin metal film are formed over the GaAs layer. A conducting grid contact and a top antireflection coating are added to complete the solar cell.

An inexpensive conducting substrate such as steel makes these solar cells less expensive. However, without a passivation layer, the substrate can alloy with the germanium or diffuse into the germanium and gallium arsenide.

The characteristics desired in a passivation layer are:

- thermal and electrical conduction,
- low contact resistance with the adjacent materials,
- strong adhesion to the adjacent materials,
- low interdiffusion of the substrate and Ge/GaAs through the passivation layer, and
- low loss of the passivating material into the adjacent materials.

Because Ge bonds, wets, and crystal-



A Tungsten Passivation Layer prevents constituents of steel from interacting with the semiconductor materials in this MOS thin-film solar cell. The thin plating of nickel on the steel improves bonding of the tungsten. The use of steel as the substrate reduces the materials cost of the solar cell.

lizes well on tungsten, vapor-deposited coatings of tungsten and of tungsten with 1 percent carbon were tested for passivation. The steel was first plated with a thin nickel coating to improve the bonding of the tungsten layer.

Studies with various growth temperatures and power levels for the laser-beam recrystallization of the germanium show no evidence of nickel or iron contamination of the Ge/GaAs. Also, the studies show that the high background temperatures and long-duration laser pulses used to melt and recrystallize the germanium cause

small clumps of tungsten to appear in the upper regions of the germanium. The appearance of the tungsten clumps, however, is not expected to affect the electrical performance of the cells. The clumps could be prevented by using lower background temperatures and higher-power-density, intermittent laser pulses to melt and recrystallize the germanium.

This work was done by Richard J. Stirn and Yea-Chuan M. Yeh of Caltech for **NASA's Jet Propulsion Laboratory**. For further information, Circle 74 on the TSP Request Card. NPO-14961

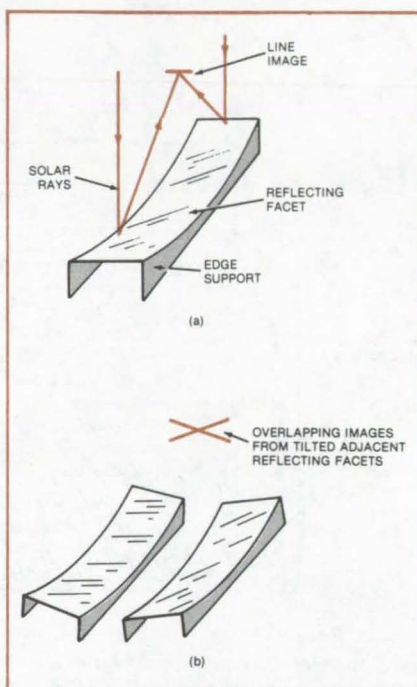
Low-Cost Concentrating Mirrors

Cost-effective concentrator mirrors are constructed from flat stock.

NASA's Jet Propulsion Laboratory, Pasadena, California

Parabolic mirrors used as concentrators in solar-energy systems are relatively expensive to manufacture. Their costs run about 15 percent of the total solar-concentrator costs. The cost, however, is reduced by constructing a parabolic reflector from many flat rectangular mirrors. Each mirror (see figure) is elastically deformed in one dimension. Several such mirrors placed adjacent to each other along a parabolic curve form an inexpensive mirror suitable for solar application.

Each reflecting facet is elastically deformed in one direction by a pair of edge supports so that incident solar rays form a short line image. When two adjacent facets are positioned at a slight tilt with respect to each other, their line images overlap. The overlap is



Rectangular Mirror Facets are slightly curved (a) by edge supports to produce line images of incident solar rays. When adjacent curved facets are tilted (b), the line images overlap to concentrate energy for solar-cell or solar-heating applications.

somewhat smeared because the focal planes for the two facets are not identical; but if the radius of curvature of the mirrors is large, the images are far away from the mirrors, the smearing is slight, and the tilt of adjacent facets for image overlap is small. By this principle, many facets can be assembled to form a concentrating mirror approximating a parabolic reflector.

This simple, low-cost reflector may be fabricated from commercially available flat stock. The edge-supports may be integrated into the mounting arrangement.

This work was done by Timothy R. Carroll of Caltech for NASA's Jet Propulsion Laboratory. No further documentation is available.
NPO-14962

Spiral-Wound Gasket Forms Low-Temperature Seal

Small when stored, a new seal is formed in place into large-diameter seal.

Langley Research Center, Hampton, Virginia

A new cryogenic seal has been tested between -320°F (77 K) and room temperature against chamber pressures up to 130 psig ($896 \times 10^3\text{ N/m}^2$). Seal pressure loads between 500 psig ($3.45 \times 10^6\text{ N/m}^2$) and 2,500 psig ($17.23 \times 10^3\text{ N/m}^2$) are applied. Fabricated from 25 percent glass-filled Teflon (or equivalent) material formed into a continuous strip gasket, the seal can be "active" (be opened and closed), or it can be permanent. It is

made from just one component, requires no encapsulant, and can be easily produced with self-locking or other features.

The seal is made by skiving a thin continuous strip from the circumference of a disk of the glass-filled material. The disk is prepared by planing both surfaces to a smooth, parallel finish. When machining the strip, a lathe turns the disk, and the lathe crossfeed is adjusted to give the

required thickness to the skived strip.

The seal is installed in a groove machined into one of the flange surfaces by wrapping successive turns of the strip spirally until the groove is filled. The thickness of the disk is the height of the seal, part of which protrudes above the groove. Closing the joint compresses the gasket, forming a tight seal. Figure 1 shows two concentric seals, and Figure 2 shows a cross section of a self-locking seal.

The new strip seal eliminates several design weaknesses of large-diameter cryogenic pressure seals. Since it is not fabricated to its final diameter by the manufacturer, as are conventional gaskets, problems of shipping and storage are minimized. Furthermore, because the seal is so small before installation, access to its location can be limited (relative to the seal final diameter), eliminating over-design and unnecessary cost.

In contrast to large-diameter segmented seals, the new strip seal does not have radial leak paths. With the continuous strip, the potential leak-path length between the spiral windings is several times the circumference; thus, the chance for leakage is only a fraction of that of a conventional segmented seal. In addition, the seal allows for the relief of thermal stresses, and cracking would not necessarily cause the seal to fail.

A variation of the basic seal has an adhesive between the strips, resulting in a bonded solid piece of material. Other forms are a tubular strip with ends that allow for pressurization after assembly and a thermally controlled seal with a heated wire embedded in the strip. Large-diameter bearings, using a suitable material, could also be

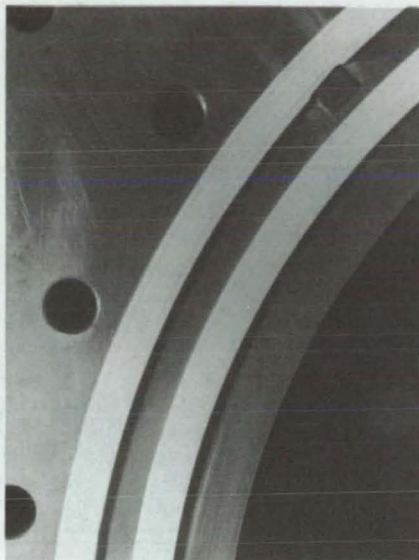


Figure 1. Two Concentric Spiral-Wound Seals are shown in their grooved flange.

constructed in the same way. The strip seal can be custom-fitted to irregular flange surfaces and to different flange shapes.

This work was done by Stephen C. Irick of Langley Research Center. For further information, Circle 75 on the TSP Request Card.

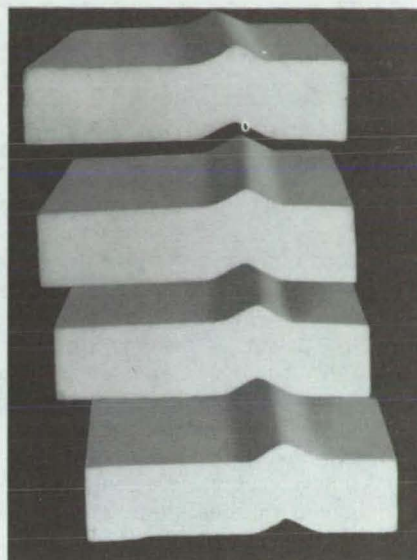


Figure 2. The Self-Locking Spiral-Wound Seal is shown in cross section.

This invention is owned by NASA, and a patent application has been filed. Inquiries concerning nonexclusive or exclusive license for its commercial development should be addressed to the Patent Counsel, Langley Research Center [see page A5]. Refer to LAR-12315.

Arc Spraying Solderable Tabs to Glass

Solder wets copper, copper bonds to aluminum, and aluminum adheres to glass.

NASA's Jet Propulsion Laboratory, Pasadena, California

Solderable tabs suitable for electrical or mechanical connections in such devices as solar cells and integrated circuits can be made by arc spraying aluminum and then copper onto glass. Arc spraying can be automated and integrated with encapsulation, eliminating hand tabbing, improving reliability, and reducing cost.

In an arc sprayer, two wires of the metal being sprayed are fed through hollow electrodes. An electric arc between the wires melts the metal; compressed air sprays the molten metal toward the surface being coated.

Adhesion tests of various metals arc sprayed on glass showed that aluminum adheres strongly but that copper can be peeled off. On the other hand, copper solders easily, but aluminum does not.

Thus, the key to making firmly-adhered solderable tabs is strongly bonding aluminum and copper so that both metals can be used. Copper and aluminum have different thermal expansion properties; the copper must be sprayed lightly, or the tab will curl like a bimetallic strip and warp. Good adhesion is obtained by spraying copper for only 2 to 3 seconds at minimum feed rate.

After soldering a tab to the copper, adhesion was tested by pulling on the

tab at a 45° angle. It took a force of about 0.4 lb (2N) or more to pull a tab off. The tabs did not peel off the glass; rather, the glass beneath the tab fractured.

The excellent adhesion is believed due to a chemical reaction between the glass and the aluminum: Glass is primarily silicon dioxide, and aluminum bonds readily to oxygen. Also, glass softens around the melting point of aluminum, 1,200° F (660° C).

This work was done by Joseph Lindmayer of Solarex Corp. for NASA's Jet Propulsion Laboratory. For further information, Circle 76 on the TSP Request Card.
NPO-14853

Back Contacts for Silicon-on-Ceramic Solar Cells

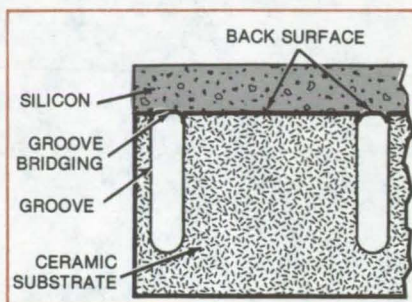
Grooved substrate gives access to back surface of photovoltaic cells.

NASA's Jet Propulsion Laboratory, Pasadena, California

Depositing polycrystalline silicon on a ceramic substrate is an economical way of mass-producing cells for solar electric power. A persistent problem with this method has been making electrical contact with the back surface of the silicon layer — the surface next to the substrate.

A new substrate configuration, containing narrow grooves, exposes part of the back surface so that a dopant can be diffused into it and electrical contact can be made without weakening the substrate. When the substrate is coated first with carbon and then with molten silicon, silicon bridges form, leaving open channels in the grooves (see figure).

Liquid silicon containing a high concentration of boron is injected into the grooves. The liquid diffuses p^+ dopant (that is, a large quantity of boron ions) into the silicon. The p^+ -



Polycrystalline-Silicon Bridges form over grooves in a ceramic substrate to expose the back surface of a solar cell. The back surface can be impregnated with dopants and can be contacted electrically. The groove spacing is 65 mils (1.6 mm).

doped silicon creates a back-surface field effect.

After removal of the oxide that forms on the silicon bridges during diffusion, contact with p^+ silicon is made by any of several methods, such as electrolytic plating or solid-metal deposition by the decomposition of a liquid. Contacts to the front surface are made by conventional methods.

For best adhesion, the substrate grooves should run perpendicular to the direction in which the liquid-silicon layer is applied. The grooves should be closely spaced to maximize the back-contact area.

This work was done by Terry L. Schuller and Shirley Marquardt of Honeywell, Inc., for NASA's Jet Propulsion Laboratory. For further information, Circle 77 on the TSP Request Card.
NPO-14809

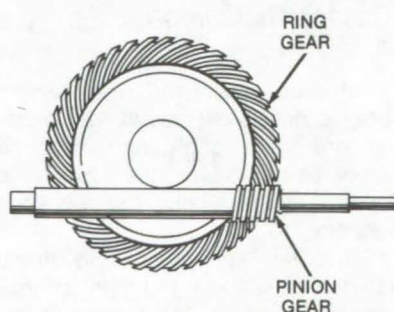
Self-Lubricating Gearset

Self-lubricating material allows attention-free operation in a vacuum and at extreme temperatures.

Lyndon B. Johnson Space Center, Houston, Texas

A skewed-axis gearset (see figure) can operate unattended for long periods if it is fabricated from a molybdenum sulfide filled polyimide (such as du Pont Vespel-SP1 or an equivalent material). The filled-polyimide gearset does not require lubrication, and it can be used in vacuum or at extreme temperatures.

Skewed-axis gearsets are often selected for slow-rotation high-torque drives because their rugged, multitooth contacts are compatible with gear ratios from as little as 10:1 to as much as 500:1. However, when the gears are fabricated of metal, the need for a lubricant restricts their use. In vacuum, for example, a lubricant would evaporate; and at extreme temperatures it can



Ring Gear Drives Pinion Gear on a shaft in a skewed-axis arrangement. Because loads are shared among multiple meshing teeth, the molybdenum sulfide filled polyimide material is strong enough to handle a high gear ratio.

burn or freeze. The metal gears are also impractical in remote installations where it is difficult to do routine maintenance.

In contrast, a skewed-axis gearset fabricated of the self-lubricating polyimide plastic retains its ruggedness and efficiency, while allowing reliable attention-free operation in environments inappropriate for metal gears. Although originally developed for use in space, the self-lubricating gearset could also be used in remote installations on Earth.

This work was done by Derek S. Binge of RCA Corp. for Johnson Space Center. No further documentation is available.
MSC-18801

Reflecting Layers Reduce Weight of Insulation

The density of insulation blankets can be halved if metalized films are placed between layers.

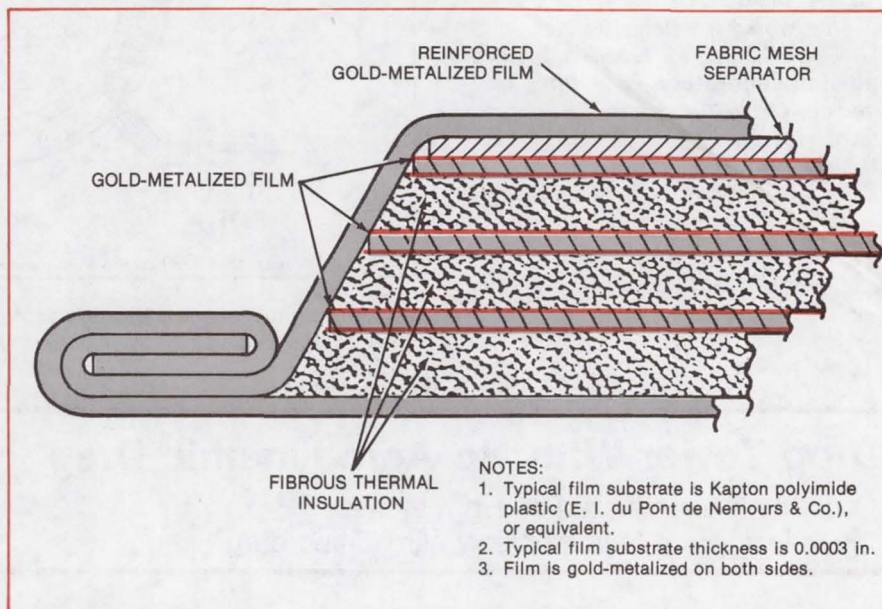
Lyndon B. Johnson Space Center, Houston, Texas

The weight of insulating blankets is reduced 40 percent by interleaving gold-metalized films of plastic between the layers of fibrous material. Use of the lighter weight material with the "goldized" film in the Space Shuttle orbiter has saved approximately 710 pounds (320 kg). It should also be useful in commercial aircraft to reduce weight and increase cargo space.

Previously, thermal conductivity was reduced in fibrous-batting insulation blankets by increasing their density (and thus increasing their weight). However, the new insulation design (see figure) reduces density and weight while maintaining equivalent thermal conductivity. Development tests indicate that insulation with a density of 1 lb/ft³ (17 kg/m³), plus reflectors of goldized film spaced between the layers of insulation, has a thermal conductivity comparable to that of 2 lb/ft³ (34 kg/m³) insulation without the films.

This work was done by James D. Cole, Edward D. Schlessinger, and Harley J. Rockoff of Rockwell International Corp. for Johnson Space Center. No further documentation is available.

MSC-18785



Lightweight Insulation batting is formed by interleaving gold-metalized films between layers of fibrous material. Because only half the density of fibrous material is required for a given thermal protection when the film is used, this construction saves 40 percent in weight.

Lightweight Cryogenic Vessel

A thin cooling jacket is contained by relatively thin walls.

NASA's Jet Propulsion Laboratory, Pasadena, California

A concept in the design of cryogenic cooling vessels would allow much lighter and more-easily fabricated vessels than are possible with conventional Dewar construction. The concept requires recirculating liquid nitrogen in a thin cooling jacket, but it does away with the evacuated insulating spaces normally required. This eliminates the need for heavy-walled shells to contain the vacuum.

The new cryogenic vessel was originally proposed for maintaining liquid fluorine, a cryogenic rocket fuel, while a spacecraft is on its launch pad. (After launch, the vacuum of space completes a Dewar-flask structure.) Since the design saves weight, it reduces fuel consumption (at the expense of increased consumption of liquid nitrogen).

The proposed design is shown in the figure, where the thickness of the outer shell has been exaggerated for clarity. The actual thickness is only about 5 mils (0.13 mm) or less. The inner shell, which holds the primary cryogenic fluid, is of conventional design.

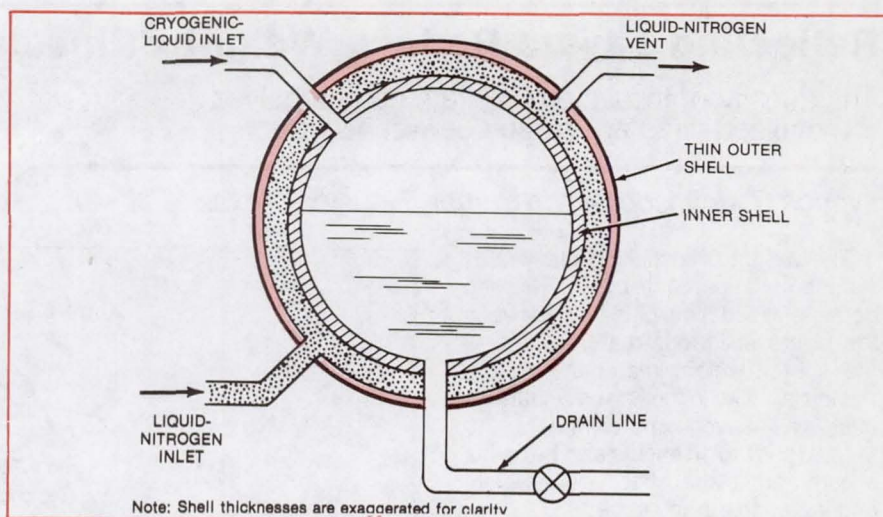
The thin wall of the outer shell is possible because it contains recirculating liquid nitrogen at only a slight positive
(continued on next page)

pressure. In conventional Dewar design, the outer shell has to withstand full atmospheric negative pressure. It must therefore be thick enough to prevent buckling.

The new design is not limited to cryogenics. It could also be used to keep liquids hot by circulating a hotter fluid instead of liquid nitrogen.

This work was done by Joseph C. Lewis of Caltech for **NASA's Jet Propulsion Laboratory**. For further information, Circle 78 on the TSP Request Card.

NPO-14794

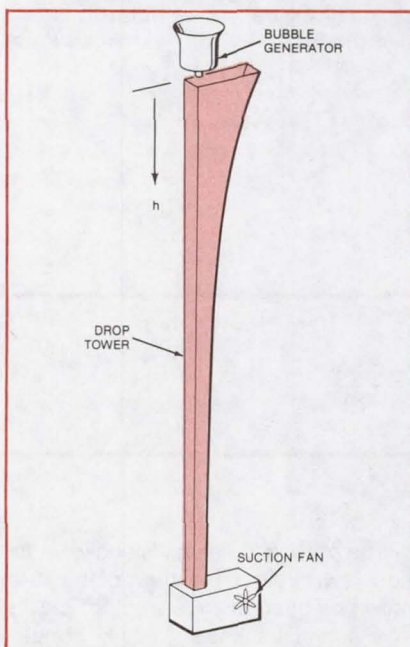


A **Lightweight Cryogenic Storage Tank** is kept cool by recirculating liquid nitrogen. The nitrogen is contained by an outer shell that can be less than 5 mils in thickness.

Drop Tower With No Aerodynamic Drag

Cooling air accelerated at 1 g matches the velocity of a falling object, eliminating drag.

NASA's Jet Propulsion Laboratory, Pasadena, California



The **Drop Tower** with no aerodynamic drag has a fan that expels air from the bottom of the tower. Ideally, the tower cross-sectional area would be proportional to $1/\sqrt{h}$ where h is the height measured from the top of the tower. In practice, an area increment is added to correct for the effects of air friction on the wall of the channel.

A prototype 3-meter drop tower has air cooling but no aerodynamic drag. The drag is eliminated by forcing cooling air downward at 1 g with a suction fan so the air velocity matches the velocity of the falling drops. The tower geometry (see figure) causes the air to accelerate downward at 1 g.

Drop towers have long been used to make lead shot. Drops of molten material released at the top of the air-filled tower cool and solidify as they fall. However, aerodynamic drag tends to distort the drops, preventing them from assuming the spherical shape that would result from surface tension.

The drag-free tower was tested with hollow waterdrops. The time of fall was 0.7 second. Photographs confirm that the drops are more nearly spherical and the bubbles within more concentric than when drag is present.

A full-scale drop tower is planned for making spherical fuel capsules for thermonuclear fusion reactors. The tower must be taller than one with drag because the spheres continue to accelerate rather than approach a limiting velocity. Thus they fall farther in a given time interval. The spheres also cool more slowly because the surrounding air moves with them, lowering the heat-transfer rate.

This work was done by James M. Kendall, Jr., of Caltech for **NASA's Jet Propulsion Laboratory**. For further information, Circle 57 on the TSP Request Card.

This invention is owned by NASA, and a patent application has been filed. Inquiries concerning nonexclusive or exclusive license for its commercial development should be addressed to the Patent Counsel, NASA Resident Office-JPL [see page A8]. Refer to NPO-14845.

Books and Reports

These reports, studies, and handbooks are available from NASA as Technical Support Packages (TSP's) when a Request Card number is cited; otherwise they are available from the National Technical Information Service.

Nickel-Doped Silicon for Solar Cells

Large grain boundaries act as gettering centers for nickel precipitates and improve cell performance.

When a p-type semiconductor crystal is grown from silicon doped with nickel, Ni precipitates in star-shaped clumps in the crystal. Heavier doping produces a higher density of larger clumps. However, in polycrystals the Ni precipitates along the grain boundaries without forming large clumps.

If the nickel-doped silicon is used for a solar cell (by the diffusion of a donor material into a wafer of the silicon, to form a pn junction), the clumps of precipitated Ni degrade the performance of the cell. The larger the size of the precipitate clumps, the more the

conversion efficiency of the cell is degraded. However, a grain boundary around the effective area of the cell acts as a gettering center for the precipitates and impurities and improves the efficiency.

These effects in Ni-doped Si are described in a report that is available on request. Three crystals were grown (by the Czochralski method) with successively greater Ni concentration. The first, a single crystal, was doped at 5×10^{14} atoms/cm³; the second, also single, at 4×10^{15} atoms/cm³; and the third, which was polycrystalline, at 8×10^{15} atoms/cm³. The examination of wafers cut from the crystals showed that the first had 400 precipitation clumps per cm², with an average size of 12 μ m. The second had 1,500 clumps per cm², with an average size of 17 μ m. However, in wafers of the third, the polycrystal, the precipitates were aligned along grain boundaries and had an average size of only 5 μ m.

Solar cells were made from wafers of each crystal by diffusing phosphorus into the top surface to form an n⁺ region. The qualities of the n⁺p junctions were determined by measurements of the electrical properties of the cells.

Data on open-circuit voltage, short-circuit current, maximum power, and conversion efficiency for the illuminated cells were compared with values for baseline (undoped) cells. The efficiencies of the solar cells made from the Ni-doped Si were lower than those of the baseline cells, with the heavier-doped single crystal degraded the most.

Dark forward current versus voltage was also measured for the cells made from the three different crystals. Both cells made from single-crystal silicon showed current leakage caused by the presence of the closely spaced arrays of precipitate clumps in the bulk of the cells. The cells made from Ni-doped polycrystalline Si, however, did not show current leakage and had near-ideal perfection factors.

This work was done by Amal M. Salama of Caltech for NASA's Jet Propulsion Laboratory. For further information, including X-ray topographs of the crystals, a SEM/EBIC micrograph of an electrically-active star-shaped precipitate clump, and a photomicrograph of a Sirtl-etched solar cell, Circle 66 on the TSP Request Card.

NPO-14780

Computer Programs

These programs may be obtained at very reasonable cost from COSMIC, a facility sponsored by NASA to make new programs available to the public. For information on program price, size, and availability, circle the reference letter on the COSMIC Request Card in this issue.

CADAT Network Translator

Cell-net data are converted to logic-gate models for test and simulation.

The CADAT network translator (NTRAN) converts cell-net data, as used by automatic layout programs, in-

to logic-gate models for use by test and simulation programs. NTRAN input consists of either a Place, Route, and Fold (PRF) or a Place-and-Route-in-Two-Dimensions (PR2D) layout data deck. Output consists of either a Test Pattern Generator (TPG) or Logic-Simulation (LOGSIM) logic-circuitry data deck.

NTRAN reduces the workload of the integrated-circuit designer. Instead of having to build both the cell-net-data circuit description and the logic-gate-model circuit description, the designer needs only to build the former. Both describe the same circuit, and NTRAN acts as a translator. Thus, once the layout cell-net data are developed, they

are translated and used as inputs for logic simulation and test pattern generation.

NTRAN is written in FORTRAN IV for batch execution and has been implemented on a Xerox Sigma V computer. It was developed in 1975. (Also see the related series of articles on the CADAT programs on pages 394 through 396 of *NASA Tech Briefs*, Vol. 5, No. 3.)

This program was written by E. R. Pitts of M&S Computing, Inc., for Marshall Space Flight Center. For further information, Circle L on the COSMIC Request Card.

MFS-25055

CADAT Integrated-Circuit Artwork Program

A versatile, ready-to-use mask-generator package

The CADAT integrated-circuit artwork program (ARTWORK) converts high-level artwork data into mask patterns. ARTWORK generates commands for a Gerber 1200 plotter or for a Mann pattern generator that select the appropriate apertures and completely expose, or "fill in," the specified areas

of a circuit mask. The program generates the commands required to produce the artwork on a "one-mask-at-a-time" basis with up to nine mask levels. The commands are written to tape, with each level being written in a separate file.

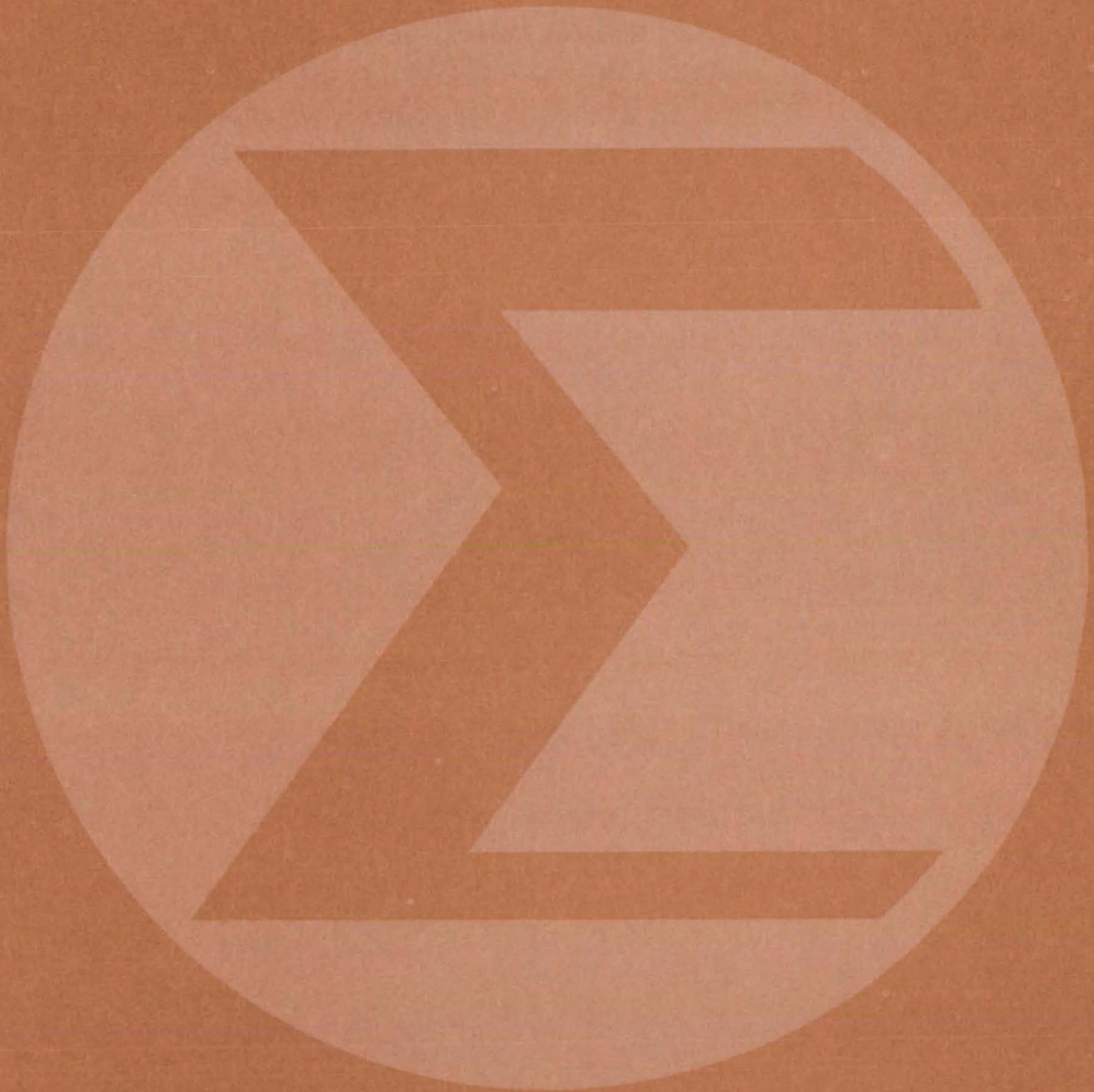
ARTWORK also contains an extensive utility package. This enables the user to create new pattern libraries, to develop new cells, to incorporate new cells into the pattern library, and to perform system orientation functions, such as pattern-library display and tape handling. Included with the COSMIC

distribution package for ARTWORK is an extensive PMOS, CMOS, and SOS pattern library.

ARTWORK is written in FORTRAN IV for batch execution and has been implemented on a Xerox Sigma V computer with a central memory requirement of approximately 20K of 32-bit words. It was developed in 1976. (Also see the preceding article.)

*This program was written by **Marshall Space Flight Center**, RCA Corp., and R. L. Kuelthau of M&S Computing, Inc. For further information, Circle M on the COSMIC Request Card. MFS-25017*

Mathematics and Information Sciences



Hardware, Techniques, and Processes

Books and Reports

Computer Programs

511 An Approximation for Inverse Laplace Transforms

511 Safety Analysis for Complex Systems

512 Evaluating Computer-Drawn Ground-Cover Maps

512 OCCULT — ORSER Complete Conversational User-Language Translator

513 Selecting Optimum Algorithms for Image Processing

513 A Universal Structured-Design Diagrammer

An Approximation for Inverse Laplace Transforms

A finite-series approximation can be run on a programmable calculator.

Lyndon B. Johnson Space Center, Houston, Texas

A finite-series approximation for Laplace transform inversions is simple enough to run on a programmable calculator. Utilizing a new family of orthonormal functions, the approximation can be used for a wide range of transforms, including those encountered in feedback-control problems.

For a Laplace transform $F(s)$, the N -term approximation to its inverse $F(t)$ is given by

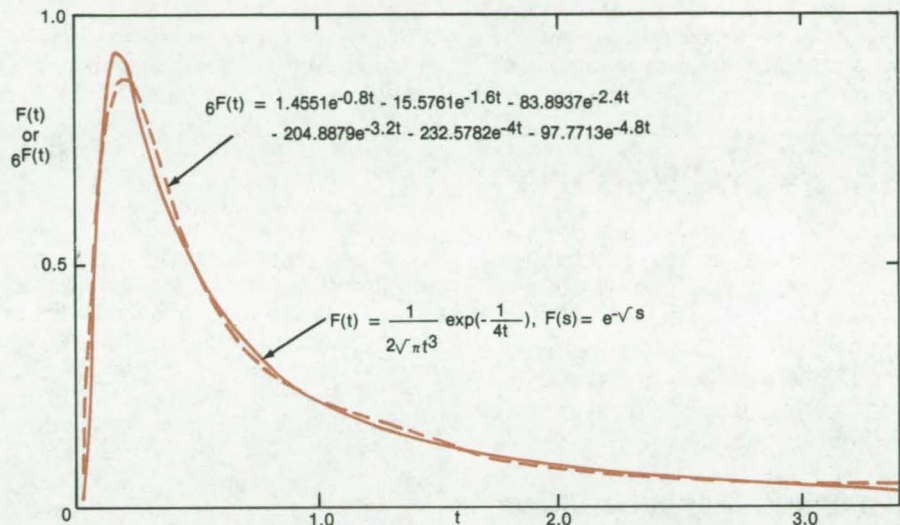
$$NF(t) = \sum_{n=1}^N A_n L_n(st)$$

where the A_n are Fourier coefficients and the $L_n(st)$ are the new orthonormal functions. The parameter s is chosen to give the best approximation, such that the integral square error

$$E(s) = \int_0^{\infty} [NF(t) - F(t)]^2 dt$$

is minimized. Each of the orthonormal functions is a power series, containing terms that are readily calculated from recursion relations given in the report referenced at the end of this article.

The new method approximates the Laplace transform by a transform with a series of simple poles along the real



A Six-Term Approximation using the new method is compared with an exact Laplace transform inversion $F(t)$. The parameter s is 0.8. The agreement is excellent, even though $F(t)$ does not at all resemble a function of the form $e^{-0.8t}$.

axis in the left-half plane. The method works well as long as $F(t)$ decays to zero as t approaches infinity, as is often the case for physical systems. An example of a six-term approximation is shown in the figure.

This work was done by William M. Lear of TRW, Inc., for **Johnson Space Center**. Further information

may be found in NASA TM-81064 [N80-25056/NSP], "Inversion and Approximation of Laplace Transforms" [\$6]. A copy may be purchased [prepayment required] from the National Technical Information Service, Springfield, Virginia 22161. MSC-18867

Safety Analysis for Complex Systems

Hardware, environment, and human factors are considered in operational risk assessment.

Lyndon B. Johnson Space Center, Houston, Texas

A technique for assessing the possible failure modes of a complex system accounts for factors introduced by the presence of human operators and by the environment. The effects of hardware failures are considered for all phases of a mission.

Some risks or hazards are inherent in a configuration; high voltages and pressurized vessels are examples. These hazards can be identified and resolved in a design-phase hazard analysis. Hazards resulting from improper performance of a function at a

time when its consequences become adverse, however, are analyzed in an operating-phase or mission-phase analysis.

The mission-phase hazard analysis technique starts with the division of a postulated mission into segments.

(continued on next page)



Each segment is then subdivided into events that must occur during the segment. The events are further broken down into operational steps (such as crew actions, hardware responses, software instructions, and data feedback required) that must occur to allow execution of the event without adverse effects on the system. For large-scale complex operations, the division process may be simplified by sketching out a logic flow diagram showing each

event in relation to preceding and/or parallel events.

The consequences of each event, nonoccurrence, premature operation, out-of-sequence operation, and inadvertent execution are all examined at the subevent, event, and phase levels. Any indication of a hazardous consequence is identified and treated on an individual basis.

This technique was used to obtain an early identification of hazards and operational risks for the Space Shuttle

mission. It has also been applied in hazard analysis for aircraft flight tests. Analysts in the fields of energy and transportation should find it of value.

This work was done by Joseph P. Onesty and Robert L. Peercy, Jr., of Rockwell International Corp. for Johnson Space Center. To obtain a copy of a report, "Risk Assessment Process as Applied to the Space Shuttle," Circle 65 on the TSP Request Card.
MSC-18745

Books and Reports

These reports, studies, and handbooks are available from NASA as Technical Support Packages (TSP's) when a Request Card number is cited; otherwise they are available from the National Technical Information Service.

Evaluating Computer-Drawn Ground-Cover Maps

Plots of remote-sensing data were compared with photos of actual ground cover.

Computer-generated character maps from Landsat data were compared to aerial photos (and actual ground cover) for two test sites in Florida. The success in extracting ground features by two analytical techniques is the subject of a 113-page report.

The test sites were each about 20 miles (32 km) square. One was characterized by hardwood forests, softwood forests, grazing lands, cultivated fields, rivers, lakes, small towns, and scattered residential areas. The other had similar features, plus part of a city and some mining areas.

The two techniques for analyzing data from the Landsat satellite were an unsupervised (i.e., operated without any human interference) clustering algorithm, called Landsat Signature Development Program (LSDP), and an interactive algorithm based on the multispectral image analyzer (Image 100) at Kennedy Space Center. LSDP computer maps were produced at a scale of 1:24,000 (the scale of U.S. Geological Survey maps). The Image 100 plots were printed at the same scale. The most promising computer maps for both test sites were compared to geological survey maps and to aerial photos. In making comparisons, attention was given to determining whether the computer-generated maps could depict characteristic ground features.

In this study the LSDP maps provided good results when the features of interest had distinct spectral signatures. Successful characterization of Landsat scenes on the Image 100 depends heavily on firsthand knowledge of ground-cover conditions and on the ability to locate features on the display console.

The exact location of such specific ground features as small residential areas, roads, small rivers, and lakes

could not be determined from any of the evaluated computer-generated maps in the study. Due to edge effects, such features were classified in one of the surrounding-cover categories. The study also found that the smaller the number of classifications used, the easier the maps were to interpret and the higher the accuracy of the maps.

Overall, the report concludes that the Landsat-generated maps are satisfactory depictions of actual ground conditions. The study was convincing that computer classification of digital Landsat multispectral data, supplemented with certain ground-cover information, may be a valuable tool in the hands of qualified scientists for the analysis of renewable resources.

This work was done by L. G. Arvanitis, R. Newburne, and R. Reich of the University of Florida for Kennedy Space Center. Further information may be found in NASA CR-154635 [N80-32805/NSP], "Evaluation of Remote Sensing Techniques on Selected Forest Sites in Florida" [\$10]. A copy may be purchased [prepayment required] from the National Technical Information Service, Springfield, Virginia 22161.
KSC-11195

Computer Programs

These programs may be obtained at very reasonable cost from COSMIC, a facility sponsored by NASA to make new programs available to the public. For information on program price, size, and availability, circle the reference letter on the COSMIC Request Card in this issue.

OCCULT — ORSER Complete Conversational User-Language Translator

A "friendly" translator for non-computer-oriented users of satellite imagery and other remotely sensed data

The ORSER Complete Conversational User-Language Translator (OCCULT) assists non-computer-oriented users to set up and submit jobs for the ORSER system developed and distributed by Pennsylvania State University. OCCULT is designed for those who would like to use ORSER but cannot justify the effort of

acquiring and maintaining the necessary proficiency in Remote Job Entry Language, Job Control Language (JCL), and control-card formats. For such users, OCCULT provides a "friendly" conversational front end to the ORSER software. OCCULT includes a data-management system and an output retrieval system.

ORSER is a collection of image-processing programs for analyzing remotely sensed data, such as those from Landsat satellites. Its use requires proficiency in editing JCL procedure files and in the details of ORSER control-card formats.

OCCULT is a set of "user-friendly" conversational programs that assists the new, or infrequent, ORSER user to set up and run ORSER jobs. OCCULT prompts the user for information, checks the validity of the answers, automatically creates the JCL and control cards, and submits the job to the computer. It also helps to retrieve the job output and provides a data-management system for storing image names and other pertinent data. OCCULT currently supports six of the available ORSER programs: SUBSET, NMAP, UMAP, STATS, CLUS, and CLASS.

OCCULT is written in FORTRAN IV and OS Assembler for interactive execution. It has been implemented on an IBM 360 computer under OS/MVT with a central memory requirement of approximately 230K of 8-bit bytes. The use of OCCULT requires interactive execution capability (e.g., with the time-sharing option, TSO). The OCCULT program was developed in 1979.

This program was written by H. K. Ramapriyan of Goddard Space Flight Center and Kenneth Young of Computer Sciences Corp. For further information, Circle S on the COSMIC Request Card.

Selecting Optimum Algorithms for Image Processing

An evaluation of registration, compression, and classification algorithms

Several algorithms process digital imagery such as Landsat data. The most common of these perform

registration, compression, and classification. Because different techniques are available for registration, compression, and classification, image-data users need a rationale for selecting one approach over others.

A collection of registration, compression, and classification algorithms allows users to evaluate the different approaches and select the best approach for an application. Routines are included for six registration algorithms, six compression algorithms, and two classification algorithms. The package also includes routines for evaluating the effects of processing on the image data.

The registration of image data involves the geometrical alteration of the imagery. Registration routines available in the evaluation package include image magnification, mapping functions, partitioning, map overlay, and data interpolation.

The compression of image data involves reducing the volume of data needed for a given image. Compression routines available include adaptive differential-pulse-code modulation, two-dimensional transforms, clustering, vector reduction, and picture segmentation.

The classification of image data involves analyzing the uncompressed or compressed image data to produce inventories and maps of areas of similar spectral properties within a scene. The classification routines include a sequential linear technique and a maximum-likelihood technique.

The choice of the appropriate evaluation criteria is quite important in evaluating the image-processing functions. The user is therefore given a choice of evaluation criteria. All of the available criteria basically compare the observed results with the expected results. For the image reconstruction processes of registration and compression, the expected results are usually the original data or some selected characteristics of the original data. For classification processes the expected result is the ground truth of the scene.

Thus, the comparison process consists of determining what changes occur in processing, where the changes occur, how much change occurs, and the amplitude of the change. The package includes evaluation routines for performing such comparisons as average uncertainty, average information transfer, chi-square statistics, multidimensional

histograms, and the computation of contingency matrices.

This collection of routines is written in FORTRAN IV for batch execution and has been implemented on an IBM 360 computer with a central memory requirement of approximately 662K of 8-bit bytes. The collection was developed in 1979.

This program was written by R. R. Jaroe, J. Hodges, R. E. Atkinson, B. Gaggini, L. Callas, and J. Peterson of Marshall Space Flight Center. For further information, Circle N on the COSMIC Request Card.
MFS-25367

A Universal Structured-Design Diagrammer

A generator of standardized flow charts and concordances for development and debugging of programs in virtually any language

The Universal Structured-Design Diagrammer (FLOWCHARTER) is a tool for documenting and understanding computer programs. FLOWCHARTER is "universal" because it produces flow charts and concordances for any program written in any language that can be described according to a defined set of rules. Because the generated flow charts are presented in a concise tree-like format appropriate for representing the flow of control in a structured program, FLOWCHARTER is termed a "structured-design diagrammer."

To flow-chart a program, the user provides FLOWCHARTER with a description of the programming-language grammar. Three sets of rules are needed: The first is a list of syntax rules in Backus-Naur form (BNF). These rewrite rules allow FLOWCHARTER to do a bottom-up parse of the input program. The next set is a list of semantic rules, in one-to-one correspondence with the syntactic rules, which specify how a particular construct is to be diagrammed. Last is a set of concordance rules, again in one-to-one correspondence with the syntactic rules, which are used to isolate positions where identifiers may appear and to classify these identifiers as variables or as procedure names. Preparing this list is not trivial;

(continued on next page)



however, the list is only prepared once for each language. (A grammar description for PASCAL is included with the FLOWCHARTER package.)

Once the grammar is described, the user supplies only the source code of the program to be diagrammed. FLOWCHARTER automatically produces a flow diagram and a concordance. The diagram is quite different from traditional flow charts. The structured-design

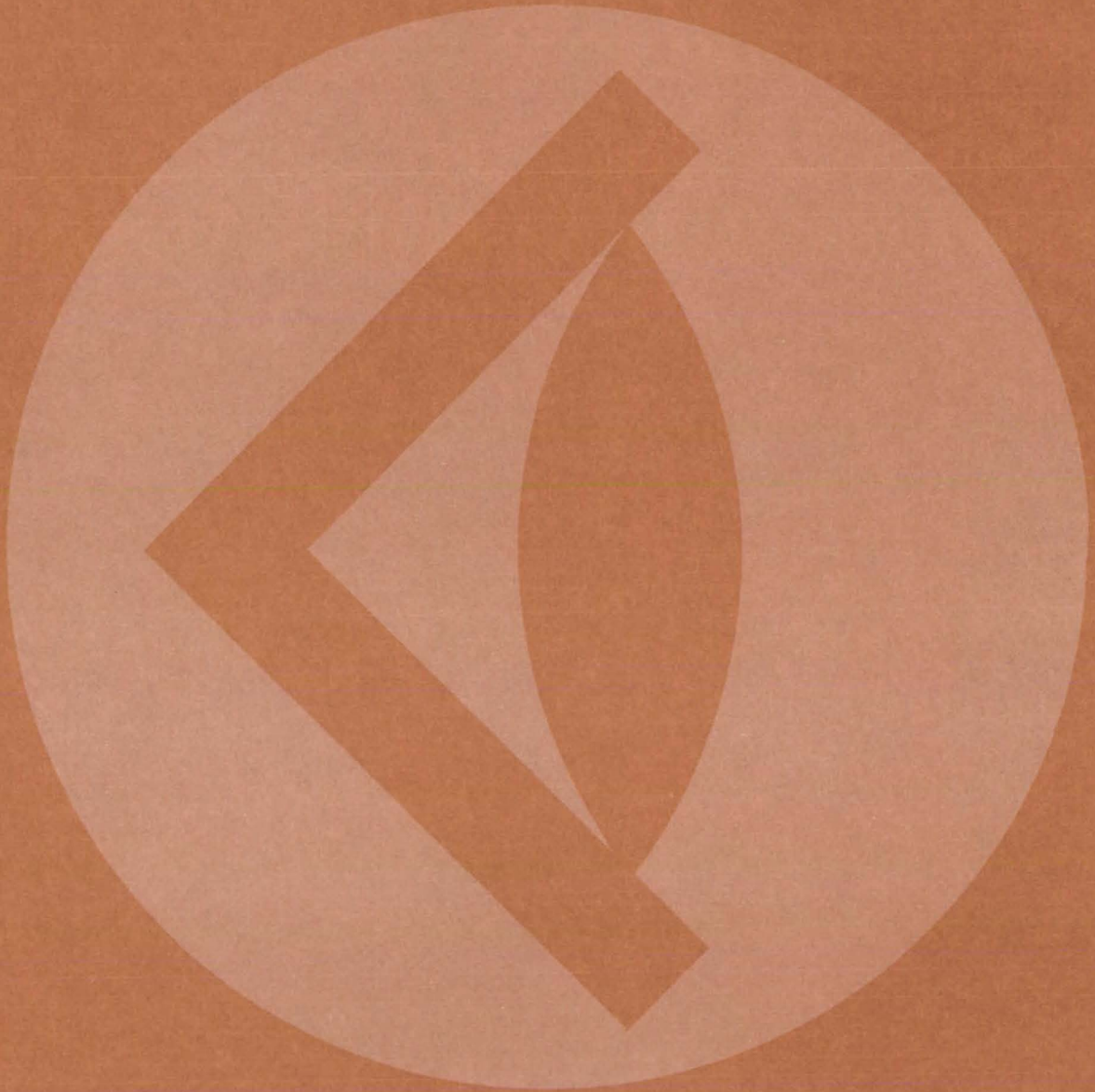
diagram represents the main flow of the program in the top-down format, with increasing levels of detail explicitly indicated. This structured-design diagram approach is particularly appropriate for languages with higher level constructs, such as case, iterative loops, or logical dependent execution blocks.

The source code for FLOWCHARTER is written for the PASCAL Release 2 compiler, as distributed by the Univer-

sity of Minnesota. FLOWCHARTER is intended for batch execution and has been implemented on a CDC 6000-series computer with a central memory requirement of approximately 100K (octal) of 60-bit words. FLOWCHARTER was developed in 1979.

*This program was written by Higher Order Software, Inc., for **Langley Research Center**. For further information, Circle P on the COSMIC Request Card. LAR-12548*

SUBJECT INDEX



ACTUATORS

Lock for hydraulic actuators
page 489 MSC-18853

ADHESIVES

New pressure-sensitive silicone adhesives
page 452 LAR-12737

AERODYNAMICS

The design and analysis of low-speed airfoils
page 481 LAR-12727
Transonic flow over wing/fuselage configurations
page 482 LAR-12702

AIR WATER INTERACTIONS

Thermodynamic and transport properties of air/
water mixtures
page 479 LEW-13432

AIRFOILS

The design and analysis of low-speed airfoils
page 481 LAR-12727

ALGORITHMS

Selecting optimum algorithms for image process-
ing
page 513 MFS-25367

ANODIZING

User chooses coating properties
page 451 LAR-12719

ANTENNA COUPLERS

High-power dual-directional coupler
page 420 NPO-14713

ANTENNAS

Cavity-backed spiral-slot antenna
page 421 MSC-18532
Trislot-cavity microstrip antenna
page 422 MSC-18793

ARC SPRAYING

Arc spraying solderable tabs to glass
page 503 NPO-14853

ARRESTING GEAR

Gentle arrester for moving bodies
page 490 LAR-12372

ARTHRITIS

Gage for evaluating rheumatoid hands
page 461 GSC-12610

AUTOMATIC TEST EQUIPMENT

Developing experiment instrument packages
page 423 GSC-12536
Solar-site test module
page 433 MFS-25543

AUTOMOBILES

Four-wheel dual braking for automobiles
page 488 LAR-12687

BAGS

Soft container for explosive nuts
page 491 MSC-18871

BATTERY CHARGERS

Improved battery charger for electric vehicles
page 411 NPO-14964

BEARINGS

Cylindrical bearing analysis
page 491 LEW-13393

BINARY ALLOYS

Diffusion in single-phase binary alloys
page 454 LAR-12665

BIOINSTRUMENTATION

Cardiopulmonary data-acquisition system
page 457 MSC-18783
Microprocessor-based cardiometer
page 459 MSC-18775

BONDING

Arc spraying solderable tabs to glass
page 503 NPO-14853
"Densified" tiles form stronger bonds
page 495 MSC-18741
Tile densification with TEOS
page 495 MSC-18737

BRAKES (FOR ARRESTING MOTION)

Four-wheel dual braking for automobiles
page 488 LAR-12687

Gentle arrester for moving bodies
page 490 LAR-12372

BRAYTON CYCLE

Gas absorption/desorption temperature-differen-
tial engine
page 474 NPO-14528

BUBBLES

Driving bubbles out of glass
page 453 MFS-25414

CABLES (ROPES)

Gentle arrester for moving bodies
page 490 LAR-12372

CALIBRATING

Fast calibration of gas flowmeters
page 476 KSC-11076

CARDIOTACHOMETERS

Microprocessor-based cardiometer
page 459 MSC-18775

CARDIOVASCULAR SYSTEM

Cardiopulmonary data-acquisition system
page 457 MSC-18783
Microprocessor-based cardiometer
page 459 MSC-18775

CATALYSTS

Improved cell for water-vapor electrolysis
page 447 MSC-16394
Photoproduction of halogens using platinized TiO₂
page 449 LAR-12713

CAVITY RESONATORS

Cavity-backed spiral-slot antenna
page 421 MSC-18532

CERAMIC COATINGS

Mobile glazing unit
page 498 KSC-11171

CHEMICAL REACTORS

Producing silicon continuously
page 497 NPO-14796

CIRCUIT BOARDS

Low-resistance continuity tester
page 415 NPO-14881

CLAMPS

Eliminating gaps in undersized split rings
page 500 MSC-18854

Lock for hydraulic actuators
page 489 MSC-18853

CLOCKS

Fiber-optic clock-signal distribution system
page 430 NPO-14749

CLOUD COVER

Instrument measures cloud cover
page 474 NPO-14936

COATINGS

User chooses coating properties
page 451 LAR-12719

COLLIMATORS

Multibeam collimator uses prism stack
page 427 GSC-12608

COMPLEX SYSTEMS

Safety analysis for complex systems
page 511 MSC-18745

COMPRESSED AIR

Pneumatic-power supply
page 486 MSC-18855

COMPUTER PROGRAMS

A universal structured-design diagrammer
page 513 LAR-12548

COMPUTERIZED SIMULATION

CADAT integrated-circuit artwork program
page 508 MFS-25017

CADAT network translator
page 507 MFS-25055

Calculating linear A,B,C, and D matrices from a
nonlinear dynamic engine simulation
page 479 LEW-13250

CONCENTRATORS

Low-cost parabolic mirrors
page 502 NPO-14962

CONNECTORS

Interlocking wedge joint is easily assembled
page 485 LAR-12729

CONTAINMENT

Soft container for explosive nuts
page 491 MSC-18871

CONTAMINATION

Bulk lifetime indicates surface contamination
page 471 NPO-14966

COOLING

Heat pipes cool probe and sandwich panel
page 478 LAR-12588

COUPLINGS

Interlocking wedge joint is easily assembled
page 485 LAR-12729

CRYOGENIC EQUIPMENT

Spiral-wound gasket forms low-temperature seal
page 503 LAR-12315

CRYOGENIC FLUID STORAGE

Lightweight cryogenic vessel
page 505 NPO-14794

DATA ACQUISITION

Cardiopulmonary data-acquisition system
page 457 MSC-18783

Microprocessor-based cardiometer
page 459 MSC-18775

Solar-site test module
page 433 MFS-25543

DATA ANALYSIS

Selecting optimum algorithms for image process-
ing
page 513 MFS-25367

DECONTAMINATION

Removing Freon gas from hydraulic fluid
page 452 MSC-18740

DEFORMETERS

Biaxial method for in-plane shear testing
page 472 LAR-12680

DENSIFICATION

"Densified" tiles form stronger bonds
page 495 MSC-18741

Tile densification with TEOS
page 495 MSC-18737

DIFFUSION

Diffusion in single-phase binary alloys
page 454 LAR-12665

DISPLAY DEVICES

Imager displays free fall in stop action
page 450 NPO-14779

DISTANCE MEASURING EQUIPMENT

Short-range self-pulsed optical radar
page 432 NPO-14901

DOPING (ADDITIVES)

Nickel-doped silicon for solar cells
page 507 NPO-14780

DRILLING

Sidewall penetrator for oil wells
page 487 NPO-14306

DROP TOWER

Drop tower with no aerodynamic drag
page 506 NPO-14845



DYNAMIC RESPONSE

An all-FORTRAN version of NASTRAN for the VAX
page 481 GSC-12600

DYNAMIC STABILITY

Isolation and measurement of rotor vibration
forces
page 468 LAR-12476

ELECTRIC CONTACTS

Back contacts for silicon-on-ceramic solar cells
page 504 NPO-14809

ELECTRIC DISCHARGES

Pulse-shaping circuit for laser excitation
page 428 NPO-14556

ELECTRICAL RESISTANCE

Low-resistance continuity tester
page 415 NPO-14881

ELECTROLYTIC CELLS

Improved cell for water-vapor electrolysis
page 447 MSC-16394

ENDOSCOPES

Fiber-optic coupler for arthroscope
page 462 LAR-12718

ENERGY CONVERSION

Solar cell is housed in light-bulb enclosure
page 413 LEW-13418

ENGINE DESIGN

Calculating linear A,B,C, and D matrices from a
nonlinear dynamic engine simulation
page 479 LEW-13250

Gas absorption/desorption temperature-differen-
tial engine
page 474 NPO-14528

ENVIRONMENT POLLUTION

Recycling paper-pulp waste liquors
page 450 NPO-14797

EXPLOSIVES

Soft container for explosive nuts
page 491 MSC-18871

FASTENERS

Eliminating gaps in undersized split rings
page 500 MSC-18854

Interlocking wedge joint is easily assembled
page 485 LAR-12729

FEEDBACK CONTROL

Speed control for synchronous motors
page 414 MSC-18680

FIBER OPTICS

Fiber-optic coupler for arthroscope
page 462 LAR-12718

FIELD-EFFECT TRANSISTORS

Simple JFET oscillator
page 413 GSC-12555

FILLERS

Repairing high-temperature glazed tiles
page 496 MSC-18736

FLOW CHARTS

A universal,structured-design diagrammer
page 513 LAR-12548

FLOW DISTRIBUTION

The design and analysis of low-speed airfoils
page 481 LAR-12727

FLOW MEASUREMENT

Fast calibration of gas flowmeters
page 476 KSC-11076

FLUID FLOW

Potential flow in two-dimensional deflected nozzles
page 481 LEW-13461

Reduced viscosity interpreted for fluid/gas mix-
tures
page 431 NPO-14976

Transonic flow over wing/fuselage configurations
page 482 LAR-12702

FLUIDIZED BED PROCESSORS

Producing silicon continuously
page 497 NPO-14796

FORTRAN

An all-FORTRAN version of NASTRAN for the VAX
page 481 GSC-12600

FREE FALL

Drop tower with no aerodynamic drag
page 506 NPO-14845
Imager displays free fall in stop action
page 450 NPO-14779

FREON

Removing Freon gas from hydraulic fluid
page 452 MSC-18740

GAS CHROMATOGRAPHY

Applying the helium ionization detector in chroma-
tography
page 448 MSC-18835

GAS FLOW

Fast calibration of gas flowmeters
page 476 KSC-11076

GAS LASERS

Gas-laser power monitor
page 430 LAR-12682

GAS TURBINE ENGINE

Gas absorption/desorption temperature-differen-
tial engine
page 474 NPO-14528

GAS-LIQUID INTERACTIONS

Driving bubbles out of glass
page 453 MFS-25414

GASKETS

Spiral-wound gasket forms low-temperature seal
page 503 LAR-12315

GEARS

Self-lubricating gearset
page 504 MSC-18801

GEOMAGNETISM

Improved LEEM ranges over four decades
page 469 LAR-12706

GLASS

Arc spraying solderable tabs to glass
page 503 NPO-14853

Driving bubbles out of glass
page 453 MFS-25414

GLAZES

Mobile glazing unit
page 498 KSC-11171

GOLD COATINGS

Reflecting layers reduce weight of insulation
page 505 MSC-18785

GONIOMETERS

Gage for evaluating rheumatoid hands
page 461 GSC-12610

GROUND SUPPORT EQUIPMENT

Developing experiment instrument packages
page 423 GSC-12536

HALOGENS

Photoproduction of halogens using plantinized TiO₂
page 449 LAR-12713

HAND (ANATOMY)

Gage for evaluating rheumatoid hands
page 461 GSC-12610

HEART RATE

Microprocessor-based cardiometer
page 459 MSC-18775

HEAT PIPES

Heat pipes cool probe and sandwich panel
page 478 LAR-12588

HEAT TREATMENT

Mobile glazing unit
page 498 KSC-11171

HEATING EQUIPMENT

Building with integral solar-heat storage—Stark-
ville, Mississippi
page 444 MFS-25559

Closed-circulation system for motel hot water—
Savannah, Georgia
page 443 MFS-25572

Economic evaluation of a solar hot-water system
page 435 MFS-25529

Economic evaluation of a solar hot-water system
—Palm Beach County, Florida
page 441 MFS-25536

Evaluation of an evacuated-tube liquid solar col-
lector
page 434 MFS-25450

Fire-station solar-energy system—Kansas City,
Missouri
page 440 MFS-25538

Five-city economics of a solar hot-water system
page 434 MFS-25532

Motel solar-hot-water installation — Atlanta,
Georgia
page 443 MFS-25564

Motel solar-hot-water system—Dallas, Texas
page 442 MFS-25575

Motel solar-hot-water system with nonpressurized
storage—Jacksonville, Florida
page 442 MFS-25569

Multimode solar-heating system—Columbia,
South Carolina
page 439 MFS-25552

One-year assessment of a solar space water
heater—Clinton, Mississippi
page 440 MFS-25539

Residential solar-heating system—Lansing,
Michigan
page 441 MFS-25530

Residential solar-heating system uses pyramidal
optics
page 436 MFS-25567

Single-family-residence solar heating—Carlsbad,
New Mexico
page 438 MFS-25528

Solar-energy heats a transportation test center—
Pueblo, Colorado
page 438 MFS-25527

Solar-energy landmark building—Columbia,
Missouri
page 437 MFS-25524

Solar-heated and cooled savings and loan building
—Leavenworth, Kansas
page 436 MFS-25520

Solar-heated bank—Marks, Mississippi
page 436 MFS-25558

Solar-heated ranger station—Glendo, Wyoming
page 440 MFS-25537

Solar-heated swimming school—Wilmington,
Delaware
page 439 MFS-25548

Solar heating for a restaurant—North Little Rock,
Arkansas
page 443 MFS-25568

Solar heating for an observatory—Lincoln,
Nebraska
page 437 MFS-25525

Solar space-heating system—Yosemite National
Park, California
page 442 MFS-25553

Solar water heater design package
page 434 MFS-25521

Solar water-heating performance evaluation—San Diego, California
page 436 MFS-25502

Two-story residence with solar heating—Newnan, Georgia
page 438 MFS-25526

Winter performance of a domestic solar-heating system—Duffield, Virginia
page 439 MFS-25540

HELICOPTER DESIGN
Isolation and measurement of rotor vibration forces
page 468 LAR-12476

HIGH PRESSURE
Vibration transducer for high temperatures and pressures
page 471 MSC-18778

HYDRAULIC EQUIPMENT
Lock for hydraulic actuators
page 489 MSC-18853

HYDRAULIC FLUIDS
Removing Freon gas from hydraulic fluid
page 452 MSC-18740

IMAGE ENHANCEMENT
OCCULT—ORSER complete conversational user-language translator
page 512 GSC-12604

IMAGERY
Evaluating computer-drawn ground-cover maps
page 512 KSC-11195

Imager displays free fall in stop action
page 450 NPO-14779

Selecting optimum algorithms for image processing
page 513 MFS-25367

INFRARED DETECTORS
Compact infrared detector
page 475 NPO-14864

INSTRUMENT PACKAGES
Developing experiment instrument packages
page 423 GSC-12536

INSULATION
Reflecting layers reduce weight of insulation
page 505 MSC-18785

INTEGRAL TRANSFORMATIONS
An approximation for inverse Laplace transforms
page 511 MSC-18867

INTERFACIAL TENSION
Driving bubbles out of glass
page 453 MFS-25414

IONIZATION COUNTERS
Applying helium ionization detector in chromatography
page 448 MSC-18835

JOINTS (ANATOMY)
Gage for evaluating rheumatoid hands
page 461 GSC-12610

JOINTS (JUNCTIONS)
Interlocking wedge joint is easily assembled
page 485 LAR-12729

JUNCTION TRANSISTORS
Simple JFET oscillator
page 413 GSC-12555

LANDSAT SATELLITES
Evaluating computer-drawn ground-cover maps
page 512 KSC-11195

LAPLACE TRANSFORMATION
An approximation for inverse Laplace transforms
page 511 MSC-18867

LASER RANGE FINDERS
Short-range self-pulsed optical radar
page 432 NPO-14901

LASERS
Gas-laser power monitor
page 430 LAR-12682

Tunable pulsed carbon dioxide laser
page 432 NPO-14984

LIGHT BEAMS
Multibeam collimator uses prism stack
page 427 GSC-12608

LIVESTOCK
Beef grading by ultrasound
page 463 NPO-14812

LOCKS (FASTENERS)
Lock for hydraulic actuators
page 489 MSC-18853

LOGIC CIRCUITS
CADAT integrated-circuit artwork program
page 508 MFS-25017

CADAT network translator
page 507 MFS-25055

MACHINE-INDEPENDENT PROGRAMS
A universal structured-design diagrammer
page 513 LAR-12548

MAGNETIC TRANSDUCERS
Vibration transducer for high temperatures and pressures
page 471 MSC-18778

MAGNETOMETERS
Improved LEEM ranges over four decades
page 469 LAR-12706

MAINTENANCE
Repairing high-temperature glazed tiles
page 496 MSC-18736

MAPS
Evaluating computer-drawn ground-cover maps
page 512 KSC-11195

MATERIALS HANDLING
Lightweight cryogenic vessel
page 505 NPO-14794

Soft container for explosive nuts
page 491 MSC-18871

MATERIALS RECOVERY
Recycling paper-pulp waste liquors
page 450 NPO-14797

MATRICES (MATHEMATICS)
Calculating linear A,B,C, and D matrices from a nonlinear dynamic engine simulation
page 479 LEW-13250

MEDICAL EQUIPMENT
Cardiopulmonary data-acquisition system
page 457 MSC-18783

Fiber-optic coupler for arthroscope
page 462 LAR-12718

Microprocessor-based cardiachometer
page 459 MSC-18775

Microprocessor-controlled ultrasonic plethysmograph
page 458 MSC-18759

METEOROLOGY
Instrument measures cloud cover
page 474 NPO-14936

MICROORGANISMS
Improved microbe detection in water samples
page 460 LAR-12709

MICROWAVE ANTENNAS
Cavity-backed spiral-slot antenna
page 421 MSC-18532

Trislot-cavity microstrip antenna
page 422 MSC-18793

MICROWAVE COUPLING
High-power dual-directional coupler
page 420 NPO-14713

MICROWAVE TUBES
Cooling microwave tube for enhanced performance
page 419 NPO-14975

MIRRORS
Low-cost parabolic mirrors
page 502 NPO-14962

MOLYBDENUM SULFIDES
Self-lubricating gearset
page 504 MSC-18801

MULTIPHASE FLOW
Reduced viscosity interpreted for fluid/gas mixtures
page 431 NPO-14976

NONNEWTONIAN FLOW
Reduced viscosity interpreted for fluid/gas mixtures
page 431 NPO-14976

NOZZLE FLOW
Potential flow in two-dimensional deflected nozzles
page 481 LEW-13461

OIL RECOVERY
Sidewall penetrator for oil wells
page 487 NPO-14306

OPTICAL COMMUNICATION
Fiber-optic clock-signal distribution system
page 430 NPO-14749

OPTICAL EQUIPMENT
Multibeam collimator uses prism stack
page 427 GSC-12608

OPTICAL RADAR
Short-range self-pulsed optical radar
page 432 NPO-14901

OPTIMIZATION
Selecting optimum algorithms for image processing
page 513 MFS-25367

Structural design with stress and displacement constraints
page 480 MFS-25235

ORTHONORMAL FUNCTIONS
An approximation for inverse Laplace transforms
page 511 MSC-18867

OSCILLATORS
Simple JFET oscillator
page 413 GSC-12555

OVENS
An oven for many thermocouple reference junctions
page 467 FRC-10112

PAPERS
Recycling paper-pulp waste liquors
page 450 NPO-14797

PARABOLIC REFLECTORS
Low-cost parabolic mirrors
page 502 NPO-14962

PASSIVATION
Passivation layer for steel substrate of solar cell
page 501 NPO-14961

PHASE LOCKED SYSTEMS
Fiber-optic clock-signal distribution system
page 430 NPO-14749

Timing signal propagates without phase shift
page 422 MSC-18777

PHOTOELECTRIC CELLS
Solar cell is housed in light-bulb enclosure
page 413 LEW-13418



PHOTOMETERS

Compact infrared detector
page 475 NPO-14864

Gas-laser power monitor
page 430 LAR-12682

PHOTOPRODUCTION

Photoproduction of halogens using platinized TiO₂
page 449 LAR-12713

PHOTOVOLTAIC CELLS

Multijunction high-voltage solar cell
page 412 LEW-13400

PLETHYSMOGRAPHY

Microprocessor-controlled ultrasonic plethysmo-
graph
page 458 MSC-18759

PNEUMATIC EQUIPMENT

Pneumatic-power supply
page 486 MSC-18855

POLLUTION MONITORING

Improved microbe detection in water samples
page 460 LAR-12709

POTENTIAL FLOW

Potential flow in two-dimensional deflected nozzles
page 481 LEW-13461

PRISMS

Multibeam collimator uses prism stack
page 427 GSC-12608

PROGRAMMING LANGUAGES

OCCULT—ORSER complete conversational user-
language translator
page 512 GSC-12604

PROTECTIVE COATINGS

Passivation layer for steel substrate of solar cell
page 501 NPO-14961

PULSE GENERATORS

Pulse-shaping circuit for laser excitation
page 428 NPO-14556

PURIFICATION

Driving bubbles out of glass
page 453 MFS-25414

RADAR

Short-range self-pulsed optical radar
page 432 NPO-14901

RADIANT HEATING

Mobile glazing unit
page 498 KSC-11171

RADIOMETERS

Compact infrared detector
page 475 NPO-14864

Field limiter for cavity solar radiometer
page 429 NPO-14781

RANGE FINDERS

Short-range self-pulsed optical radar
page 432 NPO-14901

RECYCLING

Recycling paper-pulp waste liquors
page 450 NPO-14797

REDUNDANT COMPONENTS

Four-wheel dual braking for automobiles
page 488 LAR-12687

REFLECTORS

Low-cost parabolic mirrors
page 502 NPO-14962

REMOTE SENSORS

Evaluating computer-drawn ground-cover maps
page 512 KSC-11195

RING STRUCTURES

Eliminating gaps in undersized split rings
page 500 MSC-18854

ROLLING CONTACT LOADS

Cylindrical bearing analysis
page 491 LEW-13393

RUGGEDNESS

Self-lubricating gearset
page 504 MSC-18801

SAFETY FACTORS

Safety analysis for complex systems
page 511 MSC-18745

SANDWICH STRUCTURES

Heat pipes cool probe and sandwich panel
page 478 LAR-12588

SEALING

Spiral-wound gasket forms low-temperature seal
page 503 LAR-12315

SELF LUBRICATING MATERIALS

Self-lubricating gearset
page 504 MSC-18801

SHEAR PROPERTIES

Biaxial method for in-plane shear testing
page 472 LAR-12680

SILICON

Back contacts for silicon-on-ceramic solar cells
page 504 NPO-14809

Producing silicon continuously
page 497 NPO-14796

SILICONES

New pressure-sensitive silicone adhesives
page 452 LAR-12737

SIMULATION

Wind-simulation tester for solar modules
page 477 NPO-14837

SLOT ANTENNAS

Cavity-backed spiral-slot antenna
page 421 MSC-18532

Trislot-cavity microstrip antenna
page 422 MSC-18703

SOLAR CELLS

Back contacts for silicon-on-ceramic solar cells
page 504 NPO-14809

Multijunction high-voltage solar cells
page 412 LEW-13400

Nickel-doped silicon for solar cells
page 507 NPO-14780

Passivation layer for steel substrate of solar cell
page 501 NPO-14961

Solar cell is housed in light-bulb enclosure
page 413 LEW-13418

Wind-simulation tester for solar modules
page 477 NPO-14837

SOLAR ENERGY

Building with integral solar-heat storage—Stark-
ville, Mississippi
page 444 MFS-25559

Closed-circulation system for motel hot water—
Savannah, Georgia
page 443 MFS-25572

Economic evaluation of a solar hot-water system
page 435 MFS-25529

Economic evaluation of a solar hot-water system
—Palm Beach County, Florida
page 441 MFS-25536

Evaluation of an evacuated-tube liquid solar col-
lector
page 434 MFS-25450

Fire-station solar-energy system—Kansas City,
Missouri
page 440 MFS-25538

Five-city economics of a solar hot-water system
page 434 MFS-25532

Low-cost parabolic mirrors
page 502 NPO-14962

Motel solar-hot-water installation—Atlanta, Geor-
gia
page 443 MFS-25564

Motel solar-hot-water system—Dallas, Texas
page 442 MFS-25575

Motel solar-hot-water system with nonpressurized
storage—Jacksonville, Florida
page 442 MFS-25569

Multijunction high-voltage solar cells
page 412 LEW-13400

Multimode solar-heating system—Columbia,
South Carolina
page 439 MFS-25552

Nickel-doped silicon for solar cells
page 507 NPO-14780

One-year assessment of a solar space water
heater—Clinton, Mississippi
page 440 MFS-25539

Residential solar-heating system—Lansing,
Michigan
page 441 MFS-25530

Residential solar-heating system uses pyramidal
optics
page 436 MFS-25567

Single-family-residence solar heating—Carlsbad,
New Mexico
page 438 MFS-25528

Solar-energy heats a transportation test center—
Pueblo, Colorado
page 438 MFS-25527

Solar-energy landmark building—Columbia,
Missouri
page 437 MFS-25524

Solar-heated and cooled savings and loan building
—Leavenworth, Kansas
page 436 MFS-25520

Solar-heated bank—Marks, Mississippi
page 436 MFS-25558

Solar-heated ranger station—Glendo, Wyoming
page 440 MFS-25537

Solar-heated swimming school—Wilmington,
Delaware
page 439 MFS-25548

Solar heating for a restaurant—North Little Rock,
Arkansas
page 443 MFS-25568

Solar heating for an observatory—Lincoln,
Nebraska
page 437 MFS-25525

Solar-site test module
page 433 MFS-25543

Solar space-heating system—Yosemite National
Park, California
page 442 MFS-25553

Solar water heater design package
page 434 MFS-25521

Solar water-heating performance evaluation—San
Diego, California
page 436 MFS-25502

Two-story residence with solar heating—Newnan,
Georgia
page 438 MFS-25526

Winter performance of a domestic solar-heating
system—Duffield, Virginia
page 439 MFS-25540

Field limiter for cavity solar radiometer
page 429 NPO-14781

Learning high-quality soldering
page 499 NPO-14869

Speed control for synchronous motors
page 414 MSC-18680

Pneumatic-power supply
page 486 MSC-18855

Lightweight cryogenic vessel
page 505 NPO-14794

Structural design with stress and displacement
constraints
page 480 MFS-25235

Biaxial method for in-plane shear testing
page 472 LAR-12680

Structural design with stress and displacement
constraints
page 480 MFS-25235

Biaxial method for in-plane shear testing
page 472 LAR-12680

Structural design with stress and displacement
constraints
page 480 MFS-25235

Biaxial method for in-plane shear testing
page 472 LAR-12680

Structural design with stress and displacement
constraints
page 480 MFS-25235

Biaxial method for in-plane shear testing
page 472 LAR-12680

Structural design with stress and displacement
constraints
page 480 MFS-25235

Biaxial method for in-plane shear testing
page 472 LAR-12680

Structural design with stress and displacement
constraints
page 480 MFS-25235

Biaxial method for in-plane shear testing
page 472 LAR-12680

Structural design with stress and displacement
constraints
page 480 MFS-25235

Biaxial method for in-plane shear testing
page 472 LAR-12680

STRUCTURAL ANALYSIS

- An all-FORTRAN version of NASTRAN for the VAX
page 481 GSC-12600
Structural design with stress and displacement
constraints
page 480 MFS-25235

SYNCHRONISM

- Fiber-optic clock-signal distribution system
page 430 NPO-14749
Timing signal propagates without phase shift
page 422 MSC-18777

SYNCHRONOUS MOTORS

- Speed control for synchronous motors
page 414 MSC-18680

TEA LASERS

- Tunable pulsed carbon dioxide laser
page 432 NPO-14984

TEMPERATURE CONTROL

- An oven for many thermocouple reference junctions
page 467 FRC-10112
Building with integral solar-heat storage—Starkville, Mississippi
page 444 MFS-25559
Closed-circulation system for motel hot water—Savannah, Georgia
page 443 MFS-25572
Economic evaluation of a solar hot-water system
page 435 MFS-25529
Economic evaluation of a solar hot-water system—Palm Beach County, Florida
page 441 MFS-25536
Evaluation of an evacuated-tube liquid solar collector
page 434 MFS-25450
Fire-station solar-energy system—Kansas City, Missouri
page 440 MFS-25538
Five-city economics of a solar hot-water system
page 434 MFS-25532
Motel solar hot-water installation—Atlanta, Georgia
page 443 MFS-25564
Motel solar-hot-water system—Dallas, Texas
page 442 MFS-25575
Motel solar-hot-water system with nonpressurized storage—Jacksonville, Florida
page 442 MFS-25569
Multimode solar-heating system—Columbia, South Carolina
page 439 MFS-25552
One-year assessment of a solar space water heater—Clinton, Mississippi
page 440 MFS-25539
Residential solar-heating system—Lansing, Michigan
page 441 MFS-25530
Residential solar-heating system uses pyramidal optics
page 436 MFS-25567
Single-family-residence solar heating—Carlsbad, New Mexico
page 438 MFS-25528
Solar-energy heats a transportation test center—Pueblo, Colorado
page 438 MFS-25527

- Solar-energy landmark building—Columbia, Missouri
page 437 MFS-25524
Solar-heated and cooled savings and loan building—Leavenworth, Kansas
page 436 MFS-25520
Solar-heated bank—Marks, Mississippi
page 436 MFS-25558
Solar-heated ranger station—Glendo, Wyoming
page 440 MFS-25537
Solar-heated swimming school—Wilmington, Delaware
page 439 MFS-25548
Solar heating for a restaurant—North Little Rock, Arkansas
page 443 MFS-25568
Solar heating for an observatory—Lincoln, Nebraska
page 437 MFS-25525
Solar space-heating system—Yosemite National Park, California
page 442 MFS-25553
Solar water heater design package
page 434 MFS-25521
Solar water-heating performance evaluation—San Diego, California
page 436 MFS-25502
Two-story residence with solar heating—Newnan, Georgia
page 438 MFS-25526
Winter performance of a domestic solar-heating system—Duffield, Virginia
page 439 MFS-25540
TEST EQUIPMENT
Solar-site test module
page 433 MFS-25543

TETRAETHYL ORTHOSILICATE

- Repairing high-temperature glazed tiles
page 496 MSC-18736
Tile densification with TEOS
page 495 MSC-18737

THERMAL INSULATION

- Reflecting layers reduce weight of insulation
page 505 MSC-18785

THERMOCOUPLES

- An oven for many thermocouple reference junctions
page 467 FRC-10112

THERMODYNAMIC PROPERTIES

- Thermodynamic and transport properties of air/water mixtures
page 479 LEW-13432

TILES

- "Densified" tiles form stronger bonds
page 495 MSC-18741
Repairing high-temperature glazed tiles
page 496 MSC-18736
Tile densification with TEOS
page 495 MSC-18737

TIME SIGNALS

- Fiber-optic clock-signal distribution system
page 430 NPO-14749
Time signal propagates without phase shift
page 422 MSC-18777

TRACE CONTAMINANTS

- Bulk lifetime indicates surface contamination
page 471 NPO-14966

TRANSDUCERS

- Vibration transducer for high temperatures and pressures
page 471 MSC-18778

TRANSLATING

- OCCULT—ORSER complete conversational user-language translator
page 512 GSC-12604

TRANSONIC FLOW

- Transonic flow wing/fuselage configurations
page 482 LAR-12702

TRANSPORT PROPERTIES

- Thermodynamics and transport properties of air/water mixtures
page 479 LEW-13432

ULTRASONIC TESTS

- Beef grading by ultrasound
page 463 NPO-14812
Microprocessor-controlled ultrasonic plethysmograph
page 458 MSC-18759

VAPOR DEPOSITION

- Producing silicon continuously
page 497 NPO-14796

VIBRATION MEASUREMENT

- Vibration transducer for high temperatures and pressures
page 471 MSC-18778

VIDEO EQUIPMENT

- Imager displays free fall in stop action
page 450 NPO-14779

VISCOSITY

- Reduced viscosity interpreted for fluid/gas mixtures
page 431 NPO-14976

WASTE ENERGY UTILIZATION

- Gas absorption/desorption temperature-differential engine
page 474 NPO-14528

WASTES

- Recycling paper-pulp waste liquors
page 450 NPO-14797

WATER QUALITY

- Improved microbe detection in water samples
page 460 LAR-12709

WATER VAPOR

- Improved cell for water-vapor electrolysis
page 447 MSC-16394

WEATHER FORECASTING

- Instrument measures cloud cover
page 474 NPO-14936

WEIGHT REDUCTION

- Reflecting layers reduce weight of insulation
page 505 MSC-18785
Structural design with stress and displacement constraints
page 480 MFS-25235

WHEEL BRAKES

- Four-wheel dual braking for automobiles
page 488 LAR-12687

WIND PRESSURE

- Wind-simulation tester for solar modules
page 477 NPO-14837

WIRING

- Learning high-quality soldering
page 499 NPO-14869



National Aeronautics and
Space Administration

Washington, D.C.
20546

Official Business
Penalty for Private Use \$300

THIRD-CLASS BULK

THIRD-CLASS BULK RATE
POSTAGE & FEES PAID
NASA
WASHINGTON, D.C.
PERMIT No. P-154



An engineer for a Kansas City, Missouri, corporation peers through a maze of steam and water lines — a model of a flow network that will eventually be part of a powerplant. The MEL-21 computer program, available from NASA's Computer Software Management and Information Center [COSMIC], saves design time and effort in this and other projects by analyzing pipe stresses due to temperature, weight, and flow pressure. [See the bottom of page A1.]

